

**SKB**

**TECHNICAL  
REPORT**

**89-31**

**INTERDISCIPLINARY STUDY OF  
POST-GLACIAL FAULTING  
IN THE LANSJÄRV AREA  
NORTHERN SWEDEN  
1986 – 1988**

Editors:  
Göran Bäckblom, Roy Stanfors

December 1989

---

**SVENSK KÄRNBRÄNSLEHANTERING AB**  
*SWEDISH NUCLEAR FUEL AND WASTE MANAGEMENT CO*  
BOX 5864 S-102 48 STOCKHOLM  
TEL 08-665 28 00 TELEX 13108 SKB S  
TELEFAX 08-661 57 19

**INTERDISCIPLINARY STUDY OF  
POST-GLACIAL FAULTING  
IN THE LANSJÄRV AREA  
NORTHERN SWEDEN  
1986 – 1988**



# CONTENTS

	Page
<b>ABSTRACT</b>	<b>ix</b>
<b>SUMMARY</b>	<b>xi</b>
<b>1 INTRODUCTION</b>	<b>1:1</b>
<i>Authors: Göran Bäckblom, Roy Stanfors</i>	
<b>1.1 BACKGROUND</b>	<b>1:2</b>
<b>1.2 OBJECTIVES</b>	<b>1:2</b>
<b>1.3 PREVIOUS STUDIES ON SWEDISH POST-GLACIAL FAULT MOVEMENTS</b>	<b>1:2</b>
<b>1.4 SCOPE OF PRESENT STUDY</b>	<b>1:4</b>
<b>1.5 REFERENCES</b>	<b>1:4</b>
<b>2 TECTONIC STUDIES IN THE LANSJÄRV REGION</b>	<b>2:1</b>
<i>Author: Herbert Henkel</i>	
<b>2.1 INTRODUCTION</b>	<b>2:1</b>
2.1.1 Purpose of the Project	2:1
2.1.2 Basic Data Used for this Study	2:1
2.1.3 Regional Setting	2:2
2.1.4 Results from the Nordkalott Project	2:4
<b>2.2 GEOPHYSICAL INVESTIGATIONS</b>	<b>2:5</b>
2.2.1 Magnetics	2:5
2.2.2 Electromagnetics	2:5
2.2.3 Gravity	2:6
2.2.4 Elevation above Sea Level	2:7
2.2.5 Seismic Refraction	2:7
<b>2.3 RESULTS</b>	<b>2:7</b>
2.3.1 Determination of Dip and Width of Large Fault Zones	2:7
2.3.2 Tectonic Interpretation Map	2:8
2.3.3 The NW-striking Steepdipping System of Lineaments	2:12
2.3.4 The N-S Striking Steepdipping System of Lineaments	2:13
2.3.5 The NNE-SSW Striking Near Horizontal System of Lineaments	2:14
2.3.6 Determination of Highest Shore Line (HS)	2:14
2.3.7 The Post-glacial Fault Scarps, PGF	2:15
<b>2.4 DISCUSSION</b>	<b>2:18</b>
2.4.1 Three-dimensional Network of Fault Zones	2:18
2.4.2 Summary	2:19
2.4.3 Tectonic Patterns	2:21
2.4.4 Methods	2:22
2.4.5 New Fracturing	2:22
<b>2.5 REFERENCES</b>	<b>2:23</b>

	<b>Page</b>	
<b>3</b>	<b>POSTGLACIAL FAULTING AND PALEO-SEISMICITY IN THE LANSJÄRV REGION</b>	<b>3:1</b>
	<i>Author: Robert Lagerbäck</i>	
<b>3.1</b>	<b>AIM OF INVESTIGATIONS</b>	<b>3:1</b>
<b>3.2</b>	<b>THE LANSJÄRV AREA</b>	<b>3:1</b>
3.2.1	Topography, Highest Coastline, Bedrock, Quaternary Deposits	3:1
3.2.2	Fault Scarps, Paleoseismic Records	3:3
<b>3.3</b>	<b>FIELD INVESTIGATIONS</b>	<b>3:5</b>
3.3.1	Trenching Across Fault Scarps	3:5
3.3.2	Paleoseismic Records	3:13
3.3.2.1	Landslides	3:13
3.3.2.2	Seismites	3:14
<b>3.4</b>	<b>DISCUSSION</b>	<b>3:16</b>
3.4.1	Age of Faulting	3:16
3.4.2	Fault Geometry and Style of Postglacial Faulting, some Remarks	3:17
3.4.3	Paleoseismicity	3:18
3.4.3.1	Landslides	3:18
3.4.3.2	Seismites	3:19
<b>3.5</b>	<b>CONCLUSIONS</b>	<b>3:20</b>
<b>3.6</b>	<b>REFERENCES</b>	<b>3:21</b>
<b>4</b>	<b>REACTIVATIONS OF PROTEROZOIC SHEAR ZONES</b>	<b>4:1</b>
	<i>Authors: Christopher Talbot, Raymond Munier, Lucie Riad</i>	
<b>4.1</b>	<b>PURPOSE</b>	<b>4:1</b>
<b>4.2</b>	<b>GEOLOGY</b>	<b>4:1</b>
4.2.1	Rock Types	4:1
4.2.2	Early Regional Strains	4:2
<b>4.3</b>	<b>SHEAR ZONES</b>	<b>4:4</b>
4.3.1	General	4:4
4.3.2	N-trending Shear Zones	4:4
4.3.3	NW-trending Shear Zones	4:5
4.3.4	NE-NNE Trending Shear Zones	4:5
<b>4.4</b>	<b>SHEAR ZONE HISTORIES</b>	<b>4:7</b>
4.4.1	Early Ductile Shear	4:7
4.4.2	Mylonites, Pseudotachylites & Micro-cataclasites	4:8
4.4.3	Veins Formed in Greenschist Metamorphic Facies	4:8
4.4.4	Faults	4:10
4.4.5	Possible Fault Gouges	4:10

	Page	
4.5	BLOCKS AND ORTHOGONAL JOINTS	4:11
4.6	REPEATED EPISODIC REACTIVATIONS WITH UNKNOWN TIMING	4:12
4.7	DISPLACEMENT LINKAGE	4:14
4.8	DYNAMICS	4:15
4.9	REFERENCES	4:16
5	<b>ANALYSIS OF THE EARTHQUAKE MECHANISMS IN THE NORRBOTTEN AREA</b>	<b>5:1</b>
	<i>Author: Ragnar Slunga</i>	
5.1	INTRODUCTION	5:1
5.2	THE EARTHQUAKES OCT 1987 — FEB 1989	5:1
5.3	FOCAL DEPTHS	5:1
5.4	THE EARTHQUAKE MECHANISMS	5:4
5.4.1	The Seismic Moments and Magnitudes	5:4
5.4.2	Size of the Faulting Area, Static Stress Drop, and Size of the Shear Slip	5:4
5.4.3	The Fault Plane Solutions	5:7
5.4.4	The Horizontal Stresses	5:9
5.5	THE SPATIAL DISTRIBUTION AND EXTENT OF ASEISMIC SLIDING	5:9
5.6	DISCUSSION AND CONCLUSIONS	5:11
5.7	REFERENCES	5:12
6	<b>EARTHQUAKES NEAR THE LANSJÄRV FAULT</b>	<b>6:1</b>
	<i>Author: O Kulhánek</i>	
6.1	INTRODUCTION	6:1
6.2	SEISMIC MONITORING OF THE LANSJÄRV NEOTECTONIC FAULT REGION	6:1
6.3	THE MOBILE NETWORK	6:1
6.4	DATA ANALYSIS	6:3
6.5	HYPOCENTRE LOCATIONS	6:3
6.6	FOCAL MECHANISMS	6:6
6.7	DYNAMIC SOURCE PARAMETERS	6:7
6.8	DISCUSSION AND CONCLUSIONS	6:7
6.9	SOURCE PARAMETERS OF MAJOR EARTHQUAKES IN NORTHERN SWEDEN DEDUCED FROM SYNTHETIC SEISMOGRAMS	6:10
6.10	REFERENCES	6:13

	<b>Page</b>	
<b>7</b>	<b>DRILLING AND BOREHOLE DESCRIPTION</b>	<b>7:1</b>
	<i>Authors: Bjarni Bjarnason, Olle Zellman, Peter Wikberg</i>	
7.1	INTRODUCTION	7:1
7.2	GEOPHYSICAL BOREHOLE LOGGING	7:3
7.3	CORE MAPPING	7:5
7.4	GROUNDWATER CHEMISTRY	7:8
7.5	ROCK STRESS MEASUREMENTS	7:9
7.5.1	Purpose of the Work	7:9
7.5.2	The Stress Measuring Method	7:9
7.5.3	Field Work	7:10
7.5.4	Results	7:10
7.5.5	Conclusions	7:13
7.6	REFERENCES	7:14
<b>8</b>	<b>HYDROGEOLOGICAL CONDITIONS</b>	<b>8:1</b>
	<i>Author: Nils-Åke Larsson</i>	
8.1	GENERAL	8:1
8.2	BOREHOLE TESTING IN KLJ 01	8:2
8.2.1	Hydraulic Conductivity and Groundwater Pressure	8:2
8.2.2	Hydraulic Conductivity – Comparison with other Study Sites	8:5
8.3	CONDUCTIVE FRACTURE FREQUENCY	8:5
8.3.1	Definition	8:5
8.3.2	Input Data	8:5
8.3.3	Results	8:8
8.3.4	Comparison of CFF with other Study Sites	8:8
8.4	NUMERICAL MODELLING	8:9
8.4.1	Objective and Approach	8:9
8.4.2	Verification of Hydraulic Boundaries	8:10
8.4.3	Modelled Cases and Results	8:10
8.4.4	Concluding Remarks	8:13
8.5	REFERENCES	8:13
<b>9</b>	<b>MINERALOGICAL AND GEOCHEMICAL STUDIES OF FRACTURE-INFILLINGS IN DRILLCORE KLJ 01</b>	<b>9:1</b>
	<i>Authors: Ove Landström, John Smellie, Eva-Lena Tullborg</i>	
9.1	INTRODUCTION	9:1
9.2	RESULTS FROM THE CORE LOGGING	9:1
9.3	SAMPLING AND ANALYSES	9:1
9.4	MINERALOGY — RESULTS OF MICROSCOPY	9:2

	<b>Page</b>
<b>9.5</b>	<b>CHEMISTRY</b> <span style="float: right;"><b>9:3</b></span>
9.5.1	Reference Normalized Granite v.s Fracture Filling Phases <span style="float: right;">9:6</span>
9.5.2	REE Fractionation Trends <span style="float: right;">9:9</span>
9.5.3	Depth Related Trends <span style="float: right;">9:12</span>
9.5.4	Uranium Decay Series Measurements <span style="float: right;">9:12</span>
<b>9.6</b>	<b>DISCUSSION AND CONCLUSION</b> <span style="float: right;"><b>9:14</b></span>
<b>9.7</b>	<b>REFERENCES</b> <span style="float: right;"><b>9:17</b></span>
<b>10</b>	<b>MODELLING OF ROCK MASSES</b> <span style="float: right;"><b>10:1</b></span>
	<i>Author: Ove Stephansson</i>
<b>10.1</b>	<b>INTRODUCTION</b> <span style="float: right;"><b>10:1</b></span>
<b>10.2</b>	<b>PROBLEM DEFINITION AND CONCEPTUAL MODELS</b> <span style="float: right;"><b>10:1</b></span>
<b>10.3</b>	<b>MODELLING TECHNIQUES</b> <span style="float: right;"><b>10:5</b></span>
10.3.1	Jointed Rock Continuum Model, HNFEMP <span style="float: right;">10:6</span>
10.3.2	Distinct Element Program for Modelling Jointed Rock Masses, MUDEC <span style="float: right;">10:7</span>
<b>10.4</b>	<b>AN ATTEMPT TO VALIDATION OF ROCK MECHANICS CODES AGAINST COLORADO SCHOOL OF MINES BLOCK TEST DATA</b> <span style="float: right;"><b>10::8</b></span>
10.4.1	Mechanical Properties <span style="float: right;">10:9</span>
10.4.2	Modelling with HNFEMP and Comparison of Numerical and Field Test Results <span style="float: right;">10:10</span>
10.4.3	Modelling with MUDEC and Comparison of Numerical and Field Test Results <span style="float: right;">10:14</span>
<b>10.5</b>	<b>MODELLING THE EFFECT OF GLACIATION, ICE FLOW AND DEGLACIATION ON LARGE ROCK MASSES</b> <span style="float: right;"><b>10:15</b></span>
10.5.1	Modelling with HNFEMP <span style="float: right;">10:19</span>
10.5.2	Modelling with MUDEC, Linear Fault Stiffness <span style="float: right;">10:20</span>
10.5.3	Modelling with MUDEC and Barton-Bandis Joint Model <span style="float: right;">10:26</span>
<b>10.6</b>	<b>SUMMARY</b> <span style="float: right;"><b>10:31</b></span>
<b>10.7</b>	<b>CONCLUSIONS</b> <span style="float: right;"><b>10:32</b></span>
<b>10.8</b>	<b>REFERENCES</b> <span style="float: right;"><b>10:33</b></span>
<b>11</b>	<b>GENERAL CONCLUSIONS</b> <span style="float: right;"><b>11:1</b></span>
	<i>Authors: The interdisciplinary researchers and co-ordinators</i>





## ABSTRACT

Post-glacial faults have been recognized in the northern Baltic shield for several decades.

It is important to evaluate whether such neotectonic movements can lead to new fracturing or decisively alter the geohydrological or geohydrochemical situation around a final repository for spent nuclear fuel.

The post-glacial Lansjärv fault was chosen for interdisciplinary study because of its relative accessibility.

The goals of the study were to assess the mechanisms that caused present day scarps, to clarify the extent of any recent fracturing and to clarify the extent of any ongoing movements. All these objectives were reasonably met through a series of studies.

This report describes achievements that have been gained since the study was initiated by SKB 1986.

Analysis of geology and geophysics over a 150x200 km region supplemented with seismic networks and field studies at outcrops and trenches set a framework for a cored borehole down to a depth of 500 m at the fault. The core has been studied in detail with respect to fracture-infillings in order to analyse mineralogical and geochemical alteration. The borehole has been logged for geophysics, stress, hydraulic conductivity, groundwater pressure and the chemical constituents of the groundwater. Numerical modelling has been undertaken in order to understand the effects of glaciation on the behaviour of a blocky rock mass. Several general conclusions have been made by the interdisciplinary research group. One of the major conclusions is that pre-existing old structures were reactivated by tectonic movements, possibly triggered by deglaciation. In spite of a major earthquake that may have occurred during the deglaciation, and in spite of the anomalous tectonic setting compared to study-sites within SKB's site investigation programme, the hydraulic conductivity and groundwater chemistry are comparable with results from those sites.



## SUMMARY

An in-depth analysis of the possible effects of geological processes on a final repository was initiated by SKB 1986. Essential questions are whether recent movements can lead to new fracturing and whether load changes or rock block movements can decisively alter the geohydrological or geohydrogeological situation around a final repository. A major study within this framework has been directed to the Lansjärv post-glacial fault (PGF) scarps in northern Sweden. The Lansjärv fault was chosen as the most accessible of the PGFs in Sweden. The fault complex is composed of four major and several minor fault scarps, together forming a 50 km long fault set. The longest fault-scarp segment is 17 km. The scarps generally range in height from between 5 to 10 m.

The specific goals for the Lansjärv study were to assess mechanisms that caused present day scarps, to clarify the extent of any recent fracturing and to clarify the extent of any ongoing movements. All these objectives were reasonable met through a series of studies.

In the initial stage of the Lansjärv study existing geological and geophysical data in an 150x200 km large area was compiled. The tectonic interpretation map has utilized digital imageprocessing technique for the combined interpretation of magnetic, elevation relief, geology and gravity. This analysis and geophysical ground measurement identified three regional fault systems. Major single faults of the N and NW system are about 200 m wide and have generally steep dips. The third system strikes NNE and gently dips ESE. So far no case of post-glacial fracturing in the bedrock has been observed.

By trenching across the fault scarps it has been possible to date fault movements relative to the Quaternary stratigraphy. It is concluded that the post-glacial faults in the Lansjärv area developed as single-event movements shortly after the deglaciation about 9000 years ago, possibly in connection to strong earthquakes. The scarps are developed in strongly fractured and chemically weathered zones of presumed pre-Quaternary age. The results from the trenches suggest, at least at the surface, that the faults are reverse and dipping between 40 – 50° and the vertical. It is concluded that most, if not all, the post-glacial fault movements took place along zones shattered and chemically altered long before pre-Quaternary times.

The natures, geometries, histories, kinematics and recent dynamics of geological deformation structures and fabrics exposed in the bedrock in or near the post-glacial Lansjärv fault system and N- and NW-trending geophysical lineaments was treated in a tectonic interpretation in a regional scale of the Lansjärv area. The geological and tectonic studies concluded the post-glacial fault to strike NNE and dip gently to ESE.

Two seismic networks for earthquake monitoring have been established and operated in the Lansjärv area as part of the project. Up to Feb. 1989 more than 90 events were detected by the six station permanent network with signals at 3 or more stations. The magnitudes were in the range  $M_L$  0.1 – 3.6. The released stresses have the horizontal principal compression in the NW-SE quadrant. The dominating type of fault movements is strike-slip along subvertical planes. The mobile network for detecting seismic activity registered a few events during the 1987 period. For the 1988 campaign some of the stations were relocated and 28 events were detected. Plausible focal styles have been derived for four events, showing a variety of faulting styles. Many events are located at depths of 8–10 km.

Based on the results and analysis of geophysical measurements and tectonic interpretation a site for core drilling was suggested. Three percussion boreholes and a 500 m cored hole were drilled. As the cored hole collapsed at a depth of 148 m, casing was set down to this depth. The hole was logged with several geophysical methods. Core mapping shows predominantly red-gray granite as the general rock type. Pegmatites and aplites occur as dykes and veins. Tectonic breccia occurs in some sections of the borehole. The upper part of the hole, 32 – 300 m, is very fractured, while the lower section is less fractured.

Samples of groundwater chemistry at depths of 150 m and 237 m show that the Lansjärv water belongs to the group of intermediate non-saline granitic groundwaters. Eh (redoxpotential) monitoring as well as presence of detectable amounts of ferrous iron indicate the reducing character of the water.

Rock stresses were measured by means of hydraulic fracturing. The minimum horizontal stress especially near the bottom of the hole is exceptionally low, close to 6 MPa, compared to elsewhere in Sweden. Maximum horizontal stress values are more scattered, but is in general in the same order as the vertical stress. The direction of the maximum horizontal stress is depth dependent. At 300 m the direction is NW-SE. However, it rotates rapidly and steadily with depth and at the bottom of the hole it has turned to ENE-WSW. This re-direction of stresses with depth is unusual.

Hydrogeological testings in the hole included measurements of hydraulic conductivity and observations of groundwater pressures. The hydraulic conductivity decreases slightly with depth. The highest values ( $> 10^{-6}$  m/s) are obtained in the depth interval where the fracture frequency is highest and where the hole is interpreted to intersect the post-glacial fault. There is no obvious correlation between hydraulic conductivity, fracture frequency, rock type, rock stress or infillings. Compared to other study-sites the conductivity show no clear anomaly, even though the rock may have experienced a  $M_L = 7$  earthquake. Measurements of groundwater levels, however show some peculiarities. The groundwater level is approximately 70 m below surface in the percussion hole HLJ 01 and there is a relatively large vertical gradient through the length of the borehole. Numerical modelling was done in order to study some aspects of the effects of fracture zone geometry on groundwater flow conditions. The modelling show that the existence of a continuous fracture zone with an inclination of  $15^\circ$  does not explain observed hydraulic data. A steeper inclination of the fracture zone give a better fit with data. Another possibility is several subhorizontal fracture zones.

A mineralogical and geochemical study has been performed of fracture-infillings in the drillcore in order to identify evidence that may support recent reactivation and to determine whether low temperature rock/water reactions have contributed to changes in the fracture mineralogy and chemistry. Of particular interest to this study is the variation of U, Th, REE (Rare Earth Elements) from the fracture edges into the wall rock as well as their variation with depth. The study show that the rock has been exposed to extensive hydrothermal activity especially pronounced in the upper 300 m of the drillcore. Subsequent to hydrothermal period(s) low temperature groundwaters have caused redistribution of elements as well as minerals e.g. the dissolution of calcite and the leaching of U and light REE along the flow paths in the upper part of the borehole.

Computer modelling of large-scaled bedrock has also been conducted to study effects of e.g. glaciation, ice sheet advance, deglaciation, ice sheet retreat, and melt-down.

The first part of the modelling project has been aimed at attempts to validate the numerical codes used. The Colorado School of Mines block tests have been used for checking the performance of the codes. Using the finite difference code

MUDEC, the rock is essentially treated as a discontinuum. The modelled stresses indicate features similar to those measured in the CSM block i.e. rotations from blocks to block where crossing a joint. The ranges of values for deformations are in agreement with measurements. Using the finite element code HNFEMP the rock is essentially treated as a continuum. There is fair agreement in the orientations and magnitudes of displacement vectors and direction of principal horizontal stress. The effect of glaciation and deglaciation has been studied as well. Six loading cases were modelled for a 4 · 4 km rock mass with three different fault set geometries. The results from one calculation using MUDEC show inter-block displacements in the order of 5 to 10 cm for the assumed material properties.

At the end of the research project questions were listed and answered by the interdisciplinary research group to form the general conclusions of the project. Some of the conclusions are that:

- The Lansjärv post-glacial fault reactivated pre-existing old structures. Any new fractures appear at surface or to be confined to within a few metres of the scarp.
- The causes of the post-glacial movement is a combination of plate tectonics and deglaciation.
- In spite of the very dramatic structures and events, the borehole results with respect to and hydraulic conductivity and groundwater chemistry are comparable to results from potential sites for a repository in Sweden being sited more favourable. Pre-existing, old, heavily fractured and altered zones can be avoided when making the design of a repository so that canisters of waste are not positioned in zones of potential movement.



# 1 INTRODUCTION

*Göran Bäckblom*

SKB, Box 5864, S-102 48 Stockholm, Sweden

*Roy Stanfors*

Roy Stanfors Consulting AB, IDEON, S-223 70 Lund, Sweden

The introduction provides an overview of the background to and objectives of the Lansjärv study. Earlier works on post-glacial faults in Sweden are presented. The scope of work in the Lansjärv area, Figure 1-1 are outlined.

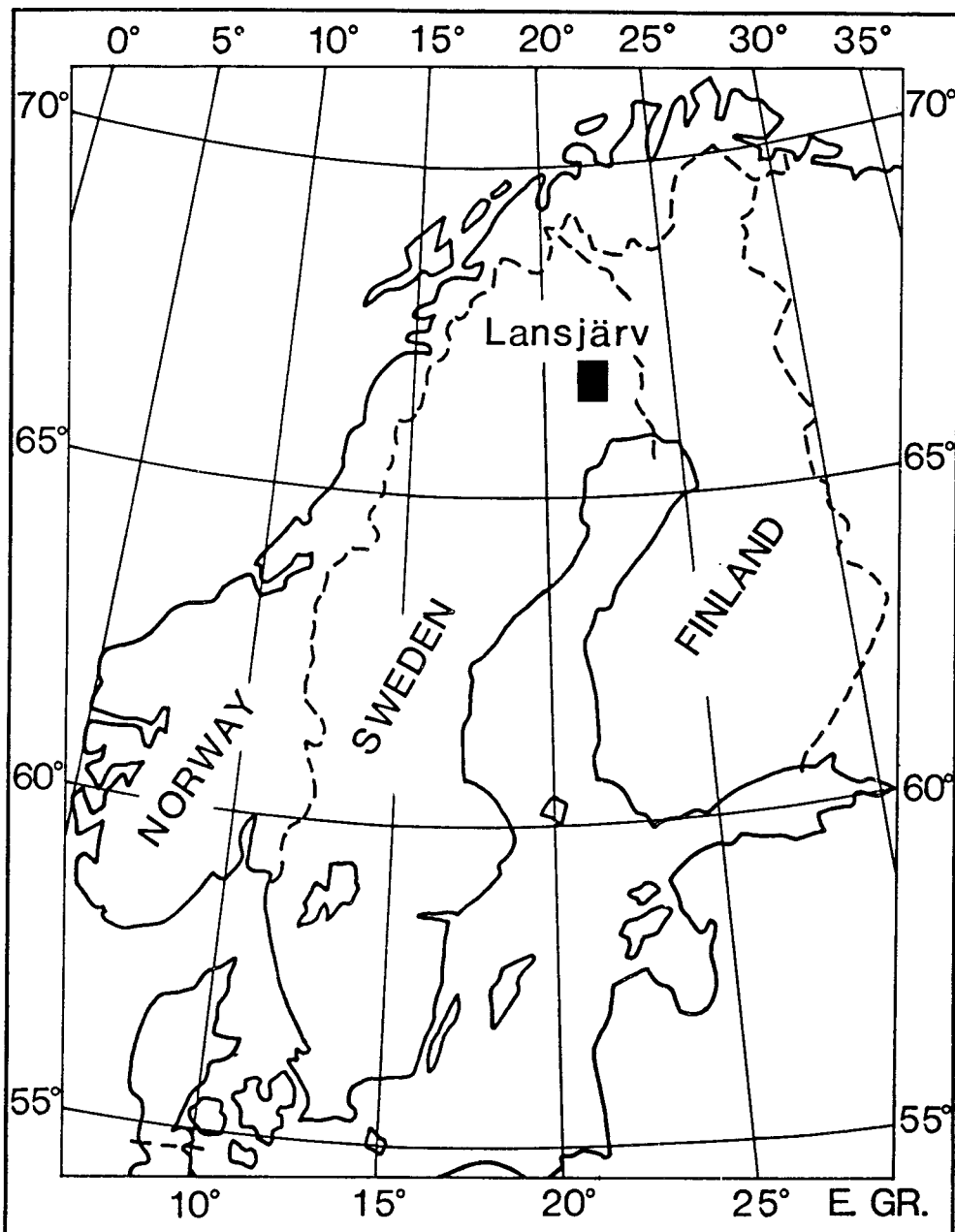


*Figure 1-1. The Lansjärv area.*



## 1.1 BACKGROUND

The long-term safety of a repository can be demonstrated by using several redundant barriers. The performance of the waste and the engineered barriers – canister and buffer – is dependent on the chemical and geohydrological conditions in the rock mass. With respect to safety it is important that the rock provides mechanical protection, low groundwater flow and a favorable chemical environment over a long period of time. In order to carry through an in-depth analysis the possible effects of geological and climatic processes several studies have been launched in accordance with the R&D-programme on handling the final disposal of nuclear waste that was presented in 1986, SKB (1986).

One essential study within the programme on bedrock stability is the analysis of post-glacial fault movement in the Lansjärv area. The post-glacial fault movements that have been detected in Scandinavia probably occurred along major fault zones that have already existed for hundreds of million years.

It is, however, of importance to evaluate whether these recent (neotectonic) movements can lead to new fracturing or decisively alter the geohydrological or geochemical situation around a final repository for spent nuclear fuel.

## 1.2 OBJECTIVES

The objectives for the R&D on bedrock stability are

- to quantify or set limits on the consequences of earthquakes, glaciations and land uplifts to the safety of a final repository for spent nuclear fuel,
- to process, evaluate and increase knowledge concerning geodynamic processes in the Baltic Shield.

Within these overall objectives, specific objectives have been set for the Lansjärv study. They are

- to assess the mechanisms that caused present day scarps,
- to clarify the extent of any recent fracturing,
- to clarify the extent of any ongoing movements.

## 1.3 PREVIOUS STUDIES ON SWEDISH POST-GLACIAL FAULT MOVEMENTS

The first paper on Swedish post-glacial fault movements was published by Lundqvist & Lagerbäck (1976). The occurrence of similar fault scarps had previously been discovered in Finland, Kujansuu (1964). Robert Lagerbäck, Swedish Geological Survey, surveyed the Lappish "Pärvie" phenomenon during 1975 by request of Mr Aslak Partapouli. Lagerbäck concluded that the Pärvie-feature was largely composed by post-glacial fault scarps and a fault-line more than 150 km long was mapped. It became obvious that the Pärvie fault movement could be an example of a more common phenomenon and continued work revealed several expected post-glacial fault movements. Lagerbäck & Henkel (1977), Lagerbäck (1979).

Preliminary geological and geophysical characterization of the faults was carried through and published. Lagerbäck & Witschard (1983), Henkel et al. (1983).

These reports included interpretations of air-borne magnetical surveys, photogrammetrical levelling, air-photo interpretation, investigations on outcrops and geophysical measurements on the ground, including seismic refraction profiling.



## 1.4 SCOPE OF PRESENT STUDY

During 1986 – 1988 a great number of investigations have been performed in the Lansjärv area. Henkel (1988) made a geophysical study in order to obtain basic data for an optional location of drill holes, excavations and deformation measurements, Chapter 2.

Lagerbäck (1988) investigated the fault scarps along excavated trenches in order to date fault movements relative to the Quaternary stratigraphy, Chapter 3.

Talbot (1986), and this volume, performed field investigations of structural geology and a tectonic interpretation on a regional scale, Chapter 4.

Slunga (1989), and this volume, reported results of the operation of seismological network with six stations in northern Sweden. A great number of events have been located and analysed for source mechanics, Chapter 5.

A mobile seismic network operated close to the faults in the Lansjärv area during two summer periods. A number of events have been registered and analysed by Wahlström et al. (1988), (1989), Chapter 6.

In order to check the hypothesis of a gently dipping fracture zone – which is considered to be activated in post-glacial time – a core borehole has been drilled to a depth of 500 m at a site 5 km NE of Lansjärv. A summary description of the borehole data is contained in this volume. Results from core mapping, geophysical logging and sampling of groundwater chemistry are presented in Chapter 7. Studies on hydrogeological conditions comprising borehole testing, analysis and modelling is presented in Chapter 8, whereas studies on mineralogy and geochemistry of fracture-infillings is contained in Chapter 9.

Chapter 10 describes the efforts to model large-scaled blocky bedrock to study effects of glaciation, deglaciation, ice flow and melt-down. The modelling was preceded by attempts to validate the models, Barton & Chryssanthakis (1988) and Stephansson & Savilahti (1988).

The final Chapter 11, presents the general conclusions of the Lansjärv study, co-authored by those participating in the project.

The quality of this summary report has been substantially improved by the keen co-reviewing of Prof Eystein S Husebye, Oslo, Prof O Stephansson, Luleå, Prof C Talbot, Uppsala and Dr Paavo Vuorela, Espoo.

During the course of the project it was not possible to resolve all issues completely. It is thus planned for a minor extension of the study focusing mainly on the dip of the post-glacial fault and evidence for seismites.

## 1.5 REFERENCES

### **Barton N, Chryssanthakis P 1988**

Validation of MUDEC against Colorado School of Mines block test data. SKB TR 88-14, Stockholm

### **Henkel H, Hult K, Eriksson L, Johansson L 1983**

Neotectonics in Northern Sweden – geophysical investigations. SKBF/KBS TR 83-57, Stockholm

### **Henkel H 1988**

Tectonic studies in the Lansjärv region. SKB TR 88-07, Stockholm

**Kujansuu R 1964**

Nuorista sirroksista Lapissa. Summary: Recent faults in Lapland. Geologi 16, 30-36, Helsingfors

**Lagerbäck R & Henkel H 1977**

Studies of neotectonic activity in the middle and north part of Sweden. Air-photo and geophysical interpretation of recent faults. (In Swedish). SKBF/KBS TR 19, Stockholm

**Lagerbäck R 1979**

Neotectonic structures in Northern Sweden. GFF 100, 263 – 269, Stockholm

**Lagerbäck R, Witschard F 1983**

Neotectonics in Northern Sweden – geological investigations. SKBF/KBS TR 83-58, Stockholm

**Lagerbäck R 1988**

Post-glacial faulting and paleoseismicity in the Lansjärv area, northern Sweden. SKB TR 88-25, Stockholm

**Lundqvist J, Lagerbäck R 1976**

The Pärvie Fault: A lateglacial fault in the Precambrian of Swedish Lapland. GFF 98, 45-51, Stockholm

**SKB 1986**

Handling and final disposal of nuclear waste. Programme for research, development and other measures. Stockholm

**SKBF/KBS 1983**

Handling of spent nuclear fuel – KBS-3. Parts I-IV. Stockholm.

**Slunga R 1989**

Earthquake measurements in northern Sweden Oct 1987 – Apr 1988. SKB TR 89-26, Stockholm

**Stephansson O, Savalahti T 1988**

Validation of the HNFEMP against Colorado School of Mines block test data. SKB TR 88-13, Stockholm

**Talbot C 1986**

A preliminary structural analysis of the patterns of post-glacial faults in northern Sweden. SKB TR 86-20, Stockholm

**Wahlström R, Linder S-O, Holmqvist C 1988**

Near-distance seismological monitoring of the Lansjärv neotectonic fault region. SKB TR 88-12, Stockholm

**Wahlström R, Linder S-O, Holmqvist C, Mårtensson H-E 1989**

Near-distance seismological monitoring of the Lansjärv neotectonic fault region. Part II. SKB TR 89-01, Stockholm



## 2 TECTONIC STUDIES IN THE LANSJÄRV REGION

*Herbert Henkel*

Geological Survey of Sweden  
Box 670, S-751 28 Uppsala, Sweden

### 2.1 INTRODUCTION

#### 2.1.1 Purpose of the Project

The purpose of this study is:

- to obtain a geological-geophysical basis for an optimal location of detailed studies of post-glacial faulting using deformation measurements, drill holes and excavations. Of special importance is to indicate where new fracturing has occurred in the bedrock of Norrbotten and
- to understand within a broader regional tectonic context where movements and earthquakes occur today.

The following sub-projects have been performed:

- 1 – Compilation of existing geological and geophysical data in an
  - a) **regional area 150 x 200 km** where gravity, magnetic, terrain elevation, terrain relief and geological data are stored digitally. The maps are reproduced in a smaller scale in plates 1–5. A set of maps in two sheets to the scale 1:250 000 have been prepared from these datasets, and in
  - b) **an local area 20 x 45 km** located around the Lansjärv PGF where existing detailed surveys are compiled in 6 map sheets to the scale 1:20 000, Henkel and Wällberg (1987).
- 2 – Additional airphoto studies to localize outcrops along large fault zones, Sundh and Wahlroos (1987).
- 3 – Additional ground geophysical measurements of magnetic field, VLF and slingram along profiles across larger fault zones. Model calculations of dip of fault zones, Arkko and Lind (1988) and Arkko (1988).
- 4 – Tectonic-geological reconnaissance in the local area, Talbot (1986).
- 5 – Photogrammetric levelling of highest shoreline, Sundh and Wahlroos (1988).
- 6 – Integrated analysis of basic data compiled in sub-project 1a. This report, plate 6, Tectonic Interpretation Map and report by Henkel (1988).

#### 2.1.2 Basic Data Used for this Study

A new image analyzing system for the combined interpretation of aeromagnetic, elevation relief and gravity data has been used. The data can now be analyzed using the maximal (with respect to the measurements) spatial and functional resolution. For the aeromagnetic measurements, this implies a functional resolution a five times better as compared to the previous available maps (i.e. 20 nT/nanoTesla/ instead of 100). The combination of aeromagnetic and elevation

data turned out to be a very efficient tool for the mapping of fault patterns. The basic datasets provided for this study have the specifications shown in Table 2-1.

**Table 2-1. Data of geophysical information.**

Type	Spatial (m) Resolution	Functional Resolution	Data provided by
Aeromagnetic total field anomaly	200 x 200	20 nT	Geological Survey of Sweden and Finland
Gravity	400 x 400	0.2 mgal	Geological Survey of Sweden and Finland and Swedish Land Survey
Elevation	100 x 100	2 m	Swedish Land Survey
Bedrock geology			Geological Survey of Sweden

A set of maps showing the study area on two sheets in the scale 1:250 000 have been prepared for each of the datasets. The functional resolution on these maps is lower than in the original datasets as only about 40 color isolines can be visually discriminated. The Tectonic Interpretation Map has been prepared with the image analyzing system in 50 x 50 km quadrangles and was subsequently compiled and plotted in the desired scale with an electrostatic plotter.

### 2.1.3 Regional Setting

The oldest rocks of the region occur in a small dome of Archean basement in the map area 25 N, plate 5. The rest of the study area is occupied by rocks which are thought to have been deformed, metamorphosed and intruded during the Svecokarelian orogeny 1.9–1.7 Ga ago (see Geological Map of Northern Fennoscandia, 1986). The area is now dominated by Svecokarelian granitoids. A few dyke swarms of younger Proterozoic age occur and at the southern margin of the area a set of alkaline dykes intruded at -1.1 Ga, Kresten et al. (1977). At the end of the Precambrian, the region was peneplained and outside the study areas, autochthonous Cambrian sediments are preserved. These occur at about 1000 m above sea level at the front of the Caledonian thrust units, about 200 km to the west of the study area and in the Muhos fault graben below sea level, about 50 km to the southeast of the study area, Wannäs (1989). It is likely that the area was again eroded during the Tertiary when the crystalline basement was deeply weathered. Remnants of this weathering may be found locally when protected in downfaulted blocks. Several glaciations in the Quaternary have changed the morphology to its present shape.

Parallel with the rock forming processes, tectonic activity displaced and deformed crustal units. Shortly after the formation of the Svecokarelian crust. Berthelsen and Marker (1986) suggest large scale displacements along strike-slip megashears along N-S lineaments in the Baltic-Bothnian zone and NW-SE lineaments in the Rahe-Ladoga zone. This zone appears about 60 km to the

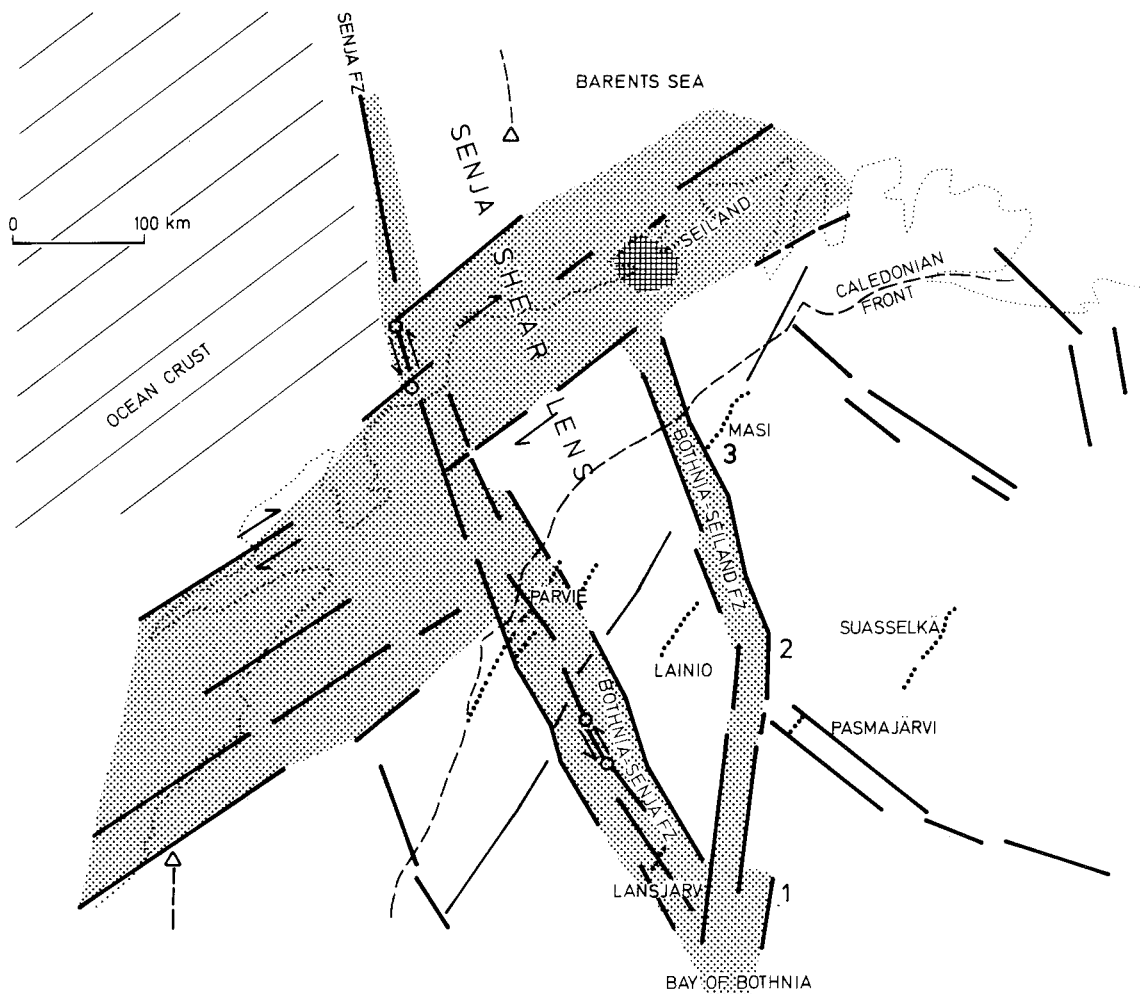


Figure 2-1. Generalized regional fault zone patterns in northern Fennoscandia. Dotted lines show known PGF scarps. 1, 2 and 3 are locations with major lithological discontinuities.

south of the study area and to the east of the Baltic-Bothnian Megashear, Figure 2-1. On these zones, movements were both sinistral and dextral and resulted in a net 120 to 160 km sinistral displacement along the N-S zone. The existence of late Paleozoic alkaline intrusives at Kalix and Paleozoic sediments in the Muhos graben indicate repeated tectonic activity and possible reactivation of the Svecokarelian Megashears.

The plate tectonic situation indicates a period during the Tertiary, when the regional lineaments again were active. The Senja fracture zone and its fossil trace along the Western Barents Sea continental edge lines up with the Bothnian-Senja system of NW-lineaments through the Lansjärv study area. It is very likely that this zone was active not only just outside Senja at -58 Ma when the first ocean crust of the Atlantic rift formed in this region, but also along its SE continuation in northern Scandinavia. In the early stages of the Atlantic opening, the Tertiary fold belt in western Svalbard, Harland (1979) and north-easternmost Greenland, Schack Pedersen and Håkansson (1987) are large scale examples of compressive strike-slip block movements. In the western Barents Sea, basin development occurs in late Tertiary times.



Present lithospheric stresses are induced by the plate motion, remaining glacial rebound, and continued changes in plate tectonic patterns. The continued cooling and thickening of the oceanic crust induces flow of mantle material under the continental lithosphere and generates continuous rise and tilt of the continental edge. Differential opening rates in the Arctic and North Atlantic oceans will induce stresses into the surrounding continental blocks which are likely to be released in existing fault systems. Several hundreds kilometer of post-glacial fault scarps have been detected in a restricted area between and around the extension of the two large fault zones of the study area – as indicated in Figure 2-1. These mark a late episode of increased tectonic activity of the area.

#### 2.1.4 Results from the Nordkalott Project

The compilation of the Aeromagnetic Interpretation Map, Henkel (1986) in the Nordkalott project shows that the linear magnetic dislocations in the Lansjärv area are part of larger structures which extend for several hundreds kilometer. They strongly disrupt the Svecokarelian lithological pattern and could be followed under the Caledonian rock units to the coast of N Norway. Across the **NW-trending set** of major structures, a change in the patterns of sub-Caledonian basin formation can be seen, indicating fault activity in late Proterozoic time. The NW-striking magnetic dislocations approach the Norwegian coast where the Senja Fracture zone formed in the oceanic crust at about -58 Ma. Single magnetic markers along the NW-dislocations show displacements in both sinistral and dextral sense up to about 45 km.

Along the **north-trending** set of major zones, several large lithological discontinuities can be seen in the interpretation map, see Figure 2-1. The most important are the termination to the east of the 60 km wide schist belt SW of Rovaniemi, the bend in the Pajala-Kolari greenstone belt and the termination to the west of the Karasjokk greenstone belt N of Kautokeino. The location of these discontinuities are marked 1-3 in Figure 2-1. Magnetically, the N-trending set of major fault zones terminates at the Seiland Caledonian intrusive. These features have also been recognized by Berthelsen and Marker (1986), who have named this zone the Bothnian Megashear and interpreted it as a repeatedly active Proterozoic shear zone.

The N-trending lineaments south of Pajala are associated with a significant change in gravity anomaly caused by an escarpment (down to the east) of intermediate density crust. This is illustrated in a series of model calculations by Arkko (1986).

## 2.2 GEOPHYSICAL INVESTIGATIONS

### 2.2.1 Magnetics

Aeromagnetic measurements, originally made with 200 m line spacing and 30 m flight altitude, were transformed to a 200 x 200 m grid by selecting every 5th measurement along the flight lines. The dataset is shown in plate 1 in Henkel (1988). These data have been used to enhance and complete the study of magnetic dislocations performed in the first Lansjärv study, Henkel et al. (1983) and in the aeromagnetic interpretation map of the Nordkalott project, Henkel (1986). The following criteria were used to identify the magnetic dislocations reported here:

- linear or curved discordant magnetic minima caused by oxidation in fracture zones,
- displacements of magnetic reference structures including magnetic contacts, patterns and dykes,
- linear or curved magnetic gradients.

The method in earlier interpretations to stress the straight lineaments has been modified to include also curved linear segments. The Lansjärv area contains numerous magnetic lithologies and structures which allow a rather detailed magnetic mapping of faults and fractures. The magnetic dislocations were digitized and entered into the image analyzing system.

Ground magnetic profiles, about 1 km long, have been measured (together with electromagnetic methods) across 34 selected major fault zones with minimum complexity. These measurements were made with 20 m spaced readings to give the necessary spatial and functional resolution. Small scale structures cause considerable noise in some of these measurements. Both the ground and aeromagnetic measurements were used for dip calculations of major faults and fractures. These calculations are based on:

- knowledge of rock susceptibilities,
- modelling where the model anomaly is iteratively brought to coincide with the measured anomaly,
- restriction of the sense of dip using the slingram anomalies.

The network pattern of larger fault zones is very obvious, see plate 1 and 6 in Henkel (1988). The width of single fault zones is often several 100 m. The entire fault system can be followed for several hundreds of kilometer to the N and NW. An example of a set of ground geophysical profiles is shown in Figure 2-2. The complete documentation of all measured profiles is given in Arkko and Lind (1988).

### 2.2.2 Electromagnetics

VLF profiles with 20 m spacing, using either the GBR or the JXZ transmitter, were made on 25 selected locations along the major fault zones. VLF anomalies arise due to conductivity changes in the uppermost 200 m of the crust. The method is very sensitive but is disturbed by power lines and telephone lines (such locations were thus avoided). In most cases the magnetic and VLF indications coincide, however, the VLF method gives additional information on smaller non-oxidized faults than the magnetic method. It also discriminates zones of different conductivity within the fault zone.

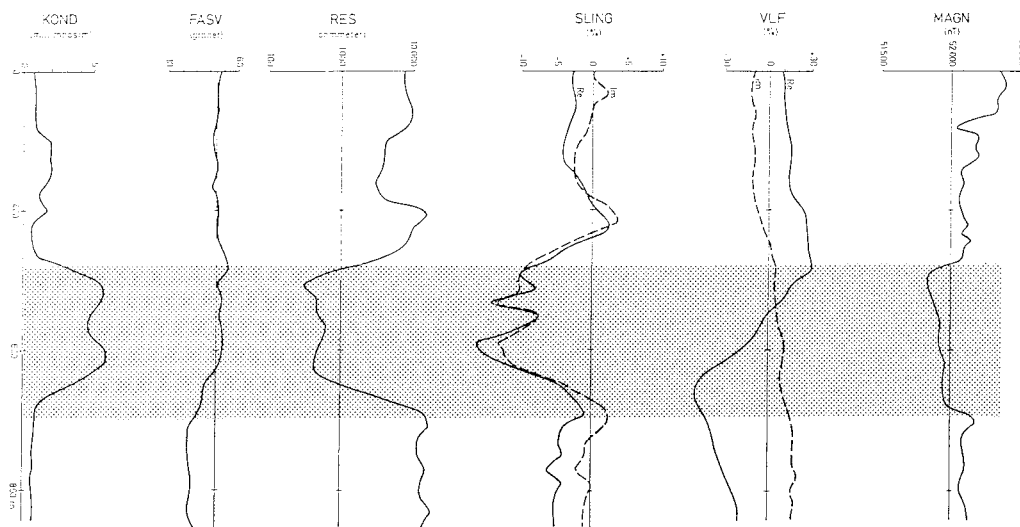


Figure 2-2. Example of combined ground geophysical profile across a NW striking fault zone segment (shaded). The measured properties are: magnetic total intensity (MAGN), VLF, Slingram (SLING), VLF-resistivity (RES and phase angle (FASV), electric conductivity (KOND).

Slingram measurements with 100 m coil spacing, using a 16 kHz signal, were made along the same profiles as the VLF and magnetic measurements. The slingram method gives information on the location width and sense of dip of conductors in the uppermost 100 m of the crust and the soil cover. These measurements were used to constrain the magnetic model calculations. The details of within zone conductivity shown by the VLF measurements are also reflected in the slingram measurements.

In-situ resistivity measurements with the VLF method and slingram with coil spacing of 4 m provide information about the soil conductivity (by the slingram method) and the conductivity of the nearest rock units (by a combination of these two measurements). Such measurements allow more detailed studies of the width of fault zones and the nature of the uppermost rocks within them by discriminating between weathered and normal crystalline rocks.

### 2.2.3 Gravity

Measurements were made with 1–3 km station spacing along roads. The dataset is presented in plate 2 in Henkel (1988). Elevations were obtained from contoured maps in the scale 1:20 000. Gravity anomalies are caused by density contrasts associated with structures and variation in the type of bedrock in the crust. Compared with magnetic and electromagnetic methods, only rather large structures will be visible. These include large displacements along fault zones, major unconformities and changes in crustal thickness. Gravity anomalies were used for calculations of the general dip of major fault zones down to about 7 km. In these calculations, the magnetic modelling results were used as constraint for the uppermost 1 km. Knowledge of rock densities is necessary for these calculations (made with the same modelling technique as for magnetics). Due to the ambiguity of the method, only limiting dips can be obtained (unless the upper surface of the buried structures can be determined independently). Combined interpretation of gravity magnetic and seismic velocity data can restrict the structural ambiguity.

#### 2.2.4 Elevation above Sea Level

In connection with studies of meteorite impact sites coloring of topographic maps has revealed the potential of tectonic information in elevation data. The relief technique demonstrated by Elvehage (1986) has further stressed the value of digital elevation information and digital image manipulation techniques. In the Lansjärv area, 100 m spaced elevation data were accessible to the project from the Swedish Geodetic Survey. These data have an elevation resolution of about 2 m. The dataset is presented in plate 3 and 4 in Henkel (1988). The tectonic information reflected in the morphology is affected by erosion and glaciation processes. Displacements of morphologic reference structures will indicate lateral movements of faults. Erosion cuts faster into the crystalline rocks where they are more fractured. Glacial processes will enhance or obliterate pre-glacial tectonic imprints depending mainly on the direction and intensity of ice flow. Post-glacial tectonics which distort glacial patterns can be recognized in the elevation data. A first glance at the elevation data gives an immediate understanding of their value for tectonic interpretations. Digital image analyzing techniques can further enhance specific trends in the data. Prominent features can be sorted out from faint or sharp features. The overall impression of obvious lens shaped topographic/tectonic units indicates the importance of longlived strike-slip fault movements. Also pull-apart basins and push-together ridges immediately show the effects of vertical displacements associated with strike-slip movements. If an age could be assigned to the morphology, it would also be possible to constrain the rate of fault movement.

#### 2.2.5 Seismic Refraction

The seismic refraction method (geophone spacing 5 m) has been used for the location of fracture zones, and determination and mapping of PGF faults down to the bedrock. Fault zones other than the PGFs were located by using ground VLF measurements. Refraction seismics also give information about the occurrence of weathered bedrock and should therefore be used more extensively for the mapping of this reference structure. Results of the seismic profiling are reported in Wällberg and Henkel (1987).

### 2.3 RESULTS

#### 2.3.1 Determination of Dip and Width of Large Fault Zones

Figure 2-3 shows an example of a dip modelling of a large fault zone by using magnetic measurements. Together with the dip, also the width of the zone is obtained. All model calculations are reported in Arkko (1988). Normally a distinct anomaly is obtained when magnetic rocks are intersected by an oxidized fault zone, Henkel and Guzmán (1977), or when fault movements have juxtaposed rocks with different magnetizations. In all these cases the shape of the anomaly is very sensitive to the dip of the most magnetic structure, which can be determined within 5 degrees. In ground magnetic profiles, small local structures can generate considerable noise and therefore a combination of aeromagnetic (lower noise level but less spatial resolution) and ground measurements (higher resolution of critical shape details) were used in the modelling. In the slingram measurements, an asymmetric anomaly indicates dipping sources which in many cases represents a definite constraint of the sense of dip. Also the VLF

anomalies tend to develop asymmetry over dipping conductors. In those cases where the magnetic anomaly is caused by one magnetic contact only, the ground VLF resistivity constrains the width of the fault zone. This width is obtained when upper layer conductivity known from slingram measurements with small coil separation is used for the determination of the bedrock resistivity.

The dips of N-S striking larger fault zones is mainly near vertical, the typical dip being 85 degrees to the east. The dips of the NW-SE striking larger fault zones have a bimodal distribution with typical dips being 65 degrees to the NE and 60 degrees to the SW respectively. The frequency of SW dips on major fault zone segments is higher.

Where large fault zones are also associated with distinct gravity gradients, a combined interpretation using magnetic and gravity modelling can give information about the deeper extension of the fault zone. The gravity anomaly arises typically when large lateral displacements juxtapose structures with different densities. Figure 2-3 gives an example of such a combined modelling. As no dense rocks are known at the surface, a buried denser body must be introduced in the model, which increases the ambiguity of the result. As constraint to the fault dip, the magnetic dip determination is used in the upper 1 km of the crust. Depending on the depth to the top of the dense body, the dip for the next few km can vary between 25 degrees and the surface dip of 70 degrees. The dip cannot be steeper than the surface dip nor dip to the other direction. More calculations can be made in the area but have not been attempted at this stage of the work.

Notice that the faulted edge of the higher density structure is obtained by strike-slip motion (and not by vertical faulting).

### 2.3.2 Tectonic Interpretation Map

The tectonic interpretation map, Figure 2-4, illustrates the interpretations of the aeromagnetic measurements, the terrain elevation and morphology, and the model calculations. A classification of smaller shear lenses and other morphologic features indicative of positive and negative block movements has also been attempted. Maximum resolution of all the datasets has been used in the digital image analyzing system EBBA II. In this system, the primary data are stored as image matrices 500 x 500 x 255 while interpretations are made and stored in up to 7 graphical matrices 500 x 500 x 1, each with its own color. The following steps were performed in 50 x 50 km areas:

- updating of previous aeromagnetic interpretations and digitization,
- updating of matrices using aeromagnetic anomalies and their relief,
- updating of matrices using terrain elevation relief,
- classification of shear lenses using updated lineaments and terrain elevation,
- addition of dip determinations, names and other symbols,
- plot of all graphical matrices to a map in the scale 1:250 000.

Three distinct systems of lineaments dominate the study area, **the steep NW-SE and N-S striking zones** and **the low angle dipping NNE-striking zones**. In addition, weak E-W and SW-NE striking morphologic lineaments occur. The steep systems contain a number of very prominent fault zones in a lens like pattern. These lenses are more elongated for the N-S system. Each swarm of steep lineaments make up an approximately 50 km wide fracture zone in which the dominant movement has been strike-slip. Significant accumulated displacements of different kinds of Precambrian reference structures can be seen in the aeromagnetic data. Morphologic features appear to be displaced. The N-S trending system of lineaments is associated with a major break in the gravity

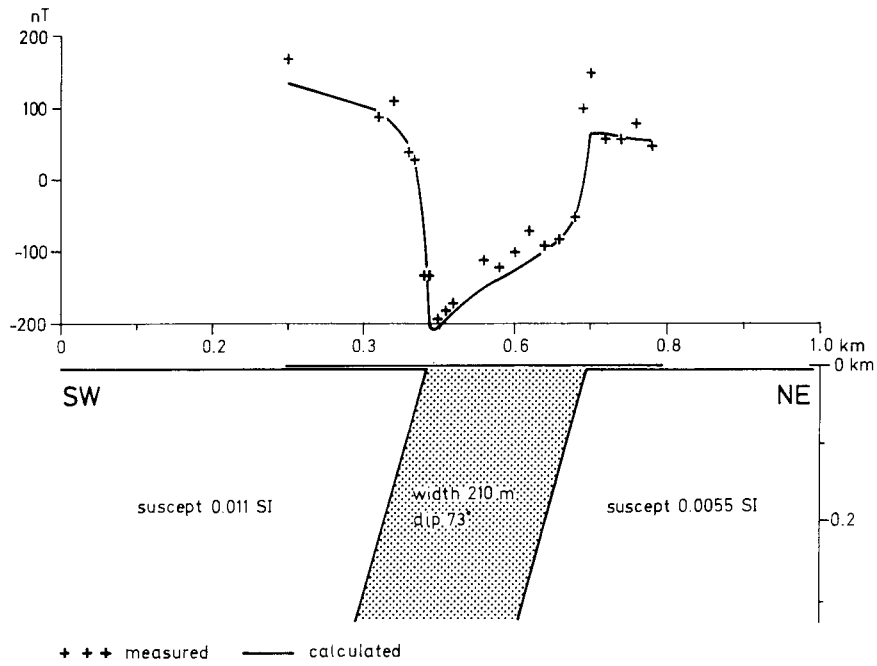


Figure 2-3A. Example of magnetic model calculation of a NW-striking fault zone segment (at profile 7).

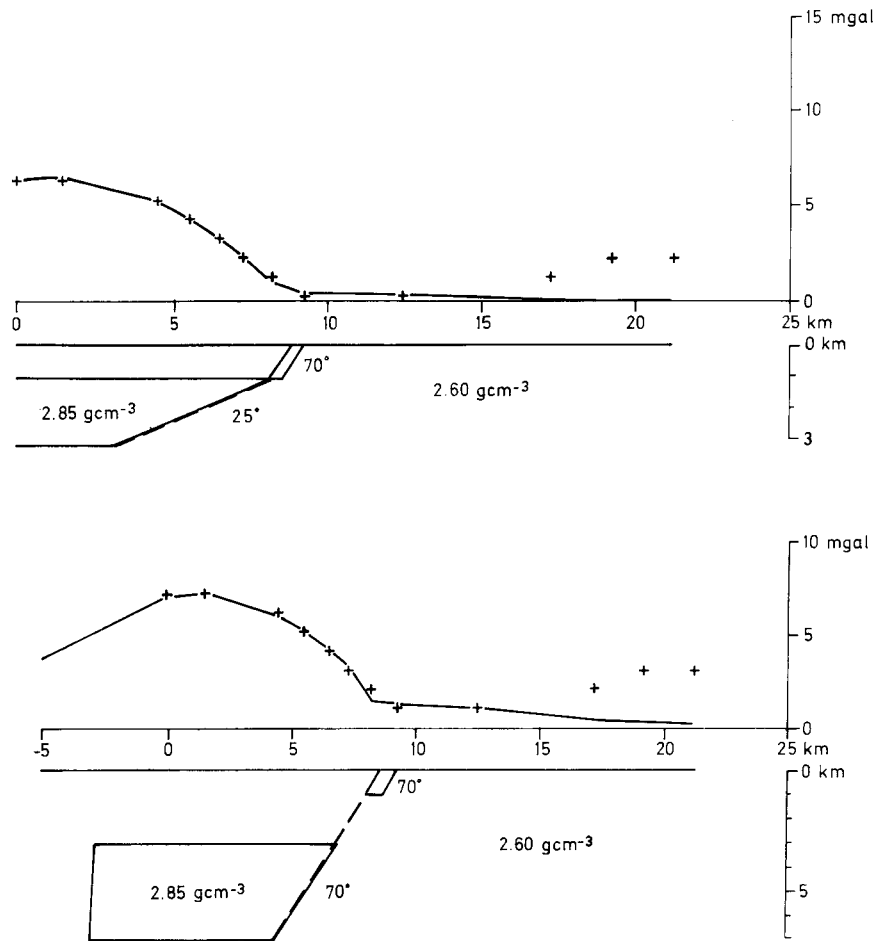


Figure 2-3B. Example of combined magnetic and gravity dip determination of a NW-striking fault zone segment (location in map area 26L 5a). The near surface magnetic model is used to constrain the surface location and dip of the zone.

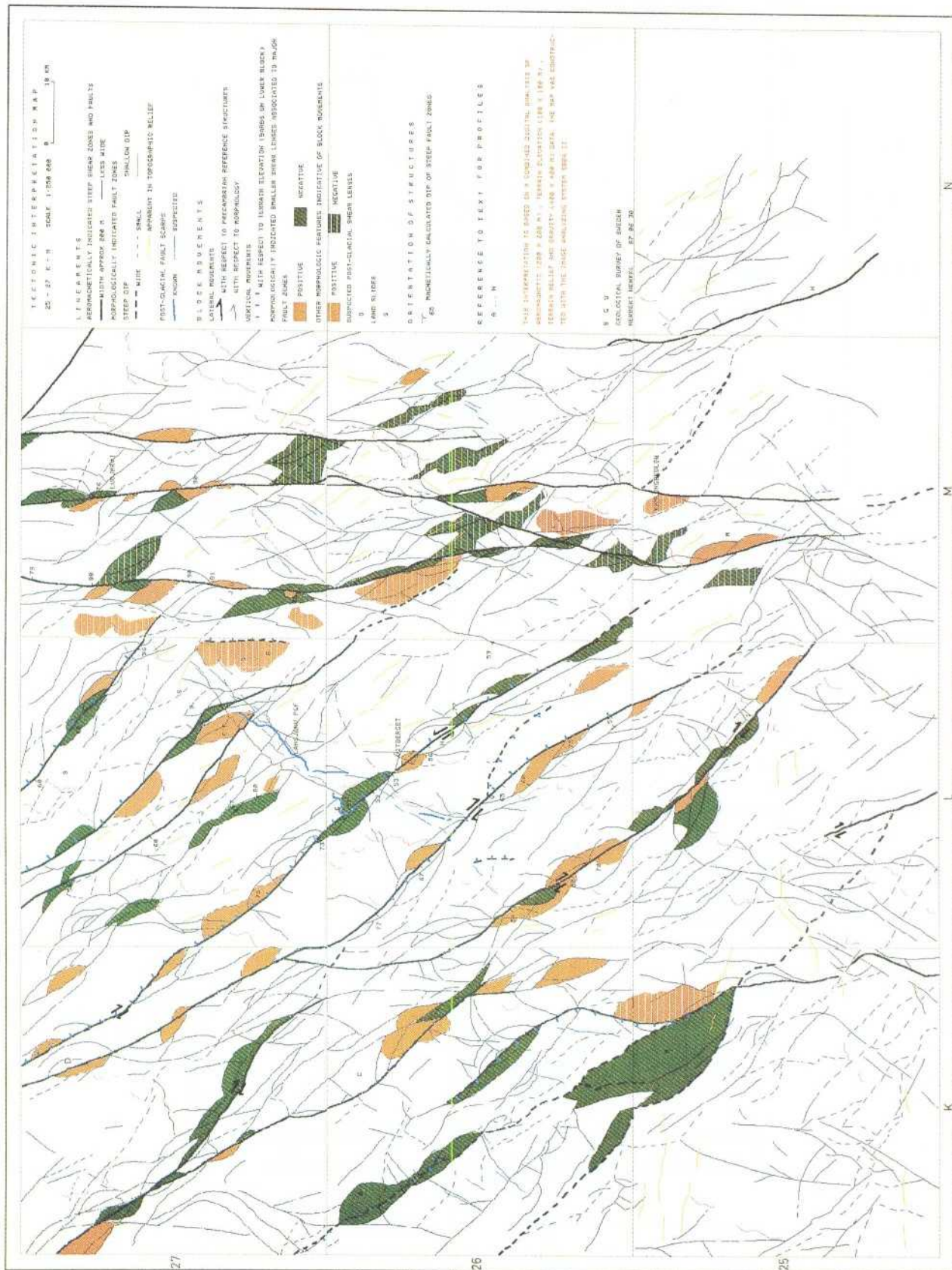


Figure 2-4. Tectonic interpretation map. After Henkel (1988).

anomalies. This indicates very different crustal structures on either sides and very large accumulated block movements. This zone has been named the Baltic-Bothnian Megashear by Berthelsen and Marker (1986), who suggested that it initiated at about -1.8 Ga. Figures 2-5 and 2-1 show the location and patterns of the three major fault zones. Together, these three fault zones define a three-dimensional regional pattern. It should be noticed that the shear lenses associated with major fault zone may have normal fault boundaries (around basins) and reverse or thrust fault boundaries (around horsts). The fault scarps along the major fault zone segments may locally face in opposite directions and look like normal faults.

A set of 14 profiles (A-N in the tectonic interpretation map) have been presented, in Henkel (1988). The maps demonstrate various aspects of the magnetic and morphologic structures associated with segments of different fault zones.

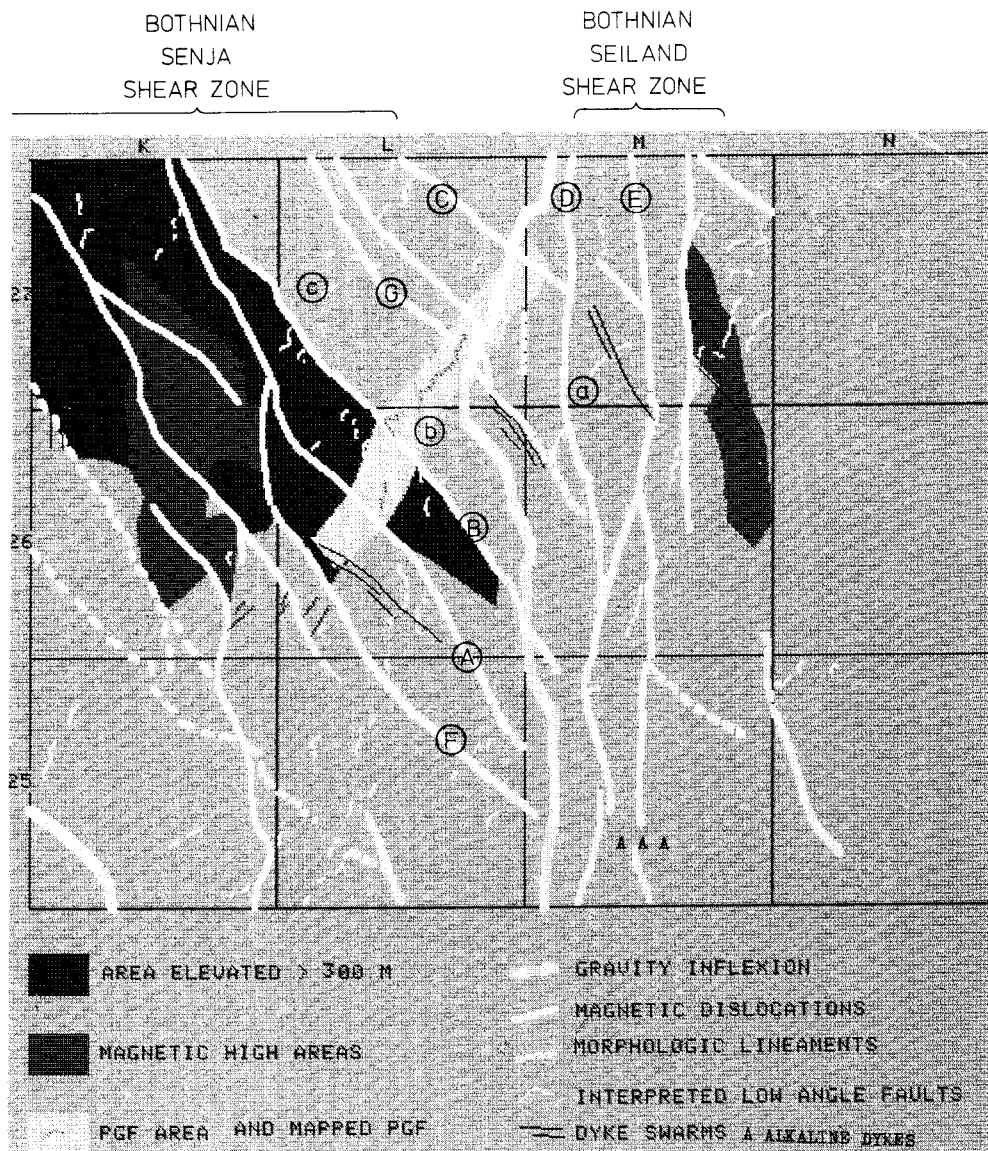


Figure 2-5. Compilation of regional lineaments. Each square is 50x50 km. Reference to map system at frame. Letters A-G and a-c denote some of the major fault zone segments treated in the text.



### 2.3.3 The NW-striking Steepdipping System of Lineaments

This approximately 75 km wide system of up to 5 prominent single faults can be followed NW from just north of the Bay of Bothnia to and beyond the Island of Senja off the Norwegian coast. In several locations very drastic changes in the magnetic patterns are observed indicating large displacements. Contours of the depth to the magnetic basement in the Aeromagnetic Interpretation Map of Northern Fennoscandia, Henkel (1986) show a change in the occurrence of late Proterozoic basins which are more frequent to the SW of the fault zone. It is not yet possible to determine the distribution in time of these displacements. In the Caledonides, however, less drastic but clearly visible effects along NW-lineaments are found in the region north of Torne Träsk (see map by Gustavsson 1974). The southwesternmost of the NW-trending lineaments is indicated by only a sharp morphologic feature – the Lule Älv valley. Displacements in magnetic reference structures are lacking, indicating that only rather small (less than 200 m) block movements can have occurred. Where the lineament bends in the map area 25 K, a large negative shear lens has developed. The distinct morphologic expression of the Lule älv lineament indicates a rather recent activation in a region with only small older block movements. This can be interpreted as a SW migration of fault zone activation associated with the Senja 1st order shear lens. The spacing to the Lule älv fault zone segment is similar as for the entire NW set of faults. The Lule älv fault zone coincides with the SW edge of the central relatively elevated block of higher (2 m) highest shore line levels. To the SW of this lineament, the fault pattern changes into an angular block type pattern with only minor block movements. Such angular patterns are typical for the regions between the large shear zones. Locally in the Precambrian terrains, rock foliations are turned into the strike of the NW-zones, see plate 5 in Henkel (1988). The general morphology is also strongly influenced along these zones, it therefore appears likely that the NW-striking fracture zones have been active since the Precambrian (and may be so at present). One of the larger lineaments acted as a local side wall to the Lansjärv PGF just W of the letter b in Figure 2-5. Other indications of very recent activity can probably be found, such as local fault scarps associated with shear lenses of different attitude. Small negative shear lenses (i.e. pull apart valleys) are most likely candidates as indicators of recent strike-slip movements. Sediments which are accumulated in these basins are probably a very good indicator of a faster rate subsidence and strain rate of the fault zone than elsewhere. The positive shear lenses (horst) are likely to be eroded immediately and thus represent only a minimum strain rate indication. A number of such features are indicated in the tectonic interpretation map and should be checked in the field. The general strike of the Lansjärv PGF is between 3 major NW-lineaments. The PGF, however, terminates within the shear lenses associated with these lineaments, indicating that such lenses act as strain traps and were deforming simultaneously. In Henkel and Wällberg (1987), an analysis of these features is made, based on detailed ground geophysical measurements.

The dip of NW-striking major fracture zones is on average 60 degrees to the SW. Edges of some associated shear lenses dip in the opposite direction, i.e. 60 degrees to the NE. These dip determinations are based on model calculations of ground or aeromagnetic profiles located at specific parts of the lineaments. The magnetic model calculations can not resolve the zones deeper than about 5 times their width (i.e. about 1 km depth), although the zones may continue to larger depths.

#### 2.3.4 The N-S Striking Steepdipping System of Lineaments

This approximately 45 km wide system of faults and lineaments can be followed from the Bay of Bothnia to the Seiland mafic intrusive province in northern Norway. In the study area, 3 to 4 distinct and prominent single zones are found. The magnetic patterns are entirely different on each side of the fault zone. On the entire length of the zone, three very prominent angular discontinuities are seen in the magnetic patterns (for location, see Figure 2-8).

- 1 – in the southern area of map 25–26 N, the distinct east-west banded pattern occurring east of the fault zone terminates and does not re-occur within the study area,
- 2 – in the central area at Pajala-Kolari (to the north of the study area), a possible large sinistral shift of magnetic patterns associated with an early Proterozoic greenstone belt can be seen,
- 3 – in the Masi-Kautokeino region in Norway, a strong angular discontinuity occurs between SW-striking early Proterozoic greenstone structures of the northeastern block and NNW-striking greenstones of the SW block.

As the main gravity inflexion lies to the west of the westernmost N-trending fault zone, a general W dip can be inferred in the upper 10 km of the crust for this fault system, despite the magnetically indicated steep E dip of the uppermost 1 km.

Over large areas, the strike of rock foliation turns into the north-south striking fault system (see geological map area 25M). The gravity anomalies reflect large scale density contrasts and changes in crustal composition and thickness. Low gravity in the eastern block changes to high gravity in the western block along a pronounced gradient close to the westernmost major magnetic lineament. Model calculations of these gradients indicate a major step down of about 5 km to the east in the crust of intermediate composition (Arkko 1986). In this respect the north-south striking system of faults represents larger accumulated displacements than the NW-system. It is yet not possible to determine the sense and amount of displacement along the N-S system but it appears to be very large sinistral. Magnetic model calculations show steep dips, on average about 90 degrees. The general appearance of single major zones is similar to the situation for the NW-system. Associated shear lenses are numerous and several show possible post-glacial deformation. An example is shown in Figure 2-9B. The shear lenses associated with the N-S system appear also to be more elongated than those in the NW-system of faults. Some of these shear lenses contain highly magnetic granites which may be of deep origin. Several disconnected NW-lineaments occur in between major N-S trending fault zones and some of these also show indications of recent movements. These lineaments strike more to the southeast, indicating a dextral rotation of the blocks between the single north-striking lineaments. An alternative explanation would be significant block movements which have juxtaposed blocks with different fabrics. The N-S lineaments continue southwards into the Bay of Bothnia. One of them defines a distinct step in the bottom morphology just south of the study area. It is associated with the occurrence of Jotnian and Cambrian sediments in the eastern block, Ahlberg (1986). At the northern shores of the Bay of Bothnia an alkaline dyke swarm intruded mainly in this fault zone at -1.1 Ga, Kresten et al. (1977).

### 2.3.5 The NNE-SSW Striking Near Horizontal System of Lineaments

These lineaments constitute sets of topographic scarps, most of which have steep WNW facing slopes rising from gently SE dipping flat areas. This pattern, which is best seen in relief maps, is interpreted as a glacial enhancement of the scarps of gently dipping fault zone segments. The slope of such gentle ESE-dipping zones is determined by the stratum contours of the fault scarp as it turns around the hills and it is generally low and is dipping only 1–5 degrees to the southeast. Geological field control by Talbot (1987) and VLF profiles show associated flat lying foliations and asymmetric anomalies typical for gently dipping conductors, respectively. Asymmetric magnetic lows are locally associated with these fault zones. The most obvious of the PGF movements appear to have occurred in zones parallel to these lineaments.

In Figure 2-5, all determined gently dipping lineaments so far are shown with thin white lines. In all five sets of such zones appear, each 5-10 km wide, at the surface (representing a width of approximately 300 m) and with 30–40 km spacing between zones in the horizontal (representing a vertical spacing of approximately 2.5 km). The gently dipping zones are interrupted by the NW- and N-striking fault systems indicating simultaneous movements of all 3 systems or younger movements of the steep faults.

Some other characteristic morphologic patterns seem to be associated with the gently dipping zones. Rather steep hillsides above several of the indicated zones rise above the surrounding, to form a WNW oriented wedge. More gentle dips are observed to the east. Within these wedges numerous gently dipping surfaces appear, so that the wedge resembles a pile of thrust flakes. It must be stressed that the NNE-system of lineaments is not verified with ground geophysical methods. Before a number of ground profiles with a combination of methods have been made, the character of these zones remains highly speculative.

Apart from the three major fault systems, no other dislocation directions seem to occur on the regional scale. In a few places, especially in the southwestern area, minor east striking lineaments can be observed in the morphology and the relief of the elevation data. These and other similar structures with small extent (and normally not visible in the aeromagnetic data) are indicated with a separate color in the map. Some represent rather sharp structures and may be of recent origin. Smaller features, clearly discordant to the glacial structures, may be of post-glacial origin and are indicated as suspected PGF:s.

### 2.3.6 Determination of Highest Shore Line (HS)

The map of the location of the highest (post-glacial) shore line is constructed from stereoscopic elevation maps on a large number of sites of different type. All determinations are reported in Sundh and Wahlroos (1987). These data were compiled to a separate map in the scale 1:250 000. The average accuracy of height is about 3 m.

The pattern of HS isolines shows a general curving trend around the Bay of Bothnia. The minimum elevation is around 160 m and the maximum elevation is around 220 m. Only a few meters local changes can be seen and it is uncertain if these reflect differential block movements. Therefore the regional trend of the highest shoreline has been constructed by smoothing the 10 m contours and by interpolating intermediate 1 m contours by eye. Next the differences between observed elevations and the regional trend were calculated. Numerous areas with deviations from 0 occur. The map area can be divided into three regions with different aspects of the HS deviations from the regional trend. This division

follows the westernmost N-trending fault zone and the southwesternmost NW-trending fault zone. The three regions are numbered I–III from SW to NE. Area II, which lies in the central part of the study area (where the regional trend is best defined), shows a positive residual distribution which is centered around +2.2 m (above the regional trend). Area III shows a negative distribution around -2 m (below the regional trend) and area I shows both a small negative and a positive residual distribution. The distributions around 0 deviation indicate the scatter in the observed HS values and in the regional fit.

The results can be interpreted as a slight rise of the central block of about 2 m with respect to surrounding areas and a slight subsidence of block III of about 2 m. The local distribution of residuals, together with the location of major fault zones, may indicate areas where measurable displacements of HS occur. More precise levellings of the indications would improve the resolution of this method in those particular areas. The expected displacements due to tectonic disturbances during the last 8000 years are rather small but the obtained results encourage further studies.

### 2.3.7 The Post-glacial Fault Scarps, PGF

The post-glacial fault scarps have previously been described in Lagerbäck and Witschard (1983) and Henkel et al. (1983). All geophysical measurements in an inner 40 x 20 km area around the faults are documented in Henkel and Wällberg (1988). The previous known faults consist of a northern, almost 15 km long scarp facing towards NW, with different scarp heights, an approximately 10 km long irregular scarp facing NW, having its sidewall in a prominent NW oriented fault zone segment, an appr. 5 km N-S oriented scarp facing east in the central area and a southern, about 5 km long scarp facing WNW, Figure 2-6. All branches except the Central N-S striking one appear to dip gently to the southeast or east. As there is normally rather small topographic relief, the dips can be estimated with stratum contours only at Mäjärverget, where it is about 12 degrees and at Storsaiviskölen, where it is about 10 degrees. The seismic refraction profiles of these low angle branches are shown in Figure 2-7 (left side from north to south). In these profiles, the topographic scarp is usually located above a bedrock surface inclined in the opposite direction. In some profiles, this surface rises again to the southeast or east. In profile 26 at the southern branch, the bedrock surface rises under the scarp. Contrary to these configurations, the bedrock surface rises under the elevated terrain in the N-S oriented fault scarp and in the sidewall of the Risträskkölen thrust flake. These faults therefore, have been interpreted as steeply dipping, Figure 2-7, right side. The post-glacial faults appear to interact with NW-trending major fault zone segments and with minor NW-trending faults. At the northern and southern terminations, the fault scarps disappear in the 3rd order shear lenses associated with large NW-trending fault zone segments.

Terrain relief studies in the area reveal several rather sharp minor steps in the terrain which can be interpreted as fault traces. The nature of these structures should be field checked. The entire set of PGF scarps is located within an approximately 5 km wide zone with several gently dipping faults interpreted from topographic maps and elevation data. This zone is about 60 km long and appears to be interrupted by transacting NW fault zone segments. The location of the PGF scarps within this NNE-trending zone indicates that most of the post-glacial fault movements may have occurred by reactivation of faults of the NNE-trending gently dipping fault zone.

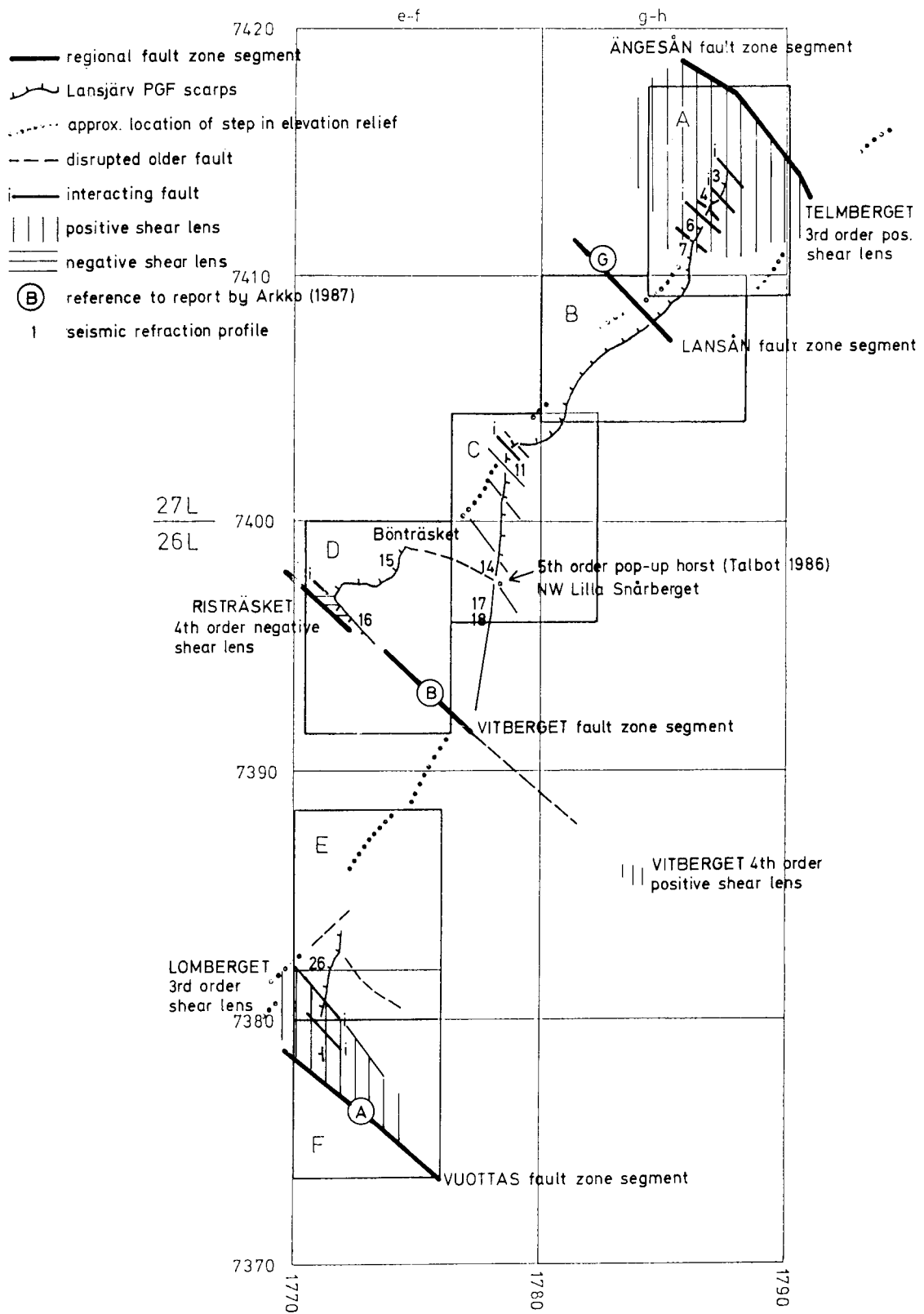


Figure 2-6. Index map of PGF-scarps. Scarps and location of refraction seismic profiles, regional fault zones and interpreted fault zone interference.

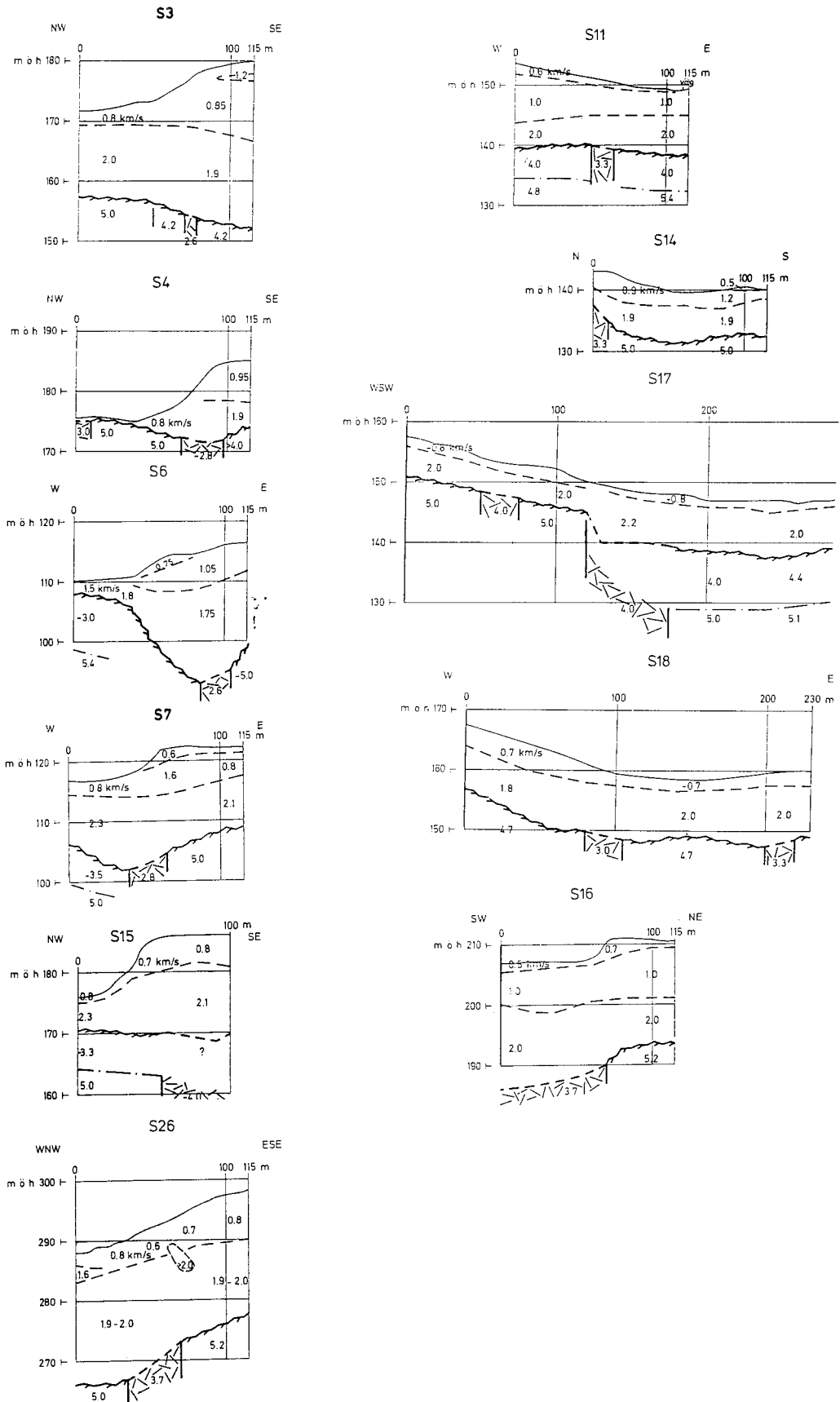


Figure 2-7. Seismic refraction profiles across PGF. Left, low angle (dip). Right, steep dipping PGF. Profile S16 is from the steep side wall of the Risträskkölen thrust flake. The ratio of vertical to horizontal scale is 4. Data from Henkel and Wällberg (1987).

## 2.4 DISCUSSION

### 2.4.1 Three-dimensional Network of Fault Zones

The structural pattern arising from the present knowledge is that of a three-dimensional network of shear zone of different magnitude, dipping to the SW in its top 1 km. The combined use of magnetic and gravity modelling and the location of seismic events in the upper crust may, however, give a clue to the deeper structure of this network. The following two hypotheses can be considered, Figure 2-8.

- a – the present erosion level is a random surface through a 3-dimensional network of shear zones with similar horizontal and vertical geometry,
- b – the observed 3-dimensional network is the result of the proximity to a free surface which can deform vertically. The network changes geometry deeper down in the lithosphere.

For case a, the deeper parts of the fracture zones would be similar to the horizontal sample we look at, down through the brittle part of the crust where it would change to a ductile set of structures continuing down through the lithosphere – this is illustrated in Figure 2-8. This hypothesis also requires a continuous variation in the dip of single fracture zones from SW to vertical NE-dip – the vertical dips being the most frequent (as the lenses are elongated in plane). This configuration is rather similar to that presented in Sibson (1977).

In case b, a structural anisotropy is caused by the steadily upward decreasing vertical load and the occurrence of a discontinuity at the surface. Shear lenses would only develop in the uppermost regions of the brittle crust. The larger shear zones would have a continuous dip down and through the ductile regime of the crust.

Case c is like case b, but the fault zone narrows in the ductile regime of the lithosphere due to strain concentration. This effect may, however, depend on the rate of displacements, being pronounced in periods of strong motions only. The strain concentration is obtained by thermal softening due to frictional heating, Brun and Cobbold (1980).

As shown previously, active strike-slip faults will induce considerable vertical displacements and changes in the morphology where they curve. When these displacements are faster than erosion, a topography will appear. A simple relation between fault displacement and shear lens subsidence shown in Henkel (1988), indicates that a lateral fault displacement of  $1 \text{ mm a}^{-1}$  will induce a subsidence of  $1 \text{ mm a}^{-1}$  in a basin which is twice as deep as it is wide and has a triangular cross section. In 10 000 years, up to 10 m subsidence will have occurred. This simple relation can be used as first approximation of strain rates when the dimensions and age of a subsidence basin are known.

Quaternary sediments and shore lines are strain indicators for the most recent fault movements. The post-glacial faults were first detected because of their conspicuous redistribution of the moraine layers. Other structures which also would be indicative of fault movements and which are observed on earth quake ruptures at the surface have not yet been looked for in a systematic way. Such structures are wrinkle ridges, tension cracks in addition to the mentioned shear lenses. Precise levelling and dating of shore lines would also reveal fault displacements. Precise levelling along roads would indicate the vertical component of any current movements.

Figure 2-9 shows structures interpreted as indications of rather recent displacements. Full lines represent segments of regional fault zone determined by aeromagnetic interpretation. Broken lines represent local faults interpreted from topography. The age of such structures are, however, unknown.

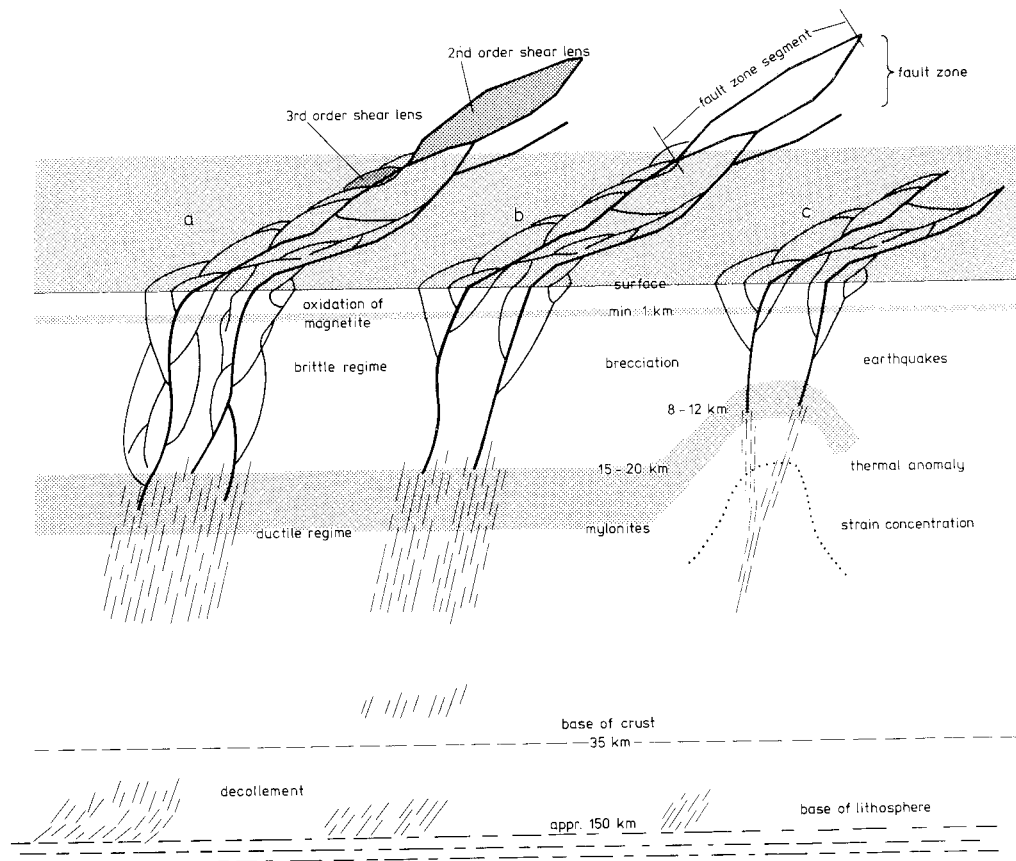


Figure 2-8. Model of deep continental faults. *a*, model with downward continuing network of shear zones is similar to the model of Sibson (1977). *b*, model where the fine structure of the network increases towards the free surface. *c*, a model similar to model *b* but with higher strain rates leading to thermal softening at depth (and rise of the brittle-ductile transition), see Brun and Cobbold (1980).

#### 2.4.2 Summary

The Nordkalott project produced the first detailed analysis of fault zones in a large region of the Fennoscandian shield. The results were used to define a critical area for possible recent crustal deformations. Several distinct systems of faults set a regional framework to the study area around Lansjärv. Close structural connections with the recent (less than 60 Ma) plate tectonic situation are apparent as one major fault system is the strike continuation of the Senja Fracture Zone in the Atlantic ocean. Along this zone the active spreading ridge of the North Atlantic steps sinistrally to the active spreading ridge in the Arctic ocean. Plate spreading at different rates in segments of the rift system could induce stresses in the continental crust. This deformation is interpreted to occur mainly connected to one or several lithospheric lenses surrounded by systems of pronounced fault zones. The Senja lens has a slightly higher elevation than its surroundings. Suggesting an ongoing transpressional slip. In the Lansjärv area, the NW and N fault zones appear as very sharp, about 200 m wide, magnetic low lineaments with associated large lateral displacements of magnetic reference structures. Many drastic changes in the bedrock lithology occur along these lineaments. Single fault zones in each system represent, on average, 200 m wide, movement zones, interconnected in an elongate lens like pattern.

For the first time, dips of fault zones have been calculated using ground and airborne magnetic and electromagnetic data. The dips of these zones are steep



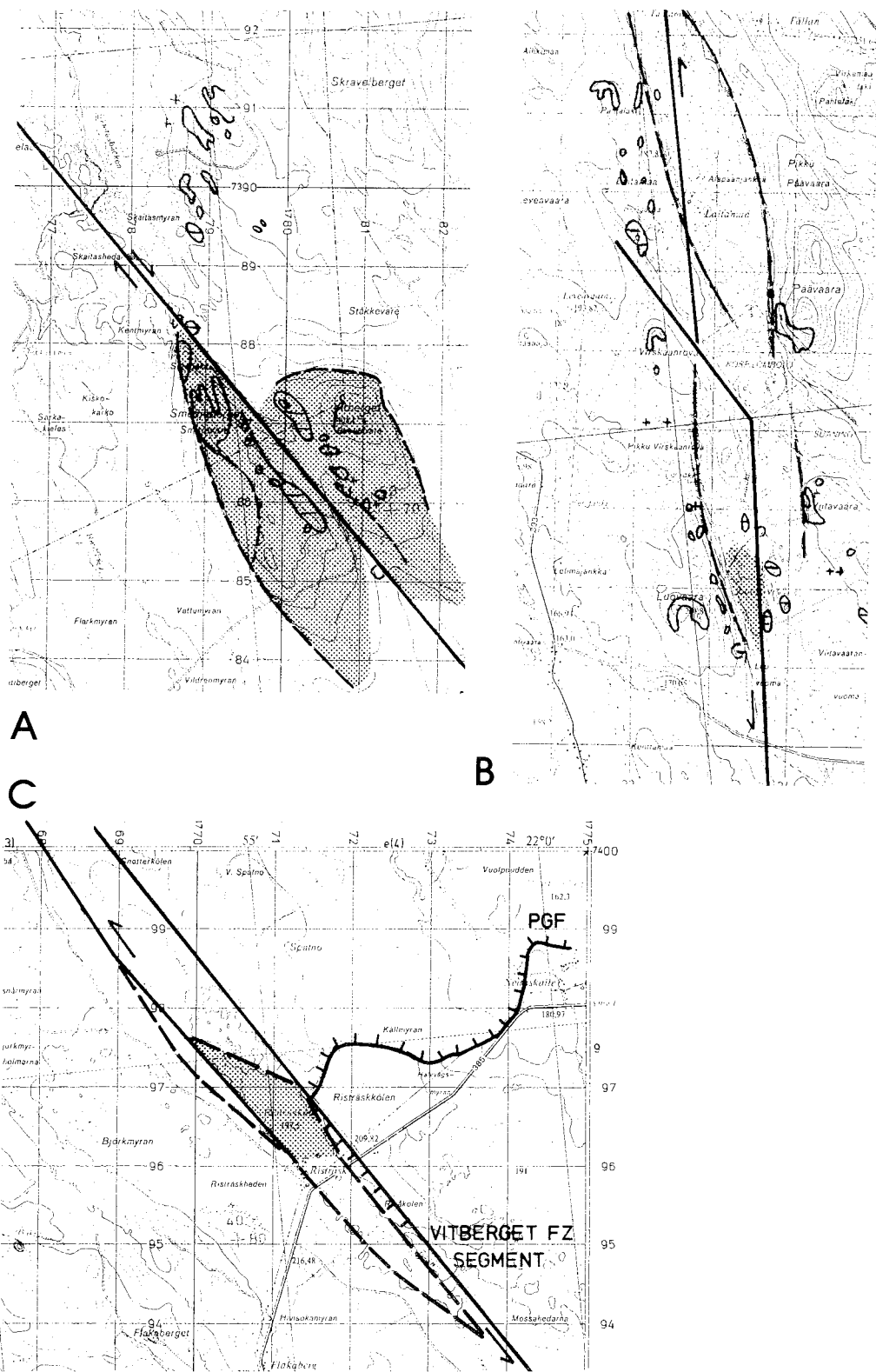


Figure 2-9. Examples of small (4th order), morphologically indicated shear lenses (shaded), located close to major fault zone segments (black full lines).

A. The Vitberget displaced positive shear. Map area 26L 7g.

B. The Luojärvi negative shear lens. Map area 27M 7e.

C. The Risträsket negative shear lens and the Risträskkölen PGF thrust flake (barbs towards lower block). Map area 26L 4e.

Grid size 1 x 1 km.

at the surface but may flatten at depth. Close to each movement zone, series of shear lenses, several km wide, can be seen cutting off arcuate segments of the surroundings.

The width of these shear lens patterns grades into the size of the network. Minor gravity lows along the strike direction of several fault zone segments, see plate 2 in Henkel (1988), can represent the effect of an increased occurrence of small shear lenses.

At outcrops close to the major fault zones, a variety of strain indicators indicating ductile to brittle deformation show that these faults have been active at very different crustal depth regimes over a very long period of time. The most recent (post-glacial) faults were detected and described by Lagerbäck (1979), Olesen (1988) and Kujansuu (1972). Today, several 100 km of PGF fault scarps are known in northern Scandinavia. Most PGF fault have NNE-strike directions and show scarps of steep to gentle SE dipping faults. They typically occur between the NW-striking major fault zones and seem to be closely related to a set of low angle thrusts. These close spatial and structural relations to the NW-zones suggest simultaneous activity along linked faults, Henkel et al. (1983). The same can be suspected for the north striking faults. A few indications of PGF scarps along single faults of both the N and NW steep as well as the gently dipping NNE regional fault systems improve this hypothesis. These features need a more detailed study in order to ensure their post-glacial nature. In Henkel and Wällberg (1987), a detailed study of the relations between sections of the PGF and local and regional faults is made. The distinct imprint of fault zones and fault movements on the morphology of the study area indicates strong activity along the three regional fault systems. One very important effect is the formation of topographically positive and negative shear lenses where steps or bends in the regional fault zones create structures which can release compressional or tensional stresses. The PGF scarps usually stop along the border to such lenses, indicating that they deformed simultaneously with the post-glacial fault movement.

All stages of shear lens development can be observed ranging from small (0.2 x 2 km) recent and sharply developed basins and horsts to very elongated narrow, graben like structures and displaced or sliced horsts. A rough estimation of the response of the free surface to a continuous strike-slip movement of 1 mm per year results in an adjustment of the horizontal surface of about 2 m in a period of 8000 years. Such figures appear to be in the correct order of magnitude judging from the depths of the smallest shear basins.

Two other features deserve attention. 1) Several, on average 15x5 km, north-south oriented areas with pronounced elevation appear not to be positive shear lenses (as they are not surrounded by major fault zones). 2) A series of northwest-southeast oriented topographic lows between major N-S lineaments are unlikely to be negative shear lenses. These features are tentatively interpreted as compressional and tensional features respectively. Profile A and J in report by Henkel (1987) show examples of these types of structures.

### 2.4.3 Tectonic Patterns

The following conclusions can summarize the tectonic patterns; see also Figure 2-7.

- The Lansjärv region is situated at the southern extremity of a 600 x 200 km. large tectonic lens (the Senja Lens).
- The southern end of the Senja Lens is limited by two sets of regional fault systems striking NW and N and has about 50 m elevation above the surroundings.

- The lens may represent a compressional structure.
- The single larger faults of each set are connected in a network of smaller lenses showing locally both compressional and tensional features.
- Major single faults of the N and NW system are about 200 m wide and have general steep dips.
- NW-zones dip in average 60 degrees to the SW- and N-zones dip generally steeply (70°) to the W.
- NNE gently dipping zones (less than 5 degrees) are a few hundreds metres wide; the width of single faults is not known,
- Each zone of steep fault zone is surrounded by a series of several kilometer wide of minor shear lenses.
- The outer faults bounding the shear lenses are less likely to be as steep as the main fault.
- The interior of lenses between major fault zones are less faulted than the main zones,
- Negative shear lenses are likely to be more brecciated than positive (Sibson 1986).
- The criteria so far cited define a pattern typical for a strike-slip fault zone of lithospheric dimensions.
- The post-glacial fault scarps may represent movements of flat lying fault system and the interaction with the free surface,
- Several other morphologic features can be interpreted as effects of post-glacial strike-slip movements (i.e. small scarps, horsts, basins etc.).

The Lule älv NW fault (zone) and a NW zone in the map area 25M have no (or very minor) magnetic dislocations.

#### 2.4.4 Methods

- Aeromagnetic measurements provide the best indicator of large fault zones (width 50 m, length 5 km) with steep dips.
- Elevation data have been most effective in locating scarps of gently dipping zones.
- A sufficiently large study area is necessary in order to understand local features of faulting.
- Detailed ground geophysical measurements with VLF and slingram are necessary for the detection of small scale faults and associated structures.
- Ground radar measurements are recommended for precise location of buried steps in bedrock.
- In combination with aeromagnetic measurements, terrain elevation data give an enhanced interpretation of fault mechanisms.

#### Improvement of Methods

Reflection seismic methods in connection with slingram should be developed for detection of fault geometries and especially flat lying faults.

#### 2.4.5 New Fracturing

So far, no evidence of post-glacial fracturing in the bedrock has been observed. This does not exclude their existence. In southern Sweden a few cases of strong, apparently recent fracturing of surface rocks have been noticed and are documented in Agrell (1984). The relation of these cases with tectonic patterns is,

however, unknown. The occurrence of distinct post-glacial scarps and the displacements of Quaternary deposits in the Lansjärv area indicate considerable block movements in the order up to tens of meters in the last 8000 years. The well developed fault systems of the area can accommodate most of the strain (especially at low strain rates) without fracturing, except in extreme situations. Some rock volumes are, however, in a position where new fracturing is likely to occur, e.g.:

- the wedge between the free surface and a activated gently dipping fault zone,
- the block between the faults in a tensional step over (shear basin),
- the hanging wall block adjacent to a tensional bend in a main fault zone. The drilling at the northern Lansjärv PGF segment is located in a wedge overlying the extrapolated location of the PGF surface. The other situations could also be tested by drilling in suitable structures.

## 2.5 REFERENCES

**Agrell H 1984:**

Dokumentationsrapport över urbergsgrottan Gillberga gryt, Trollegatar m fl strukturer.

Sveriges Geologiska Undersökning

**Ahlberg P 1986:**

Berggrunden på kontinentsockeln.

Sveriges Geologiska Undersökning, Rapporter och meddelanden nr 47

**Arkko V 1986:**

The Nordkalott project – model calculations of magnetic and gravimetric data. SGU BRAP 86409

**Arkko V, and Lind J 1988:**

SKB projekt bergets stabilitet. Tektoniska studier i Lansjärv. Lägesrapport över kompletterande markgeofysikmätningar.

SKB AR 88-03

**Arkko V 1988:**

SKB projekt bergets stabilitet. Tektoniska studier i Lansjärv. Report of the magnetic dip determinations. SKB AR 88-04

**Berthelsen A, and Marker M 1986:**

1.9–1.8 Ga old strike-slip megashears in the Baltic shield and their plate tectonic implications.

Tectonophysics 128 pp 163–181

**Brun J P, and Cobbold P R 1980:**

Strain heating and thermal softening in continental shear zones: A review.

Journal of Structural Geology, Vol 2 Pt 1–2, pp 149–158

**Elvehage Chr, and Andersson P 1986:**

The use of elevation data bases in computer assisted cartography. National Land Survey of Sweden. Professional Papers. Report 1986,17

**Gustavsson M 1974:**

Berggrundskart Narvik 1:250 000.  
Norges Geologiske Undersökelse

**Hanks C Th 1979:**

Seismic width of active crustal fault zones.  
In: Proceedings of Conference VIII Analysis of fault zones in bedrock.  
US Geological Survey Open File Report 79-1239

**Harland W B 1979:**

A review of major fault zones in Svalbard. In Proceedings of Conference VIII.  
Analysis of actual fault zones in bedrock.  
US Geological Survey. Open file Report 79-1239

**Henkel H 1986:**

Aeromagnetic Interpretation Map of Northern Fennoscandia. Geological Surveys of Finland, Norway, and Sweden.  
ISBN 91-7158-376-9

**Henkel H, and Guzmán M 1977:**

Magnetic features of fracture zones.  
Geoexploration 15

**Henkel H, Hult K, Eriksson L, and Johansson L 1983:**

Neotectonics in northern Sweden – Geophysical investigations.  
SKBF/KBS TR 83-57

**Henkel H 1988:**

SKB projekt bergets stabilitet. Tektoniska studier vid Lansjärv. Dokumentation av profiler över olika exempel på tektoniskt-morfologiska strukturer i undersökn.området 25-27 K – N.  
SKB AR 88-07

**Henkel H 1988:**

Tectonic studies in the Lansjärv region.  
SKB TR 88-07

**Henkel H, and Wållberg B 1988:**

The post-glacial faults at Lansjärv.  
Ground geophysical measurements and interpretations in a 40 x 20 km surrounding area.  
SKB AR 88-05

**Kresten P, and Printzlau I et al., 1977:**

New ages of carbonatitic and alkaline ultramafic rocks from Sweden and Finland.  
GFF 99 pp 62–65

**Kujansuu R 1972:**

On landslides in Finnish Lapland.  
Geol. Survey Finland Bull. 256, pp 1–22

**Lagerbäck R 1979:**

Neotectonic structures in northern Sweden.  
GFF 100 pp 263–269

**Lagerbäck R, and Witschard F 1983:**

Neotectonics in northern Sweden-Geological investigations.  
SKBF/KBS TR 83–58

**Olesen O 1988:**

The Stuoraguna fault, evidence of neotectonics in the Precambrian of Finnmark, northern Norway – Norsk Geologisk Tidsskrift. 68, pp 107-118.

**Schack Pedersen S A, and Håkansson E 1987:**

Structural styles of the Wandel Hav strike-slip mobile belt.  
In: Abstracts of the 18th Nordic Geological Meeting – Geological Survey of Denmark.  
ISBN 87-88640-07-08

**Sibson R H 1977:**

Fault rocks and fault mechanisms.  
Journ Geol Soc London 133 pp 191–213

**Sibson R H 1986:**

Brecciation process in fault zones: Interference from earthquake rupturing.  
PAGEOPH 124 Pt 1–2 pp 159–176

**SKB 1986:**

Kärnkraftavfallets behandling och slutförvaring, del III.  
Forskningsprogram 1987–1992

**Sundh M, and Wahlroos J E 1988:**

SKB projekt bergets stabilitet – Tektoniska studier i Lansjärv. Dokumentation av hålltolkning och fotogrammetriska avvägningar av högsta kustlinjen.  
SKB AR 88-06

**Talbot C 1986:**

A preliminary structural analysis of pattern of post-glacial faults in northern Sweden.  
SKB TR 86-20

**Wannäs K 1989:**

Seismic stratigraphy and tectonic development of the Upper Proterozoic and Lower Paleozoic of the Bothnian Bay, Baltic Sea.  
Acta Universitatis Stockholmiensis.  
Stockholm Contributions in Geology. 40(3), 168 pp.



# 3 POSTGLACIAL FAULTING AND PALEO-SEISMICITY IN THE LANSJÄRV REGION

*Robert Lagerbäck*

Geological Survey of Sweden  
Box 670, S-751 28 Uppsala, Sweden

## 3.1 AIM OF INVESTIGATIONS

The present study involved excavations across till-covered fault scarps and brief investigations of paleoseismic structures in the unconsolidated Quaternary overburden.

The aim of the study was;

- To attempt to elucidate when the different major fault scarps developed in relation to the melt-away of the most recent ice-sheet and the postglacial land-upheaval.
- To attempt to determine whether the morphologically identifiable fault scarps developed as a rapid single event, step by step, or by creep over a long period.
- To investigate the geographical extent and characteristics of secondary, fault-induced seismic distortions in different types of glacial and postglacial sediments.

Compared with the original plans, and in agreement with the commissioner, the problems concerning timing of fault movements were stressed at the expense of the paleoseismic aspects. The field work was carried out between Sept. 26 and Nov. 4, 1987. The results of the investigations are summarized in SKB Technical Report 88-25 (Lagerbäck 1988b). The present contribution is a condensed version of that report.

## 3.2 THE LANSJÄRV AREA

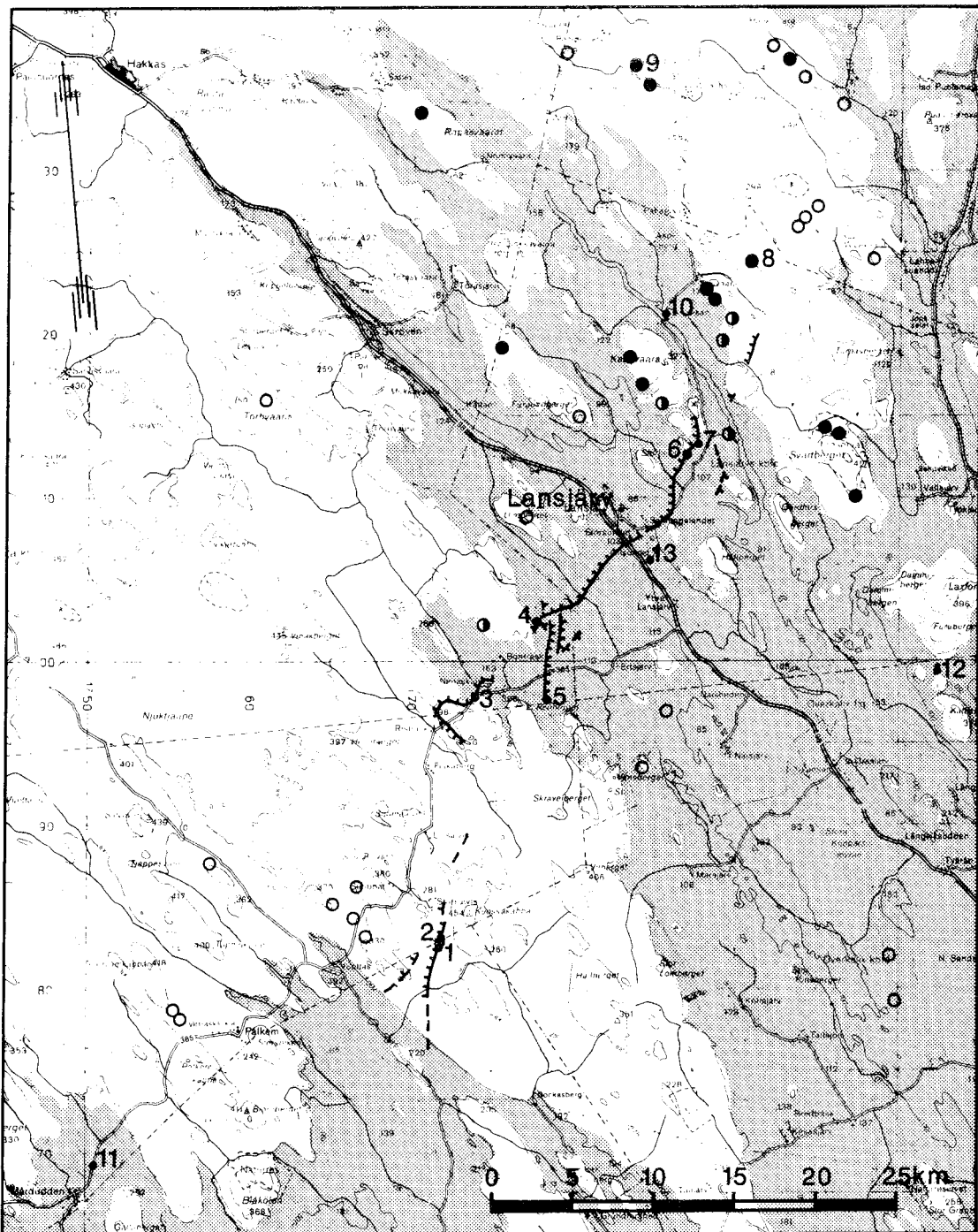
### 3.2.1 Topography, Highest Coastline, Bedrock, Quaternary Deposits

The Lansjärv area is situated in the forested part of northernmost Sweden and is crossed by the Arctic Circle. Topographically it is a weakly undulating terrain with scattered hills. The area is situated between about 50 and 470 m above sea level and the terrain generally rises from the east towards the west.

The southern, eastern and central parts of the area are largely located below the Holocene, highest coastline (Figure 3-1), which varies between about 205 m in the south-eastern part and 175 m in the north-west. The Late-Quaternary fault set is largely situated at, or below, the highest postglacial coastline, a fact which theoretically offers a good opportunity for dating the fault movements in relation to early postglacial land-upheaval.

The bedrock (see Nordkalott Project 1987) is dominated by granites of which the late orogenic Svekokarelian Lina Granite (c. 1800-1750 Ma) is the most common. The Lina Granite varies in texture/structure from aplitic to pegmatitic and it is generally reddish or pinkish in colour. Sometimes an older, characteristically well foliated, granite is met with. This granite occurs as large xenoliths floating in the "sea" of Lina Granitoids. Also greyish, granodioritic to dioritic, early orogenic granitoids, belonging to the Haparanda suite (c. 1900–1860 Ma) are frequently found as xenoliths or as more continuous areas. Further, various











-  Fault scarp, barbs turned towards the lower block
-  Landslide
-  Landslide, somewhat uncertain
-  Landslide, uncertain
-  Area below the highest coastline
-  Site mentioned in the text

Figure 3-1. Post-glacial fault scarps, landslides, areas below the highest coastline and investigated sites in the Lansjärv area. Sites: 1. Mainekjaura 2. Storsaiviskölen 3. Neitaskaite 4. Molberget 5. Stupforsen 6. Mäjärnberget 7. L. Telmträsket 8. Elmaberget 9. Repovaara 10. Angeså 11. Slättheden 12. L. Furuberget.

gneissose and migmatitic rocks, probably representing various metasupracrustal rocks, occur in the area.

Exposed bedrock constitutes only a few per cent of the area and generally the outcrops are extensively frost-shattered. This shattering dates from an Early Weichselian interstadial characterized by strong periglacial conditions and is indicative of an extremely sluggish Middle and Late Weichselian ice-sheet (Lagerbäck 1988a). Talbot (1986) suggested that this widespread shattering had a seismic origin and was related to the postglacial fault movements in the Lansjärv area (Talbot's so-called "Jericho syndrome").

Glacial till is the predominant Quaternary deposit. The tills in general have a sandy composition and often constitute morphologically prominent features such as hummocky moraines and drumlins. The drumlinoid features mainly belong to a north-westerly directed ice-flow system deriving from the first Weichselian glaciation (Lagerbäck & Robertsson 1988). Features belonging to this system are spread over the entire area and they are generally very well preserved despite being exposed to younger glaciations.

The Quaternary stratigraphy is complex. Two or more till beds, often intercalated with water-laid sediments, appear to be the rule rather than the exception down to 4–6 m below ground surface. The typical sequence is one (or occasionally two) brown or greyish brown, fairly thin till bed(s), often no more than 0.5 m thick, resting on a thick, grey till. The complex stratigraphy in the Lansjärv area offers excellent reference structures for dating of fault movement relative to the Late Quaternary glacial and non-glacial stages.

### 3.2.2 Fault Scarps, Paleoseismic Records

The Late Quaternary fault complex is composed of four major and several minor fault scarps (Figure 3-1), together forming a 50 km long fault set with a SSW-NNE orientation. The longest continuous fault-scarp segment is 17 km. The identified fault scarps generally range in height from between 5 to 10 m, with slightly more than 20 m as a single exception. Most of the scarps downthrow to the west but some segments in the central and northern parts of the fault set show an eastward downthrow. The bedrock along the fault scarps are almost entirely covered by Quaternary deposits, mainly glacial till, and repose angles generally vary between 20 to 30 degrees.

The different fault segments generally have a straight or gently winding course. At some places the scarps appear to bend as a response to differences in topographic level, indicating a shallow easterly dip (c.f. Talbot 1986). However, at other places the tendency is the opposite or there appears to be no response at all to changes in elevation and some segments obviously bend independently of topography (Figure 3-2). Highly varying dips and a strong influence of local bedrock properties on the configuration of the fault surfaces appear likely if judging from the course of the scarps.

The bedrock along the scarps is generally covered by Quaternary deposits. Exposed bedrock in direct connection to the scarps is observed only at two localities. At one of these localities, situated at the edge of the strongly angled scarp in the central part of the fault set (Figure 3-2), the bedrock is strongly fractured and shattered and it is difficult to define which fault surface was active during the Late Quaternary movement. The repose angle (about 30°) of the till covering the bedrock, the configuration of the outcrops and the relation between the outcropping bedrock, shatter debris and overburden indicate a moderately steep, reverse fault. Large quantities of ground water leaking from the scarp suggest an extensive system of open fractures in the fault zone and adjacent parts of the bedrock.

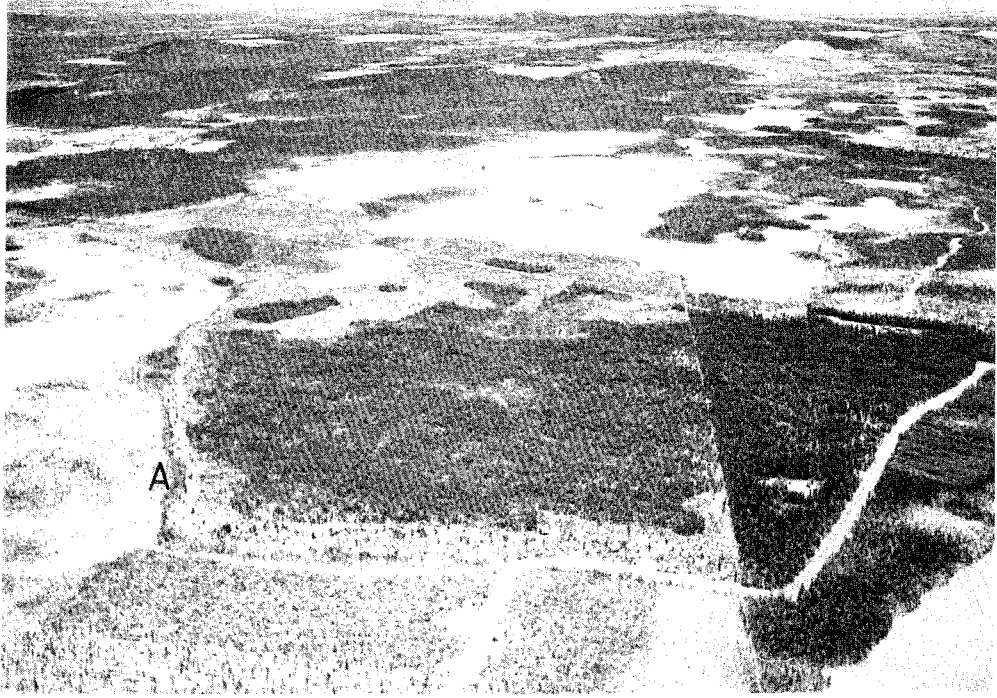


*Figure 3-2. The strongly angled postglacial fault scarp at the Risträskkölen plateau. The scarp in the foreground is about 20 m high. Bedrock outcrops occur at A. Photograph looking east. Photo: R. Lagerbäck 1976. Approved for publication.*



*Figure 3-3. Exposed bedrock at the fault scarp east of Karhuvaara 13 km NE of Lansjärv. The height of the scarp visible on the photograph is about 10 m. Photo: R. Lagerbäck 1987.*

Exposed bedrock in the fault scarp occur also at the northernmost fault scarp segment (Figure 3-3). Here, bedrock outcrops occur along a several hundred meter long section. The bedrock in the hanging wall forms vertical or steeply overhanging cliffs, also perpendicular to the main fault scarp, indicating steeply dipping fault planes and block movements.

There are strong indications that the Late-Quaternary faulting was associated with intense seismic activity. In Sweden (Lagerbäck & Witschard 1983; Lagerbäck 1989, in manuscript) as well as in Finland (Kujansuu 1972) a large number of landslides have occurred in the same region as the fault scarps. In the Lansjärv area there are some ten well identified landslide scars representing major slides ( $> c. 100\ 000\ m^3$ ) and in addition to these there are some thirty somewhat uncertain scars (Figure 3-1). The landslide scars, in Sweden as well as in Finland, are all stabilized and vegetated. Several slides are radiocarbon dated to be older than 8000 years and some demonstrably moved in direct connection with the local deglaciation, that is, from the period when the faulting occurred.

Distortions of the internal structures of different types of Quaternary deposits is another phenomenon interpreted to be related to the faulting. The distortions occur mainly in layered sandy and silty sediments but have also been found in glacial till (Lagerbäck 1989, in manuscript). The distortions include different types of convolution, corrugation, flamelike structures and sizesorting of clasts. These phenomena are interpreted to be due to seismically induced liquefaction and tremor in connection with the faulting.

### 3.3 FIELD INVESTIGATIONS

#### 3.3.1 Trenching Across Fault Scarps

In connection with this project, excavations across the fault scarps were made at five localities not investigated previously (sites 1, 2, 3, 4 and 6 in Figure 3-1). Two previously investigated sites (5 and 7 in Figure 3-1), of which one was now reinvestigated (5), are included in the study. Three of these sites (4, 5 and 6 in Figure 3-1) are described in what follows. For an account of the other sites, see Lagerbäck (1988b).

The excavations were made as trenches at right angles to, and crossing, the fault scarps. The excavators theoretically reached depths of 5.5 and 6.5 m. However, in practice it was often not possible to dig very deep into the ground as soils were wet and unstable due to rainy weather during the summer and great quantities of water leaking from the fault zones.

The profiles and sections along the trenches were levelled and recorded by sketches and photographs. The sections shown in Figures 3-4, 3-8 and 3-11 are simplified and stylized versions of the sketches made in the field. A schematic illustration of the interpreted course of events in connection with faulting and subsequent repose is given at each section. (Note that these sketches are not to be viewed literally!). A restricted number of samples of the bedrock and overburden were collected for later examination and analysis.

**MOLBERGET** (Figures 3-1 and 3-4). This site is situated just below the highest coastline and the till on the raised block is largely affected by wave-erosion. Even though the visible fault scarp was not more than 1–2 m high, a 4 m high and vertical bedrock scarp was met with only two metres beneath the ground (Figures 3-5 and 3-6). The bedrock, composed of pegmatites and granodioritic granitoids, was excessively fractured and weathered in a wide zone on both sides of the scarp (Figure 3-7). Two samples of the weathered bedrock were analysed with respect to clay minerals. A sample of the red, clayey saprolite in the very fault zone was dominated by vermiculite and expandable mixed-layer minerals.

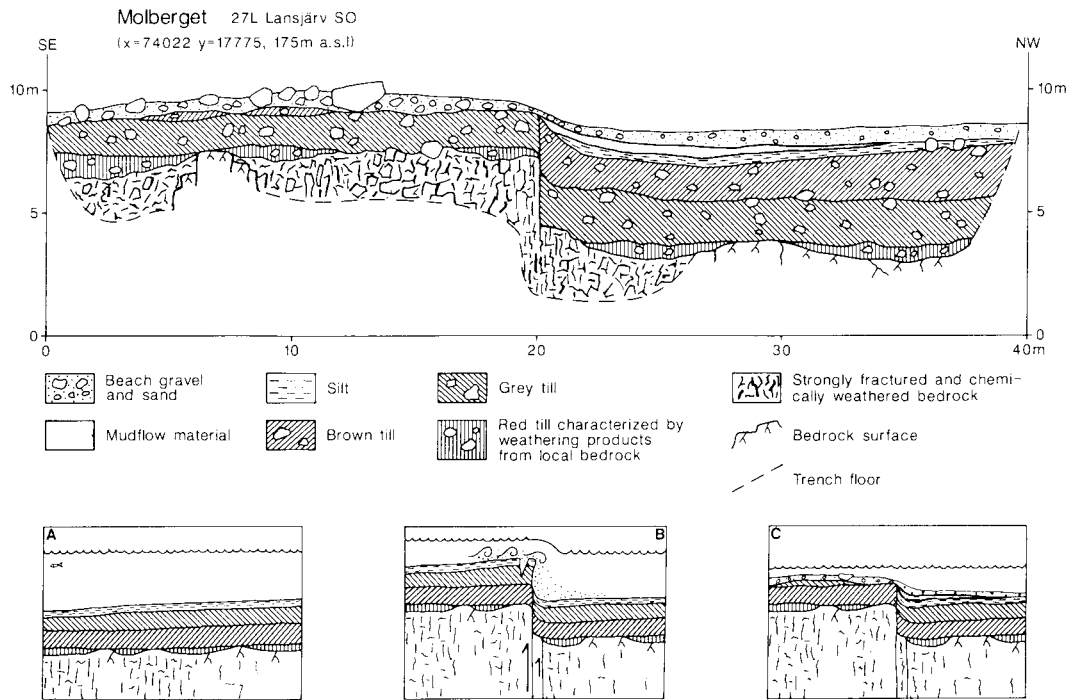
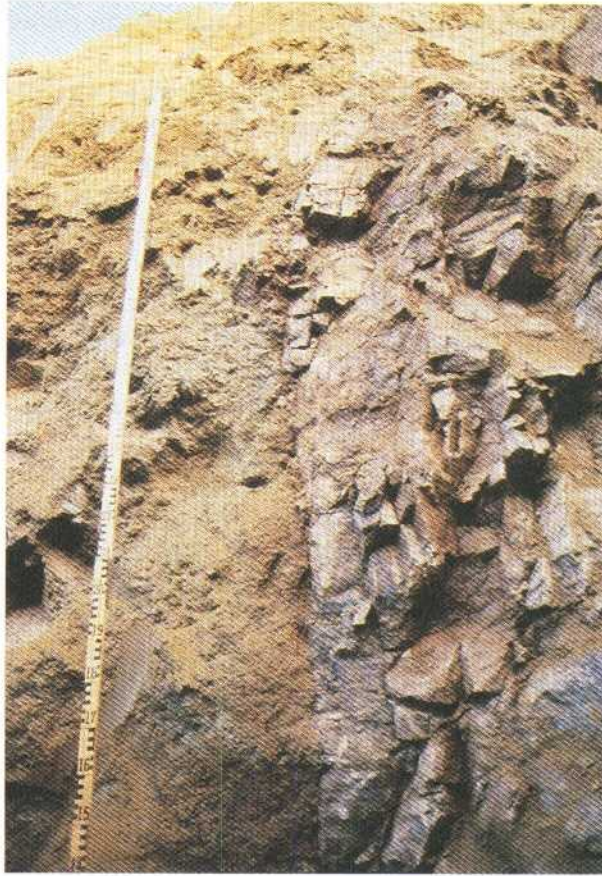


Figure 3-4. Trench section across the fault scarp at Molberget (site 4 in Figure 3-1). Inferred development: A. Previous to faulting. The recently deglaciated locality is covered by the postglacial sea, deposition of fairly fine-grained littoral sediments. B. Faulting. Movement occurs in an existing, strongly weathered fracture zone. The fine-grained sediments on the lower block becomes covered by debris and mud from the collapsing overburden on the rim of the raised block. C. Wave-erosion of the till on the raised block and deposition of sand on the lower block during the land upheaval masks the originally more marked fault-scarp.



Figure 3-5. The strongly fractured edge of the raised bedrock block at Molberget. The contact between bedrock and till is stippled. Photo: R. Lagerbäck 1987.



*Figure 3-6. The sharp, vertical contact between bedrock and till in the fault-zone at Molberget.*

Photo: R. Lagerbäck 1987.



*Figure 3-7. Strongly fractured and chemically weathered bedrock of the raised block at Molberget. Contact between till and bedrock in the upper part of the photograph.*

Photo: R. Lagerbäck 1987.

The other sample, from the red, sandy weathering residual of the raised block, consisted of vermiculite, expandable mixed-layer minerals, illite, plagioclase and potassium feldspar.

Three different till beds were present in the section, and they were all cut by the fault. Debris and mud-flow material, deriving from the collapsed till beds, covered postglacial fine-grained water-laid sediments on the down-faulted block, demonstrating that faulting occurred after local deglaciation. The ground on the raised block was excessively wave-abraded, and covered by residual till boulders and coarse gravel. On the down-thrown block, situated in a more protected position, fine grained littoral gravel and sand covered the remaining, not eroded deposits, including the fault-induced debris and mud-flow material. The littoral gravel and sand were unaffected by the faulting, making it obvious that no movements have occurred in the fault zone since the site was raised above the sea.

**STUPFORSEN** (Figures 3-1 and 3-8). This site has been studied previously and was now only partially re-excavated. Two till beds were cut by a well-defined, reverse fault scarp dipping some 45° to the west (Figure 3-9). The hanging-wall bedrock, composed of coarse grained Lina granite and pegmatite, was heavily fractured and weathered (Figure 3-10), similar to that described from Molberget. The clayey saprolite in the fault zone displayed beautiful, dip-slip slickensides. The clay-minerals in the saprolite were dominated by chlorite, vermiculite and expandable mixed-layer minerals. The footwall rock was not reached because of large quantities of water pouring out from the fault zone. A surficial bed of undisturbed littoral gravel demonstrates that no fault movements have occurred after the site was raised above the sea.

**MÄJÄRVBERGET** (Figures 3-1 and 3-11). This locality is situated at about the same level as the highest coastline and a minor wave-cut bench is developed in the scarp. Three till units were identified in the trench (Saalian or older, Early and Middle/Late Weichselian) and they were all affected by the fault movement. The bedrock was met with at a depth of between 1.5 and 6 metres but it was not possible to reach the bedrock within the 20 metres nearest to the fault scarp on the foot-wall block. The bedrock 20 m away from the scarp was a continuous and not significantly weathered granite, pinkish in colour, medium grained and possibly belonging to a granite generation older than the Lina Suite, T. Sjöstrand, pers. comm.. The bedrock in the fault zone, which was at least some 15 m wide, was extremely fractured and weathered. It was composed of Lina granite, pegmatite and biotite gneiss, the latter possibly a metasediment or otherwise a variety of the Haparanda Suite, T. Sjöstrand, pers. comm..

Two samples of the weathering products in the fault zone were analysed with regard to clay mineralogy. A clayey sample from the granitic rocks showed illite, expandable mixed-layer minerals, potassium feldspar and plagioclase. A more sandy sample from the weathered gneiss showed illite, vermiculite, plagioclase, potassium feldspar and amphibole.

No well defined, single fault plane occurred in the bedrock scarp. Fault displacement was instead more evenly spread within the zone and it was difficult to define the dip of fault movement more precisely. Minor fault planes, fractures, fissility and contacts between different rock units dipped some 40°–50° to the southeast, which is judged to be the most likely dip of the near-surface fault movement. A minor dextral, strike-slip movement was indicated by the way the fault-zone bedrock intruded into the lower brown till bed.

The bedrock at the surface of the raised block, composed of a greyish, medium grained Lina granite, was chemically unweathered but shattered into blocks (Figure 3-12). Fresh, open fractures were cutting the glacially polished rock indicating violent breakage (Figure 3-13). These fractures were generally

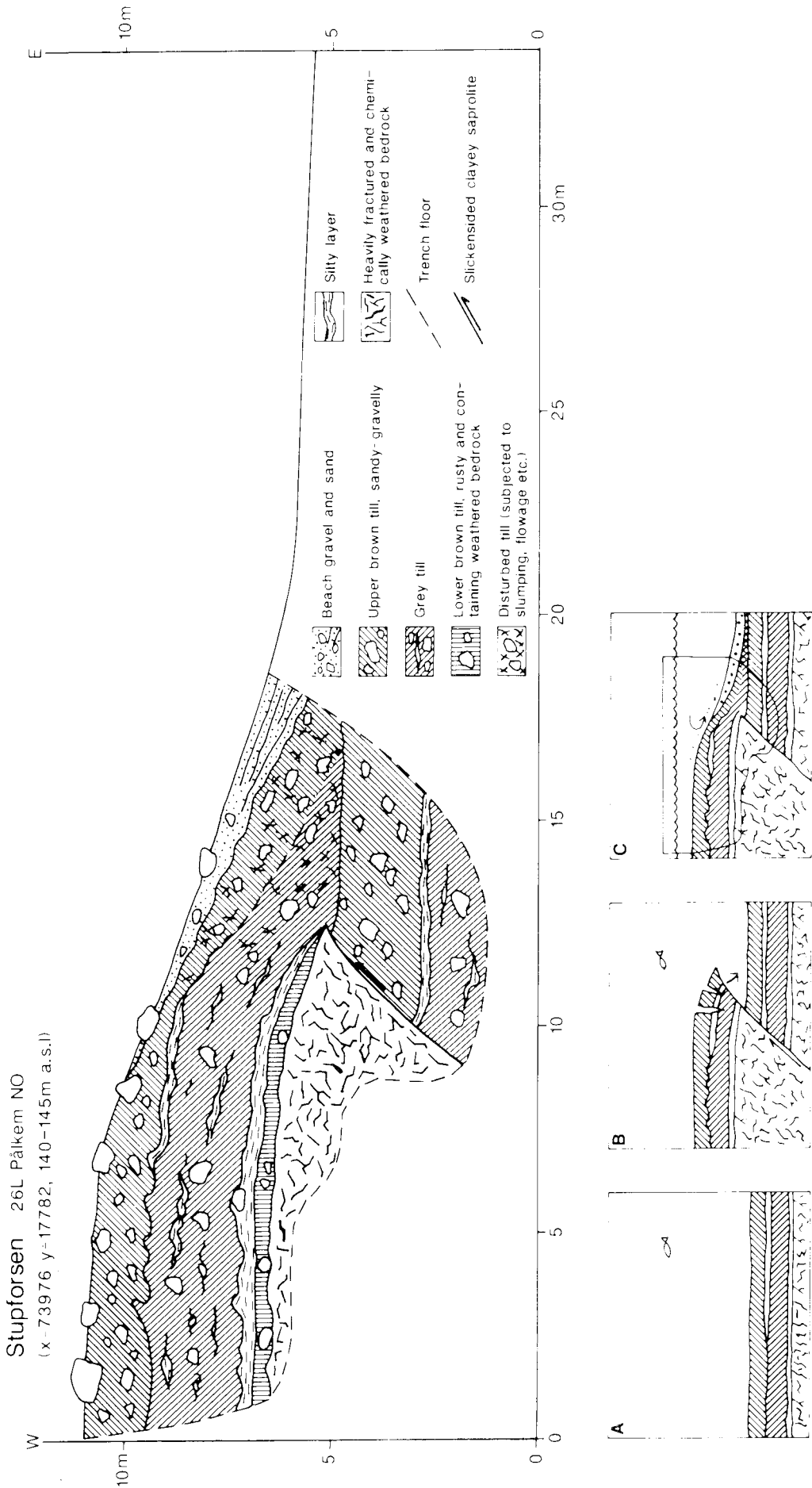


Figure 3-8. Trench-section across the fault-scarp at Stupforsen (site 5 in Figure 3-1). Inferred development: A. Previous to faulting. The locality is covered by the postglacial sea. B. Faulting. Fault movement occurs in an existing, strongly fractured and chemically weathered fault zone. The overburden on the edge of the raised block collapses during faulting and slumps and flows to cover the deposits on the lower block. C. During the land up-heaval the raised block is abraded by waves while sand and gravel is deposited on the lower block.





*Figure 3-9. The edge of the raised block at Stupforsen. Dip-slip slickensides occur in clayey saprolite on the fault surface. The height of the fault scarp visible on the photograph is about 2.5 m.*

Photo: R. Lagerbäck 1987.



*Figure 3-10. The fractured and chemically weathered bedrock in the hanging wall at Stupforsen. The bedrock was easily cut through by the excavator.*

Photo: R. Lagerbäck 1987.

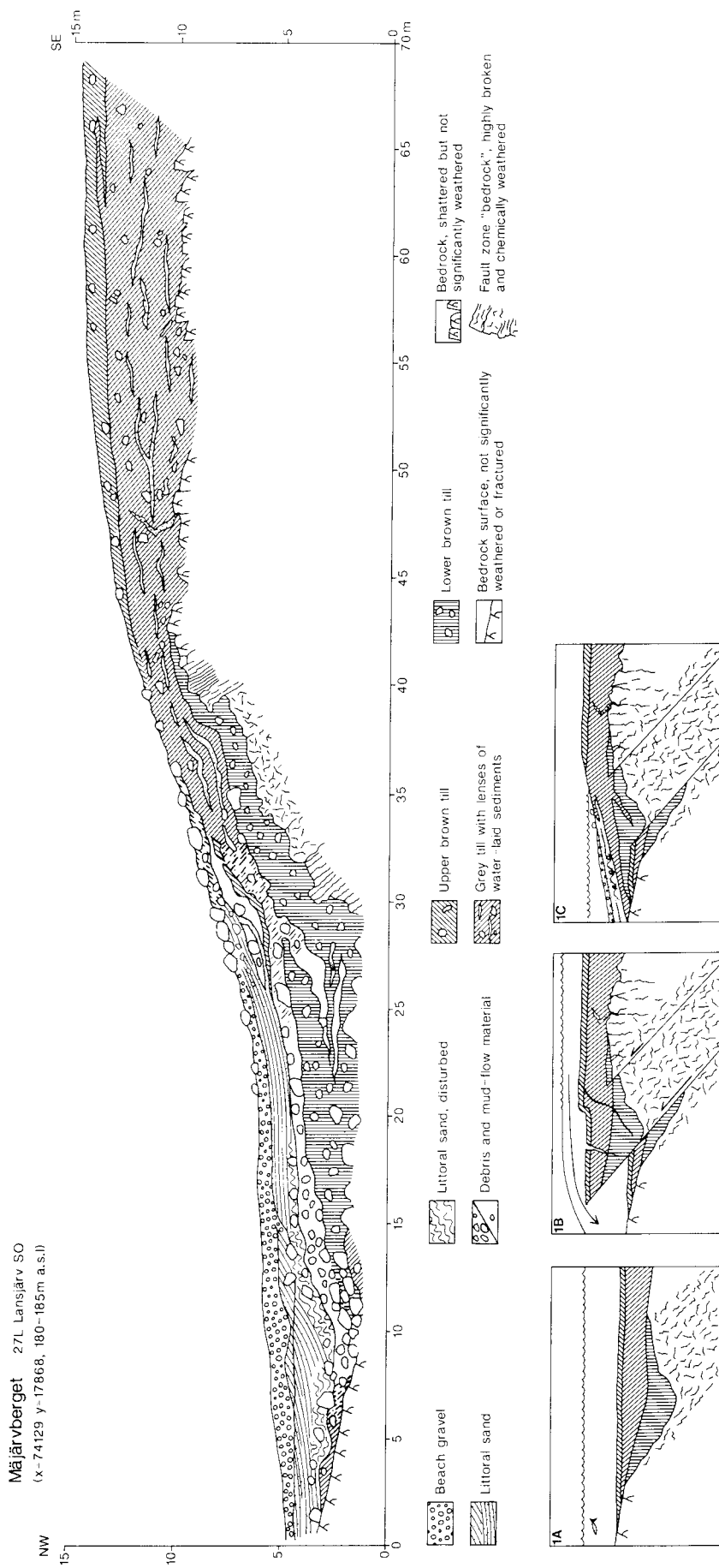


Figure 3-11. Trench-section across the fault scarp at Mäjärverket. Inferred development: A. Previous to faulting. The recently deglaciated locality is covered by shallow water. A pocket of pre-Weichselian till occurs in an existing, strongly fractured zone B. Faulting. Fault movement is spread throughout the zone. The bedrock in the raised block becomes fractured and water and sand is extruded through the fractures. The overburden on the rim of the raised block collapses. A minor strike-slip component in fault movement is indicated by the configuration of protruding bedrock. C. Stabilization of the fault scarp by slumping, wave erosion and flowage of till material. The present-day form occurs as soon as the locality is raised above the sea.



*Figure 3-12. Part of the trench at Mäjärvberget showing the shattered bedrock surface on the raised block. The rock is very hard and unaffected by chemical weathering. The thickness of the till-cover is 4–5 m.*

Photo: R. Lagerbäck 1987.



*Figure 3-13. Shattered, glacially polished bedrock boss at the surface of the raised block at Mäjärvberget. Note exposed part of open fracture in the lower part of the photograph and sand-filled veins emanating from the open fractures to the right. The picture measures about 3 m across.*

Photo: R. Lagerbäck 1987.

directed in NNE-SSW, that is, roughly parallel to the fault, and they dipped some 80° to the southeast.

The Quaternary stratigraphy and the deformational structures related to the faulting were complicated. Breakage and collapse of the till bed, debris flow from the broken till, injection of sand and silt and littoral processes have been interacting in an intricate manner. The interrelationship between the littoral sand at the foot of the scarp, debris flows and boulders which have tumbled down the slope of the scarp, demonstrates that fault movement occurred at the time when the early postglacial sea was still covering the locality. The fact that coarse beach gravel, representing the last stage of wave-activity, has not been affected by any disturbances or interruptions shows that no movements occurred subsequent to that time.

### 3.3.2 Paleoseismic Records

#### 3.3.2.1 Landslides

Several circumstances indicate that the faulting within the Lansjärv area was associated with strong seismic activity. The most striking phenomena in this context are landslides occurring in the same area as the faults. One of these slides, at **ELMABERGET** (Figure 3-14) some 15 km to the northeast of Lansjärv, has previously been investigated by excavations and was now reinvestigated with respect to stratigraphy and mechanical composition of the deposits involved. The landslide scar measures about 300x300 m and approximately some  $5 \cdot 10^5$  m<sup>3</sup> of glacial till was mobilized. Most of the material obviously moved in a liquefied state but big chunks of the more coherent, surficial parts of the overburden were

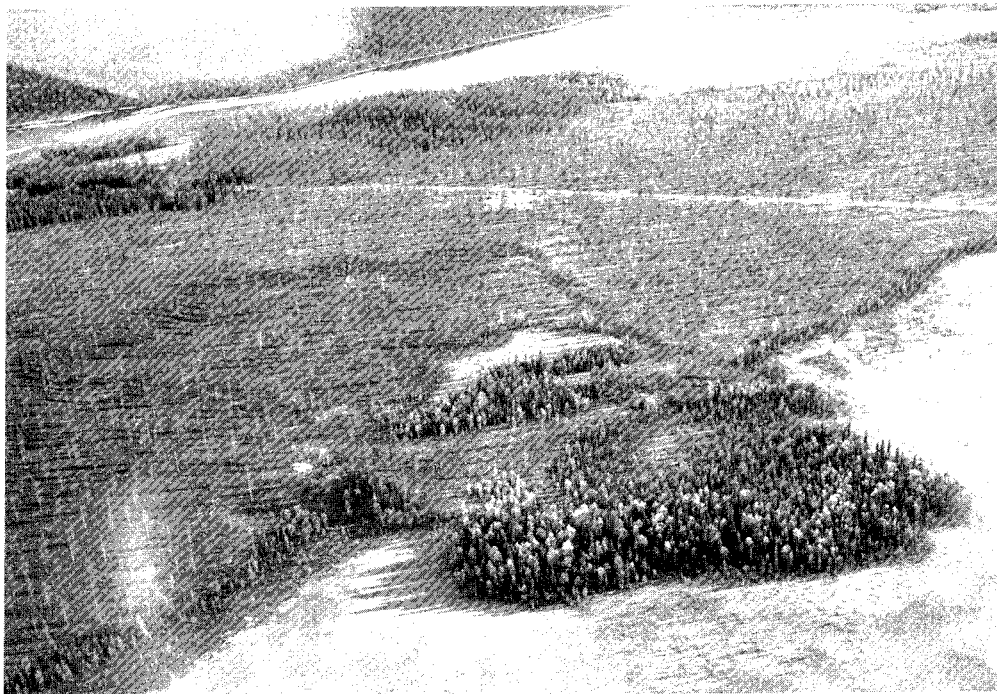


*Figure 3-14. Landslide in glacial till at Elmaberget (8 in Figure 3-1). The landslide developed in a slope with an inclination of only 3–4 degrees. It is radiocarbon dated to an age of more than 8000 years and was probably triggered in close connection to the deglaciation of the area.*

Photo: R. Lagerbäck 1981. Approved for publication.

also transported downslope. The slide has been radiocarbon dated using peat formed inside the scar and gives a date older than 8000 years. The landslide is developed in an ordinary sandy till. This most probably is valid also for the other slides within the region. The fact that these slides are developed in till is remarkable as sandy tills are not expected to slide and as the slides generally occur in gentle slopes.

Excavations were also made in some peculiar hollows and troughs situated close to the slide and suspected to be genetically related to it. Some of these most probably were created by expulsions of groundwater from the bedrock, or from the overburden in connection with a rise in pore pressure due to seismically induced compaction, while others are interpreted to have formed by subsidence of the ground due to subsurface outflow of liquefied till.

At **REPOVAARA** (site 9 in Figure 3-1), about 25 km north of Lansjärv, two minor pits were dug in connection to a fairly large slide ( $\geq 1 \cdot 10^6$  m<sup>3</sup>). This slide was also developed in a gentle hillside with an ordinary sandy till. The distribution of the mobilized material demonstrates that the slide was triggered while remnants of the down-wasting ice-sheet were still present at the place.

### 3.3.2.2 Seismites

Seismically induced disturbances of the primary structures of different types of Quaternary deposits is another effect of earthquakes associated with the faulting. Such disturbances are the result of liquefaction and occur in unconsolidated, water saturated frictional soils when affected by seismic acceleration. Disturbances in different types of soils have previously been actively searched for, and have also been found in many places within the Lansjärv area (Lagerbäck 1989, in manuscript). Deposits, interpreted as being significantly distorted by seismic acceleration, are collectively called here seismites, a term introduced by Seilacher (1969).

In connection with the present project, waterlain sediments interpreted to be seismically disturbed were examined in two areas; at Slättheden some 50 km to the southwest of Lansjärv and at L. Furuberget 25 km northwest of Överkalix.

**SLÄTTHEDEN** (site 11 in Figure 3-1) is a large delta built up more or less to the level of the highest coastline. The purpose of excavating here was to check if seismically induced disturbances of any significance exist at a considerable distance from the fault area. The locality is situated about 25 km to the southwest of the southernmost part of the Lansjärv fault and about 50 km from its center. Four trenches were made. Two of them revealed disturbances of a type very similar to those found earlier in the Lansjärv area, the most typical features being a considerable compaction and a transformation of the original layers into different types of convolutions, "ripples" and "flames" (Figure 3-15). The most surficial layers were not affected by these disturbances.

At **L. FURUBERGET** (site 12 in Figure 3-1), some 25 km northwest of Överkalix, phenomena interpreted as seismically induced were come across during reconnaissance for suitable sites for excavation. In a gully, cut by meltwater during the spring of 1987, extensive distortions of the primary sedimentary structures were found in littoral sand (Figures 3-16 and 3-17). The disturbances seemed to be restricted to a certain stratigraphic level and the uppermost layers were quite unaffected. These circumstances demonstrate that the agents generating the distortions were acting only during a short period, probably at one single occasion, during the early postglacial period and before the locality was raised above the sea.



*Figure 3-15. Small scale convolutions and corrugations in silty and fine-sandy layers at Slättheden. Features very similar to the “flames” developed in the darker, silty layer in the middle of the picture are produced experimentally by shaking of sand overlying mud (Dzulynski & Walton 1963, plate XX11B). Scale in cm.*

Photo: R. Lagerbäck 1987.



*Figure 3-16. Strongly corrugated sandy and silty littoral deposits at L. Furuberget. Note that the uppermost part of the picture (above the scale) shows undisturbed layering. The phenomenon is interpreted as being caused by seismically induced liquefaction, compaction and dewatering during the build up of the sequence.*

Photo: R. Lagerbäck 1987.



*Figure 3-17. Convoluted sandy deposits at L. Furuberget. Pseudo-nodules very similar to the one in the center are produced experimentally by simulating earthquake effects on sand overlying mud (Kuenen 1958). The material above the scale is artificial filling.*

Photo: R. Lagerbäck 1987.

## 3.4 DISCUSSION

### 3.4.1 Age of Faulting

The different stratigraphical units of the Quaternary overburden are the only adequate reference structures for dating the fault movements, visual as scarps in the ground surface. The fact that the scarps cut the till cover, and protrude as morphologically prominent scarps extending over long distances, does not necessarily imply that the faulting occurred postglacially. The reason for this is that the last two ice-sheets in this area were very sluggish and had a generally weak impact on the previous glacial landscape (Lagerbäck & Robertsson 1988; Lagerbäck 1988a).

However, a complex stratigraphy, with different till beds together with other stratigraphical units, offer a good potential background for dating of fault movement relative to glaciations and ice-free periods. The fact that the fault scarps are largely situated below the highest coastline means that it is theoretically possible to also date fault movement relative to deglaciation and local land-upheaval. These circumstances make trenching across the scarps a very promising tool in this context.

At Molberget and Mäjärvberget it is evident that faulting occurred after local deglaciation, but previous to the rise above the postglacial sea. Taking into consideration the location of these sites close to the highest coastline, the fault scarps must have developed within a very limited time period after local deglaciation. In principle the situation is identical at the sites Neitaskaite and L. Telmträsket, see Lagerbäck (1988b) for these localities. Nothing contradicts that the scarps at Storsaiviskölen, Mainekjaure (Lagerbäck 1988b) and Stupforsen

(above) are also of the same age, as the stratigraphy at these sites does not allow such precise dating. On the contrary it is of course most likely that these scarps all developed at the same time as shown by their similarity and while together they form a connected fault complex.

At Mäjärvberget sedimentary structures and the appearance of the interface between bedrock and till indicate that the fault may have been active during the deposition of the grey, Early Weichselian till. However, this is uncertain and the distribution of the different deposits and their relation to the bedrock surface clearly indicates that at least the main part of the fault scarp height developed postglacially.

The stratigraphies at Neitaskaite, Molberget, Mäjärvberget and Telmträsket obviously were cut abruptly by the fault movement and the scarps were here most probably developed as a one-step event. Nothing, except for what has been said about the section at Mäjärvberget, indicates that the scarps developed by repeated movements. Creeping over a long period of time is definitely ruled out. Also the slickensides at Stupforsen, speaks in favour of rapid fault movements.

Thus, there is strong stratigraphical evidence for a rapid fault-movement, most probably a one-step event, shortly after local deglaciation. The occurrence of landslides and seismites, if the causal relationship and interpretation of origin is accepted, also favours the conception of short-lived, co-seismic faulting of great magnitude (see further below). Minor contributions to the fault scarp development during previous glaciations, or ice-free periods, cannot be excluded but there is not much evidence in favour of them.

However, there is no doubt that the fault **zones** met with at Stupforsen, Molberget and Mäjärvberget pre-date not only the last glaciation but probably also the Quaternary. The possibility that the extensive weathering of the fractured rock should have developed postglacially is excluded and it is thought doubtful that 2–3 million years of cold Quaternary conditions are sufficient for the thorough chemical decomposition of the rock fragments. According to A. Sjödin (Geological Survey of Sweden, pers. comm.) the composition of clay-minerals in the samples from the fault zones, when taking into consideration the local rock-type, indicates that the weathering probably took place independently of atmospheric influence and that it might have occurred at a considerable depth.

### 3.4.2 Fault Geometry and Style of Postglacial Faulting, some Remarks

It is beyond the scope of this study to speculate on fault scarp geometry and tectonic style but some remarks might be justified. Henkel et al. (1983) interpret the postglacial faults as steeply dipping zones involved in block movement tectonism. Talbot (1986) arrives at a different interpretation and concludes that the postglacial fault system involves “gently dipping anastomosing thrusts with N to NE strikes and steep contemporaneous NW-EW-trending sidewalls as well as steep E or ESE dipping reverse faults”. The fault system is considered a possible “positive flower structure extruded by transpression along a NE trending master zone of weakness inherited from Proterozoic time” (Talbot 1986).

Inspired by Talbot, Henkel (1988) re-interprets the geophysical data and claims that the postglacial faults belong to a system of gently dipping (near horizontal) thrusts. The seismic refraction profiles performed across the fault scarps (Henkel 1988 Figure 16; Henkel & Wällberg 1987) are said to indicate “shallow dip” and “low angle thrusting” for several or most of the fault branches and scarps. However, all fracture-zones are marked as vertical in the figures presented. It is difficult to see in what way these profiles support an interpretation of the faults as gently dipping. Besides, the excavated fault zone bedrock is strongly fractured and weathered and therefore not possible to identify as rock



by seismic refraction sounding. Therefore, the seismic profiles probably do not reflect the true configuration of the bedrock fault scarp (see e.g. the Mäjärverget section; Figure 3-11 in this paper and seismic profile S4 (Figure 16) in Henkel 1988).

By using “terrain elevation data” (digital 100 m spaced data with an elevation resolution of about 2 m, see Plate 4 in Henkel 1988) Henkel also defines a great number of “suspected postglacial fault scarps” spread over a large area, (Plate 6 in Henkel 1988) and several “suspected postglacial shear lenses” associated with the major aeromagnetically indicated shear zones. The “suspected postglacial fault scarps” are not described and no evidence for a postglacial age of any of these features is presented.

The naturally exposed bedrock outcrops, and those met with in the trenches, give some guidance to fault scarp geometry and the near-surface dip of the postglacially activated fault zones. The bedrock plinths protruding through the till at Risträskkølen (Figure 3-2) are largely shattered and it is difficult to reconstruct the original configuration, but a reverse fault dipping some 40–60° is inferred. At Karhuvaara the fault scarp constitutes a steep cliff (Figure 3-3). At Stupforsen (Figures 3-8 and 3-9) the fault is reverse, dips some 45° and displays fresh dip-slip slickensides. Talbot (1986, Figure 3-13) suggests that strike slip movement occurred along this scarp during the postglacial faulting. At Molberget (Figures 3-4, 3-5 and 3-6) the fault surface is vertical and at Mäjärverget (Figure 3-11) fault movements are interpreted as occurring along planes dipping some 45°.

Thus, field evidence suggests it to be more likely that the faults, at least where outcropping, are reverse and dip between the vertical and some 40 – 50°. Dips of that order also seem reasonable if considering the appearance of the scarps and the deformations of the overburden stratigraphy along the scarps.

Gently dipping faults (a few degrees), as suggested by Talbot (1986) and Henkel (1988) are less likely along most of the scarps for geometrical reasons. It is difficult to see how such gently dipping faults could produce scarps of the type in question. The typical scarp is developed as a very distinct step in the ground surface, with a steep repose angle and a stable configuration for most of its extension. Faults dipping only a few degrees should result in scarps either with more gentle slopes, or, more likely with accumulations of loose deposits pushed to ridges along the fault outcrops. A much more complicated and distorted Quaternary stratigraphy than those recorded, should also be expected in the fault scarp.

### **3.4.3 Paleoseismicity**

#### **3.4.3.1 Landslides**

The landslides within the Lansjärv area, (Figures 3-1 and 3-14) like all the other landslides in Norrbotten (Lagerbäck & Witschard 1983; Lagerbäck 1989, in manuscript) and Finland (Kujansuu 1972), are developed in gentle slopes (3–10°) with a considerable cover of glacial till. The tills involved in the sliding have a sandy composition and do not differ from ordinary tills in the region. Tills of this composition are not expected to flow under normal conditions, especially not in slopes with a low gradient.

It has been demonstrated that the slides are fossilized and that they all probably developed shortly after, or in direct connection with, local deglaciation, that is, about some 9000 years ago. What anomalous circumstances prevailed during the deglaciation in the Lansjärv area and large parts of the rest of northern Fennoscandia? Kujansuu (1972) suggests that a permafrost table may have

occurred at some depth in the ground. The permafrost would serve as a slip plane and also prevent the downward percolation of water, thereby forcing a soaking of the till. The southward orientation of most of the Finnish slides, resulting in a fast thawing of the permafrost, is taken as support for this interpretation.

However, Kujansuu (1972) also suggests that earth tremors accompanying the contemporaneous faulting (Kujansuu 1964) may have triggered the landslides and he points to the regional connection between the two phenomena in Finnish Lapland. There is also an obvious distributional connection between landslides and fault scarps in northern Sweden (Lagerbäck & Witschard 1983). The correspondence in geographical distribution of the two phenomena is hardly accidental but most likely reflects a causal relationship. The occurrence of permafrost may have had an influence over the distribution of landslides but more important is that a triggering mechanism is a prerequisite for the development. The contemporaneous faulting, associated with strong seismic activity, offers an obvious explanation to the phenomenon.

It is well known that large earthquakes often initiate landslides. Keefer (1984) compiled data from 40 historical worldwide earthquakes and several hundred earthquakes from the U.S.A. in order to study the relations between landslide distribution and seismic parameters. Accepting the causal relationship between faulting, earthquakes and landslides in the Lansjärv region, and translating Keefer's results to this area, it seems that several earthquakes with a magnitude of M 6.5–7.0, or higher, occurred during the deglaciation of the region.

Magnitudes of this order are also in agreement with the horizontal extension and the displacement of the faults. Inserting the figures of fault length (almost 50 km) and fault displacement (5–10 m, with about 25 m as an extreme) of the Lansjärv fault complex into the diagrams given by Bonilla et al. (1984), showing relations among earthquake magnitude, surface rupture length and surface fault displacement, indicates that the faulting was accompanied by an earthquake with a magnitude of M 7.0–7.5 or higher.

#### 3.4.3.2 Seismites

Distortions of primary sedimentary structures similar to those found in the Lansjärv area are described from many places and from different environments. They occur not only in unconsolidated sediments but are also found lithified in sedimentary rocks. The features are generally explained in terms of load casting, liquefaction and dewatering, but opinions differ about the conditions and factors responsible. Differences in composition of the beds involved, heterogeneities of the sediments, rapid sedimentation, impact of big waves etc. are suggested to initiate the deformational processes. Many authors also stress the importance of earthquakes and seismically induced liquefaction for the development of distortions.

Convoluted and corrugated beds similar to some of those at L. Furuberget and Slättheden are explained by load casting caused by heterogeneities of the sediments and/or thixotropic behaviour (e.g. Davies 1965). The importance of differential loading (density), slumping and water seepage is stressed by e.g. Dionne (1971). Many authors stress the importance of external disturbances acting as triggers of liquefaction and fluidization. Lowe (1975) suggests that a rapid deposition by itself, resulting in consolidation and dewatering of subjacent units, may lead to liquefaction, fluidization and associated distortion of sandy deposits, but also indicates that earthquakes or other disturbances are probably influential in some instances.

However, features similar to some of those found in the Lansjärv area have also been produced experimentally by vibrating waterlogged sediments at the laboratory. Kuenens (1958) experiments are classical in this context and some of the features found at for instance L. Furuberget are more or less identical with those published by Kuenen (Figure 3-17). Structures very similar to the small scale deformations at Slättheden (Figure 3-15) have been produced experimentally by shaking sand overlying mud (Dzulynski & Walton 1963).

Sims (1973, 1975) claims that earthquakes are critical for the formation of different features found in young lacustrine sediments in California and points to the correspondence of these features and experimentally formed structures. Sims also correlates some of the features with known recent seismic events and stresses the importance of the deformational structures for determination of earthquake recurrence intervals.

The beds described from Slättheden (Figure 3-15), L. Furuberget (Figures 3-16 and 3-17), and many other sections in the Lansjärv area (Lagerbäck 1989, in manuscript) are considered seismites and caused by earthquakes associated with the postglacial faulting. The interpretation of the features as seismically induced is supported by, among others, the following reasons:

- They occur in sediments with a grain size favourable for liquefaction when affected by earthquake vibration (e.g. Lee & Fitton 1969).
- They occur in mainly frictional deposits, of a similar grain-size throughout the sections, not expected to develop load-cast structures unless liquefied.
- They occur in flat-lying or very gently sloping terrain and, thus, provide no reason to expect that slumping or sliding contributed to the deformation.
- They occur in sediments deposited during the early postglacial period, that is, contemporaneous to the faulting, but have not been found in younger sediments in the area.
- On each site they appear to be developed at a certain stratigraphical level and they are covered by undisturbed sediments. This demonstrates that the phenomenon was syn-depositional, occurred at a particular time, and before the sites were raised above the sea when the sedimentation then ceased. The distortions developed in the uppermost, least consolidated strata, which were most sensitive to liquefaction at the time of deformation.
- The features fit perfectly into a pattern of extensive faulting, accompanied by large earthquakes triggering a great number of landslides in the Lansjärv area. The features were found, when actively sought for, in deposits and environments where they were expected according to the theory of early postglacial seismogenic faulting in the Lansjärv area.

### 3.5 CONCLUSIONS

Based on the results from the present and previous investigations the following conclusions can be drawn:

- The morphologically expressed fault scarps in the Lansjärv area were formed in connection with co-seismic faulting during, or shortly after, the local deglaciation. There are no indications of fault movement after that time.
- The scarps generally developed as rapid single events but it cannot be excluded that some of them were partially developed prior to, or developed in connection with, an earlier glaciation.
- The different fault-scarp segments in the area most probably developed simultaneously, or at least in close conjunction with each other.

- The postglacial faulting at least partly (that is, at least where met with in connection with excavation) took place along heavily shattered, strongly water-bearing and chemically weathered (fault-) zones of presumably pre-Quaternary age.
- Extensive fracturing and weathering of the fault zones makes it difficult, or impossible, to use seismic refraction sounding for detailed investigation of bedrock surface and fault scarp geometry.
- The observed bedrock fault scarps and dislocated Quaternary sequences give no support for an interpretation of the faults as very gently dipping thrusts. The faults, when judged from the outcrops, appear to be reverse and dip between the vertical and some 40°.
- Fault movements were mainly dip-slip but a minor strike-slip component is indicated locally.
- The earthquakes associated with the faulting reached magnitudes of at least M 6.5–7.0, they triggered landslides in glacial till and produced extensive deformations of sandy sediments in vast areas.
- An active search for seismically induced deformations has proved fruitful if concentrated to deposits and environments favourable for the development of such structures. The investigations of seismites should be continued in the Lansjärv area in order to elucidate the variation of their appearance in different environments.
- In order to elucidate the significance of late-to postglacial paleoseismicity in wider areas the search for seismites should be extended to comprise other and larger parts of Sweden. A systematic study of favourable sediments at strategically located sites would probably contribute to a better understanding of the late- and postglacial seismotectonic evolution of Sweden.

### 3.6 REFERENCES

**Bonilla M G, Mark R K & Lienkaemper J J 1984**

Statistical relations among earthquake magnitude, surface rupture length, and surface fault displacement.

Seismological Society of America, Bulletin 74. No. 6, 2379–2411.

**Davies H G 1965**

Convolute lamination and other structures from the Lower Coal Measures of Yorkshire.

Sedimentology 5, 305–325.

**Dionne J-C 1971**

Contorted structures in unconsolidated Quaternary deposits, Lake Saint-Jean and Saguenay Regions, Quebec.

Revue Géographique Montreal XXV, no. 1, 5–33.

**Dzulynski S & Walton E K 1963**

Experimental production of sole markings.

Geological Society of Edinburgh Transactions 19, 279–304.

**Henkel H 1988**

Tectonic studies in the Lansjärv region.

SKB TR 88-07, Stockholm. 66 pp.

**Henkel H, Hult K, Eriksson L & Johansson L 1983**  
Neotectonics in northern Sweden – geophysical investigations.  
SKBF/KBS TR 83-57, Stockholm. 64 pp.

**Henkel H & Wällberg B 1988**  
The post-glacial faults at Lansjärv. Ground geophysical measurements and interpretations in a 40 x 20 km surrounding area.  
SKB AR 88-05. Swedish Nuclear Fuel and Waste Management Co, Stockholm.  
49 pp.

**Keefer D K 1984**  
Landslides caused by earthquakes.  
Geological Society of America, Bulletin 95, 406–421.

**Kuenen P H 1958**  
Experiments in Geology.  
Geological Society of Glasgow, Transactions 23, 1–28.

**Kujansuu R 1964**  
Nuorista siirroksista Lapissa. Summary: Recent faults in Lapland.  
Geologi 16, 30–36.

**Kujansuu R 1972**  
On landslides in Finnish Lapland.  
Geological Survey of Finland, Bulletin 256, 22 pp.

**Lagerbäck R 1979**  
Neotectonic structures in northern Sweden.  
Geologiska Föreningens i Stockholm Förhandlingar 100, 263–269.

**Lagerbäck R 1988a**  
Periglacial phenomena in the wooded areas of Northern Sweden – relicts from the Tarendö Interstadial.  
Boreas 17, 487–499.

**Lagerbäck R 1988b**  
Postglacial faulting and paleoseismicity in the Lansjärv area, northern Sweden.  
SKB TR 88-25. Stockholm. 37 pp.

**Lagerbäck R 1989**  
Postglacial faulting and paleoseismicity in northern Sweden.  
(In manuscript).

**Lagerbäck R & Witschard F 1983**  
Neotectonics in northern Sweden – geological investigations.  
SKBF/KBS TR 83-58, Stockholm. 58 pp.

**Lagerbäck R & Robertsson A-M 1988**  
Kettle holes – stratigraphical archives for Weichselian geology and palaeoenvironment in northernmost Sweden.  
Boreas 17, 439–468.

**Lee K L & Fitton J A 1969**

Factors affecting the cyclic loading of soil. In: Vibration effects of earthquakes on soils and foundations.  
ASTM STP 450, 71–95.

**Lowe D R 1975**

Water escape structures in coarse-grained sediments. *Sedimentology* 22, 157–204.

**Lundqvist J & Lagerbäck R 1976**

The Pärve Fault: A lateglacial fault in the Precambrian of Swedish Lapland. *Geologiska Föreningens i Stockholm Förhandlingar* 98, 45–51.

**Nordkalott Project 1987**

Geological map, Northern Fennoscandia, 1:1 mill.  
Geological Surveys of Finland, Norway and Sweden.

**Olesen O 1984**

Sen-/post-glaciale forkastningar ved MASI, Finnmark.  
NGU, Rapport 84.171, 27 pp.

**Seilacher A 1969**

Fault-graded beds interpreted as seismites.  
*Sedimentology* 13, 155–159.

**Sims J D 1973**

Earthquake-induced structures in sediments of Van Norman Lake, San Fernando, California.  
*Science* 182, 161–163.

**Sims J D 1975**

Determining earthquake recurrence intervals from deformational structures in young lacustrine sediments.  
*Tectonophysics* 29 (1–4), 141–152.

**Talbot C 1986**

A preliminary structural analysis of the pattern of post-glacial faults in northern Sweden.  
SKB TR 86-20, Stockholm. 36 pp.

**Tanner V 1930**

Studier över kvartärsystemet i Fennoskandias nordliga delar IV. *Bulletin de la Commission Géologique de Finlande* 88, 594 pp.



## 4 REACTIVATIONS OF PROTEROZOIC SHEAR ZONES

*Christopher Talbot, Raymond Munier, Lucie Riad*

Hans Ramberg Tectonic Laboratory  
Uppsala University  
Box 555, S-751 22 Uppsala, Sweden

### 4.1 PURPOSE

This study reports:

- the natures, geometries, histories, kinematics and recent dynamics of geological deformation structures and fabrics exposed in bedrock in or near:
  - the end-glacial Lansjärv fault system, Lagerbäck (1979),
  - examples of the N- and NW-trending geophysical lineaments, Henkel (1988),
  - and the intervening blocks.

The geology of the Proterozoic bedrock is outlined. Early ductile deformations are described as having localised into steep N-trending zones of ductile shear before c.1.7 Ga, and into steep NW-trending (and gently dipping zones?) in amphibolite facies after c.1.7 Ga. These zones reactivated repeatedly at unknown time intervals to generate increasingly brittle vein systems, faults and fracture zones. This occurred as the region cooled during its rise to exposure in Jotnian (c.1 Ga) or Cambrian (0.6 Ga) times, subsequently to be buried by Lower Palaeozoic sediments before being re-exhumed. Constraints on timing are very poor for, apart from the Quaternary glacial surfaces and deposits, the youngest known markers common in the region are c.1.7 Ga granites.

Kinematic arguments suggest that the NNE to NE-trending shear zones which reactivated to form the end-glacial fault scarps are probably only the most obvious component of a more general story of end-glacial reactivation. The NNE-, N- and NW-trending shear zones have acted as a linked system of dislocations which have displaced together at irregular time intervals, if not continuously, during the last c.1.7 Ga, and are still doing so. A final section suggests how the end-glacial reactivations were so much more violent than the current regional strain.

### 4.2 GEOLOGY

#### 4.2.1 Rock Types

The Proterozoic Svecokarelian rocks of the Lansjärv region consist of small volumes of supracrustal rocks amongst huge volumes of coarse-grained granitoids. The region can be divided into two: an eastern area dominated by NS strands of the Baltic-Bothnian shear zone, BBSZ: Berthelsen and Marker (1986) with subsidiary NW-trending shears, and, west of the very abrupt western margin of the BBSZ, another area dominated by the multiple NW-trending shears of the Senja-Bothnia zone, Henkel (1988), this volume. Another, unnamed zone of N-trending shears exists about 50 km to the west of the BBSZ.

The differences between these two areas are that supracrustal gneisses in the BBSZ belong to the c.2.45 Ga Korpilombolo Group and were foliated during



two phases of migmatisation. West of the BBSZ, most of the supracrustals belong to the c.2.05 Ga Råneå Group and record only the younger migmatisation. The N to NE-trending penetrative foliation imposed by the first migmatisation throughout the region probably accounts for the texture of conformable aeromagnetic anomalies seen between the various individual shear strands, Henkel (1988) & this volume. This magnetic pattern indicates layered rocks intruded by plutons of the oldest grey Haparanda diorite to granodiorite facies and red uniform medium-grained hornblende Skröven granites during the Svecokarelian orogeny at c.1.85-1.9 Ga.

The syn-Svecokarelian Haparanda and Skröven granites are injected by large sheets of less-foliated 1.7 Ga red megacrystic Hällberget granite. Irregular sheets of graphic (Brännan) pegmatite and (Hatton) aplites, which range in thickness from cm in the metabasics to at least hundreds of metres in the granitoids, appear to be contemporaneous facies of the Hällberget granites. All three together are referred to as the Lina granite facies and post-date the first phase of crustal building in the region. The emplacement of 1.8-1.7 Ga Lina granitoids west of the BBSZ probably accounts for the second pervasive synkinematic regional migmatisation, and Rb/Sr whole-rock ages of that age in the rocks they intrude, Skiöld (1982). The second regional migmatisation is recorded by thin quartzo-feldspathic veins in the supracrustal gneisses between the shears of the BBSZ. Undeformed examples of these second generation migmatite veins can be found superimposed on the oldest mylonites of the BBSZ. The BBSZ therefore began to develop after the Svecokarelian orogeny and before the emplacement of the Lina granitoids. However, the BBSZ has reactivated many times since it first formed, and parts of it are still active now. Only the kinematics and deformation mechanisms have changed with temperature and time.

#### 4.2.2 Early Regional Strains

A steep NE penetrative foliation with a subvertical lineation is most obvious axial planar to km-scale upright folds in the supracrustals, but is almost ubiquitous throughout the Lansjärv region. Haparanda granitoids of uniform grain size were rendered gneissose by aligned hornblende aggregates and ellipsoidal quartz and feldspar grains with axial ratios approaching 3:2:1.

Lina granitoids are undeformed with isotropic fabrics in the northern third of map sheet 27L (Figure 4-1). Previous workers have supposed the Lina facies to post-date all deformations in the region. However, although Lina granitoids foliate less readily than their surroundings, they generally display, faintly but clearly, the steep N or NE-trending gneissose foliation of the region. Furthermore, some of the thinner (<1m) sheets of Lina aplites and pegmatites are clearly folded about, or boudinaged in, the steep N-NE trending penetrative foliation superimposed on their country rocks.

No attempt was made to distinguish an earlier foliation reported by others as unique to the older Haparanda and Skroven granites because field work was generally confined to the vicinity of the aeromagnetic and topographic lineaments.

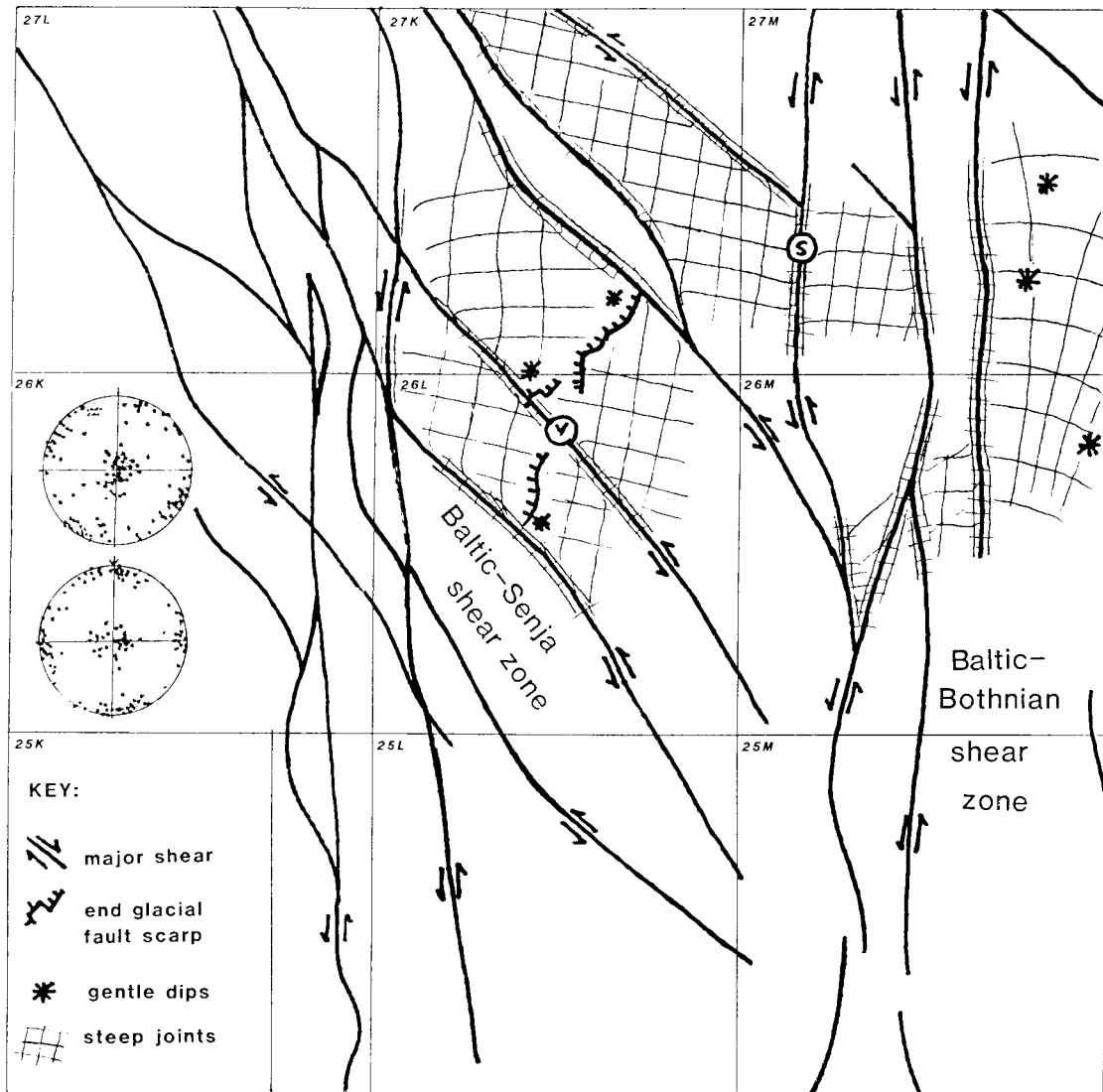


Figure 4-1. The nine 50 x 50 km map squares of the Lansjärv region showing the irregular traces of strands of the main shear zones, simplified after Henkel (1988). Thin lines extrapolate measured strikes of subvertical joints and indicate two orthogonal fracture patterns (insert stereograms: joints near NW-trending shear zones (top), and N-trending zones (bottom)). Fractures with dips <20 degrees occur in all outcrops.

## 4.3 SHEAR ZONES

### 4.3.1 General

Sets of shear zones with three strikes (N, NW, and NE-NNE) are common in the Lansjärv region (see Figure 4-4 for summary of structural data). All examples visited on the ground generally appear to have had similar histories. They originated as ductile zones of hot penetrative ductile shear in amphibolite metamorphic facies. They all narrowed with successive increments of displacement through mylonites (+/pseudotachylites) in greenschist facies before broadening to later vein systems and still later brittle fracture zones (Figure 4-6).

N- and NW-trending aeromagnetic lineaments up to 200 m wide and hundreds of km long have been mapped in the Lansjärv region using digitised topography and aeromagnetic maps of unusual detail, Henkel (1979) supplemented by local ground geophysics, Henkel (1988), this volume. All the N- and NW-trending aeromagnetic lineaments visited on the ground are marked by coincident low topographic lineaments infilled by glacial deposits, post-glacial marine sands, organic mires, or lakes. Many of these linear depressions are flanked by fault (or fault-line) scarps hundred of metres long in either the soils or bedrock.

Although the central 50—200 m is never exposed in major N- and NW-trending shear zones, the regional foliation in outcrops near shear zones of all three orientation-sets is rotated and intensified and commonly joined by a later penetrative foliation due to the growth of biotite and magnetite. All rocks, even the Lina granitoid facies, develop pronounced gneissose foliations in shear zones a few metres wide, mylonites <1 m thick and rare mm thick pseudotachylites or faults. Repeated semi-ductile and brittle reactivations of the early zones of ductile shears led to complex vein systems infilled by successive generations of minerals of the greenschist facies. In drill cores and some road cuts, later veins are found infilled by laumontite, zeolites and calcite, but such minerals have been lost by solution from all natural exposures. This means that most brittle structures at the surface appear “unfilled” and that very few can be dated relative to others.

### 4.3.2 N-trending Shear Zones

Anastomosing N-trending shear zones define the 50 km wide Baltic-Bothnian shear zone (BBSZ) adjacent to the border between Sweden and Finland, Berthelsen and Marker (1986), Henkel (1988) and a similar but narrower NS zone exists 50 km further west. Most of the N shear strands visited on the ground dip 80 degrees to the west /as predicted by remote geophysics, Henkel (1988), and all were generally left-handed during ductile deformations both before and after the 1.7 Ga Lina granitoids. However, they exhibited temporary normal dip-slip motions in greenschist facies (Figure 4-6).

The foliation in N-trending shear zones of the BBSZ is axial planar to folds which are themselves commonly refolded about steep N-trending axial surfaces and hinges which plunge steeply S. These, the latest folds in any outcrop, have chevron-like styles and range continuously in scale from at least tens of metres to a microscopic crenulation cleavage. Sets of stress-relief fractures with three orientations in the N-trending shear zones define a pattern orthogonal to the main shear foliation which is essentially similar (but not as closely spaced) in the adjacent blocks (see later).

### 4.3.3 NW-trending Shear Zones

Although these shear zones are also characterised by anastomosing strands of schist and mylonite zones with generally left handed ductile shear, most are narrower and only a few hundred metres wide. Most appear to have initiated later than the NS zones (after the Lina granitoids) and, as inferred by Henkel (1988), they appear to dip steeply SW in outcrop. NW-trending zones appear to have displaced by right handed oblique-slip during part of their passage through greenschist facies (Figure 4-6). Three sets of stress-relief fractures in NW-trending shears define a pattern distinctive of these zones, but still orthogonal to the foliation (see later).

### 4.3.4 NE-NNE Trending Shear Zones

Shear zones which dip to the ESE-SE at angles of c.30 and 10 degrees were first recognised in the Lansjärv region during the construction of structural contours for the end-glacial fault (EGF) scarps mapped by Lagerbäck, Talbot (1986), see Figures 4-2 and 4-3 here. The large scale geometry of the Lansjärv fault system suggests a long history of transpression along a steep NNE-trending shear zone which locally extruded shallow thrust flakes, Talbot (1986) and Figure 4-2. Ground studies near the Lansjärv EGF system found that the regional gneissose foliation generally has dips c.70 degrees to the NW or SW but locally intensifies as it curls to dips of 30 to 10 degrees in zones up to c.50 metres thick (Figure 4-3b). Some of these zones are mylonitic, others develop a biotite + magnetite schistosity, particularly where their dips are gentlest (<20 degrees) near their structural bases. Vein systems and fracture zones are associated with most, but not all, of these old ductile shears. Several such gently dipping ductile shears

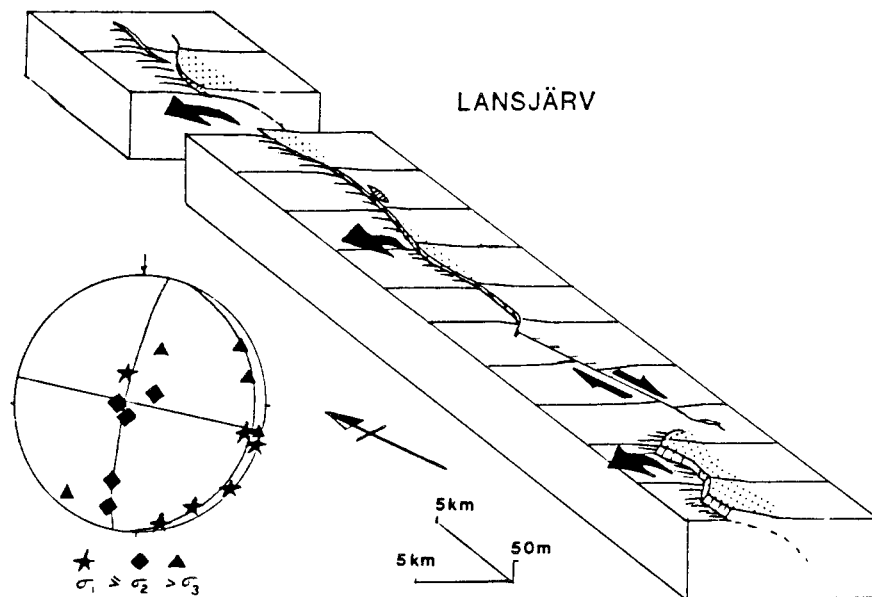


Figure 4-2. A schematic block of the end-glacial Lansjärv fault system (NE of Ris-träskkölen) to illustrate its general steep oblique reverse slip (transpressive) nature with locally extruded shallow thrust flakes. Equal-area lower-hemisphere stereogram shows principal stress axes determined from open fractures in the few rock exposures along the EGF. Notice that thrust, wrench and normal fault regimes are all represented, commonly in outcrops only mere apart, from Talbot (1986).

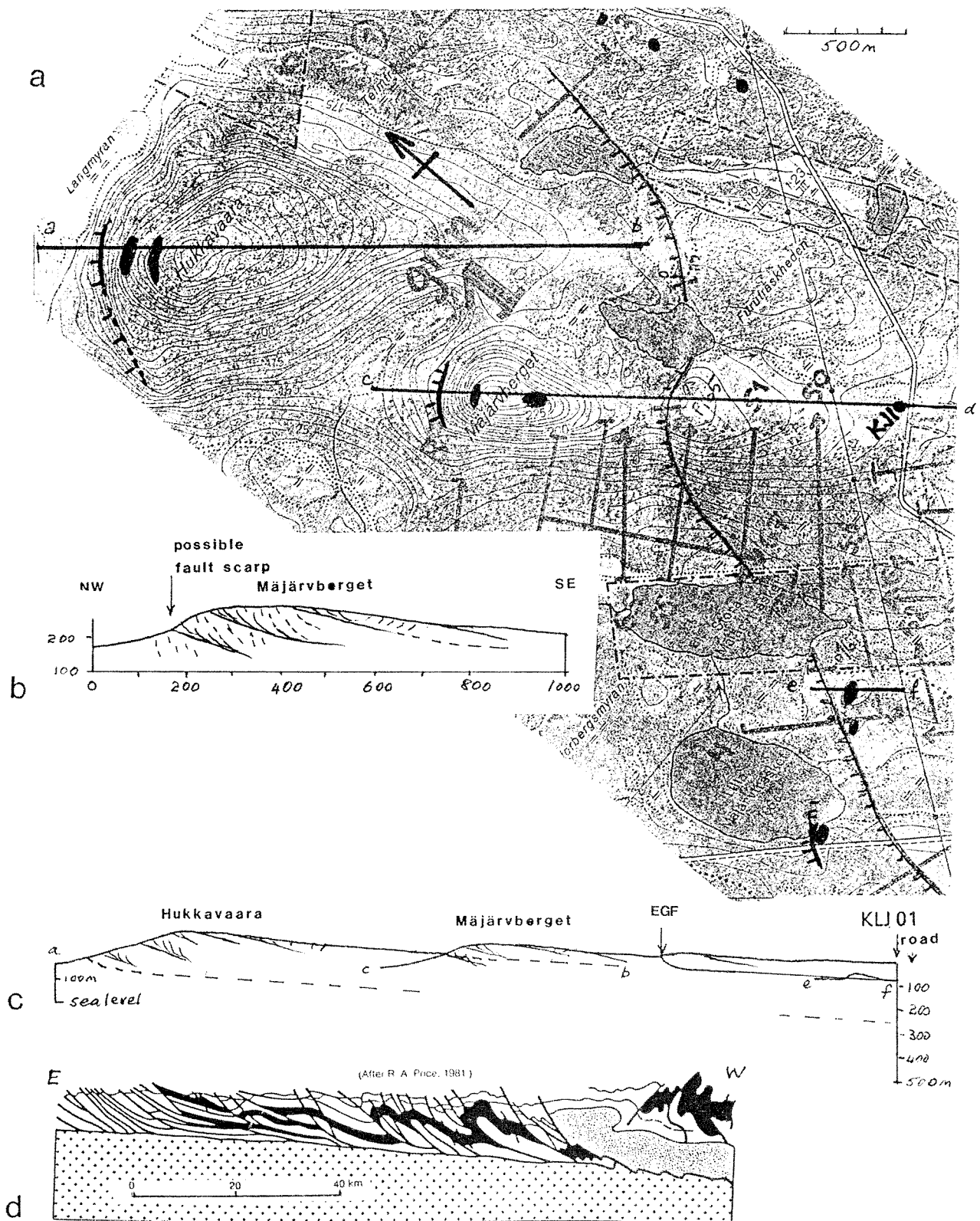


Figure 4-3. Map (a), sketch profile (b), compound cross section (c) and larger scale analogue (d=Canadian Rockies) of the northern end of the end-glacial Lansjärv fault scarp, from Lagerbäck. Outcrops of gently dipping foliation are black on map which also shows other possibly recent fault scarps.

crop out on Mäjärverget and Hukkavaara to the NW of where Borehole KLJ 01 was drilled (Figure 4-3c). Other outcrops of penetrative foliations with gentle dips occur (a) near the lakes to the SW of KLJ 01, (b) west of the road 1—2 km to the NNE of KLJ 01, (c) in the toe of the largest rock outcrop in the EGF scarp at Risträskkolen, and (d) just beyond the southernmost end of the Lansjärv EGF.

Borehole KLJ 01 was drilled into, what appears to be, an imbricate thrust zone (compare Figures 4-3c and d). This has been thrusting generally northwestward along a complex pattern of anastomosing shear zones at irregular intervals for at least the last c.1.7 Ga. Stratum contours suggest that different parts of the mapped EGF scarp mark the reactivation of examples of such zones as thrust ramps (with dips of c.30 degrees) and thrust flats (with dips of c.4—5 degrees: Figures 4-3a-c). In the NW flanks of Mäjärverget and Hukkavaara other potential fault scarps are less obvious and, if their dips are about 30 degrees, project beneath KLJ 01. Alternatively, if they flatten to a sole thus parallel to the flat where the definite EGF crosses the lower ground, they extrapolate to about 300 m in KLJ 01. However, still deeper thrust zones may crop out even further NW of Hukkavaara.

Although gently dipping shear zones may only represent local segments of steep NNE-trending zones, they are potentially of great significance. This is because they probably limit the depth of the surface rock blocks defined by the far more obvious steep shear zones. It seems likely that more may exist in the region but dip too gently to produce obvious anomalies in the (total field) aeromagnetics. Irregular asymmetric anomalies along the Lansjärv EGF have been distinguished in the topography and magnetic, electrical (VLF) and seismic refraction ground measurements, Henkel (1988). An extensive programme of ground geophysics was considered impractical, so further examples were sought largely on the basis of morphological similarities to the Lansjärv EGF system. Five swarms of similar irregular lineaments with a general NE trend considered as possible candidates for the outcrops of subhorizontal shear zones were interpreted in the Lansjärv region by Henkel (1988). Zones of anastomosing mylonites, schists, veins and fractures with gentle dips have been found exposed near only four of these, all in the BBSZ (Figure 4-1). However, outcrops along these lineaments are very few and many other gently dipping shear zones could exist beneath the extensive glacial and post-glacial deposits.

## 4.4 SHEAR ZONE HISTORIES

### 4.4.1 Early Ductile Shear

The general NE trace of the regional foliation can be seen to curl within a few km to parallel long segments of both the major N and NW lineaments on aeromagnetic maps, Henkel (1988). Field work confirms that the regional foliation increases in intensity where, in hot ductile conditions, it sheared into individual strands of the major shear zones with all three orientations. Individual shear strands in steep N-trending gneiss zones tend to be hundreds of metres wide, noticeably wider than equivalents in major NW- and NE-trending zones which rarely exceed thicknesses of 50 m. The sense of early ductile shear is left-handed in N- and NW-trending steep zones, and thrusting to the WNW in gently dipping NNE-NE trending shears.

The slight NE subvertical gneissose foliation in some megacrystic granites rotates and intensifies but remains coarse-grained. However, most protoliths diminished in grain size by dynamic recrystallization so that gneisses become schists or mylonites where they subparallel the shear zone. Foliated metabasic sheet intrusions display mullioned folds with axial planes parallel to the shear

zone. A “late” cleavage develops close to the centre planes of many, but not all, shear zones of all three orientations. Single penetrative foliations in schistose rocks, and spaced S +/- C crenulations imposed on gneisses, were associated with the regression of any hornblende surviving in the regional foliation to biotite with magnetite and, very locally, synkinematic garnet.

Rotation of the regional foliation occurred in a variety of styles on all scales which presumably reflect the metamorphic grade and rate of strain at which they developed. The curl of the pre-existing foliation can be smooth over zones many tens of metres thick, or irregular, so as to define a crenulation cleavage with lithons tens of metres to cm in thickness. The ductile curl is commonly truncated by mylonites or faults on one wall so that few of the major shear zones are symmetrical. All the N-trending shear zones appear to be asymmetric with more brittle disruption pronounced on the western wall even if the lithologies are similar on either side; however, the western blocks are rarely exposed within a km of them.

#### **4.4.2 Mylonites, Pseudotachylites & Micro-cataclasites**

Mylonite zones up to a metre or so thick occur in shear zones with all three orientations. They are generally several times less wide in pegmatites than other protoliths nearby. Most occur along the central surface of more coarse-grained zones of shear, but some are superimposed on relatively undeformed granitoids and some of these can be at high angles to any earlier foliation. Insufficient numbers are exposed to exploit their sense of shear and construct the 3d kinematic picture, but most are left-handed.

Some mylonites in the BBSZ contain post-kinematic garnets and others are crossed by undeformed quartz-feldspar pegmatites which can be attributed to heating by 1.7 Ga Lina granitoids. However, some mylonites with all three orientations are healed by recrystallization. Similarly, some of the oldest epidote + quartz veins were deformed in some of the youngest mylonites with all three orientations. Such evidence for annealing probably records changes in strain rate at constant temperatures.

Thin (<1 mm) sheets of black recrystallised pseudotachylites (seismic fault melts) and microscopic cataclastic zones appear to be rare. Most are superimposed on mylonites (and some epidote + quartz veins?) but others have been found in unfoliated aplites suggesting that these were brittle asperities that failed seismically.

#### **4.4.3 Veins Formed in Greenschist Metamorphic Facies**

Successive generations of quartz, epidote + quartz, epidote, epidote + chlorite +/- hematite? (with some chalcopyrite and arsenopyrite in one example) occur in zoned or uniform veins with, or without, angular fragments of feldspar torn from their walls. Such veins are usually a few mm wide, but some of epidote exceed a dm; their exposed lengths range from a few cm to many metres. Most are simple dilational veins but others are sheared and various surfaces within them display strike-slip, oblique, or dip-slip slickensides.

Some of these veins parallel the foliation in gneissose, schistose or mylonitised zones, but the majority are en-echelon at various angles to the earlier ductile fabrics in the shear zones in which they occur (Figure 4-4). The poles to sets of brittle fractures which formed and deformed at greenschist metamorphic facies can be interpreted in terms of the three principal stress axes in many

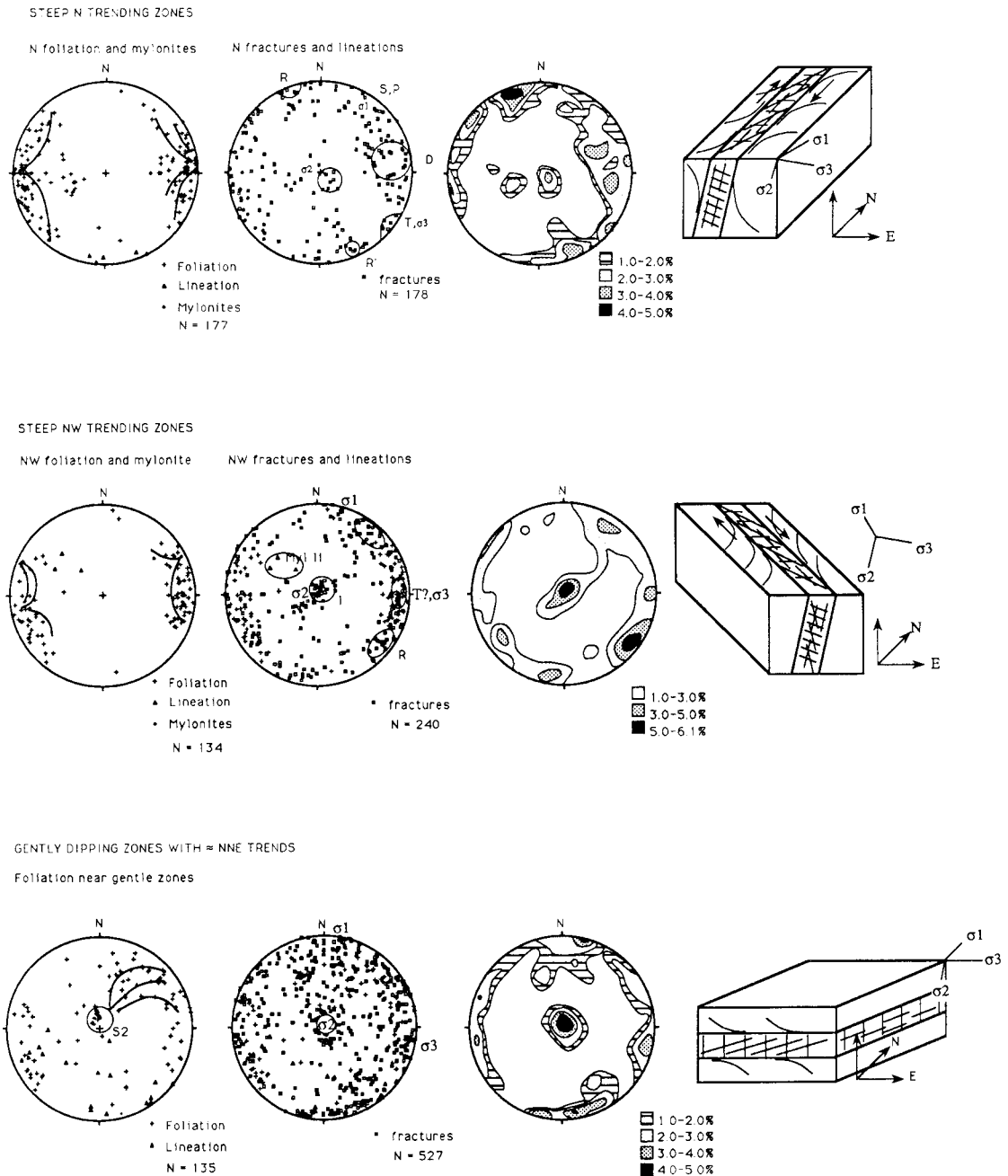


Figure 4-4. Equal-area lower-hemisphere stereograms and block diagrams showing structural data collected from major shears zones with each of the three orientation sets, data from Raymond Munier. Note how the pattern characteristic of one set also appears in the others.

vein zones. Such studies indicate that steep N-trending zones were strike-slip for most of their history, but reactivated as normal faults in greenschist facies.

Later vein infillings such as laumontite, prehnite, zeolites and calcite have been lost by solution from all the natural exposures visited. These all had to be categorised as open fractures (Figure 4-4).



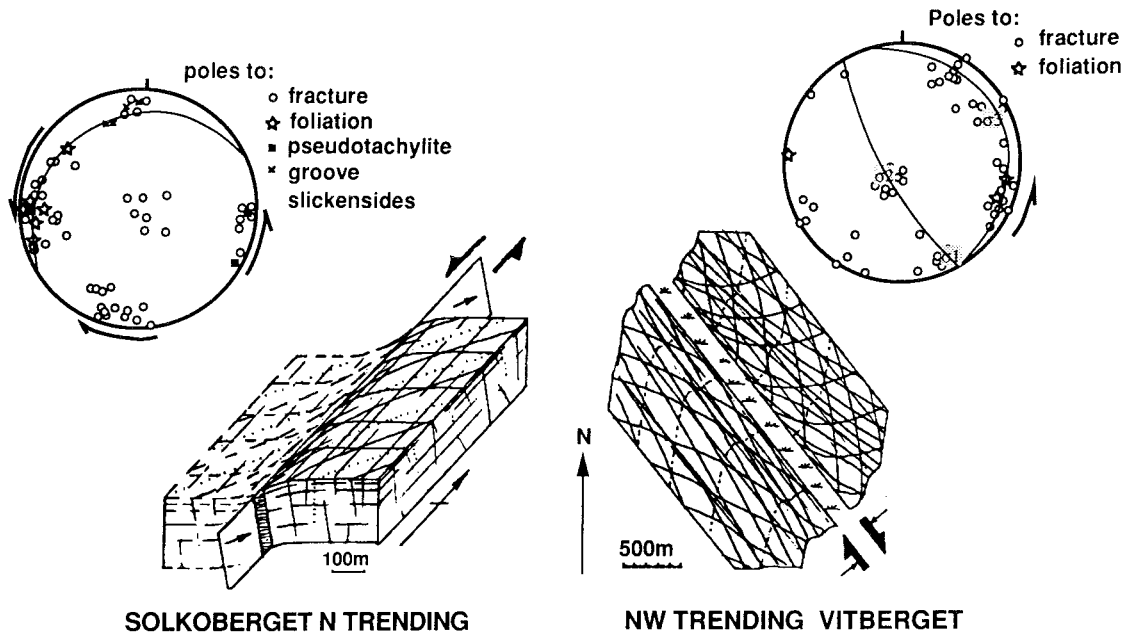


Figure 4-5. Stereograms and stylised maps showing how the orthogonal fracture sets follow the regional foliation into examples of NW and N striking shear zones, from Talbot (1986).

#### 4.4.4 Faults

Apart from the EGFs, only short segments of a few faults have been found actually exposed in the bedrock of the Lansjärv region. All appear to have played the roles of metre-scale, transpressional palm-tree structures formed in the greenschist facies.

One exposed fault thrust westward out of a N-trending, strike-slip fault duplex (near Solkoberget, Figure 4-5). Another, thrust SE out of a NW-trending strike slip fault (at Vitberget, Figure 4-5 right) and is marked by a metre or two of metabasic rocks fractured to a block volume of <1 cubic cm and extensively altered and veined by epidote and chlorite; the juxtaposed graphic granitoids are seamed by illite. A third fault is a metre-scale, transpressional strike slip imbricate zone along a NW-trending shear zone.

#### 4.4.5 Possible Fault Gouges

None of the oxidised and saturated fault breccias or gouges of the types indicated by geophysics, Henkel, this volume, seismology, Slunga, this volume, and holes drilled into the Lansjärv fault system, Stanfors et al., this volume, have been found exposed in the Lansjärv region. Such zones of dilational cataclasis are assumed to have developed by near-surface Phanerozoic-Recent reactivations. Saturated grain flow in such gouges are inferred to allow the current aseismic strike-slip displacements. All are hidden beneath the soils infilling the 50—200 m wide topographic depressions which are so obvious on the maps and on the ground.

## 4.5 BLOCKS AND ORTHOGONAL JOINTS

The N & NW trending shear zones divide the Lansjärv region into a number of major blocks (Figure 4-1) with bases probably dependant on gently dipping shear zones.

Ödman (1957) and Högbom (1925) reported cubic joint patterns to be ubiquitous to all outcrops of the Lina granite in Norrbotten. This study found one of two orthogonal joint patterns not only in the Lina granitoids, but in ALL the exposed rocks visited in the Lansjärv region. Orthogonal fracture patterns occur not only in the blocks (where individual joint blocks can reach volumes >30 cubic metres), but also in the shear zones, where they join shear-induced fractures to locally decrease the block volume below cubic cms, Tälbot (1986). Block volumes also decrease to the free surface, particularly in the hills.

A stereogram showing poles to joints measured throughout the Lansjärv region would obscure a general simplicity: only three orthogonal joint sets are usual in most outcrops. Such orthogonal patterns conform to one of two general orientations. In every outcrop, one of the three orthogonal joint sets parallels any foliation, another parallels the local free surface, and the third is close to perpendicular to the other two. Subhorizontal fractures are ubiquitous to all outcrops in the region.

Poles to joints measured near the NW-trending shear zones are shown on the upper stereogram on Figure 4-1 and poles to joints measured near the N-trending zones are shown on the lower stereogram on Figure 4-1. The subvertical fractures with NNE and ESE-trends found in the blocks are sufficiently similar in orientation to those in the N-trending shear zones for them to be treated as a single common pattern. This underlying pattern has a nearly constant orientation over most parts of the region studied (Figure 4-1). It varies only along NW-trending shear zones and near the summits of rounded hills.

The second orthogonal joint pattern consists of subvertical fractures with NW and NE-trends. This pattern is confined to comparatively narrow zones along the ductile NW trending shear zones (Figure 4-1). Very few exposures display elements of both orthogonal patterns although many other sets are present in the shear zones themselves. Two orthogonal fracture patterns with orientations similar to those in the Lansjärv region are known in SE Sweden, Tiren and Beckholmen (1988); the only significant difference in SE Sweden appears to be that both orthogonal joint sets are general and the NW-NE pattern does not seem to be as clearly concentrated to NW shear zones as in the Lansjärv region.

Epidote coats a few examples of the E to ENE subvertical fracture set within N-trending shear zones, and chlorite fills some examples of all sets in artificial excavations in the same zones. Such infillings indicate that some orthogonal fractures began to open, at least in the shear zones, while they were still in the greenschist facies. It is not known whether they began to form as early in the NW shears or in the intervening blocks.

Variations in the orientation of joints with relief is particularly obvious on the rounded summits of monadnocks above the highest marine shore line. Joint sets are everywhere parallel and perpendicular to the local free surface on such bare hills. Other symptoms of stress-relief jointing (banking) are present: all three orthogonal sets become less planar as their spacings decrease towards the nearest (subvertical or subhorizontal) free surface.

The two orthogonal joint patterns in the Lansjärv region are attributed here to the relief of in-situ stresses as the rocks approached exposure at c.1-0.6 Ga. (Close to Övertorneå in the BBSZ, a single (Cambrian?) clastic dike trends 060 degrees, dips 80 degrees SE, and reaches at least 12 m below the top of a granite cliff; this appears to be the first report of a clastic dike in Northern Sweden, Henkel, pers. comm. (1988). Fractures in the "subhorizontal" set commonly dip

up to 20 degrees. This suggests that, although the first stress relief was predominantly upward, the planar mechanical anisotropy in the fabric of the jointing rock mass (the foliation) had even more influence than the free surface. Thereafter, the principal axes of in-situ stress swapped in sign twice to induce extensional failure in two sets of joints orthogonal to both the foliation and the free surface. In areas where the foliation and free surfaces are not parallel, the initial significance of the foliation appears to diminish with block size so that the youngest fractures parallel the free surface in preference to the foliation.

Where the foliation in the blocks intensifies and rotates into any of the shear zones, all three orthogonal joint sets remain generally orthogonal to the foliation and curve with it (Figure 4-5). Talbot (1986) considered that such rotation of the joint sets into shears could indicate later ductile shearing of older joints. It is now considered more likely that younger stress-relief joints were merely guided by the orientation of the pre-existing mechanical anisotropy.

#### **4.6 REPEATED EPISODIC REACTIVATIONS WITH UNKNOWN TIMING**

Both the 1.8–1.9 Ga (Svecokarelian) and the c.1.7 Ga crustal building events in the Lansjärv region imposed pervasive foliations at (upper?) amphibolite metamorphic facies. The NS shear zones were initiated before 1.7 Ga, and the NW zones after 1.7 Ga; whether the gently dipping zones were initiated before or at 1.7 Ga is unclear (Figure 4-6). The region continued to strain after 1.7 Ga, but this became less obvious as the cooling and stiffening rock-mass partitioned the bulk strains into increasingly localised zones of shear.

Successive episodes of regional strain became less penetrative with decreasing metamorphic grade and, by inference, decreasing depth and age. Both the individual structures and, to a lesser extent, the zones defined by them, tended to narrow with decreasing temperature during compressional ductile shear and then to widen again during brittle dilational shear.

The most localised zones of amphibolite gneissose shear are at least 10–100s m wide. Later movements along these zones resulted in individual mylonites typically only a few m wide; these mylonites anastomose along zones about 50 m wide (Figure 4-6). Most veins of greenschist facies minerals are cm wide and the zones containing them appear to be still narrower than any precursor ductile shear zones. The narrowest individual shears are mm thick pseudotachylites, but these are so rarely recognised it is not known if these anastomose along broad zones. By contrast, brittle dilations later widened individual shear zones. Exposed zones of decreased block volume due to brittle shear failure are usually wider than the individual mylonites but narrower than zones defined by the anastomosing mylonite strands (Figure 4-6).

Much the same zones of shear reactivated again and again, but the kinematics varied, and not all individual components reactivated each time.

There are indications of strains in every metamorphic facies at various localities in all three sets of major shear zones. Slickensides with a variety of orientations in the same vein infilling (eg epidote) provide abundant evidence for several reactivations in the same metamorphic facies. This does not necessarily mean that the region strained either continuously or at constant rate. However, the constraints on temperature with time (or ages of infilling) are so poor that such possibilities cannot be excluded. Rather, the general picture is more likely to be of episodes with different kinematics occurring as oceans opened and closed elsewhere.

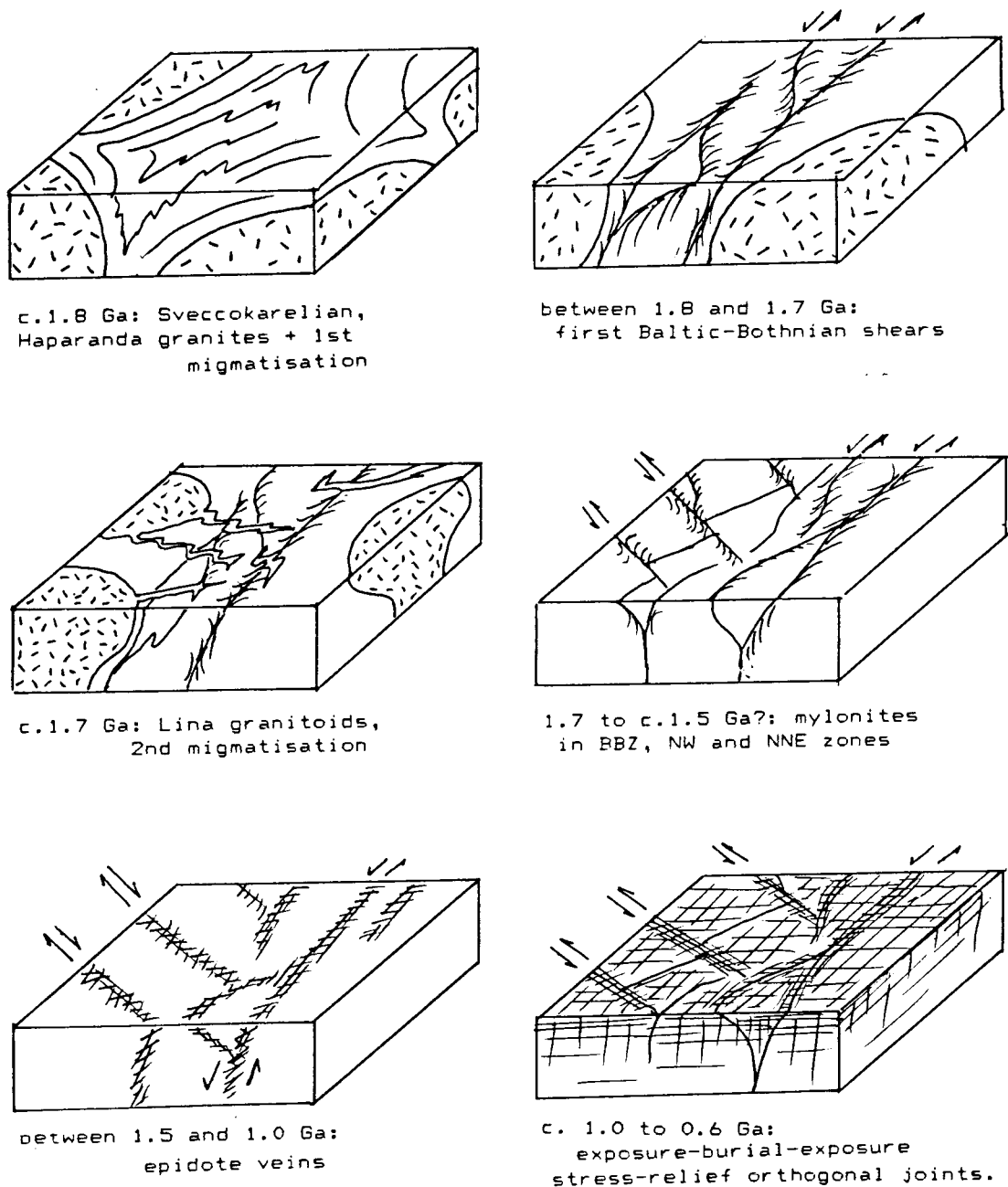


Figure 4-6. Cartoon indicating the histories of the shear zones and how they narrowed during reactivations at decreasing metamorphic grade during unroofing in the Lansjärv region.

Particular elements of the pre-existing dislocation pattern, but not necessarily the whole pattern, reactivated many times. Not all the shear zones active at one metamorphic grade were active at another. Some of the early gneissose shears, like some of the mylonitic zones, show few signs of veining or later fractures. Some of the early zones of ductile shear therefore have never reactivated after they cooled below greenschist facies.

To a lesser extent, successive reactivations tended to add minor new elements to the dislocation pattern. Many zones of veins or fractures are not superim-

posed on earlier zones of ductile strain. The poor correlation between the locations of individual zones of ductile shear fabrics, vein systems, fracture zones, and hydrological conductors in Borehole J1 demonstrate that new fractures must have developed new zones in brittle conditions. Veins and fracture zones can apparently spread through shear pods defined by older mylonites or faults; they probably developed to break through local “locks” or pod-jams within the regional dislocation pattern.

Alteration and slickensided mineral infillings indicate that most of the fractures exposed in the EGF scarps and associated minor pop-ups reactivated old fractures, Talbot (1986), Henkel, this volume. However, whether particular fractures are 1 Ga, or only 9 000 years old, cannot always be determined by visual inspection. Discriminating tools or criteria are needed to distinguish old from recent fractures.

## 4.7 DISPLACEMENT LINKAGE

The strains that a fractured body can undergo depend on the orientations and spacings of its internal dislocations. A set of dislocations with a single orientation allows only a simple shear. Dislocations with two sets of appropriate orientations allow only small biaxial strains; three orientations are necessary for significant biaxial bulk strains. Dislocations with at least five orientations are necessary for significant triaxial strains, eg. Angelier (1979).

The dislocations in the Lansjärv region appear to have been part of a single kinematically linked pattern on the regional scale throughout the last 1.7 Ga. This is illustrated by the general similarities of:

- \* fabrics and structures in shears of all three orientations
- \* at every distinguishable metamorphic grade,
- \* the fact that elements of shears with all three orientations have been found in shears of every other orientation (see Figures 4-2, 4-4 and 4-6).
- \* contemporaneous kinematics appear to have been compatible at equivalent metamorphic grades.

This linkage is amply illustrated by the end-glacial displacements in different parts of the Lansjärv EGF fault system. In one event, Lagerbäck, this volume, thrusts with NNE to NE-strikes and SE-ESE-dips ranging from 10—30 degrees (Figures 4-2, 4-3 and 4-7) moved tens of metres in the same event as 80 degree E or ESE-dipping left-handed oblique-reverse faults, and left-handed strike-slip occurred along the NW-trending sidewall of Risträskkölen (Figure 4-7). These contemporaneous displacements allowed the Lansjärv region to shorten tens of metres along a general subhorizontal WNW axis (Figure 4-7) during a single c.Ms 7 to 8 earthquake about 9,000 years ago, Lagerbäck (1979), Talbot (1986), Muir Wood, in press.

The thrust displacements are obvious because they offset the low glacial relief. However, not obvious are the equally large contemporaneous strike-slip fault displacements suggested by both the general kinematics of the linked dislocation pattern and the locations and solutions of current earthquakes. Quite large strike-slip displacements would not be discernable in the loose glacial soils with their low relief.

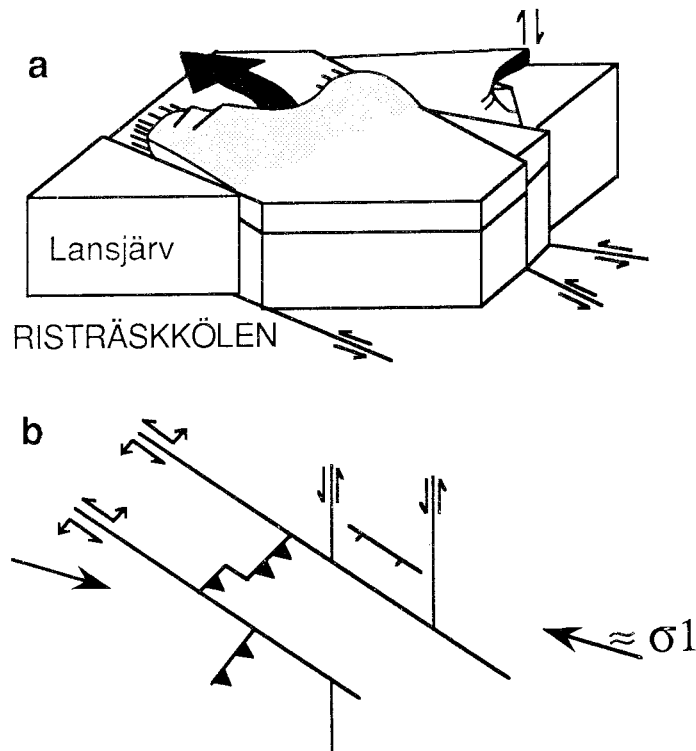


Figure 4-7. a: Block diagram of a particular part of the Lansjärv EGF fault system indicating the linage likely between faults of all three main orientations in one unusually major increment about 9 000 years ago.  
 b: Diagram indicating current kinematics indicated by structural geology, seismology, and in-situ stress determinations.

#### 4.8 DYNAMICS

Until recently the dynamics of the 500 km or so of EGFs in Lapland were attributed to post-glacial recovery uplift. However, instead of the horizontal extension radial or concentric to contours of uplift-rate expected of this model, shortening occurred across old faults with inappropriate orientations. The NNE or NE reverse faults or thrusts cross the contours of post-glacial uplift-rate. Instead of fitting the post-glacial uplift pattern, the kinematics of the EGFs + linked-faults and current seismicity appear to be part of a Fennoscandian-wide pattern which relates active faulting to the lithospheric plate margins. Corridors of differential NW strike-slip cross the European lithosphere between offsets in the active margins in the opening mid-Atlantic and shortening Mediterranean-Himalayan plate margins, Talbot and Slunga (1989). This pattern is likely to have been active at least since the Atlantic started to open c.58 Ma ago, although variations record changes in plate displacement directions at 38 and 5 Ma.

The present lack of significant earthquakes beneath Greenland and Antarctica suggest that normal plate tectonic forces are suppressed and stored elastically by the load and insulation of ice sheets, Johnston (1987). The EGFs and contemporaneous landslides in Lapland can be interpreted as recording a series of major earthquakes as the last ice front retreated c.2 000 km in about as many years, Lagerbäck, this volume, Muir Wood, in press, Talbot (1986), Talbot and Slunga (1989). The rapid unloading and escape of large volumes of melt water under high hydraulic head could have led to the sudden release of long-term plate tectonic strains stored in the Fennoscandian lithosphere. Similar major earthquakes presumably accompanied the melting of earlier Quaternary

ice sheets and will presumably accompany the next, c.40 000 to 80 000 years in the future?: Björk, in press.

If the present seismicity, Slunga, this volume and Wahlström, this volume, is typical of time intervals between ice sheets, it probably characterises the neotectonic strains of Fennoscandia through most of the opening of the Atlantic during the last c.58 Ma. Seismic solutions and structural geology combine to indicate largely left-handed strike slip along the old N- and NW-trending shear zones, shortening at shallow depths along the old NE-trending thrusts or reverse faults, and extension across old faults paralleling the maximum horizontal compression axis ( $\sigma_1$ ). The sense of displacement along the pattern of EGFs suggests that the end-glacial sigma 1 generally trended approximately NW horizontal and that sigma 2 was horizontal NE. This picture is also reinforced by in-situ stress determinations, Bjarnason, this volume. Swapping or rotation of the principal stress axes occurs at levels where intense breakage by reactivation de-stresses sigma 1, or even sigma 2, below the vertical load.

Current seismicity indicates that some of the Proterozoic shears are still active. Although the current kinematics are similar to those during long periods of their history, present seismic activity appears to be noticeably less violent than during the melting of the Quaternary ice sheet(s). Active displacements in the uppermost 3—5 km of the Lansjärv region, Slunga, this volume, probably occur by aseismic granular flow in saturated clay-gouges out of sight beneath the soils hiding the most fractured shear zones. End-glacial thrust displacements are obvious in the low relief glacial surface of Lappland, but suspected, equally large, contemporaneous strike-slip fault displacements are not so recognizable. The lack of appropriate geological strain markers means that only direct measurement can determine whether the strike-slip faults in Sweden are as active as the Egersund fault in southern Norway. This currently undergoes a vertical displacement of 1.7 (+/-0.3) mm/a, Bakkelid (1988) even though its principal displacements are probably strike-slip.

## 4.9 REFERENCES

### **Angelier J 1979**

Determination of the mean principal direction of stress for a given fault population.

Tectonophysics, 56, T17-T26

### **Bakkelid S 1988**

Statens Kartverk's engagement in active fault localization. PPPL report 1988.

Inst. of Geol. S-106 91 Stockholm, PP 46-50

### **Berthelsen A and Marker M 1986**

1.9-1.8 Ga old strike slip meagshears in the Baltic shield and their plate tectonic implications.

Tectonophysics, 128, 163-181

### **Björk S in press**

Pleistocene climatic changes and consequences for radioactive waste disposal.

Geol. Fören. Stockholm Förh

### **Henkel H 1979**

Dislocation sets in northern Sweden.

Geol. Fören. Stockholm Förh. 100, 271—278

**Henkel H 1988**

Tectonic studies in the Lansjärv area.  
SKB TR 88-07

**Högbom I 1925**

Der Berg Luppjo. Bull Geol.  
Inst of Uppsala, Vol XIX

**Johnston A C 1987**

Suppression of earthquakes by large continental ice sheets. Nature, 330, 467—469

**Lagerbäck R 1979**

Neotectonic structures in northern Sweden.  
Geol. Fören. Stockholm Förh, 100, 263—269

**Muir Wood R 1989**

Extraordinary deglaciation reverse faulting in northern Fennoscandia. In Gregersen & P W Basham (Eds): Earthquakes at North-Atlantic passive margins: Neotectonics and postglacial rebound. 143—174, Kluwer Academic Publishers, Netherlands

**Skiöld T 1982**

Radiometric ages of plutonic and hyperbyssal rocks from the Vittangi-Karesuando area, N Sweden.  
Geol. Fören. Stockholm Förh. 103, 317—329

**Talbot C J 1986**

A preliminary structural analysis of the Patterns of post-glacial faults in northern Sweden.  
SKB TR 86-20

**Talbot C J & Slunga R 1989**

Patterns of active shear in Fennoscandia, IN S. Gregersen & P W Basham (Eds): Earthquakes at North-Atlantic Passive margins: Neotectonics and postglacial rebound. 441—466, Kluwer Academic Publishers, Netherlands

**Talbot C J, Riad L and Munier R in prep**

The geological structures and tectonic history of the Lansjärv region, N. Sweden.

**Tiren S A, Beckholmen M 1988**

Structural analysis of contoured maps of Äspö and Ävrö, Simpevarp area, SE Sweden.  
SKB PR 25-87-22.

**Ödman O H 1957**

Beskrivning till berggrundskarta över urberget i Norrbottens Län.  
SGU ser. Ca Nr 41





# 5 ANALYSIS OF THE EARTHQUAKE MECHANISMS IN THE NORRBOTTEN AREA

*Ragnar Slunga*

Inst. for hydroacoustics and seismology, Foa 26,  
National defence research institute  
S-102 54 Stockholm, Sweden

## 5.1 INTRODUCTION

Within the SKB project at Lansjärv the earthquakes play a key role: they show directly the present tectonic movements of the faults in the area. Therefore seismic networks for earthquake monitoring were established and operated as part of the project. Foa (National defence research institute) established a permanent network of six stations distributed up to 100 km from the Lansjärv faults while Uppsala University during the summer halfyears has operated mobile stations closer to the faults. This chapter about earthquake mechanisms is based on the recordings collected by the permanent Foa network, Slunga (1989a), this volume.

The Foa network consisted of six stations equipped with 1 Hz vertical seismometers (type S-13). The signals were frequency-modulated and continuously transmitted on permanent telephone lines to the computer at Stockholm. The signals were continuously sampled (12 bit) at a rate of 60 Hz. Automatic detection and event location algorithms were used.

## 5.2 THE EARTHQUAKES OCT 1987 – FEB 1989

Up to February 1989 more than 90 earthquakes with signals at three or more stations have been recorded and analysed. Figure 5-1 shows the locations of the earthquakes. The magnitudes were in the range  $M_L$  0.1–3.6.

The relation to the previous seismicity is shown in Figure 5-2.

## 5.3 FOCAL DEPTHS

Figure 5-3 shows the estimated focal depth distribution.

One can divide the crust in at least three layers, the upper crust 0–15 km with the highest earthquake frequency, the middle crust 15–35 km with a lower activity rate, and the completely aseismic lower crust 35–45 km. In estimating the focal depth distribution the estimated uncertainties of the focal depth determination have been included. The uncertainties depend on the location of the epicenter in relation to the network and on the focal depth. Typically the estimated standard deviations are 1–3 km.

In Southwestern Sweden the boundary between the more active upper crust and the middle crust is 5 km deeper than for Northern Scandinavia as shown in Figure 5-3 (20 km instead of 15 km).

The drop in seismic activity at 15 km may indicate a lithologic boundary or structural boundary, the drop at 35 km (found also in Southwestern Sweden) is most probably a temperature dependent boundary.

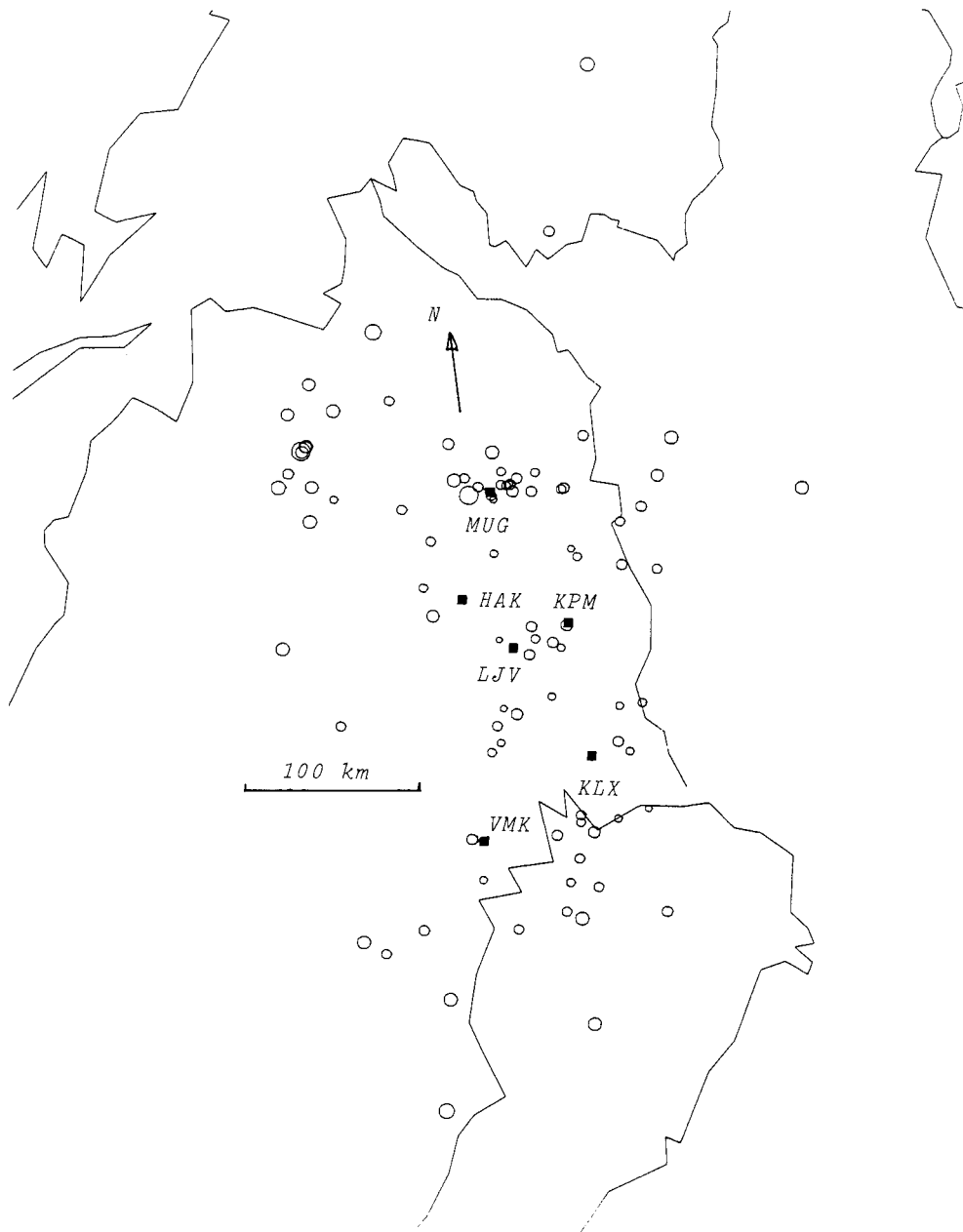


Figure 5-1. The earthquakes detected by the permanent network during the time interval Oct 1987 – Feb 1989. The solid squares show the positions of the six vertical seismometers constituting the permanent Foa network operated within this project.

An interesting similarity between the southern Sweden and northern Sweden seismic activity exists: the b-value (for the Gutenberg cumulative size distribution) is lower for the middle crust than for the upper crust. In both cases there seems to be more larger events (above about  $M_L=3$ ) in middle crust and more smaller events (less than  $M_L=3$ ) in the upper crust. See further paragraph 5.4.1.

There is no clear indication of variation of the size of the stress drop with focal depth for the earthquakes of the same size. See further paragraph 5.4.2.

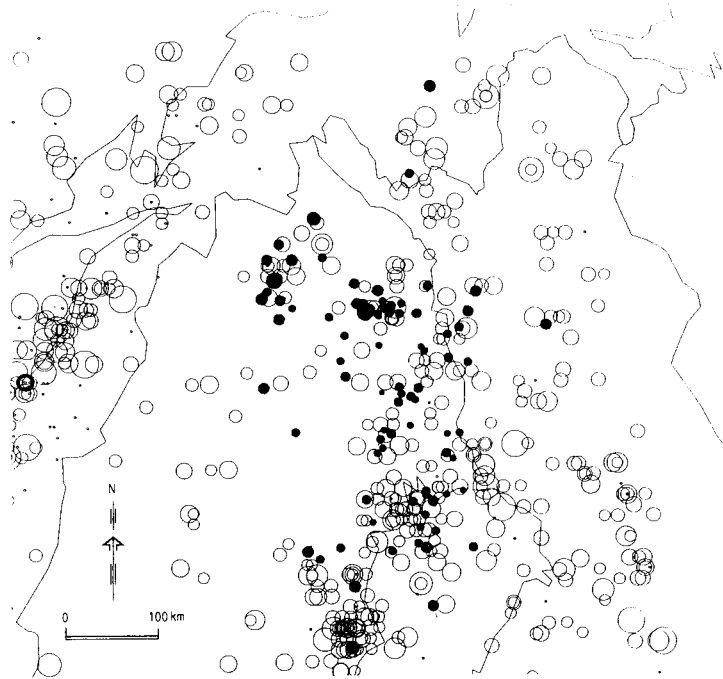


Figure 5-2. The earthquakes detected by the permanent network in operation within this project are shown by solid circles. The previous earthquakes of the area as given by FENCAT (1987) are shown by the open circles.

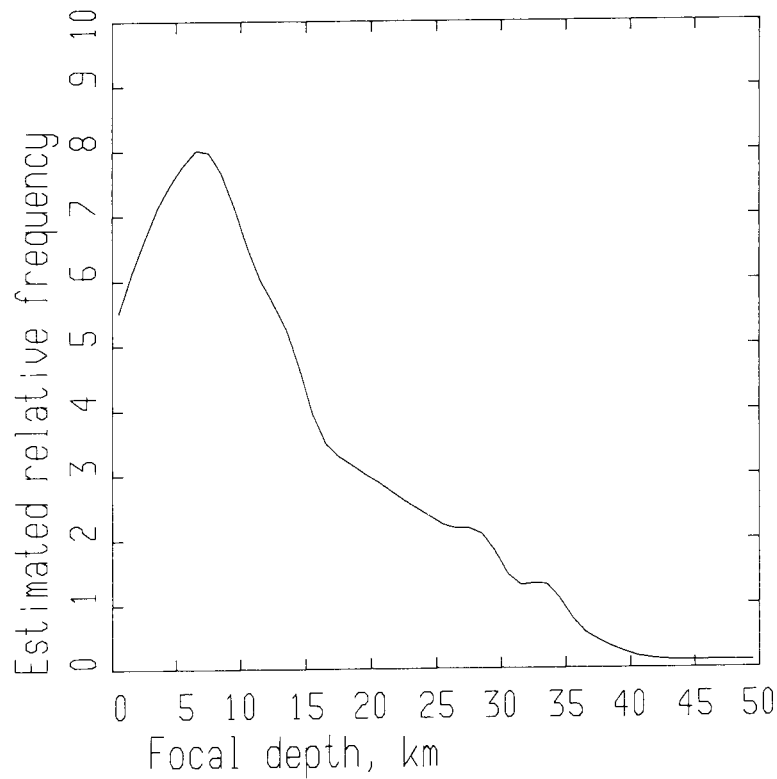


Figure 5-3. The estimated focal depth distribution for the earthquakes detected and located by the Foa network. The uncertainties of the depth estimates have been included in the estimate of the distribution.

## 5.4 THE EARTHQUAKE MECHANISMS

The earthquake source mechanisms has been analysed based on the following assumptions:

- they are pure shear slip of planar surfaces
- the slip direction is the same over the whole earthquake fault surface and do not change during the slip (unidirectional slip),
- the corner frequencies are related to the size of the fault surface (circular) in the way found by numerical shear dislocation models, Savage (1974), Madariaga (1976), Boatwright (1980), Silver (1983).

Thus the mathematical double-couple point dislocation model was assumed for the wave radiation from the earthquakes. With the given assumptions the low frequency amplitude spectrum level of the waves will be proportional to the seismic moment (the product of shear modulus, faulting surface area, and size of the shear slip), Ben-Menahem and Singh (1972, 1981), Slunga (1981a, 1982).

### 5.4.1 The Seismic Moments and Magnitudes

I estimate the seismic moment ( $M_o$ ) together with the fault plane solution, that means the source orientation is also considered, Slunga (1981a, 1982). The local magnitude ( $M_L$ ) is computed from the seismic moment by the formula:

$$M_L = 10\log(M_o) - 10, \text{ where } M_o \text{ is expressed in Nm.}$$

This formula is valid up to  $M_L=3.5$ , Slunga (1982), Slunga, Norrman and Glans (1984), and gives magnitude values in agreement with Wahlström (1978).

The distribution of the seismic moments are shown in Figure 5-4. The very irregular curves may have several explanations. The geographical area included has very varying seismicity and detection threshold and there have been long windy periods with quite different noise conditions. The data shown in Figure 5-4 indicate that the middle crust has a smaller b-value (slope of the curve defined by the circles) than the upper crust. This is very similar to the situation known for the southern Sweden earthquakes, Slunga et al (1984). The crossover between the cumulative curves for upper and middle crust is at  $M_L=3-3.5$  ( $M_o=1.E+13$  Nm) both in northern and southern Sweden. At magnitudes larger than the crossover earthquakes are more common in the middle crust.

### 5.4.2 Size of the Faulting Area, Static Stress Drop, and Size of the Shear Slip

Circular extension of the fault areas have been assumed for the study. The estimated radii are given in Figure 5-5. We see that earthquakes larger than  $M_L=2$  (seismic moment  $M_o=1.E+12$  Nm) have fault radii larger than 100 m. Smaller estimated fault radii are common for events smaller than  $M_L=2$ . The scatter is large and the estimated radii are independent of the seismic moment for magnitudes less than  $M_L$  2.5.

The estimated static stress drops are given in Figure 5-6. Note the strong correlation between the size (the logarithm of seismic moment,  $M_o$ ) and the logarithm of the static stress drop. One possible qualitative explanation is that the size variation of these small earthquakes is mainly due to variation in effective normal pressure (for instance at corners of blocks). This could be true at least up to  $M_L=2-3$ , above that the correlation between seismic moment and static stress drop is weaker.

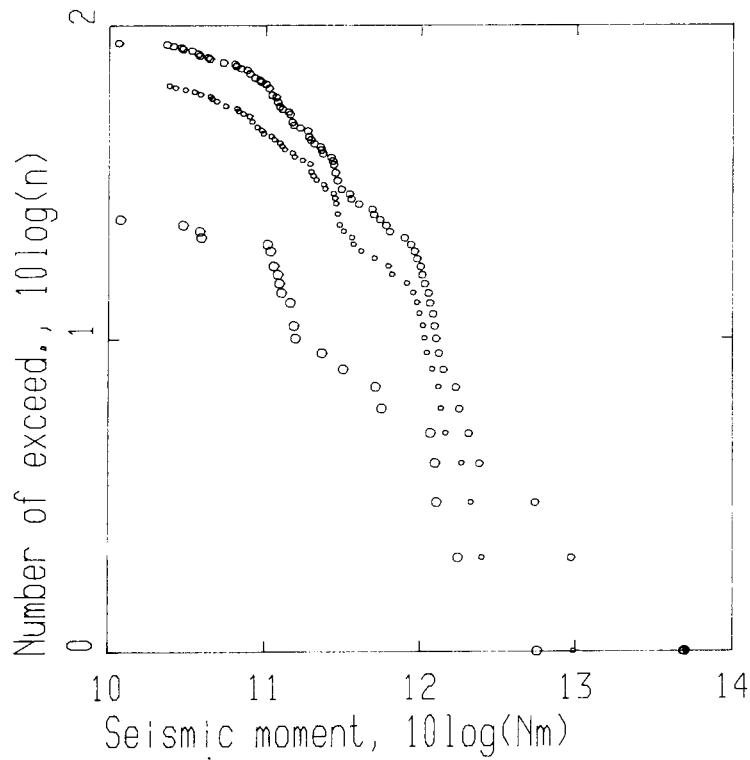


Figure 5-4. The distribution of the seismic moments given in the form of Gutenberg curves (number of events exceeding the value given by the seismic moment axis). The lower (large) circles pertain to earthquakes deeper than 15 km (middle crust), the smallest circles pertain to earthquakes in the upper crust (0–15 km), while the upper medium size circles shows all earthquakes.

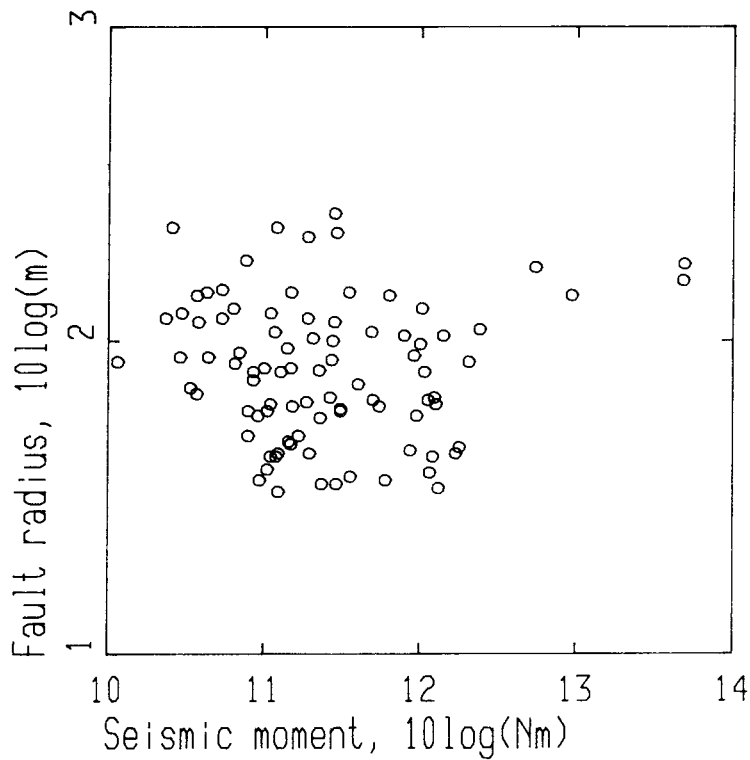


Figure 5-5. The fault radii as function of the seismic moment. Each point is one earthquake. Above  $M_L=2$  (seismic moment  $M_o=1.E+12 Nm$  or  $10 \log(M_o)=12$ ) the fault radii are typically larger than 100 m.

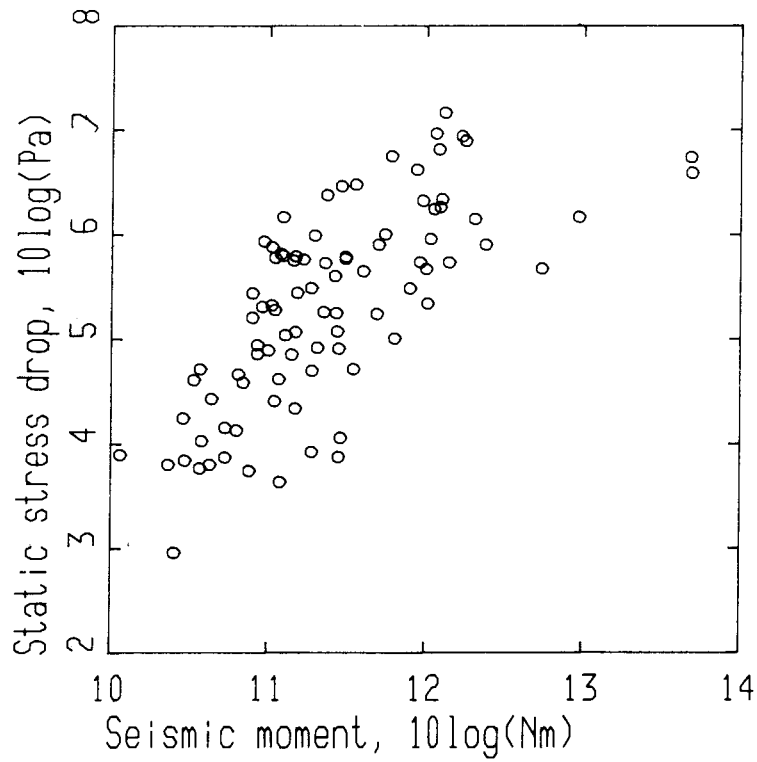


Figure 5-6. Estimated static stress drop, each point is one earthquake. Logarithmic scales are used.

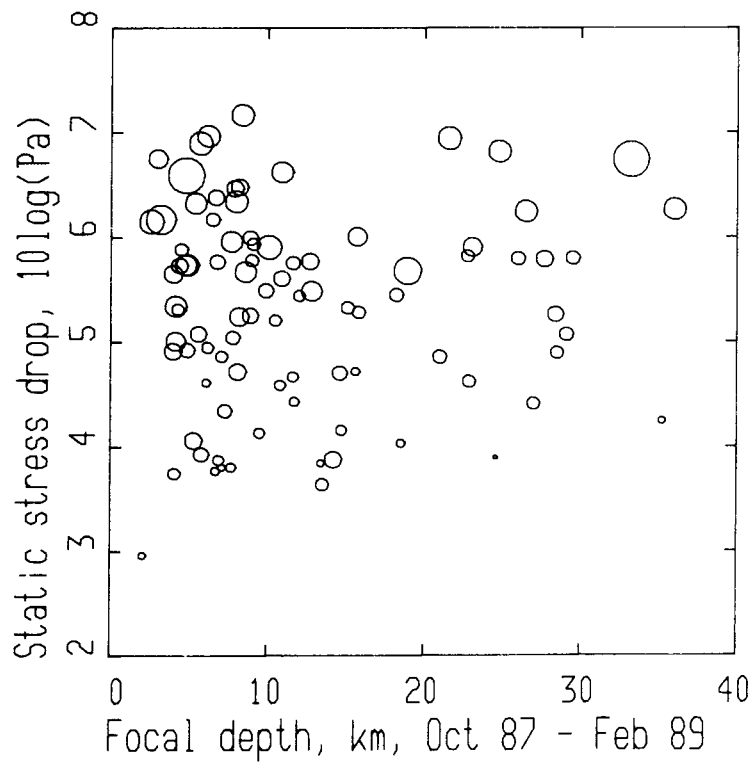


Figure 5-7. Estimated static stress drop and focal depth. Each circle is one earthquake. The size of the circle shows the earthquake magnitude (from  $M_L$  0.1 to 3.6).

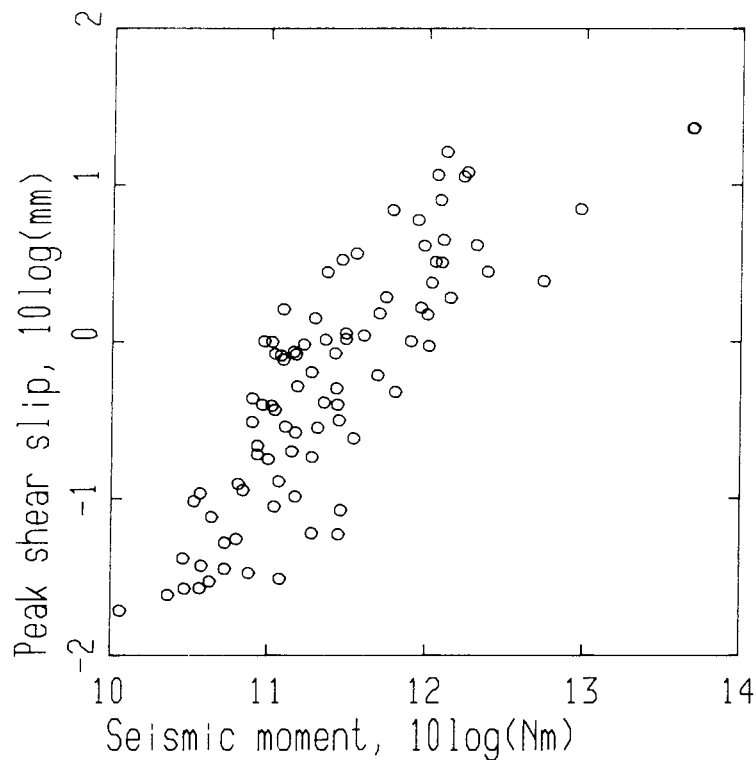


Figure 5-8. Estimated peak shear slip, each circle is one earthquake. For the alternative view on the Baltic shield seismicity, presented by Slunga (1989) and discussed in paragraph 5.5 below, this may be the tectonically most interesting dynamic parameter of these small earthquakes.

As seen in Figure 5-7 there is no obvious correlation between earthquake depth and static stress drop. This supports the idea presented above that the size variation up to  $M_L=2-3$  is mainly due to variation in the effective normal stress across the fault at the point of the earthquake (at the asperity). The lithostatic pressure may then be part of the explanation to why smaller events are relatively less common in the middle crust than in the upper crust.

The estimated peak shear slips are shown in Figure 5-8. For  $M_L=1-2$  the mean value is about 1 mm. Above  $M_L=3$  ( $\log M_o = 13$ ) the peak slip is 5–20 mm.

### 5.4.3 The Fault Plane Solutions

The fault plane solution is the description of the fault plane orientation and the direction of the shear slip across this plane. Due to a fundamental nonuniqueness of the double-couple point source description the fault plane solution consists of two possible fault planes at right angle to each other. Further the slip of one plane is in the other plane. What is unique (theoretically) is the orientation of the deviatoric stresses released by the earthquake slip. This stress is defined by the orientations of the P-axis (pressure) and T-axis (tension). These axes are at 45 degree angle to the two possible fault planes. The principal rock stresses are not at all well constrained by the fault plane solution. If one is interested in the orientation of the horizontal deviatoric stresses strikeslip earthquakes on subvertical faults give best constraints. It is also obvious that in the long run the stress release should equal the stress buildup. One complication is given by the possibility that by far most of the fault movements (more than 10000 times more according to Slunga (1989b) are aseismic, see further paragraph 5.5 below.



## Northern Sweden earthquakes

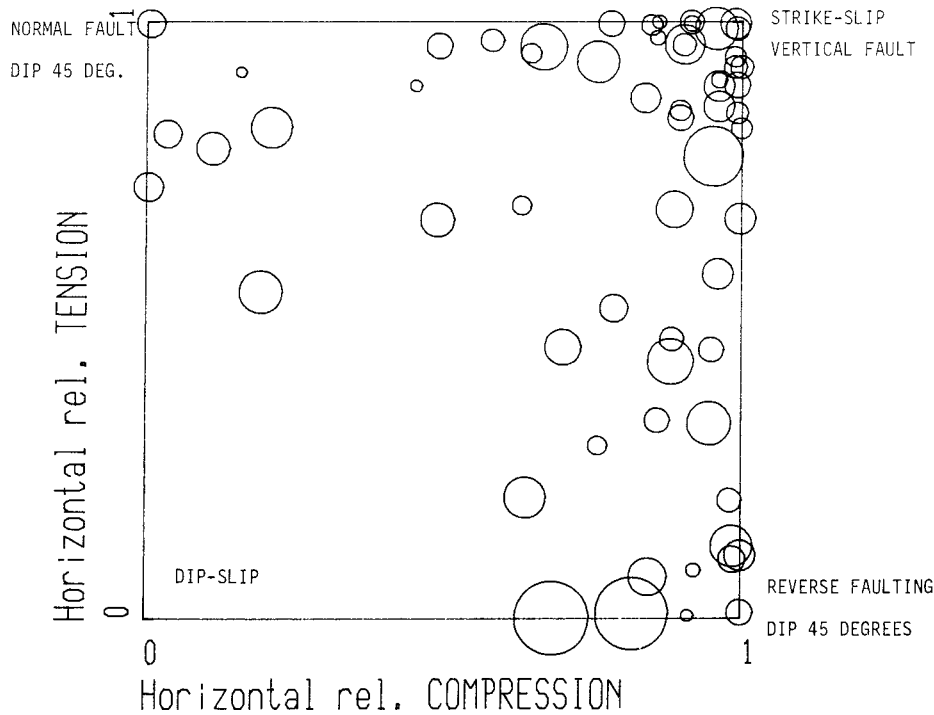


Figure 5-9. Mechanisms of earthquakes in Northern Sweden. Each circle denotes one earthquake.

There are thus fundamental possibilities of large discrepancies between the true rock conditions and what seismically can be observed.

Figure 5-9 shows the fault plane mechanisms for the best constrained earthquakes in Norrbotten. One can see that the largest cluster is at the strike-slip corner but that both normal faulting and reverse faulting is common. The number of reverse faulting events is larger than the number of normal faulting, and the two largest events ( $M_L=3.6$ ) are both close to the reverse faulting corner. This is a very interesting result for the Lansjärv project. It supports the view that the present tectonic activity is the same as the tectonic activity which built up the reverse stresses released during the deglaciation and manifested in the extensive neotectonic faulting, Lagerbäck (1979), Lagerbäck and Witschard (1983), Henkel et al (1983), Henkel (1988).

Another interesting observation from Figure 5-9 is that there are few events close to the dip-slip corner. This illustrates that it is the horizontal plate movements and deformations, and not the land uplift, that is the primary cause of the northern Sweden seismic activity.

Where an earthquake will be placed depends on the orientation of its best fitting fault plane solution (on the directions of its P- and T-axes). The horizontal axis shows the relative size of the horizontal compression of the stress released by the earthquake, the vertical axis shows corresponding horizontal tension. Each corner corresponds to different "pure" mechanisms: dip-slip (one vertical and one horizontal of the two possible fault planes), strike-slip (both planes horizontal), normal faulting (both planes at 45 deg from the vertical, tension), and reverse faulting (again both planes 45 deg from the vertical, compression). The concept of relative size of the horizontal stresses is introduced by Slunga (1981b) and described further by Slunga et al (1984).

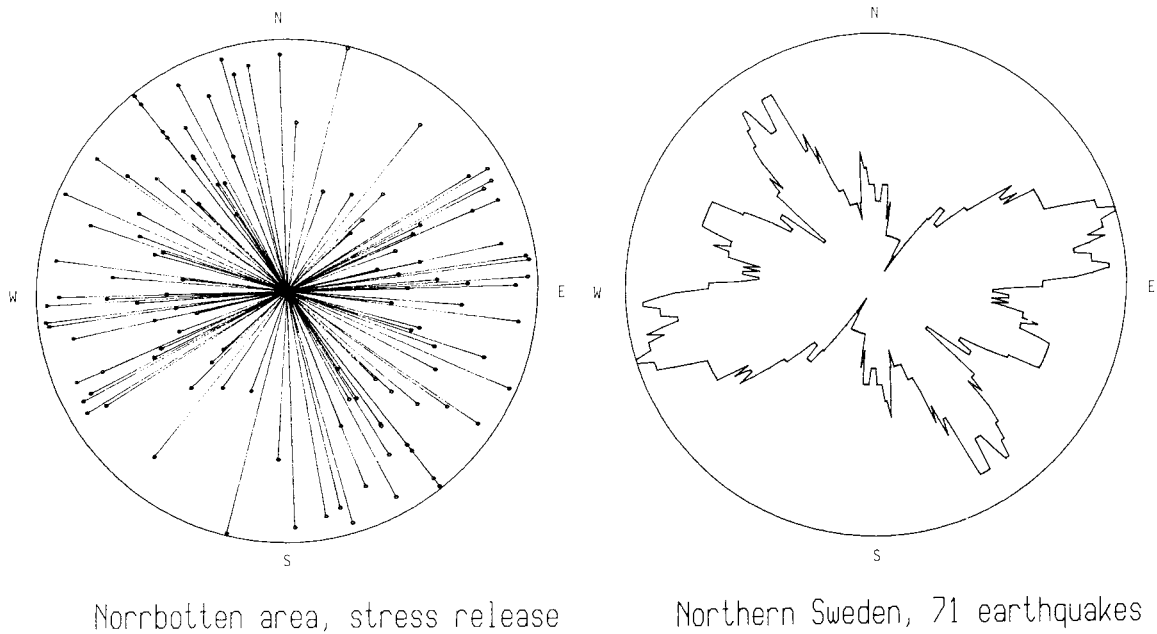


Figure 5-10. The orientation and relative size of the horizontal deviatoric stress released by the earthquake. The two figures show the same data (Norrbotten is the Swedish name of Northern Sweden). The lines in the left figure are in the direction of the principal compression. Each line is computed from the best fitting fault plane solution of an earthquake. To the right the circular frequency of the direction of the principal compression of the released stresses.

#### 5.4.4 The Horizontal Stresses

Figure 5-10 shows the orientation and relative size of the horizontal deviatoric stresses that have been released by the seismic slips. These stresses are defined by the fault plane solution and pertain to the best fitting fault plane solution for each earthquake. The concept “relative size of the horizontal deviatoric stress” is fully described by Slunga et al (1984) and was introduced into the discussion of earthquake stress release by Slunga (1981b).

### 5.5 THE SPATIAL DISTRIBUTION AND EXTENT OF ASEISMIC SLIDING

One of the most interesting results from the studies of the seismic activity in southern Sweden is the remarkable spatial distribution of the events, Slunga (1989). The simplest model of the Baltic shield seismic activity that will give such a spatial distribution assumes that aseismic sliding (stable sliding, creep) is extended over fault surfaces 10 000–40 000 times larger than the seismic sliding (the earthquakes). In Figure 5-11 the distribution of the distance to closest later event is shown for the Norrbotten (Northern Sweden) earthquakes. The distribution is very similar to the one from southwestern Sweden. The parameter “closest later event” was chosen because of its simpleness. For each (but the last) earthquake within the sample, in this case 80 events, the distance to the closest later event was computed. The distribution of this parameter is the ir-

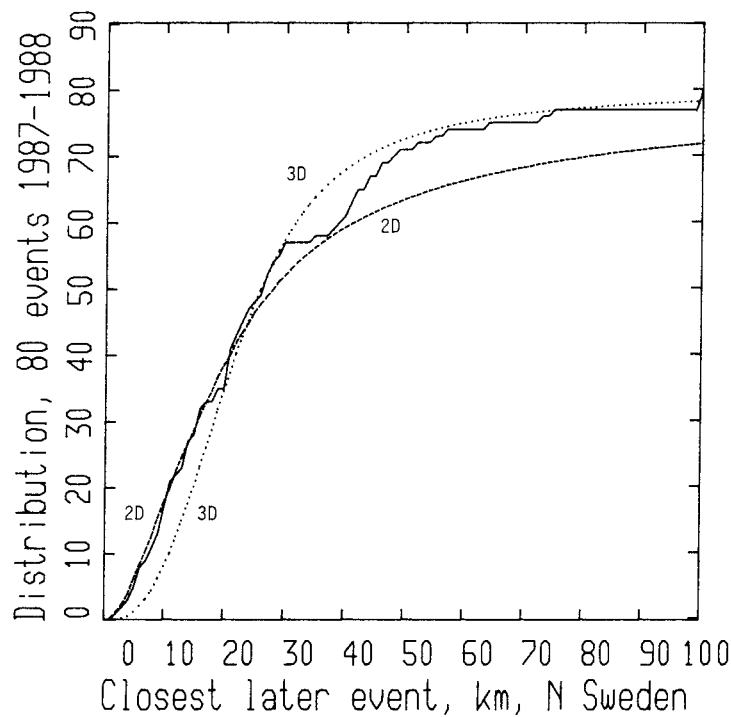


Figure 5-11. The spatial distribution of the earthquakes in Norrbotten has been studied by use of the distance to closest following event. The solid line is the observed distribution for 80 events. The dashed line with a good fit at small distances is the theoretically expected distribution if the earthquakes have a laterally homogeneous distribution on a plane (through the hypocenter). The dotted curve is the theoretical expected distribution for laterally homogeneous 3D-distribution. The 3D-curve gives a good fit at 20–30 km.

regular curve in Figure 5-11. The corresponding statistically expected distribution curves for 80 events laterally uniformly two-dimensionally and three-dimensionally distributed are given by the smooth curves.

One sees from Figure 5-11 that:

- in the range 20–30 km the observed distribution gives a close fit to a laterally uniform 3D-distribution; this is of course expected for distances large compared to the distances between seismically active faults, the 3D-curve has been adjusted to this part,
- there is an increased earthquake probability (compared to the laterally uniform 3D-distribution) at distances up to 17 km; an area of dimension 30–35 km thus must have been affected in such a way that an increased earthquake probability has been established,
- there is no indication of an increased activity at very small distances (less than 3 km) which would be expected if all fault movements were seismic,
- in the range 0–17 km (the range of increased activity) the observed distribution fits closely the laterally uniform 2D-distribution; thus the close events show up as distributed on planes through the hypocenter.

These observations strongly support the asperity model, namely that the earthquakes occur at locked points on fault segments that have previously slid

quietly. The locked “asperities” (possibly points of increased effective normal pressure) seems to be rather uniformly distributed over the slid fault surfaces.

In computing the theoretically expected curve of the laterally uniform 2D-distribution the only free parameter was the earthquake density per fault length, or, in terms of the asperity model, the fault length sliding stably per earthquake. The theoretical 2D-curve in Figure 5-11 corresponds to one earthquake per 21 km of fault length.

If the size of the aseismic fault sliding is assumed to equal the peak slip of the subsequent earthquake one can estimate the amount of aseismic fault sliding in comparison to the seismic sliding: a 21 km times 35 km (the thickness of the seismic crust) area is more than 20 000 times larger than the seismic surface (100 m radius). This is an important possibility in the planning of further research on the geodynamic processes in the Baltic shield crust.

## 5.6 DISCUSSION AND CONCLUSIONS

From the results of the analysis of the Norrbotten area earthquakes one can conclude:

- the seismicity indicates a three-layered crust, the upper crust 0–15 km with highest earthquake frequency, the seismically active middle crust 15–35 km, and the seismically quiet lower crust at depths exceeding 35 km,
- the stresses released by the earthquakes are in agreement with the general features of the models of global tectonics (horizontal compression in the direction of the expected “ridge push”),
- an excess of horizontal compression is indicated by the fault plane solutions, this is in agreement with what is known about the neotectonic fault movements in the area,
- the size of the fault slip (as given by the estimates of the peak shear slip of the earthquakes) is 0.1–10 mm for earthquakes in the range  $M_L=1-3$ ,
- the correlation between earthquake size (magnitude or seismic moment) and static stress drop indicates that the sizes of the earthquakes for events below magnitude  $M_L=3$  may be determined by the local effective normal pressure,
- the difference in b-value (the relation between the number of larger and smaller events) between upper and middle crust supports the view that the effective normal pressure determines the size of the earthquake,
- the spatial distribution of the earthquakes is in close agreement with what one would expect from the “asperity” model for the earthquake generation: the earthquakes are locked parts (possibly parts of increased effective normal pressure) at which shear stresses are concentrated due to aseismic slip (stable slip, “creep”) of the surrounding parts of the fault,
- for the observed spatial distribution to fit the “asperity” model it is needed that in mean about 20 km of fault length slips quietly (aseismically, stably) per detected earthquake, this means that for a good fit it is required that the total fault movements are more than 20000 times more extensive than the seismic fault movements observed during this project.

One must note that these conclusions are valid only as stated. Together they do show that the complex pattern of the seismicity is in agreement with a simple model of the generation of the earthquakes. The estimate of the only free parameter: the relation between the extension of the aseismic fault movements and the number of detected earthquakes, is rather stable. The high similarity be-

tween the spatial distributions in Norrbotten and Southwestern Sweden supports this view. Other circumstances in favour of this interpretation are:

- the consistency of the microseismicity, in itself the fault movements of a  $M_L=1$  earthquake are insignificant, still the picture given by such small events is very similar to the picture given by the events in the range  $M_L=3-5$ . With the “asperity” model the consistency is expected, the aseismic fault movements preceding the  $M_L=1$  earthquake are significant,
- geodetic measurements in the nordic countries have indicated fault movements much more extensive than indicated by the seismicity. The geodetic measurements show differential movements interpreted as fault movements with rates up to over 1 mm/year both vertically and horizontally, Talvitie (1977), Veriö (1982), Bakkelid (1986), Anundsen (1988).

The earthquake study presented here show the need of geodetic measurements to get direct constraints on the amount of aseismic fault movements. Monitoring of the earthquake activity is still of great importance in the understanding of the crustal deformations. The interpretation of geodetic observations gains quite a lot if one can point out which faults are likely to have moved and the direction of the movements.

## 5.7 REFERENCES

### **Anundsen K 1988**

Variations in Quaternary (Late Weichselian relative sea-levels in southwest Norway; observations of isostatic/eustatic movements and active faulting. Paper presented at the Neotectonics Symposium at Lejondal Sept 5–6 1988. (Karl Anundsen, Dept. of Geology, Section B, Univ. of Bergen, N-5007 Bergen, Norway).

### **Bakkelid S 1986**

The discovery in Norway of a strongly active geological fault and some of its practical consequences. Proceed. of the 100th General Meeting of the Nordic Geodetic Commission, Sept–Oct, Helsinki, pp 237-245.

### **Ben-Menahem A, and Singh S J 1972**

Computation of models of elastic dislocations in the earth, in *Methods in Computational Physics*, 12, pp. 299–375, Academic Press, New York.

### **Ben-Menahem A, and Sing S J 1981**

*Seismic waves and sources*, Springer-Verlag, New York.

### **Boatwright J 1980**

A spectral theory for circular seismic sources; simple estimates of source dimension, dynamic stress drop and radiated seismic energy. *Bull. Seism. Soc. Am.*, 70, pp. 1–27.

### **FENCAT 1987**

Fennoscandian seismic event catalogue.

Compiled by Institute of Seismology, University of Helsinki.

**Henkel H, Hult K, Eriksson L, and Johansson L 1983**

Neotectonics in northern Sweden – geophysical investigations. SKBF/KBS TR 83-57, Stockholm.

**Henkel H 1988**

Tectonic studies in the Lansjärv region.  
SKB TR 88-07, Stockholm.

**Lagerbäck R 1979**

Neotectonic structures in northern Sweden. Geol. Fören. i Stockholm Förh., 100, pp. 263–269.

**Lagerbäck R, Witschard F 1983**

Neotectonics in northern Sweden – geological investigations. SKBF TR 83–58.

**Madariaga R 1976**

Dynamics of an expanding circular fault. Bull. Seism. Soc. Am., 66, pp. 639–666.

**Savage J C 1974**

Relation between P-wave and S-wave corner frequencies in the seismic spectrum. Bull. Seism. Soc. Am., 64, pp. 1621–1627.

**Silver P G 1983**

Retrieval of source-extent parameters and the interpretation of corner frequency. Bull. Seism. Soc. Am., 73, pp. 1499–1511.

**Slunga R S 1981a**

Earthquake source mechanism determination by use of body-wave amplitudes – an application to Swedish earthquakes. Bull. Seism. Soc. Am., 71, pp. 25–35.

**Slunga R S 1981b**

Fault mechanisms of Fennoscandian earthquakes and regional crustal stresses. Geol. För. i Stockholm Förhandlingar, 103, pp. 27–31.

**Slunga R S 1982**

Research on Swedish earthquakes 1980–1981. FOA Report C 20477-T1.

**Slunga R S, Norrman P, and Glans A-C 1984**

Baltic shield seismicity, the results of a regional network. Geophys. Res. Letters, 11, pp. 1247–1250.

**Slunga R S 1989a**

Earthquake Mechanisms in Northern Sweden, Oct 1987 – Apr 1988. SKB TR 89-28.

**Slunga R S 1989b**

Focal mechanisms and crustal stresses in the Baltic Shield, in Earthquakes at North-Atlantic Passive Margins: Neotectonics and Postglacial Rebound edited by Gregersen S, and Basham P, pp. 261–276.

**Talvitie J 1977**

Seismotectonics of northern Finland and the Fennoscandian shield. Univ. of Oulu, Dep. of Geophysics, Contrib. 82.

**Veriö A 1982b**

På jakt efter den obekanta mekanismen i landhöjningen. Nordiskt symposium: Landhöjning och kustbygdsförändring Luleå 2-4 juni 1982, symposiepublikation volym 1.

**Wahlström R 1978**

Magnitude scaling of earthquakes in Fennoscandia, Seismological Institute, Uppsala University, Report 3-78.

## **6 EARTHQUAKES NEAR THE LANSJÄRV FAULT**

*O Kulhánek*

Department of Seismology  
University of Uppsala  
Box 12019, S-750 12 Uppsala, Sweden

### **6.1 INTRODUCTION**

During the time period 1987–1988, two research groups at the Seismological Dept., Uppsala University, carried out investigations relevant for the understanding of the seismotectonics of northern Sweden. The first group consisted of R Wahlström, S-O Linder, C Holmqvist and H-E Mårtensson and conducted a study of neotectonic features in the vicinity of the Lansjärv fault in Swedish Lapland. Their work is described in Wahlström et al. (1987,1989) to be referred to as paper I and II. The second group included W Y Kim, E Skordas, Y P Zhou and the present author. The work of this group was focused on investigations concerning source parameters of major earthquakes near Kiruna, northern Sweden, deduced from synthetic seismograms. Results of this study may be found in Kim et al. (1988), henceforth referred to as paper III.

The purpose of this chapter is to provide a detailed summary of papers I and II and a rather brief summary on work included in paper III.

### **6.2 SEISMIC MONITORING OF THE LANSJÄRV NEOTECTONIC FAULT REGION**

Along the Lansjärv fault region there is geological evidence that the spectacular Lansjärv fault, with up to more than 20 m vertical uplift of one block, was created by one or a few large earthquakes during the late phase of the last deglaciation in Fennoscandia some 9 000 years ago. Our main objective in the investigation was to monitor the current seismic activity within the area by means of a mobile network of analog and digital seismic stations. Monitoring was carried out during two field campaigns, each of approximately five month, in 1987 and in 1988 when the weather conditions permitted.

### **6.3 THE MOBILE NETWORK**

The network used along the Lansjärv fault consisted of four three-component digital stations and two vertical-component analog stations. In the 1987 campaign, one vertical-component digital station with telemetric signal transmission was also operated. Station locations are listed in Table 6-1 and also displayed in Figure 6-1. Periods of operation and further technical data (filter and gain setting) can be found in paper I and II.

The 1987 monitoring revealed that the seismicity is concentrated to the south-eastern part of the surveyed area and hence in the 1988 campaign, some of the stations were relocated to obtain a better coverage of the active region.



**Table 6-1. Location of stations used.**

Station name	Code	Type	Location	
			Lat (°N)	Lon (°E)
Brakarberget	A	ANA	66.651	22.368
Nitsån	B	DIG	66.692	22.224
Kängelberget	C	DIG	66.636	22.112
Renberget	D	ANA	66.543	22.075
Passeberget	E	DIG	66.514	21.854
Kuossakåbbå	F	DIG	66.442	21.962
Årjekvare	G	DT	66.456	21.957
Livasape	H	DIG	66.405	21.814
Långberget	J1	DIG	66.358	22.182
Skravelberget	J2	DIG	66.369	22.177
Skaitas	K	DIG	66.478	22.069
Kalvberget	L	ANA	66.413	22.160

ANA Analog vertical-component station. Teledyne Geotech Portacorder RV-320B and seismometer S-500. Continuous recording.

DIG Digital 3-component station. Lennartz Encoder 5000 (station B 5800) and Mark seismometer L4A-3D. Trigger mode recording.

DT Digital vertical-component station. Telemetric transmission to station F Lennartz transmitter 4001 and Mark seismometer L4A. Triggered simultaneously with parent station.

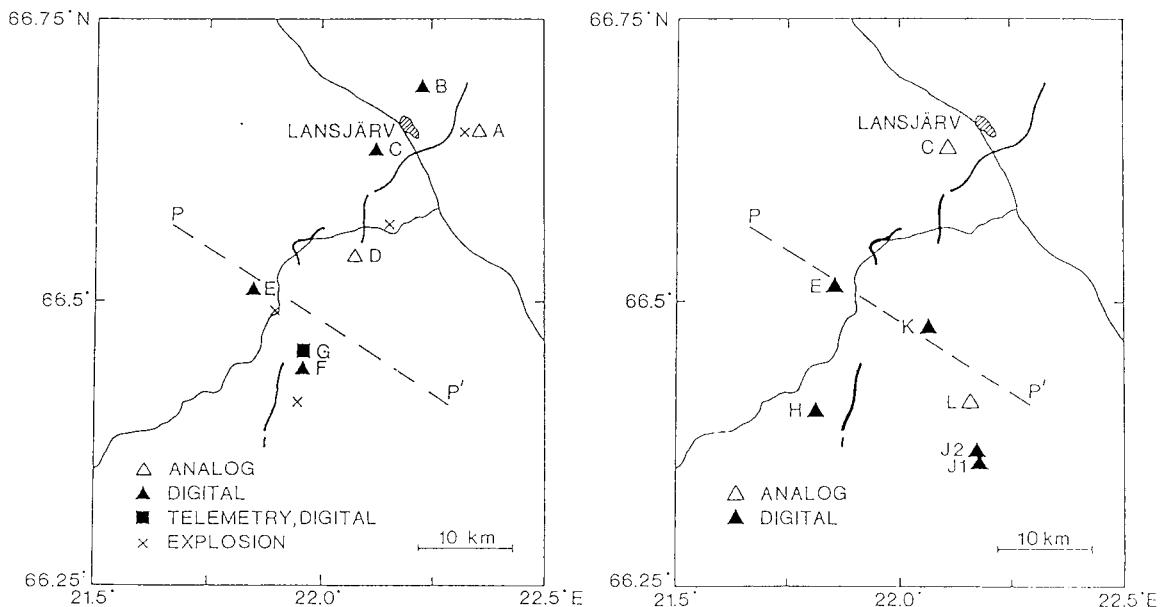


*Figure 6-1. Location of stations during the 1987 (left) and 1988 (right) campaigns. P-P' denotes the surface projection of the vertical plane on which the located earthquakes are projected in Figure 6-6.*

In 1987, several shorter intermissions at the digital stations can be ascribed to factors like bad weather (rain, wind), presence of animals, and other sources of disturbance, which have caused “false” triggers and rapid consumption of tapes. The stations F and G (Kuossakåbbå + telemetry) ceased to function in late August (encoder breakdown) and during the last 2–3 weeks the station B (Nitsån) had an error in the memory playback, causing loss of the initial P-wave coda (S properly recorded). The analog stations, especially D (Renberget), had reliable operations. In 1988, technical and maintenance problems were of similar nature, but of smaller extent than those in 1987. Two larger interruptions were due to encoder breakdown at station E (from October 10) and motor failure at station C (most of August). The station Långberget (J1) was moved to Skravelberget (J2), about 1.5 km to the north, on August 1 due to “cultural noise” (curious people).

The time signal from OMEGA in Norway was used for most of the recording time period. It was disconnected for one week in August 1987 and again for a period in August 1988, during which the time signal from DCF in Germany was received.

## 6.4 DATA ANALYSIS

The 1987 digital records were processed with a Lennartz Decoder 5000/5800 and Hewlett-Packard computer HP-1000. From the trigger lists, several thousand “events” had to be examined. After various automatic and manual steps, at which false triggers, teleseismic events, and regional events at distances larger than 40 km, including hundreds of mine explosions in Swedish Lapland, were eliminated, the number of nearby earthquakes had narrowed to about 20. The 1988 data reduction was performed according to similar procedures as the year before. An improvement was that a computer search algorithm was used to identify events simultaneously recorded at different digital stations. As an example, digital and analog records of the event of June 9, 1988 made at stations Passeberget and Kalvberget, respectively are exhibited in Figure 6-2.

To obtain, at least, rough velocity estimates of the propagating P and S waves, four test explosions, each of 5 kg dynamite, were carried out in the area (Figure 6-1, left part). Pg waves were excellently recorded with sharp onsets, whereas Sg waves were not. Only one clear S onset was observed. No exact shot times were recorded. Thus, there is some uncertainty in the simple constant-velocity model with Pg velocity of 5.82 km/s and Sg velocity of 3.36 km/s. Also alternative models have been attempted in the location procedure, and rather drastic velocity changes (10%) do not move the epicentres by more than a few km, at most. After many trials, a one layer velocity model with wave velocities of 5.76 and 3.33 km/s for Pg and Sg, respectively, was introduced to locate events at distances smaller than 40 km (travel-time difference Sg-Pg less than 5 s) from the nearest station.

## 6.5 HYPOCENTRE LOCATIONS

The location program HYPOINV1, Klein (1978) has been used for nine nearby 1987 earthquakes, for each of which the set of digital-data onsets is sufficient to provide a unique solution. The precision of arrival times is about 0.001 s from this kind of data; it is almost 2 orders lower from analog records. Note that the analog stations were operated with the main purpose to quickly and easily identify local events. In the nine cases, three or more digital stations have readable

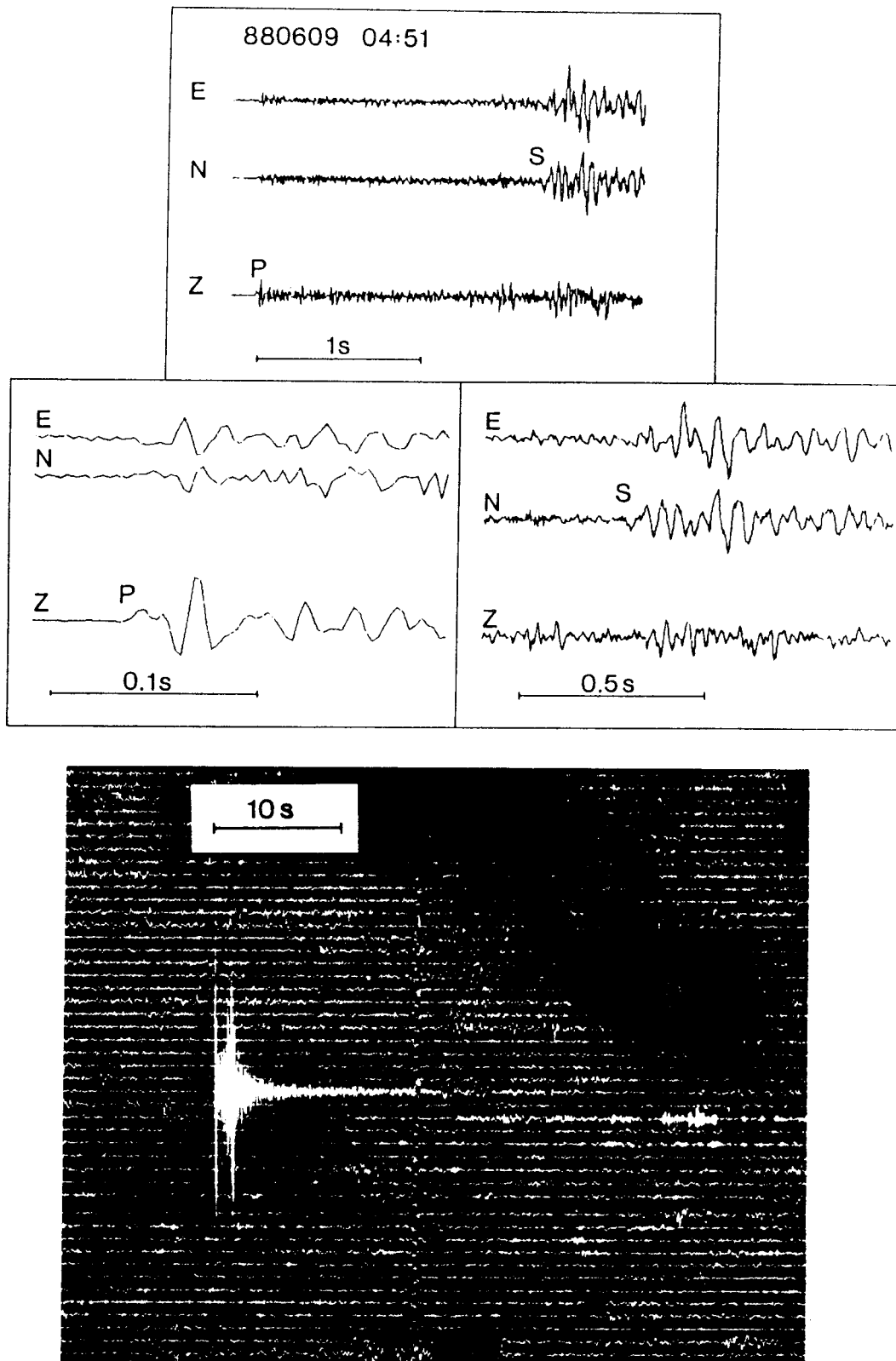


Figure 6-2. Record sections from stations Passeberget (E; digital, top) and Kalvberget (L; analog, bottom) for the event on June 9, 1988 at 04:51. For station E, P- and S-wave onsets are marked on playouts with different time resolution, and upward trace motion corresponds to ground motion to the W, S and down, respectively. For station L, upward trace motion corresponds to downward ground motion.

Pg or Sg onsets, and at least one of the stations provides both Pg and Sg readings. Two solutions give also stable focal depths of, 8 and 9 km, respectively. From the 1988 campaign, 13 events have sufficient arrival time data to be located with the HYPOINV1 program. Six of the solutions have a reliable estimate of the focal depth. They range from 5 km to 12 km; four of them are between 8 km and 10 km, similar to the two reliable focal depths obtained from the 1987 data. Five more events, although recorded by only two stations, can also be uniquely located, in most cases thanks to azimuthal discrimination from three-component digital data. Kinematic source parameters of the 27 located earthquakes are listed in Table 6-2 and the epicenters are plotted in Figure 6-3 on a tectonic map of Henkel (1988). Besides the events listed in the table, about 20 more nearby events have been recorded in 1987 and 1988. However, for these events it was not possible to obtain unique locations and in most of the cases it was also hard to decide whether or not they are earthquakes. Hence, these events have been omitted in Table 6-2 and in Figure 6-3. For more details the reader is referred to paper I and II.

**Table 6-2. Kinematic source parameters of the located earthquakes.**

Event No.	Date y m d	Origin time h m s (GMT)	Location		Focal depth km
			Lat.(°N)	Lon.(°E)	
1	870527	11 55 56	66.609	22.419	
2	870623	20 52 14	66.393	22.032	
3	870623	22 26 42	66.392	22.029	
4	870627	15 42 06	66.376	21.753	
5	870627	21 04 59	66.501	22.143	8
6	870718	04 02 32	66.505	21.234	
7	870724	17 22 41	66.392	22.071	9
8	870905	09 15 21	66.512	22.162	
9	871015	02 27 40	66.426	22.129	
10	880609	04 51 42	66.461	22.025	9.5
11	880715	00 49 08	66.458	22.141	8.6
12	880718	04 04 58	66.364	21.987	8*
13	880731	20 58 11	66.501	22.004	8.1
14	880809	18 28 46	66.581	21.880	(0)
15	880902	13 53 38	66.438	22.157	4*
16	880904	00 20 18	66.597	22.343	8.5
17	880911	06 28 12	66.409	22.089	8*
18	880913	15 11 47	66.545	22.260	8*
19	880927	01 09 23	66.628	22.732	(5)
20	880928	04 24 46	66.350	21.941	(1)
21	881009	15 54 19	66.467	22.141	6*
22	881010	12 47 15	66.746	22.387	(1)
23	881011	02 39 25	66.464	22.237	(3)
24	881019	03 29 01	66.395	22.133	5.3
25	881020	11 48 41	66.647	22.693	(6)
26	881022	06 00 04	66.674	22.322	12
27	881026	09 29 12	66.456	22.244	(2)

\*Marks the assumed focal depth for graphically located events. It is 8 km, if hypocentral distances (S-P times) do not indicate smaller depth.

The focal depth for computer-located events (no \*) is in brackets, if the solution is not well restrained as to depth.

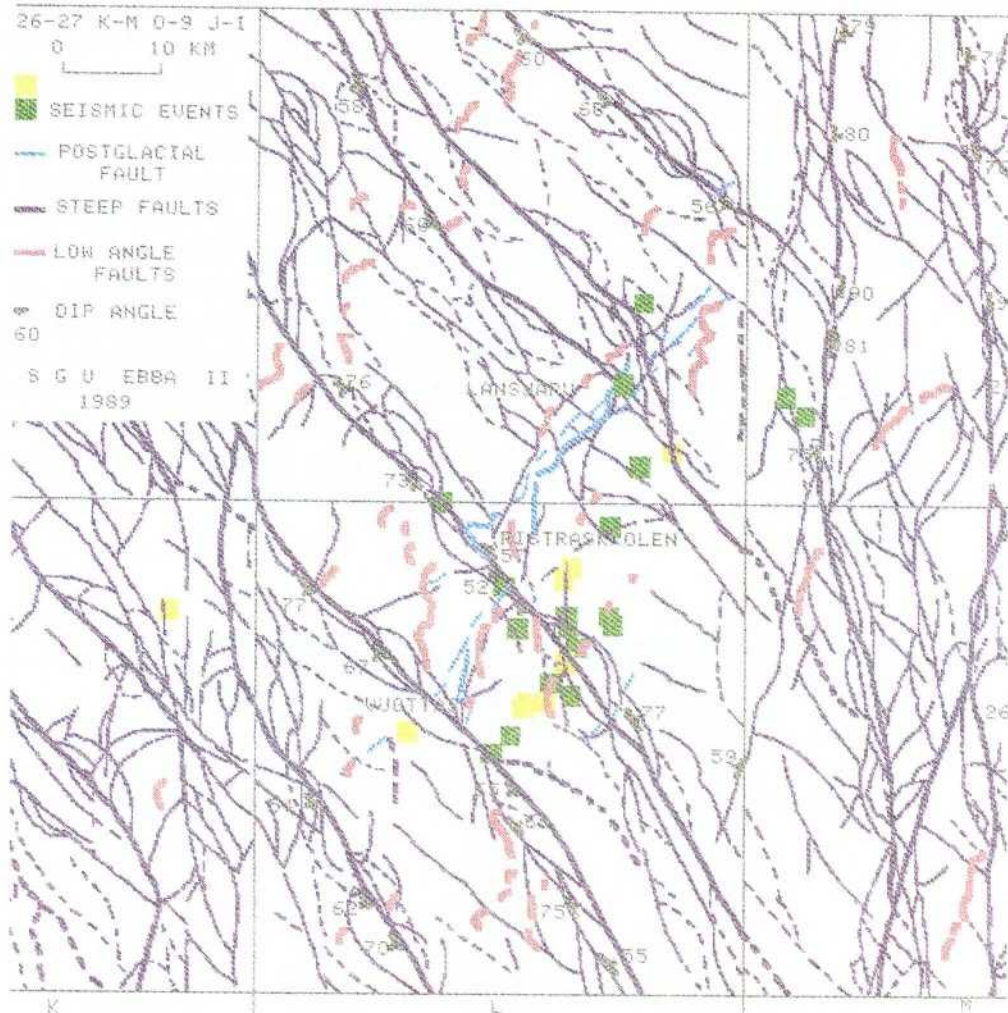


Figure 6-3. Epicenters of 27 earthquakes, from 1987 (yellow squares) and 1988 (green squares) campaigns, with unique locations (see Table 6-2) plotted on a tectonic map of the Lansjärv area, kindly provided by H. Henkel (1988).

## 6.6 FOCAL MECHANISMS

Pg polarities and Sg/Pg amplitude ratios were used as entries to a modified version of the computer program FOCMEC, Snoke et al. (1984); Wahlström (1987), to derive fault styles with orientations and deviatoric stress axes associated with the located earthquakes. The program requires at least four Pg polarities or Sg/Pg amplitude ratios to provide a solution. Due to the low number of stations and to their rather poor azimuthal coverage, plausible solutions were obtained only for four earthquakes (events 2, 6, 11 and 22 in Table 6-2). The event of June 23, 1987 is a normal-fault event with the pressure (P) axis trending roughly NW-SE and dipping about 45°. The event of July 18, 1987 shows thrust faulting with a horizontal pressure axis in the NW-SE direction. The July 15, 1988 event exhibits a strike-slip mechanism with a strong horizontal component of the pressure axis with a trend roughly SW-NE. The October 10, 1988 event shows a clear dip-slip faulting with an almost vertical pressure axis. Obviously, there is a variety of faulting styles represented by the four earthquakes.

A horizontal P axis trending roughly NW-SE, i.e., opposite to that found for the July 15 and October 10 events, would be expected to explain the mechanisms with ridge push from the North Atlantic plate boundary, a plausible cause of the Fennoscandian seismicity, see Wahlström (1989). However, we must remember that the sparse input data make the obtained mechanisms not very well constrained, and tectonic implications are uncertain. Constructed fault plane solutions are displayed in Figure 6-4.

## 6.7 DYNAMIC SOURCE PARAMETERS

Sg signals recorded by digital 3-component seismographs were converted to radial and transverse components. The ground-amplitude spectrum of the larger-amplitude transverse component was then computed. The low-frequency level and the corner frequency were measured from each spectrum which has the expected simple shape. As an example, Figure 6-5 shows the recorded signals and S-wave spectrum for event 10 (Table 6-2) recorded at station E (Passeberget, Figure 6-1).

Based on the spectral level and the corner frequency, the seismic moment, radius of focal area, average relative displacement and stress drop are computed, under the assumption of Brune's (1970, 1971) circular-fault model. Spherical spreading is assumed at these small distances. Table 6-3 shows the resulting values. Corner frequencies range from 10 to 57 Hz and the spectral low-frequency level from  $4 \times 10^{-5}$  to  $6 \times 10^{-3}$  m-s. Seismic moments range from  $10^{10}$  to  $10^{12}$  Nm, fault radii from 30 to 100 m, average displacements from 0.03 to 8 mm, and stress drops from 0.01 to 7 MPa.

## 6.8 DISCUSSION AND CONCLUSIONS

For the first time, a close-in seismic network has been operating in Sweden during a time period of several months.

The frequency of local earthquakes in the vicinity (<40 km) of the Lansjärv neotectonic region is somewhat greater than one event per week. Lacking detailed investigations from other parts of Sweden, it is hard to say if this represents an abnormally high rate. The vast majority of the events occurred to the east of the mapped segments of the postglacial fault, several of them within a smaller area. In part, this result may be a bias of the location of the station network, although there are indications that the seismicity is partially related to other, older large regional fault systems (Figure 6-3). Figure 6-6 exhibits the available hypocenters projected onto a vertical plane roughly perpendicular to the Lansjärv fault system (see Figure 6-1). Even though some of the solutions are poorly restrained as to depth, the suggested systematics in the hypocenter distribution with respect to depth, imply a rather unexpected surface dipping about  $30^\circ$  to the NW.

Excellent Pg first-motion, and Pg- and Sg-amplitude data are obtained, but unfortunately the number of stations is not large enough to provide well constrained mechanism solutions. The addition of two or three digital stations would have significantly increased the number and reliability of obtained mechanisms, and facilitated a more detailed seismotectonic description of the region.

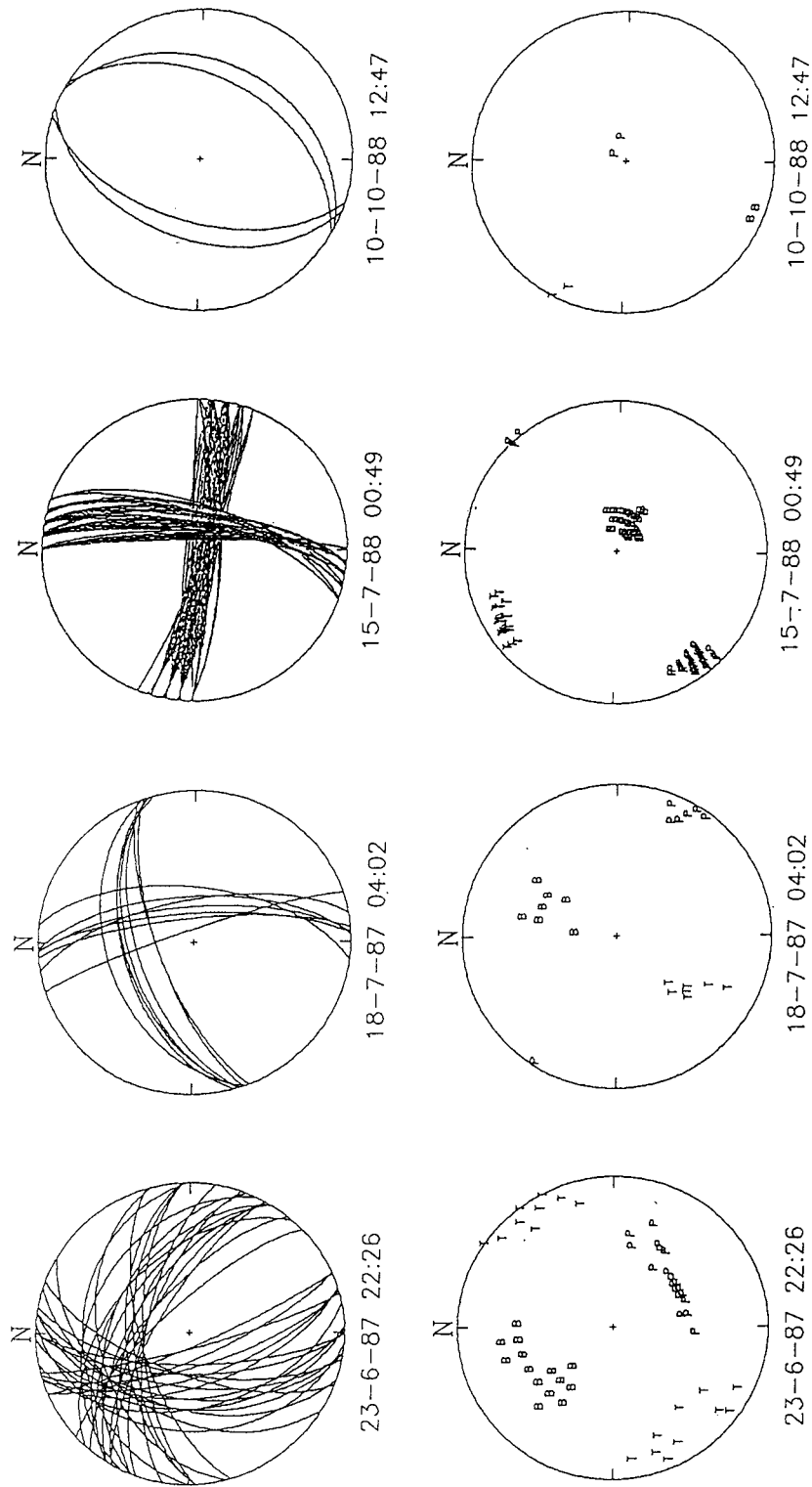


Figure 6-4. Fault-plane diagrams (lower hemisphere plot) for earthquakes 2, 6, 11 and 22 from Table 6-2. P = compression axis, T = tension axis, B = null vector.

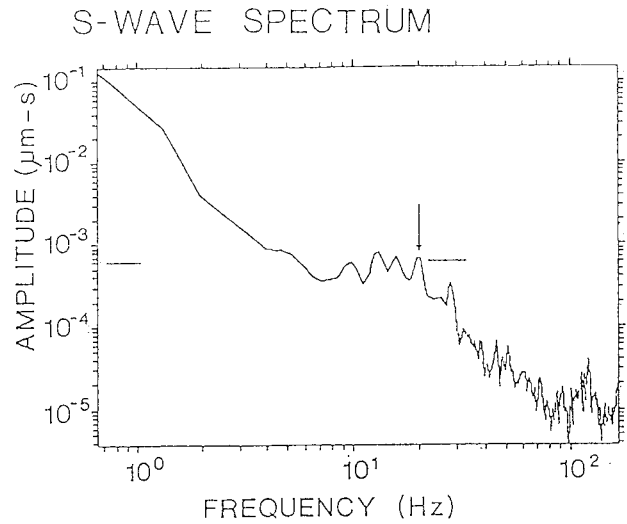
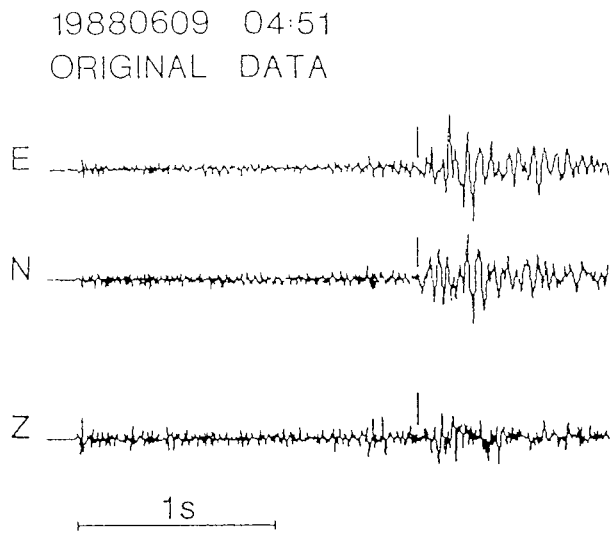


Figure 6-5. Record sections (left) and spectrum (right) for the event of June 9, 1988 observed at station Passeberget. The constant low-frequency level and corner frequency are marked in the spectrum.

Table 6-3. Dynamic source parameters.

Event No.	Seismic moment (Nm)	Fault radius (km)	Displacement (mm)	Stress drop (MPa)
1	$0.3 \times 10^{12}$	0.1	0.3	0.1
2	$0.8 \times 10^{11}$	0.07	0.2	0.2
3	$0.5 \times 10^{11}$	0.07	0.1	0.05
4	$0.1 \times 10^{12}$	0.08	0.2	0.09
5	$0.2 \times 10^{11}$	0.06	0.07	0.05
6	$0.1 \times 10^{13}$	0.04	8	7
7	$0.2 \times 10^{12}$	0.06	0.7	0.4
8	$0.5 \times 10^{12}$	0.08	0.8	0.5
9	$0.2 \times 10^{12}$	0.07	0.4	0.3
10	$0.1 \times 10^{12}$	0.06	0.4	0.2
11	$0.4 \times 10^{11}$	0.07	0.09	0.07
14	$0.4 \times 10^{12}$	0.06	1	0.7
16	$0.1 \times 10^{13}$	0.08	2	0.9
17	$0.4 \times 10^{11}$	0.03	0.7	1
18	$0.1 \times 10^{11}$	0.04	0.06	0.06
19	$0.2 \times 10^{11}$	0.03	0.4	0.6
20	$0.2 \times 10^{12}$	0.03	3	4
21	$0.4 \times 10^{11}$	0.07	0.1	0.06
22	$0.7 \times 10^{12}$	0.1	0.7	0.3
23	$0.1 \times 10^{12}$	0.06	0.3	0.5
24	$0.2 \times 10^{11}$	0.06	0.07	0.05
25	$0.1 \times 10^{13}$	0.08	2	0.9
26	$0.2 \times 10^{11}$	0.09	0.03	0.01
27	$0.9 \times 10^{11}$	0.05	0.3	0.2



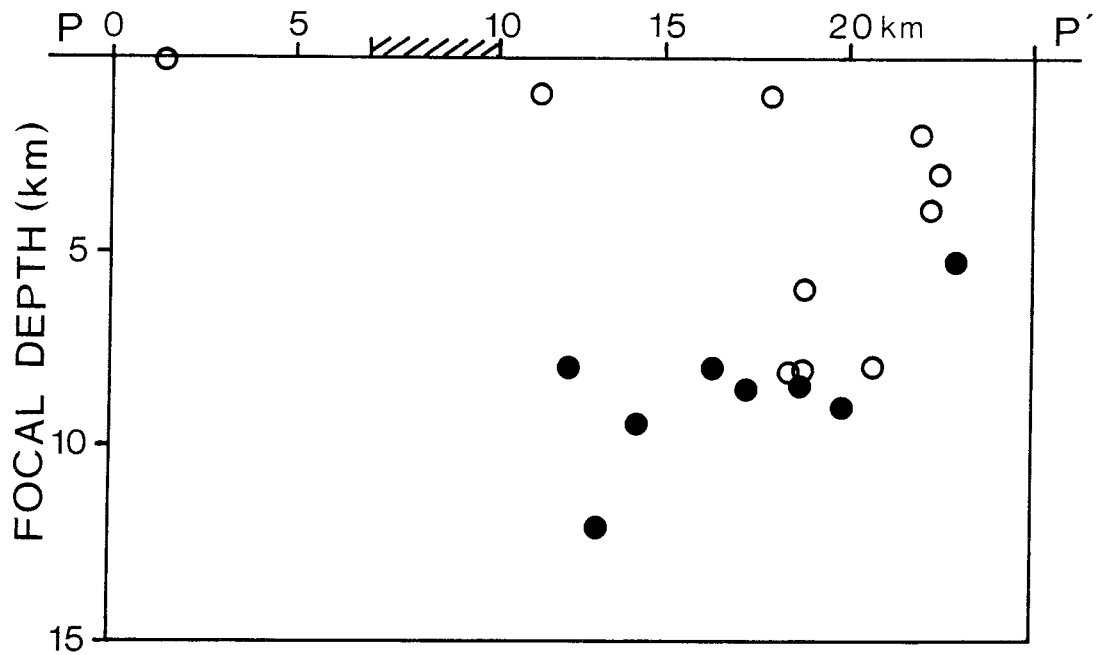


Figure 6-6. Seismicity of the Lansjärv area viewed along the cross section P-P' shown in Figure 6-1. Solid circles exhibit well restrained hypocentral locations with errors of the order of several hundred meters. Open circles show poorly restrained hypocenters with location errors probably of the order of one or a few kilometers. The shaded section indicates the location of the Lansjärv fault system.

## 6.9 SOURCE PARAMETERS OF MAJOR EARTHQUAKES IN NORTHERN SWEDEN DEDUCED FROM SYNTHETIC SEISMOGRAMS

The scope of work described in paper III does not include the area of Lansjärv. However, due to its relevance for understanding the seismotectonics of northern Sweden, a brief summary is presented below. For more exhaustive presentation the reader is referred to paper III where data, analysis techniques and results are discussed in greater detail.

The main objective of paper III is to determine seismic source parameters, such as seismic moment, source radius and stress drop, as well as to estimate the focal depth and source mechanism of earthquakes which have occurred around Kiruna, in northern Sweden and to study the seismicity of the region in detail. All earthquakes with magnitude greater than 3.0 ( $M_L$ ) that occurred during the period between 1967 and 1985 in the region bounded by 66.5°–69° N and 19°–25° E are studied (Figure 6-7, Table 6-4).

The source region under study is a typical intraplate region with low seismicity characterized by the occurrence of small crustal earthquakes. The major problem to study the seismicity of the region is that the events in question are small. Thus, they are recorded by only a few short-period seismograph stations operating at regional distances (100 – 500 km). Hence, it is very difficult to determine the source parameters reliably due to the lack of good quality data.

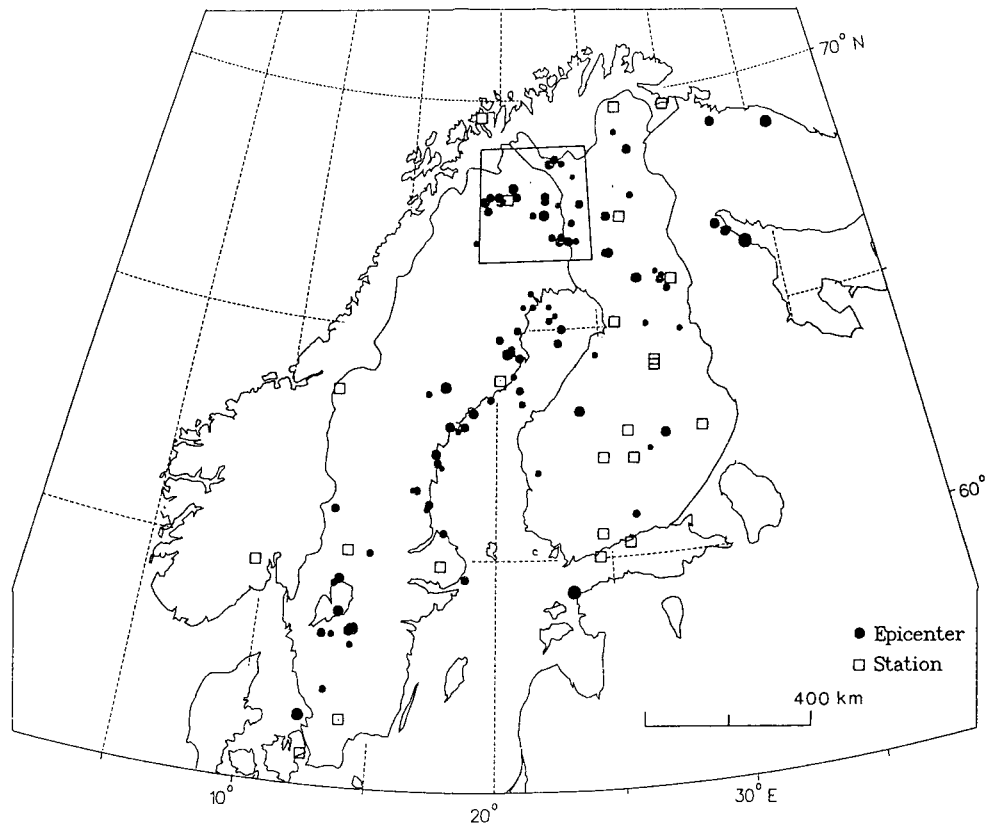


Figure 6-7. Epicentral distribution of earthquakes in the Fennoscandian shield, 1961-1986 and locations of seismograph stations (squares). All events with magnitude greater than 3.5 ( $M_L$ ) are plotted and some of the events within the magnitude range 2 to 3.4 are included. Solid circles denote epicenters and their sizes are proportional to the magnitude of the events. Note that the solid circle given in the legend corresponds to magnitude 4. The inset indicates the northern Sweden seismic zone, bounded by 66.5° – 69° N in latitude and 19 – 25°E in longitude.

Table 6-4. Major earthquakes around Kiruna, northern Sweden.

Event No.	Date y m d (GMT)	Origin time h m s	Location		Magni- tude $M_L$
			Lat(°N)	Lon(°E)	
1	670104	04 44 18	67.9	21.0	3.2
2	670413	08 46 19	68.1	20.8	3.7
3	680904	17 09 14	66.9	23.8	3.4
4	690704	22 28 54	67.6	19.4	3.1
5	710417	08 05 03	67.8	22.6	3.1
6	730417	06 17 59	67.9	20.0	3.3
7	741201	19 35 58	67.8	20.1	3.2
8	750811	18 28 09	67.5	22.5	3.9
9	780116	02 28 24	67.9	22.6	3.2
10	800528	10 36 45	67.7	24.5	3.1
11	820131	03 38 51	68.7	23.2	3.1
12	830104	20 51 04	68.6	22.9	3.4
13	840825	19 39 14	67.9	19.5	3.1
14	850402	19 29 40	66.9	23.3	3.2

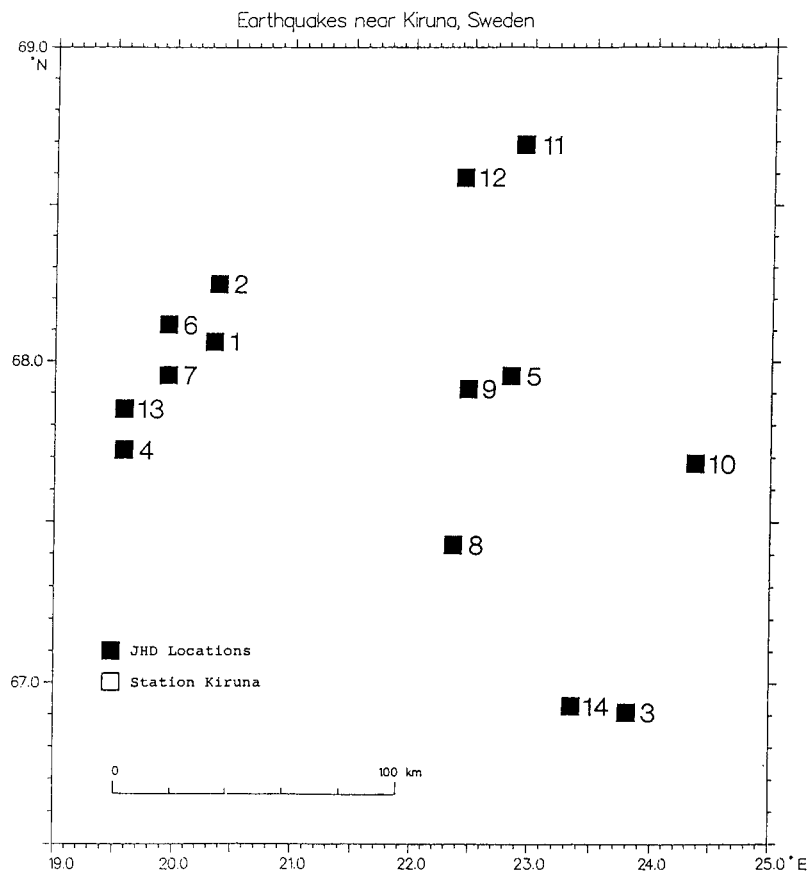


Figure 6-8. Epicenters of earthquakes near Kiruna, northern Sweden, that occurred between 1963 and 1986, studied in paper III.

In order to study the characteristics of the events, all available seismogram data have been collected and digitized for quantitative analysis. The data set consists of three-component short period seismograms recorded by stations in Finland, Norway and Sweden. Altogether, about 200 seismograms were collected and photographically enlarged for further analysis and digitizing. The enlarged seismograms are digitized using a data acquisition system which consists of an electronic digitizing table and personal computer with high resolution graphic display screen. The digitizing table has a resolution limit of about 0.125 mm and converts analog seismogram traces into digital form suitable for quantitative analysis.

For the 14 events studied (Table 6-4), arrival times of the major crustal phases, such as Pn, Pg, Sn and Sg, are measured and the events are relocated by using the method of Joint Hypocenter Determination. As follows from Figure 6-8, relocated epicenters exhibit a cluster of events in a direction NE-SW at the western side of the region close to Kiruna. Though, the focal depths of the events are not very well constrained, the relocation results suggest that the events in this cluster might have occurred at focal depths between 15 and 25 km. At the eastern side of the region, the epicenters are roughly aligned along an elongated area trending NNW-SSE. The focal depths of the events in this area tend to be shallow and are probably in the upper crust at the depth range from 5 to 16 km.

Spectral analyses of Lg waves on vertical-component seismograms are performed to determine the source parameters. Three-component digitized seis-

mograms are analysed and corresponding synthetic seismograms are calculated to constrain the focal depth and source mechanisms. The earthquakes studied show nearly constant source radii of about 0.4 – 0.6 km over the seismic moment range from  $10^{20}$  to  $10^{21}$  dyne-cm. Consequently, the events studied are characterized by a steadily increasing stress drop relative to increasing seismic moment. Calculated dynamic source parameters are listed in Table 6-5.

**Table 6-5. Dynamic source parameters of earthquakes in northern Sweden.**

Event No.	Seismic moment (dyne-cm)	Magnitude $M_L$	Source radius r (km)	Stress drop (bars)
1	$1.6 \times 10^{20}$	3.2	0.47	0.69
2	$5.3 \times 10^{20}$	3.7	0.47	2.19
3	$4.2 \times 10^{20}$	3.4	0.46	1.92
4	$2.0 \times 10^{20}$	3.1	0.41	1.27
5	$1.0 \times 10^{20}$	3.1	0.47	0.42
6	$2.8 \times 10^{20}$	3.3	0.54	0.77
7	$1.1 \times 10^{20}$	3.2	0.56	0.29
8	$1.1 \times 10^{21}$	3.9	0.45	5.31
9	$1.6 \times 10^{20}$	3.2	0.48	0.63
10	$1.2 \times 10^{20}$	3.1	0.47	0.52
11	$1.8 \times 10^{20}$	3.1	0.50	0.64
12	$3.0 \times 10^{20}$	3.4	0.45	1.46
13	$1.0 \times 10^{20}$	3.1	0.46	0.48
14	$1.5 \times 10^{20}$	3.2	0.50	0.53

The source mechanisms obtained for the two largest earthquakes of April 13, 1967 and August 11, 1975 suggest that the mechanisms are dominated by normal faultings on the near-vertical fault planes trending almost E-W and N-S, respectively.

## 6.10 REFERENCES

### **Brune J N 1970**

Tectonic stress and the spectra of seismic shear waves from earthquakes.  
J. Geophys. Res., 75, 4997–5009

### **Brune J N 1971**

Correction of “Tectonic stress and the spectra of seismic shear waves from earthquakes”.  
J. Geophys. Res., 76, 5002

### **Henkel H 1988**

Tectonic studies in the Lansjärv region.  
SKB TR 88-07, 66 pp, Stockholm

**Kim W Y, Skordas E, Zhou Y-P, and Kulhánek O 1988**

Source parameters of major earthquakes near Kiruna, Northern Sweden, deduced from synthetic seismogram computation.

SKB TR 88-23, 45 pp, Stockholm

**Klein F W 1978**

Hypocenter location program: HYPOINVERSE, Part 1: User's guide. Open-File Report 78-694, Geological Survey, Menlo Park, Calif.

**Snoke J A, Munsey J W, Teague A G, and Bollinger G A 1984**

A program for focal mechanism determination by combined use of polarity and SV-P amplitude ratio data.

Earthquake Notes 55:3, 15

**Wahlström R 1987**

Focal mechanisms of earthquakes in southern Quebec, southeastern Ontario, and northeastern New York with implications for regional seismotectonics and stress field characteristics.

Bulletin of the Seismological Society of America 77, 891–924

**Wahlström R 1989**

Seismodynamics and postglacial faulting in the Baltic Shield. In S Gregersens and P Basham (editors): Earthquakes at North-Atlantic Passive Margins: Neotectonics and Postglacial Rebound (Proceedings of NATO Advanced Research Workshop in Vordingborg, Denmark, May 9-13, 1988).

Kluwer Academic Publishers, 467–484. Publication No. 159 of the International Lithospheric Program

**Wahlström R, Linder S-O, and Holmqvist C 1987**

Near-distance seismological monitoring of the Lansjärv neotectonic fault region.

SKB TR 88-12, 27 pp, Stockholm

**Wahlström R, Linder S-O, Holmqvist C, and Mårtensson H-E 1988**

Near-distance seismological monitoring of the Lansjärv neotectonic fault region. Part II.

SKB TR 89-01, 17 pp, Stockholm

# 7 DRILLING AND BOREHOLE DESCRIPTION

*Bjarni Bjarnason – Olle Zellman, Peter Wikberg*

Renco AB, Köpmangatan 40A, S-951 32 Luleå, Sweden –  
SKB, Box 5864, S-102 48 Stockholm, Sweden

## 7.1 INTRODUCTION

Based on the results and analysis of geophysical measurements and tectonic interpretation in the Lansjärv study area a site for core drilling was suggested c. 5 km NE Lansjärv, Henkel (1988) Figure 7-1. The main aim of the core borehole (KLJ 01) was to penetrate the post-glacial fault zone and to investigate the rock mass close to this zone primarily with respect to the hydraulics and fracture minerals, Figure 7-2.

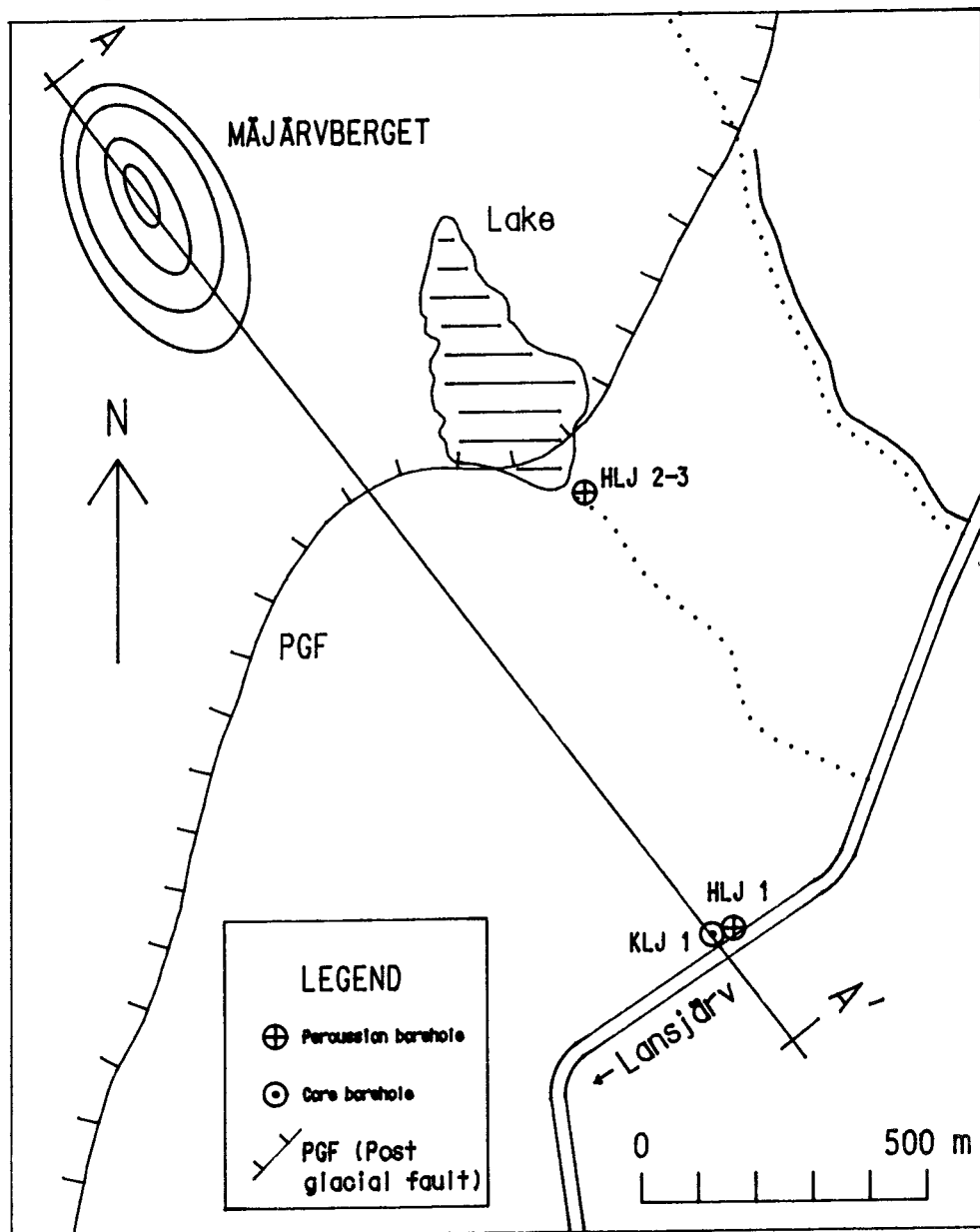


Figure 7-1. Location map of the boreholes NE Lansjärv.

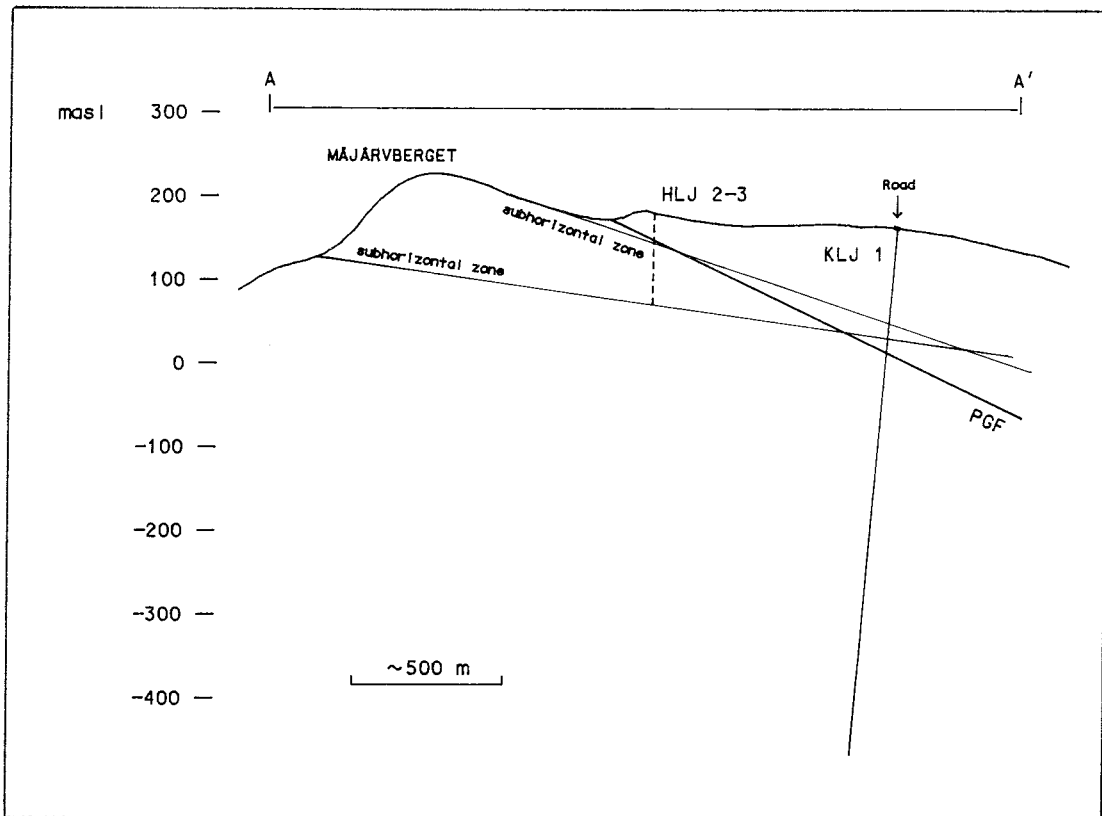


Figure 7-2. Estimated dip of low angle faults at Mäjärverket. After Henkel (1988).

Three percussion boreholes were also drilled. Borehole HLJ 01 was drilled to support this hole with drilling water. The percussion hole HLJ 02 was planned to penetrate the suggested PGF about 400 m to the west of KLJ 01, Table 1. At a depth of 84 m the drilling equipment was stuck in a highly fractured zone. All attempts to rescue the equipment failed. All air pressure produced by the compressor, 20 m<sup>3</sup>/min vanished in the bedrock. In a second attempt to intersect the fault zone hole HLJ 03 was drilled. At a depth of about 90–92 m a highly fractured zone was registered and to avoid the same problems as in HLJ 02 the drilling was stopped.

**Table 1. Data on boreholes at Lansjärv.**

	KLJ 01	HLJ 01	HLJ 02	HLJ 03
RAK X-coordinate	7412150	7412175	742926.13	7512925.87
RAK Y-coordinate	1781450	1787510.43	1787276.77	1787275.87
RAK Z-coordinate (msl)	+153.98	+154.23	+177.91	+172.74
Borehole length (m)	500.60	75	84	92
Declination (degrees)	315.0	–	–	–
Inclination (degrees)	85.0	70	85	85

Z = top of casing

Investigation performed in the core borehole KLJ 01:

1. Geophysical borehole logging
2. Core mapping
3. Water chemistry
4. Rock stress measurements
5. Fracture mineral study
6. Hydrogeological measurements

Results from investigations 1–4 are presented in this chapter, studies 5 and 6 in separate chapters.

## 7.2 GEOPHYSICAL BOREHOLE LOGGING

Geophysical logging was performed in KLJ 01 on two different occasions. As the borehole collapsed at 148 m it was necessary to case the borehole to continue drilling. Before this was done the borehole was logged down to 145 m. After completed drilling logging was conducted in the remaining part of the borehole. Measurements were done with the following methods:

- Resistivity – normal
- Resistivity – lateral
- Single Point Resistance
- Natural Gamma Radiation
- Borehole Deviation
- Sonic
- Self Potential
- Temperature
- Borehole Fluid Resistivity

Magnetic susceptibility was not possible to perform due to instrument failure. No logging has been performed in the percussion boreholes. The logging results are presented as a complot figure, Figure 7-3. Information from the fracture mapping and hydraulic injection tests have been included.

Fractures are mainly indicated by resistivity/resistance and sonic measurements. In Lansjärv the bedrock consists of granite and pegmatite with a few short sections of mafic rocks (amphibolite and dolerite). This is a favourable situation for fractures recognition.

A brief study of the logs shows that the borehole can be divided into two sections. The upper section, 32–300 m, is very fractured, while the lower section, 300–500 m, has fewer fractures. Sehlstedt (1988).

Two sections with deformed granite, 241–245 m and 255–280 m, are clearly indicated by all electrical methods. The latter is also shown on the sonic log. Both sections have less fractures than the surrounding sections. The anomalies are thought to be caused by higher porosity due to alteration.

The gamma measurements generally show spike-like positive anomalies which often correlates with single fractures indicated by single point resistance and sometimes also by sonic measurements.

A very low gamma value was recorded in the borehole at 148 m. This is probably due to the cavity from the borehole collapse at this depth.

The deformed granite at 255–280 m shows the highest gamma radiation in the borehole. This may be caused by one of the following reasons:

- radium and/or radon in the pore water,
- high content of U/Th/K in the rock.



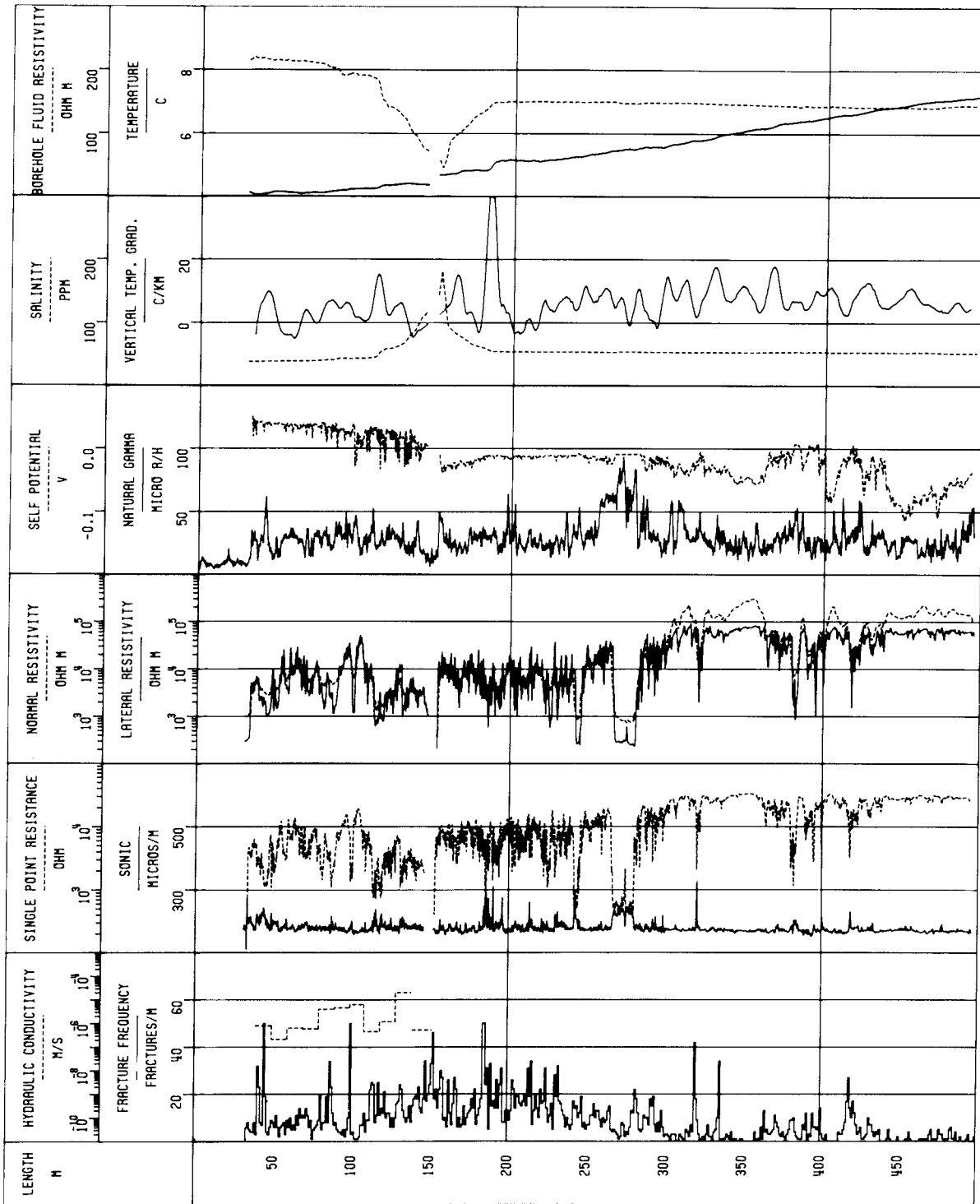


Figure 7-3. Geophysical logging. KLJ01 - Lansjärv.

Some gamma anomalies are probably caused by radium on fracture surfaces since the granite in the area is radium rich, G Åkerblom per comm.

Using the temperature and fluid resistivity measurements it is possible to gain information about water flow in the borehole. Like the rest of the measurements, these have been made on two different occasions. Data from both measurements show a rather disturbed temperature graph, indicating water circulation in the borehole.

### 7.3 CORE MAPPING

Fracture characteristics, fracture orientation and fracture minerals, Albino (1988) was distinguished in the examination of the core.

Within the investigated area the predominant rock is a red-grey granite. The granite changes appearance depending how much the rock has been tectonized. Minor amount of pegmatite, aplite and quartz veins intersect the granite. Small sections of other rocks, such as amphibolite, tectonic breccia and intermediate hypabyssal volcanics also occur in the drillcore, Figure 7-4.

The granite is medium-grained and rather uniform within most of the borehole, but foliated granite exists. The foliation is defined by a parallel arrangement of minerals predominantly biotite. The character of the granite is locally changed due to deformation (cataclasis) or hydrothermal alteration (red-colouring).

Pegmatites and aplites occur as dykes and veins cutting the granite throughout the drillhole. Most of the dykes are small, 0.20 – 0.40 m wide. There are 37 pegmatites with widths ranging from 0.2 to 3.55 m. The pegmatites are often zoned with a coarse-grained central part and an outer medium-grained rim.

Only two aplitic dykes have been observed. Quartz veins exist with widths of 0.06 – 0.18 m. The sections in the borehole are characterized by a higher fracture frequency than normal.

Small sections of a black or dark green amphibolite also occur. This rock is medium-grained with a distinct foliation with amphibole as the dominant mineral. The amphibolite is most frequent near the bottom of the borehole.

Short sections of cataclastic breccia have been observed in the core. At depths of 127 m, 131 m and 236 m this rock is very fine-grained with distinct secondary banding and normally impregnated with epidote. At the depths 206 m and 241 m broken fragments of granite occur in the breccia. Finally there is one section, 274 m, of an intermediate volcanite which is indistinctly porphyritic.

Where it exists, the single foliation is moderate to strong and dips from 30° to 60°. This foliation is sigmoidal in dark inclusions but generally axial-planar to minor folds in a few acid veins. Angular discontinuities (<30°) in the foliation appear to be coarse-grained and annealed hot shears. Instead of grain size reduction by ductile processes, dilational cataclasis led to brecciation at greenschist facies temperatures. With progressive rotation, angular clasts in dense networks of hematite veins became misaligned and angular to rounded clasts in a fine grained matrix. Although many (but not all) hematite veins are vertical, the fracture and/or cataclastic zones cannot be orientated. Epidotic, cataclastic zones are rare, thin and mainly fine grained and appear to be horizontal or dip 30°.

The frequency of coated fractures in borehole KLJ 01 can be seen in Figure 7-5. In the upper part of the borehole – down to c. 265 m – fracturing is generally high (8–15 fractures/m).

The fracture frequency plot indicates a zone with anomalously high fracture frequency between 100–265 m and the most tectonically affected part of the

LANSJÄRV  
Core borehole KLJ01

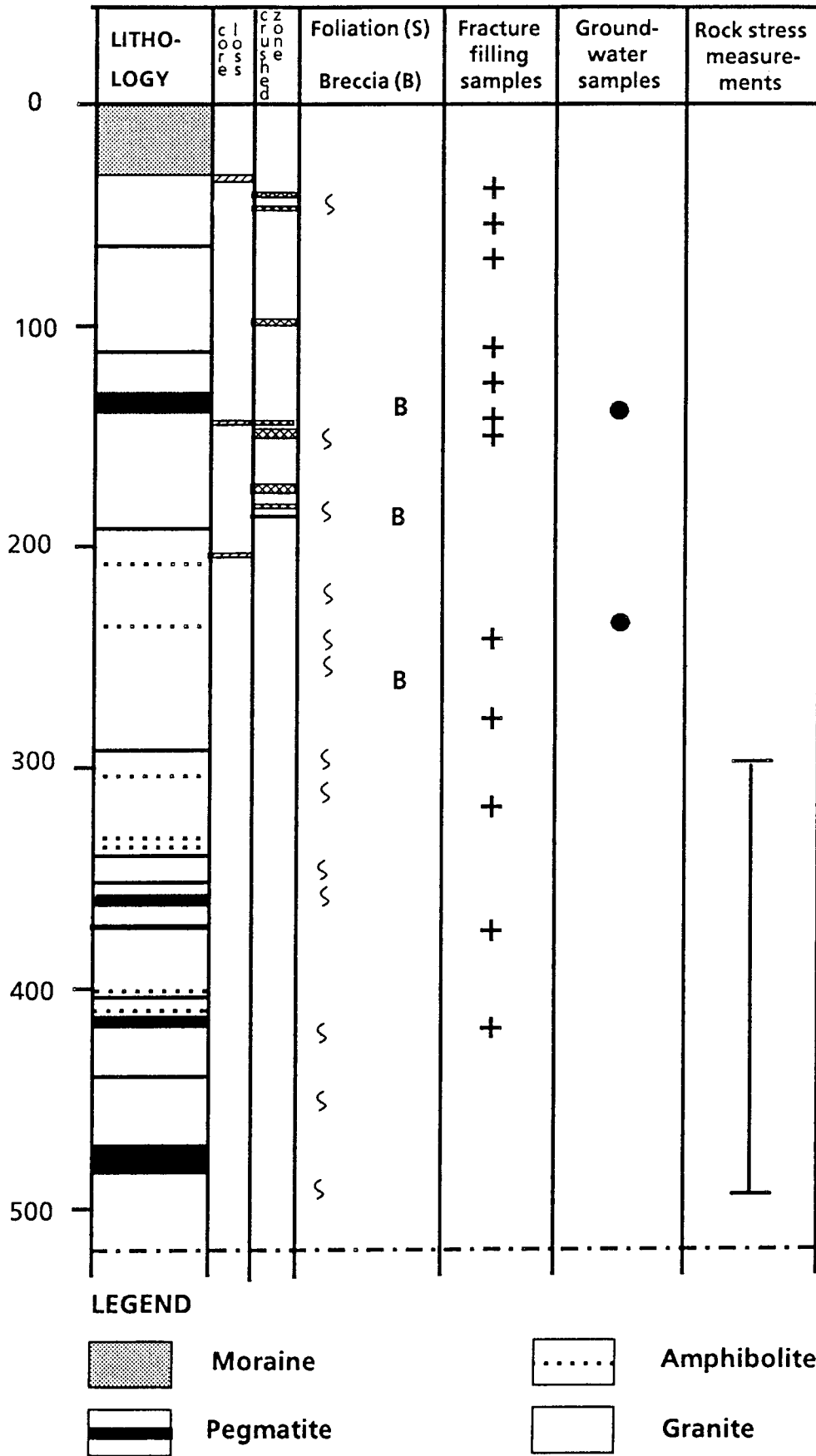


Figure 7-4. Investigation performed in the core borehole KLJ 01.

LANSJÄRV KLJ01  
FRACTURE FREQUENCY/1M  
TOTAL FRACTURE FREQUENCY

MAP SHEET : 27 L SE  
ID NUMBER : 88003  
SCALE : 1:2000

PROJECT : LANSJÄRV  
ENGINEERING GEOLOGY  
SWEDISH GEOLOGICAL CO

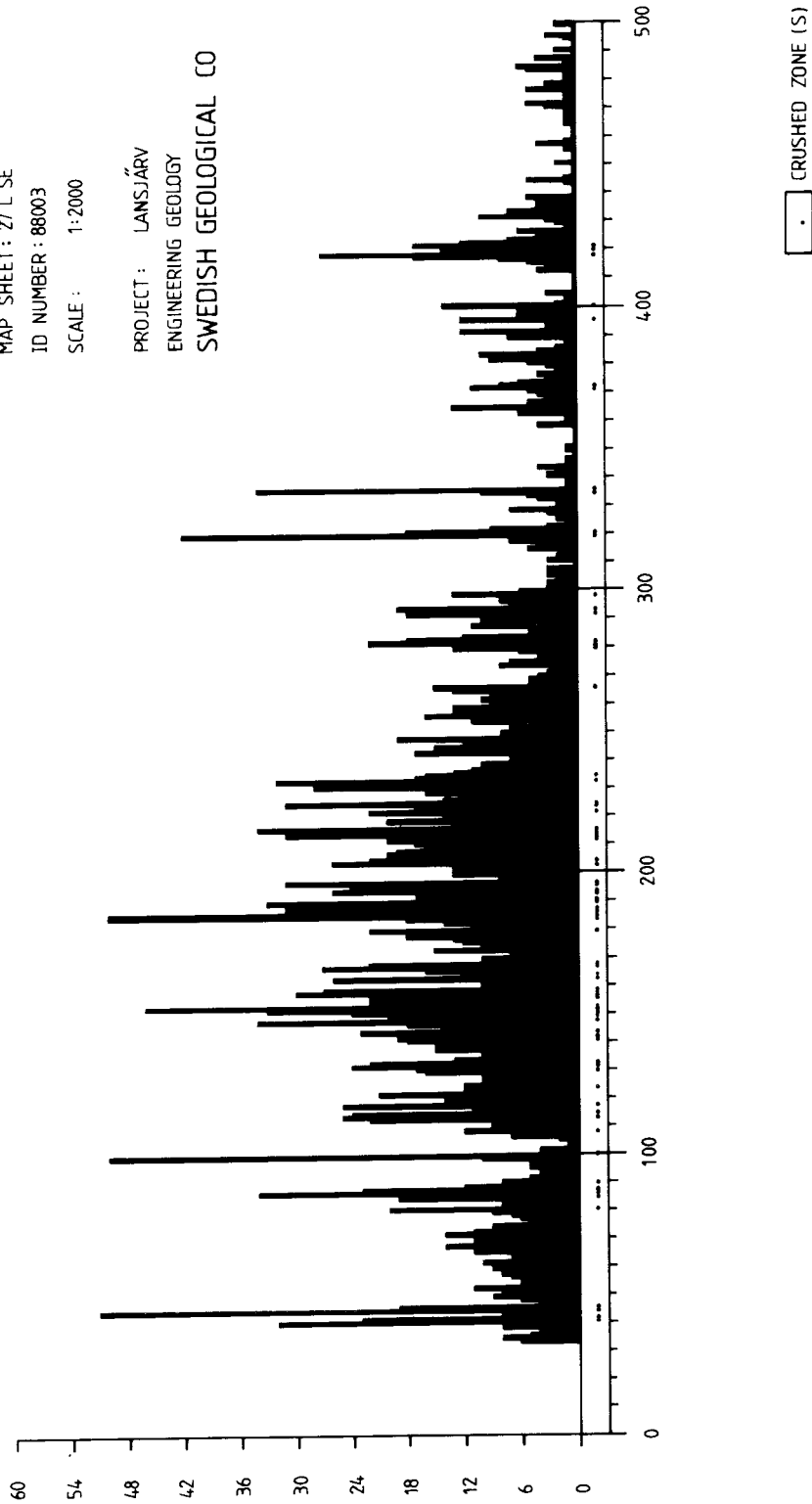


Figure 7-5. Fracture frequency of core from borehole KLJ 01 at Lansjärv.

zone seems to be at 185 m. The highest fracture frequency is within the section 147–215 m. The coating mineral that exist in this zone seem to be hematite and chlorite, especially hematite. Other, less frequent fracture fillings that have been observed are calcite and prehnite. Hematite and clay mineral alteration intensifies in porous but non-permeable zones with secondary vugs.

Below c. 265 m the fracture frequency declines and is normally very low except in four sections (279–294 m, 319–321, 334–336 m and 417–423 m) with 15–20 fractures/m.

## 7.4 GROUNDWATER CHEMISTRY

The groundwater from the borehole has been sampled and analysed on two different occasions, one at a depth of 150 m and the other at a depth of 237 m. In both cases the bottom section of the hole was sealed off by an inflatable rubber packer and the water was continuously pumped out of the bottom section. The first sampling occasion was when the hole had been drilled through a fractured zone at 150 m. The second and more extensive sampling campaign was performed when the drilling of the hole was completed. Table 7-1 summarizes the results of the analyses made on the samples collected from 237 m depth. The composition of the water collected at 150 m was the same as the one at 237 m.

**Table 7-1. Typical values of the chemical composition of the groundwater sampled from 237 m depth at Lansjärv. All concentrations are given in mg/l, except for pH and Eh.**

pH	9.0	Eh (mv)	-200
Na	10	HCO <sub>3</sub>	40
K	2	SO <sub>4</sub>	3
Ca	7	Cl	1
Mg	1	F	1.3
Al	0.2	TOC	7
Fe	0.01	HS	< 0.01
Mn	0.03	PO <sub>4</sub>	< 0.004
Li	0.006	NO <sub>3</sub>	< 0.01
Sr	0.06	NO <sub>2</sub>	< 0.001
NH <sub>4</sub>	< 0.005	SiO <sub>2</sub>	3

The concentration of dissolved species in the water is low. This is an observation which has been made at other locations in Norrbotten, e.g. Kamlunge, Laurent (1983). Despite the low salt content the water can be classified by the use of a modified Piper plot. In Figure 7-6 the water composition in Table 7-1 is plotted together with other typical water compositions from the SKB site investigation program. From the figure it is obvious that the Lansjärv water belongs to the group of intermediate non saline groundwaters from granitic terrains.

The concentration of redox sensitive elements in the water is also low. However, the Eh monitoring, as well as the presence of detectable amounts of ferrous iron indicate the reducing character of the water.

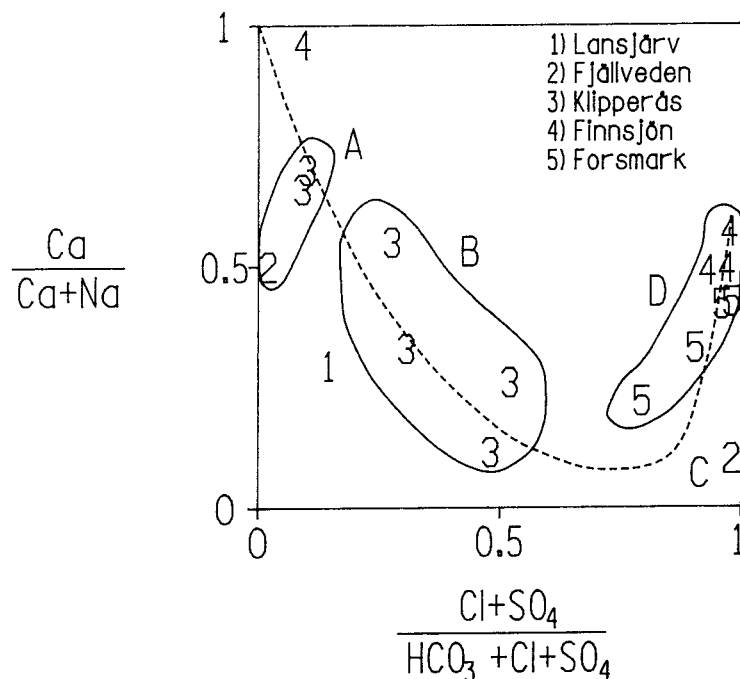


Figure 7-6. Anion versus cation ratios (Piperplot) of groundwaters from Lansjärv in comparison to other investigated waters from Fjällveden, Finnsjön, Klipperås and Forsmark. The groundwater evaluation line is dashed. The different groups are

- A: Calcium – Sodium – Bicarbonate type.
- B: Sodium – Calcium – Bicarbonate – Chloride type.
- C: Sodium – Chloride type.
- D: Calcium – Sodium – Chloride type.

The evaluation of the groundwater is from A to D.

## 7.5 ROCK STRESS MEASUREMENTS

### 7.5.1 Purpose of the Work

Rock stress measurements were conducted by means of the hydrofracturing method in borehole KLJ 01 during the autumn 1988. The purpose of the work was to measure magnitudes and orientations of horizontal stresses in the rock mass adjacent to the postglacial fault. Earlier hydrofracturing stress profiles in Sweden have mostly been measured in stable rock volumes. The measurements at Lansjärv were expected to show differences in stress magnitudes and relative stress orientations between stable and tectonically active rock mass.

### 7.5.2 The Stress Measuring Method

The conventional hydrofracturing method, as applied in this project, is two dimensional. It only measures stresses in a plane perpendicular to the axis of the borehole. In tectonically stable areas with flat topography the principal stress directions in the rock mass are assumed to be horizontal and vertical. Hydrofracturing measurements in vertical boreholes will in such cases give magnitudes and orientations of horizontal principal stresses. The near distance of borehole KLJ 01 to a fault plane precludes the assumption of vertical and horizontal orientation of principal stresses. Stress magnitudes and orientations are therefore given for the minimum and maximum horizontal stress components,  $S_h$  and  $S_H$  respectively.

Field data are treated according to the classical hydrofracturing analyzing method, Hubbert and Willis (1957), Bjarnason et al., (1988):

$$S_h = P_s \quad (1)$$

$$S_H = 3S_h - P_r \quad (2)$$

where:

$S_h$  = minimum horizontal stress

$P_s$  = shut-in pressure on the fracture plane

$S_H$  = maximum horizontal stress

$P_r$  = reopening pressure of the hydrofracture.

The magnitude of the vertical stress at every depth is assumed to be equal to the overburden pressure:

$$S_v = \gamma z \quad (3)$$

where

$S_v$  = vertical stress

$\gamma$  = unit weight of the rock mass

$z$  = depth below ground surface.

The strike of the induced hydrofracture give the orientation of the maximum horizontal stress at the measuring point.

### 7.5.3 Field Work

Casing in the borehole down to 152 m depth, precluded measurements at shallow levels. High fracture frequency and crushed rocks from the end of the casing down to approximately 300 m depth resulted in unsuccessful measurements in this interval. Difficulties were experienced in the borehole work from the beginning due to instability of the borehole walls along some of the crushed zones.

### 7.5.4 Results

Measurements were attempted at 27 different levels in the borehole. Six of the points, located between 200–300 m, did not give successful results due to difficult wall conditions. Between 300–500 m 20 points from a total of 21 gave useful results. Calculated stresses and stress ratios from these 20 points are presented in Table 7-2.

**Table 7-2. Stresses and stress ratios from hydrofracturing tests in borehole KLJ 01, Lansjärv.**

Depth (m)	$S_v$ (MPa)	$S_h$ (MPa)	$S_H$ (MPa)	$\frac{S_H}{S_h}$	$\frac{S_h}{S_v}$	$\frac{S_H}{S_v}$
308.5	8.1	4.6	7.8	1.7	0.6	1.0
323.5	8.5	5.6	9.7	1.7	0.7	1.1
352.0	9.3	7.6	12.5	1.6	0.8	1.3
354.0	9.3	8.4	14.5	1.7	0.9	1.6
356.5	9.4	8.8	16.4	1.9	0.9	1.7
378.4	10.0	9.2	16.4	1.8	0.9	1.6
410.3	10.8	7.5	13.4	1.8	0.7	1.2
440.4	11.6	7.3	14.4	2.0	0.6	1.2
442.5	11.7	8.0	14.0	1.8	0.7	1.2
447.0	11.8	6.3	12.6	2.0	0.5	1.1
449.0	11.8	6.2	11.7	1.9	0.5	1.0
452.0	11.9	5.5	10.4	1.9	0.5	0.9
455.0	12.0	6.0	6.9	1.2	0.5	0.6
462.5	12.2	5.7	9.6	1.7	0.5	0.8
469.3	12.4	7.2	12.0	1.7	0.6	1.0
474.5	12.5	5.8	9.5	1.7	0.5	0.8
480.3	12.7	7.3	13.9	1.9	0.6	1.1
489.3	12.9	6.1	10.6	1.7	0.5	0.8
491.8	13.0	6.2	10.8	1.7	0.5	0.8
494.0	13.0	6.4	12.6	2.0	0.5	1.0

$S_v$  = Calculated vertical overburden stress

$S_h$  = Minimum horizontal stress

$S_H$  = Maximum horizontal stress according to eq. (2)

The table shows extremely low values for the minimum horizontal stress, especially near the bottom of the borehole. Between 450–500 m the average value for  $S_h$  is only 6.2 MPa, compared to a theoretical value for the vertical stress of 12.6 MPa at 475 m depth. The low values of  $S_h$  are exceptional among the bulk of data obtained by the hydrofracturing method in Sweden where the values tend to be twice as high for these depths.

The maximum horizontal stress values are more scattered than the minimum stress. At depths between approximately 350–450 m,  $S_H$  is larger than  $S_v$ . At 450–500 m the  $S_H$  values are scattered around the assumed vertical stress and, are somewhat smaller than generally measured in Sweden. Stress magnitudes as a function of depth are plotted in Figure 7-7.

Fracture orientations were measured by the impression packer method at 20 test points. Results of orientation are shown in Table 7-3.



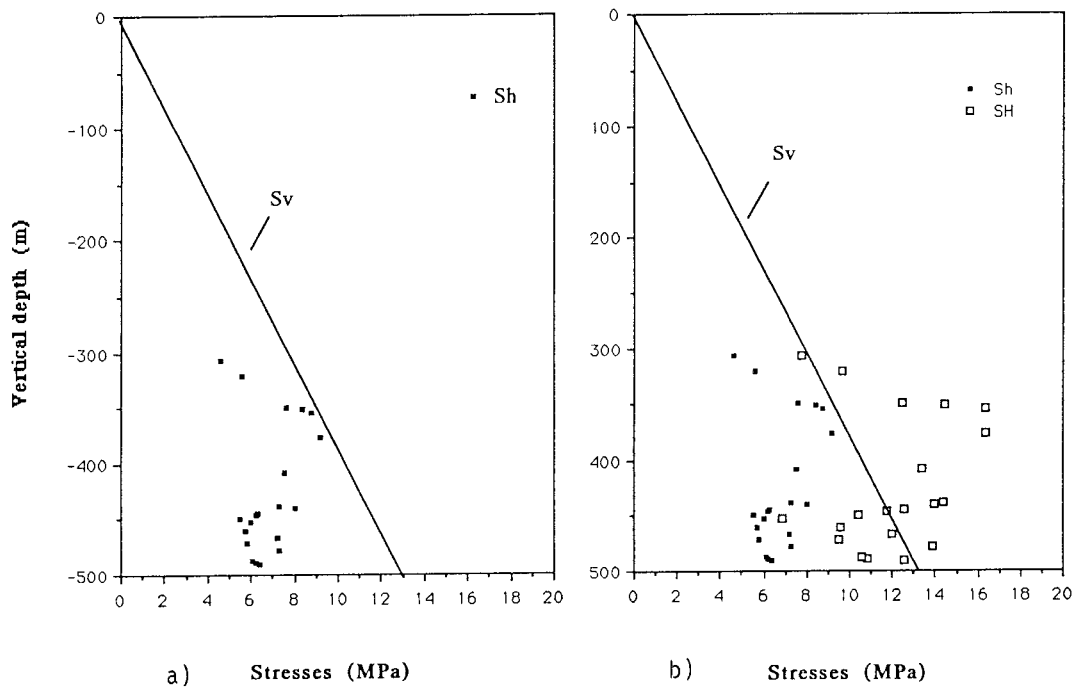


Figure 7-7. Measured stresses for borehole KLJ 01. a)  $S_h$  versus depth, b)  $S_h$  and  $S_{H1}$  versus depth. The vertical stress,  $S_v$  is calculated according to eq. 2.

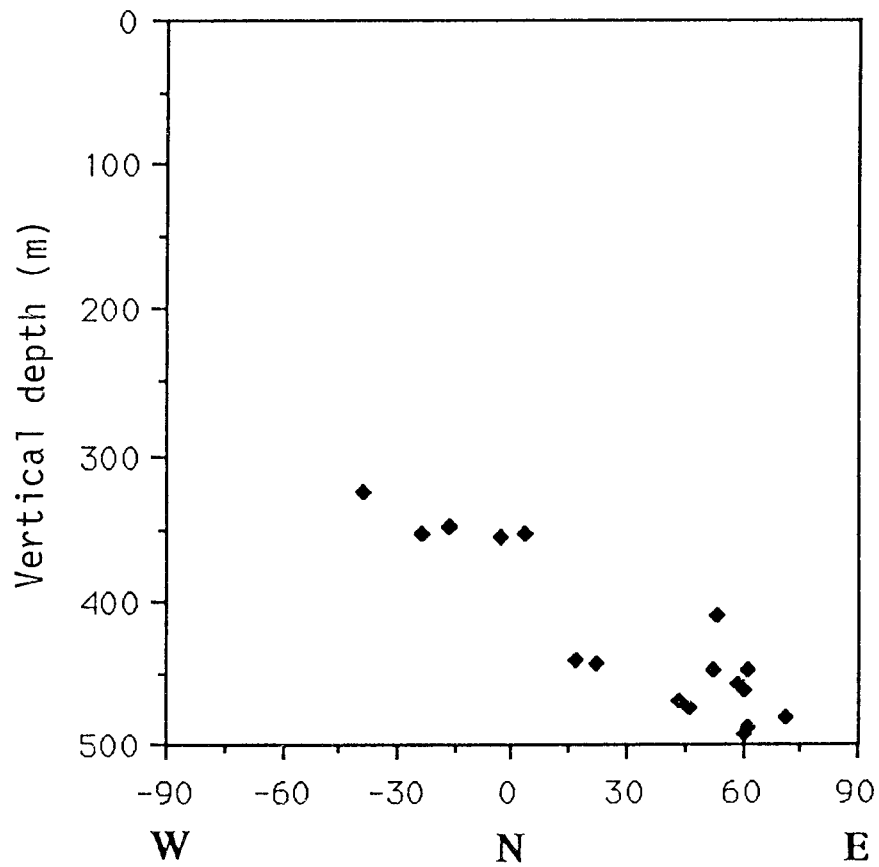


Figure 7-8. Orientation versus depth of the maximum horizontal stress,  $S_{H1}$ , as inferred from hydrofracture orientations.

**Table 7-3. Orientation of hydraulic fractures at Lansjärv.**

Depth (m)	Tool face (°)	F1 (°)	F2 (°)	S <sub>H</sub> (°)
308.5	239	No reliable vertical fracture		
323.5	119	81	265	39W
347.5	185	168	337	17W
352.0	274	90	336	24W
354.0	37	4	181	3E
356.5	254	175	359	3W
378.4	295	No reliable vertical fracture		
410.3	51	53	171	(53E)
440.4	157	21	193	17E
442.5	237	22	201	22E
447.0	228	62	239	61E
449.0	77	50	233	52E
455.0	58	60	237	59E
462.5	19	60	208	44E
469.3	300	43	223	43E
474.5	48	48	223	46E
480.3	140	70	252	71E
489.3	117	56	236	61E
491.8	193	65	240	60E
494.0	No orientation, bottom of borehole			

Tool face = Orientation of reference line on packer referred to N. F1 = Orientation of fracture 1. F2 = Orientation of fracture 2. ( ) = Fracture orientation not reliable S<sub>H</sub> = Orientation of maximum horizontal stress with respect to north.

The results in Table 7-3 are interesting. At 300 m depth the maximum horizontal stress is oriented close to NW–SE. It rotates rapidly and steadily with depth and at the bottom of the hole it has turned about 90°, to become ENE–WSW.

General results from previous stress profiling by the hydrofracturing method in stable Swedish rock masses, show more or less constant maximum stress orientations irrespective of test depth. For intact, isotropic rocks the orientation of hydrofractures is only controlled by stress directions. In layered or foliated rocks, or rocks containing other types of anisotropy, the initiation of hydrofractures may be controlled by the inherent weakness planes. The larger the S<sub>H</sub>/S<sub>v</sub> ratio is, the smaller the influence from rock structures. The S<sub>H</sub>/S<sub>v</sub> ratio in borehole KLJ 01 is generally high. Therefore, the rotation in measured hydrofracture orientations probably reflects a true rotation of S<sub>H</sub> caused by the local tectonics in the vicinity of the borehole.

### 7.5.5 Conclusions

Rock stress measurements in borehole KLJ 01 at Lansjärv reveal extremely low minimum stress magnitudes compared to existing data on rock stresses in Sweden.

The maximum horizontal stress rotates about 90°, from approximately NW–SE to ENE–WSW, over a depth interval of only 200 m in the bottom part of the borehole.

Due to local tectonic disturbances the minimum and maximum horizontal stresses measured in the borehole are probably not principal stresses.

## 7.6 REFERENCES

**Albino B 1988**

Results from the core mapping in KLJ 01, Lansjärv.  
SKB Borrhålsrapport KLJ 01, Stockholm

**Bjarnason B, Ljunggren C and Stephansson O 1988**

New developments in hydrofracturing stress measurements at Luleå University of Technology.  
International J. of Rock Mechanics and Geomechanics Abstracts (In press).

**Hansson K 1988**

Hydrogeological investigations in the Lansjärv area.  
SKB AR 89-11, Stockholm

**Henkel H 1988**

Tectonic studies in the Lansjärv region.  
SKB TR 88-07, Stockholm

**Hubbert M K and Willis D G 1957**

Mechanics of Hydraulic Fracturing.  
Trans. A.I.M.E., 210, pp 153–168

**Sehlstedt S 1988**

Geophysical borehole logging in Lansjärv, KLJ 01.  
SKB Borrhålsrapport KLJ 01, Stockholm

# 8 HYDROGEOLOGICAL CONDITIONS

*Nils-Åke Larsson*

Swedish Geological Co

Box 1424, S-751 44 Uppsala, Sweden

## 8.1 GENERAL

The hydrogeological investigations have comprised hydraulic testing in one borehole, KLJ 01, observations of groundwater levels and compilation of a groundwater level map of the area. In addition, generic numerical modelling has examined to what extent the hydrogeological conditions, in particular groundwater pressure distribution, can be explained by current geological interpretations of the area.

The groundwater level map, Figure 8-1 is based on the general assumption that the groundwater level conforms with the topography. It is thus assumed that wetlands and streams coincide with the groundwater table and that the groundwater level under hill areas is located some 10–15 m below the ground surface. The measured groundwater levels in the boreholes are presented in Table 8-1.

GROUND WATER LEVEL MAP

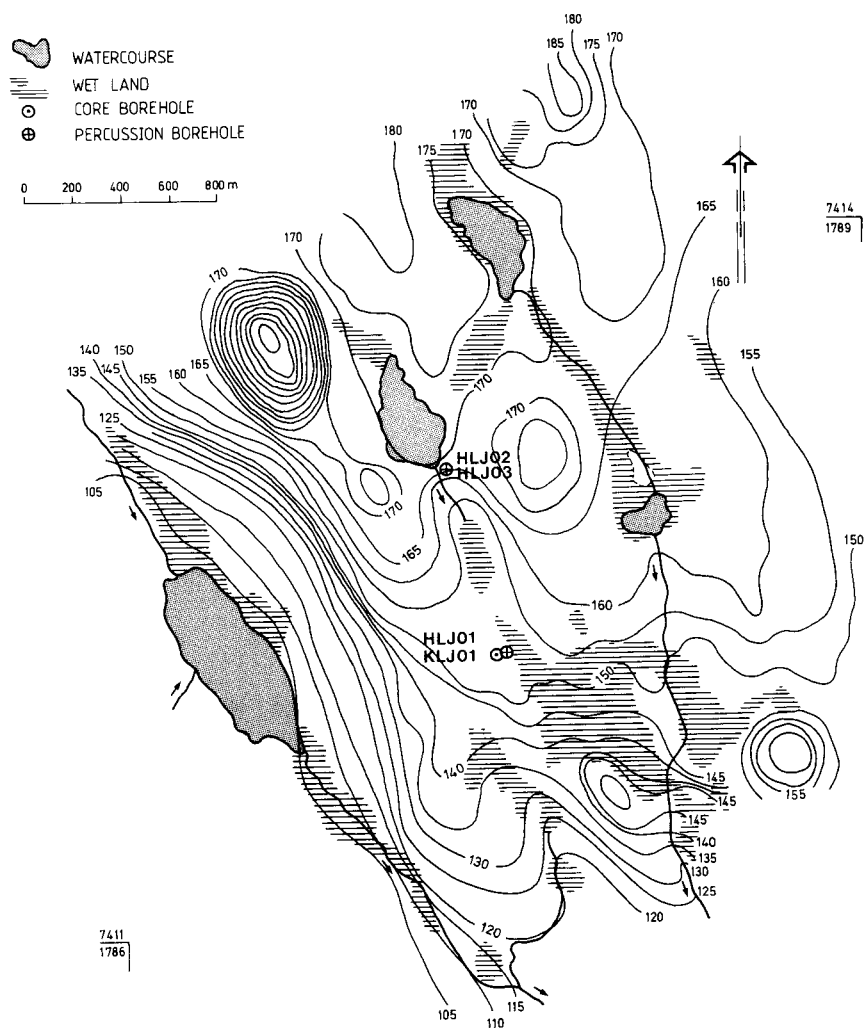


Figure 8-1. Groundwater level map of the Lansjärv area.

**Table 8-1. Altitude of the groundwater level in Lansjärv.**

Bore hole	Borehole length (m)	Borehole incl (°)	Ground level (m a s l)	Groundwater level	
				88-06-11 (m a s l)	88-10-17 (m a s l)
KLJ 01	500	85	+153.5	+134.0	+135.3
HLJ 01	75	70	+153.7	-	+151.1
HLJ 02	84	85	+177.9	-	+121.0*
HLJ 03	92	85	+172.2	+102.5	+105.7

\* uncertain value

## 8.2 BOREHOLE TESTING IN KLJ 01

### 8.2.1 Hydraulic Conductivity and Groundwater Pressure

Steady state injection tests were conducted in 10 m sections down to 150 m depth and in 30 m and 3 m sections in the rest of the borehole. The test sequence was changed for the tests below 150 m depth in order to accommodate the low groundwater pressures that were expected to prevail at depth, according to the low groundwater levels in some of the percussion holes, c.f. Table 8-2. Further details on equipment, test procedure and measurement limits are given by Hansson (1989).

**Table 8-2 Test sequence for the steady state injection tests in KLJ 01.**

	B O R E H O L E L E N G T H		
	0 – 150 m	154 – 490 m	
Test section length (m)	10	30	3
Packer inflation (min)	15	30	15
Pressure adjustment (min)	5–15	15–60	10–15
Water injection (min)	15	15	10
Packer deflation (min)	10	10	10

The tests were evaluated assuming steady state conditions. The hydraulic conductivity in the 10 m and 30 m sections in KLJ 01 is illustrated in Figure 8-2. The in situ groundwater pressure calculated from the testing in 30 m sections is also presented in the Figure; Crosses represent the pressure after 60 minutes of pressure adjustment with inflated packers and dots represent pressures extrapolated to one week. The solid line corresponds to the hydrostatic pressure in the open borehole.

The hydraulic conductivity in KLJ 01 decreases slightly with depth and varies within the interval that can be expected according to the geological environment. The greatest hydraulic conductivities ( $\geq 1 \cdot 10^{-6}$  m/s) are obtained in the depth interval where the fracture frequency is highest and where the borehole is interpreted to intersect the post-glacial fault (PGF).

At greater depth the hydraulically conductive parts are concentrated to a few 3 m sections, see Figure 8-3. For some of these sections the hydraulic conductivity is probably caused by weathering, intense fracturing and/or pegmatite dykes or veins (e.g. 181–190 m, 193–196 m, 205–208 m, 316–322 m and 415–424 m).

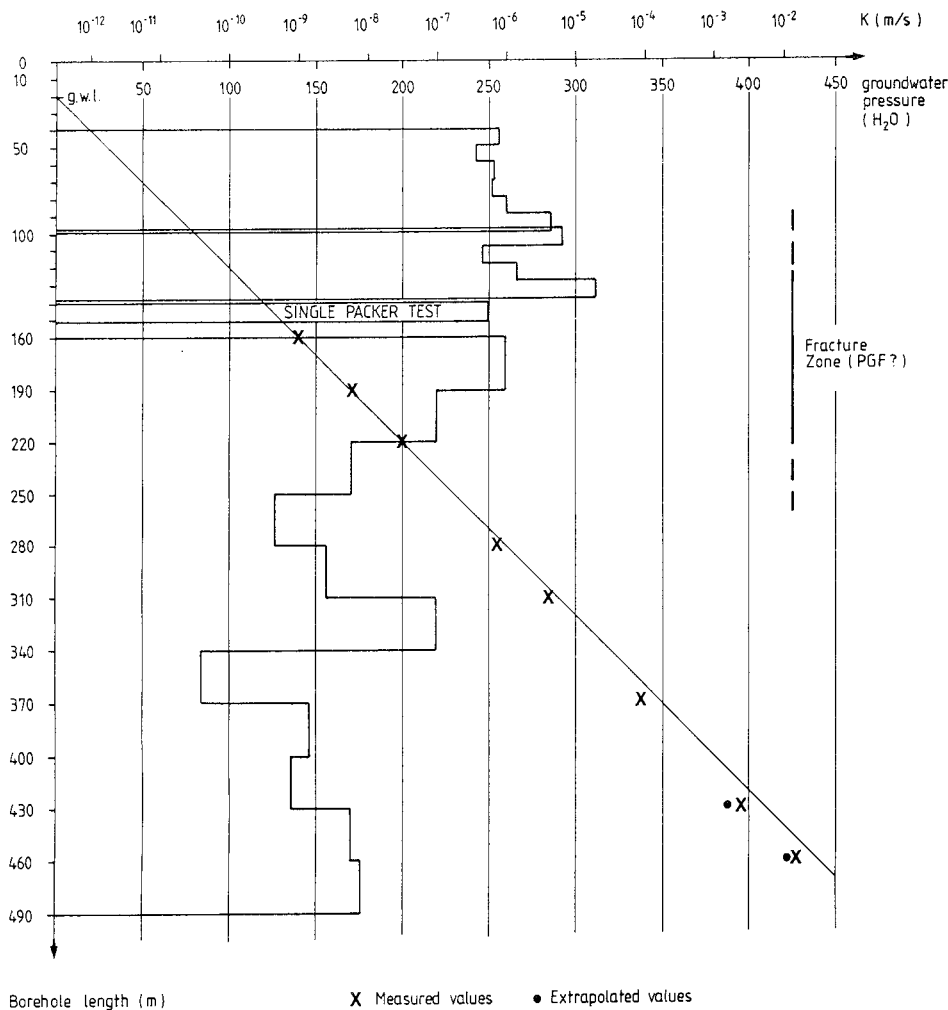


Figure 8-2. Hydraulic conductivity and groundwater pressure in borehole KLJ 01, Lansjärv.

In other sections the conductivity seems to be caused by single fractures, e.g. 406–409 m, 451–457 m. In the latter sections the maximum horizontal rock stress ( $S_H$ ) is rather low and becomes smaller than the calculated vertical overburden stress ( $S_v$ ), i.e.  $S_H/S_v < 1$ . There exists, however, no obvious correlation between hydraulic conductivity and fracture frequency, rock type, rock stress or fracture infillings; For example, the intense fracturing in the sections 280–283 m and 337–340 m is not linked with high hydraulic conductivities.

The same situation is apparent for the geophysical logging, Sehlstedt (1988), even though most of the conductive 3 m sections are indicated in the Single point resistance, Sonic and Resistivity logs, see Figure 8-3. One important deviation is identified at approx. 265–280 m; here the geophysical logs clearly indicate an extreme anomaly which is not related to intense fracturing. The anomaly is caused by increased porosity due to alteration of the granite; cavities of some 5 mm was identified in the drill core. Nevertheless, the low hydraulic conductivity in the section imply that the cavities are isolated features in the rock mass.

The borehole fluid temperature profile indicate groundwater flow along the borehole, see Figure 8-3. The temperature gradient, approx.  $7.5^\circ\text{C}/\text{km}$ , is low according to measurements at other sites in the region. For example, the temperature gradient at the study site Kamlunge is generally greater than  $9^\circ\text{C}/\text{km}$ ,

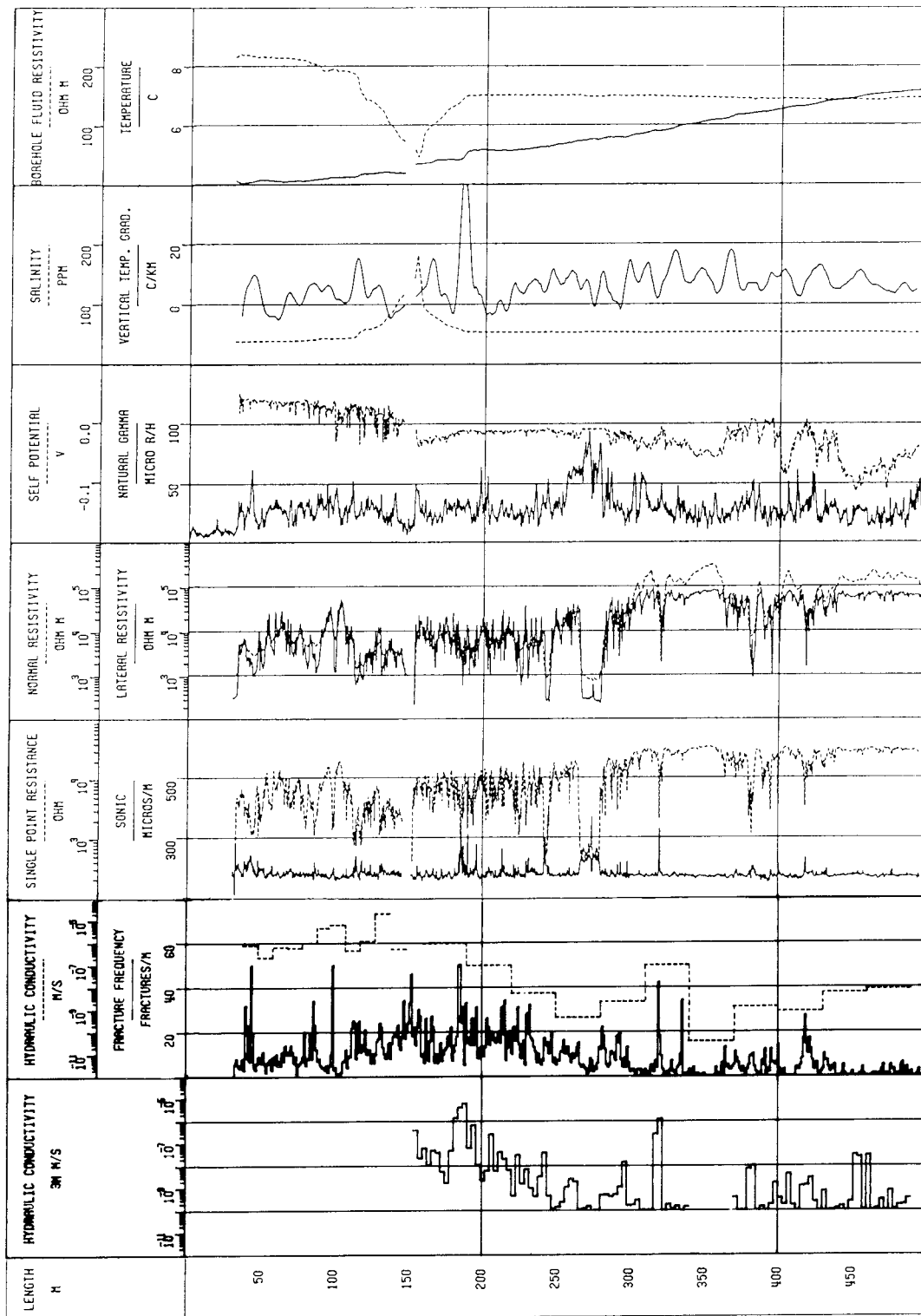


Figure 8-3. Complot diagram of borehole measurements in KLJ 01, Lansjärv.

Lindholm et al. (1983). According to the groundwater pressure measurements in KLJ 01 the groundwater transport is in the downward direction, see Figure 8-2.

### **8.2.2 Hydraulic Conductivity – Comparison with other Study Sites**

The hydraulic conductivity in KLJ 01 have been compared with data from other study sites investigated by SKB. The hydraulic conductivity from steady state tests in 2 m and 3 m sections from all core boreholes in Finnsjön (KFI01–11), Fjällveden (KFJ02), Gideå (KGI07, 09, 11), Kamlunge (KKM02) and Karlshamn (KKA01–05) have been selected.

The geometric and arithmetic means and standard deviations of the hydraulic conductivity for the boreholes of these study sites have been calculated for every vertical depth interval of 100 m.

In Figure 8-4 the geometric means, i.e. arithmetic mean of  $\log(K)$ , are plotted for Lansjärv, Karlshamn, Finnsjön and for the “KBS-3 sites” (Fjällveden, Gideå and Kamlunge). The calculated values for KLJ 01 are given larger circles than the other boreholes.

In Figure 8-5 the arithmetic means and the standard deviations from all boreholes are plotted. (The arithmetic mean differ from the geometric mean in that large K-values have relatively great influence on the arithmetic mean).

The geometric mean below 200 m depth implies that KLJ 01 is somewhat more conductive than the boreholes from the KBS-3 sites and slightly less conductive than the Karlshamn site. The lower measurement limit is not the same for the different boreholes but that does not affect this conclusion. Based on KFI04–07, which are the only comparable holes from the site, Finnsjön is much more conductive than KLJ 01.

From Figure 8-5 it can be seen that KLJ 01 is “normal” compared to the other holes. If looking more in detail one will of course find that some boreholes (e.g. KKM02 and KKA01) have lower mean values than KLJ 01.

## **8.3 CONDUCTIVE FRACTURE FREQUENCY**

### **8.3.1 Definition**

The conductive fracture frequency (CFF) implies the hydraulically conductive portion of the total number of fractures mapped over a given length in a borehole or an underground opening.

Statistical techniques to calculate CFF, which utilize information from hydraulic tests and core logs, yield an estimate of the probability that one fracture is conductive. A hydraulic conductivity equal to the lower measurement limit is regarded as non-conductive in this context. Combined with the average fracture frequency in the studied domain, an estimate of CFF is obtained. Statistical homogeneity and independence is assumed in the rock volume studied. The basic theory for calculations of CFF is presented by Carlsson et al. (1984) and is further developed in Andersson et al. (1988).

### **8.3.2 Input Data**

Two basic input data groups are essential to the calculation of the conductive fracture frequency; a suite of data on the hydraulic conductivity of a fixed section length and the corresponding number of coated fractures, i.e. discontinuities with fracture infillings along which the core is parted, per test section.



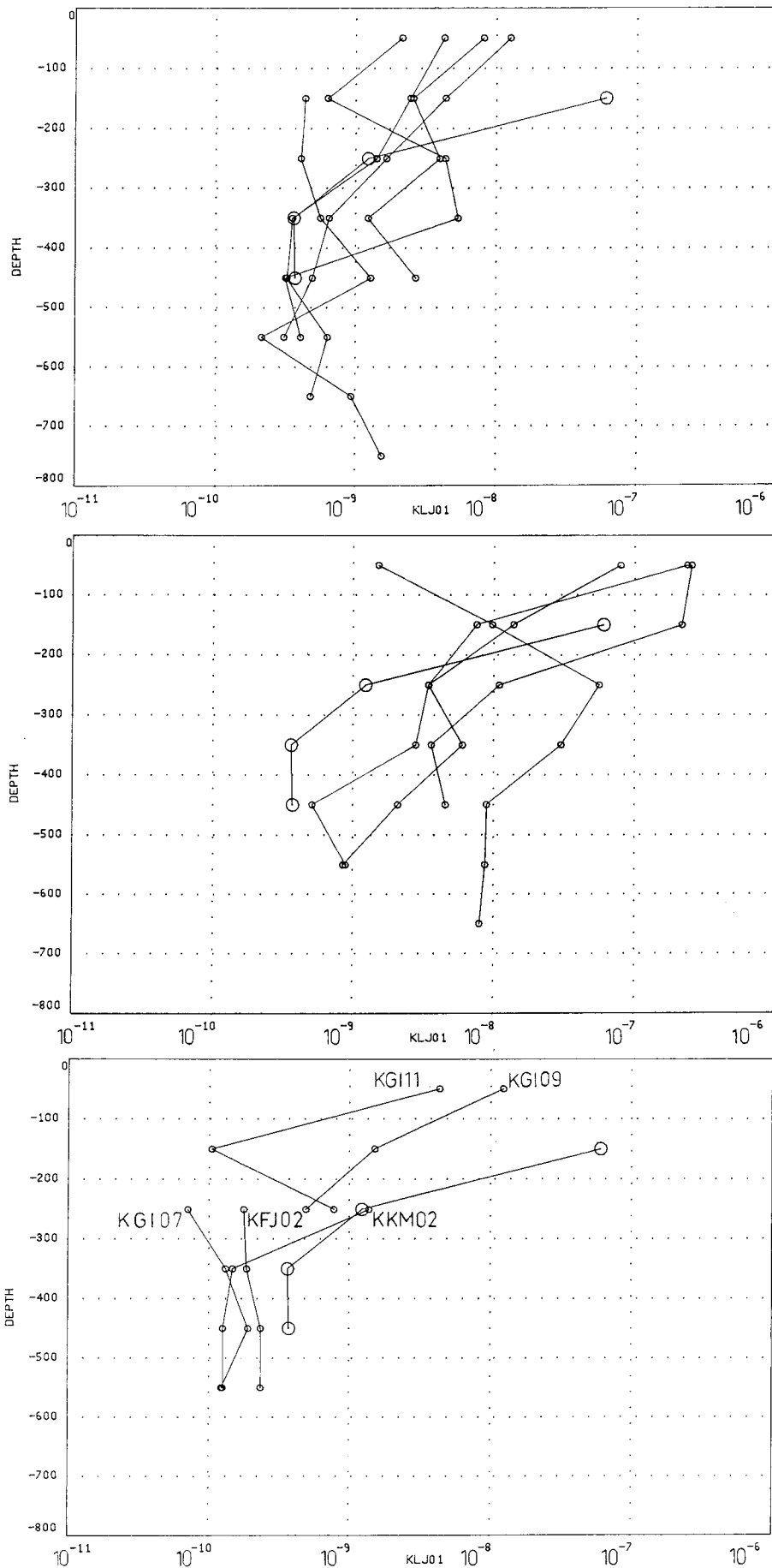


Figure 8-4. Geometric mean of hydraulic conductivity from Lansjärv, Karlshamn (top), Finnsjön (middle) and KBS-3 sites (bottom). Data are calculated for 100 m vertical depth interval. Data from Lansjärv (KLJ 01) have large circles.

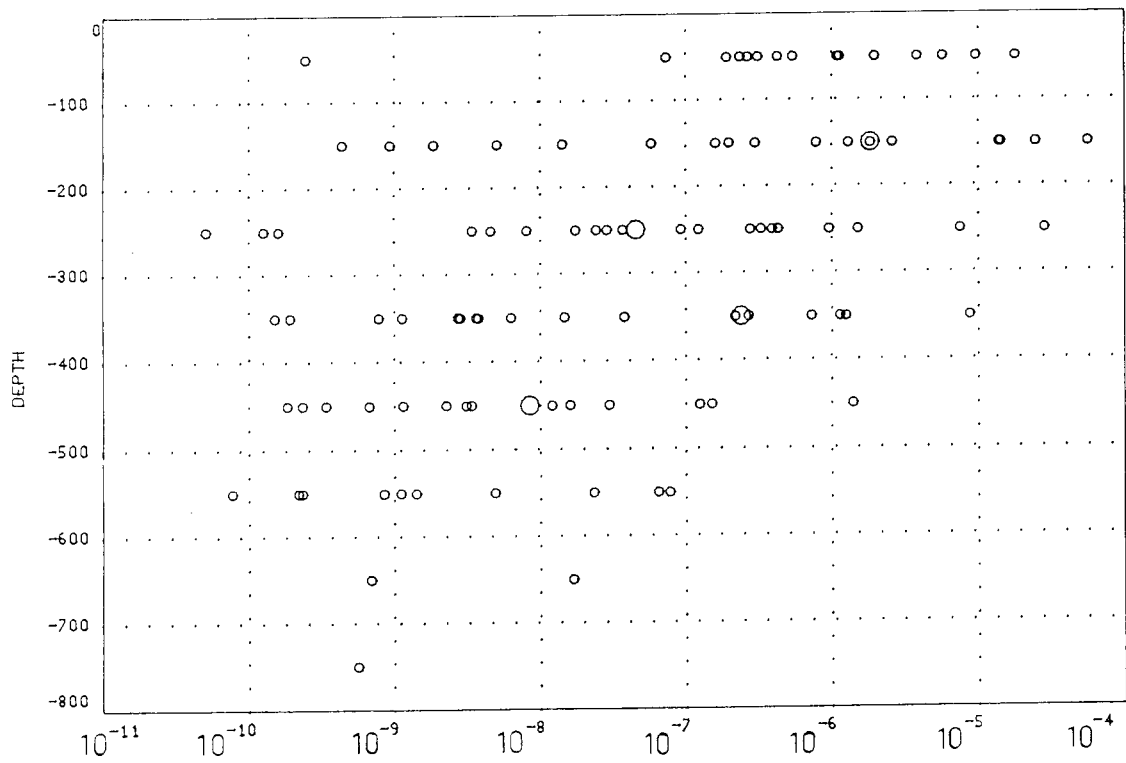
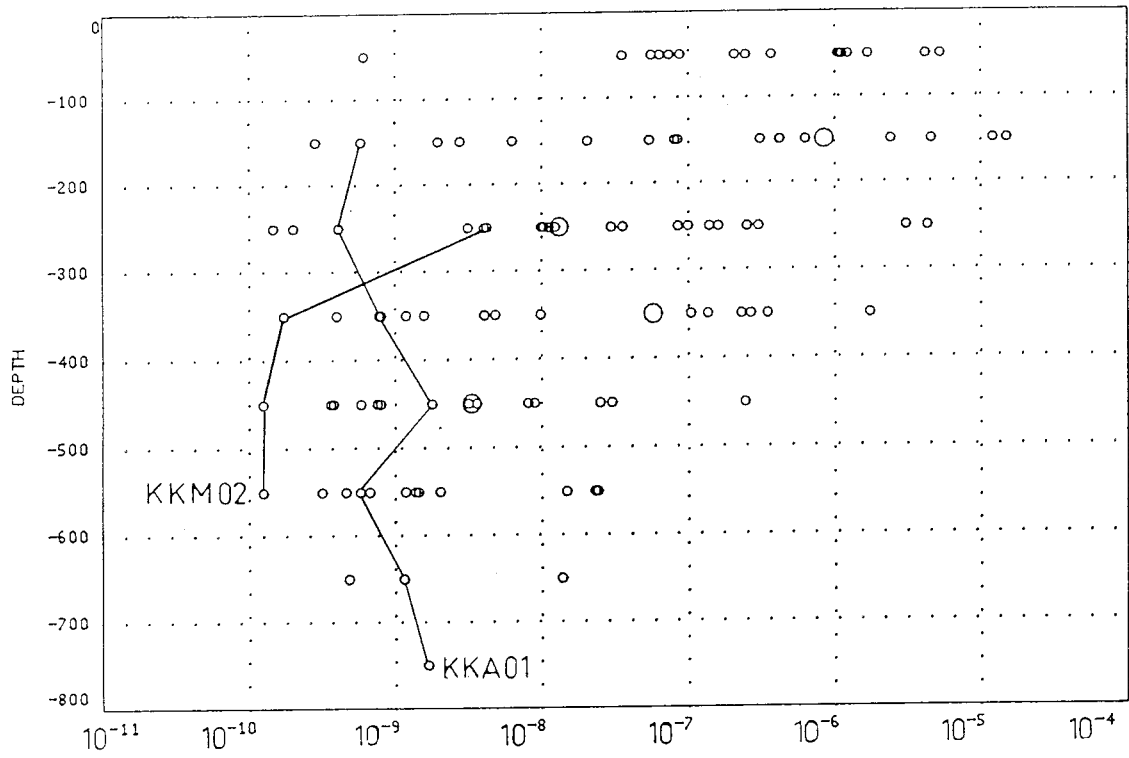


Figure 8-5. Arithmetic mean (top) and standard deviation (bottom) of hydraulic conductivity from 22 boreholes in SKB's study sites. Data are calculated for 100 m vertical depth interval. Data from Lansjäv (KLJ 01) have large circles.

The total number of data on hydraulic conductivity in 3 m sections from KLJ 01 is 105. The number of coated fractures are in this case defined as the sum of individual coated fractures plus the contribution of fracture groups and occurring crushed or core loss intervals (the latter defined as contributing 50 fractures/m).

The data set collected within the depth range 154–490 m may be subdivided into two subsets. One between 154–265 m (37 data) defining the lower parts of the actual interpreted post-glacial fault zone (A) and a second between 265 and 490 m (68 data) (B). The latter subset (B) represents the naturally fractured rock mass below the zone. This subdivision is evident and substantiated by the core log, the geophysical logs and the hydraulic conductivity log. The conductive fracture frequency has been analysed for the two defined subsets.

### 8.3.3 Results

The analysis of the data from subset (A) soon revealed that none of the measured test sections were at the measurement limit ( $1 \cdot 10^{-10}$  m/s). This fact naturally did not provide a numerical solution and consequently, by definition, implies that all fractures are conductive, i.e. CFF equals the average frequency of coated fractures which is 14.2 fractures/m. However, it should be appreciated that the true in situ CFF may be lower.

The data set (B) contains 20 test sections (29%) with a hydraulic conductivity equal to the measurement limit. The average frequency of coated fractures in the studied domain is 4.5 fractures/m. The calculated probability 1-P is 0.192 which yields a conductive fracture frequency of 0.86 fractures/m, c.f. Table 8-3.

**Table 8-3. Calculation of the conductive fracture frequency based on 3 m data from bore-hole KLJ 01 at Lansjärv.**

<b>Bedrock unit</b>	<b>1-P</b>	<b>n<sub>r</sub></b>	<b>CFF</b>	<b>±</b>	<b>C.I.</b>	<b>S</b>	<b>M</b>
PGF (A)	1.0	14.2	14.2		0.07	37	
below PGF (B)	0.192	4.5	0.86		0.41	1.16	68

1-P = probability that one fracture is conductive

n<sub>r</sub> = average frequency of coated fractures

C.I. = 95% confidence limit

S = average distance between conductive fractures

M = number of test sections in the studied domain

### 8.3.4 Comparison of CFF with other Study Sites

Calculations of CFF have previously been made on data from most of the SKB's study sites. Bearing in mind the comparably surficial nature of the Lansjärv data together with the impact of the studied fracture zone, the closest comparable datasets would be those from the Brändan area in Finnsjön and data from the Repository for Reactor Waste (SFR) at Forsmark.

The data from SFR indicated a CFF of approximately 0.3 fractures/m for the rock mass, the mean value being rather constant with depth (0–200 m), Carlsson et al. (1987). The probability 1-P was on the order of 0.11.

In the Brändan area, comparisons between the CFF of the subhorizontal 100 m thick fracture zone (Zone 2) in Finnsjön and that of the rock mass was made. The zone itself and the rock mass above indicated a CFF of approximately 1 frac-

ture/m whereas the CFF of the rock mass below the zone was reduced with approximately 50%. The probability 1-P varied between 0.2 and 0.3.

In summary, the conductive fracture frequency (CFF) of the rock mass at Lansjärv is on the order of 0.9 fractures/m whereas no numerical result was obtained for data related to the PGF itself, indicating that the CFF in this case is remarkably high.

The value of CFF for the sub-PGF rock mass at Lansjärv, is comparably high when considering the depth range of the analyzed data. This fact is attributed to an average frequency of coated fractures which is approximately a factor 2 higher than at the average KBS-3 sites.

The CFF of the rock mass at Lansjärv is comparable to values on CFF calculated for the subhorizontal Zone 2 at Brändan and the rock mass above that fracture zone. This striking and contradicting correspondence in CFF between Zone 2 at Brändan and the sub-PGF rock mass is interpreted as an effect of the highly heterogeneous nature of Zone 2 and the above mentioned high fracture frequency in KLJ 01.

## **8.4 NUMERICAL MODELLING**

### **8.4.1 Objective and Approach**

The objective of the numerical modelling has been to study some aspects of the effects of fracture zone geometry on groundwater flow conditions. The observations from hydraulic measurements that need to be explained can be summarized as:

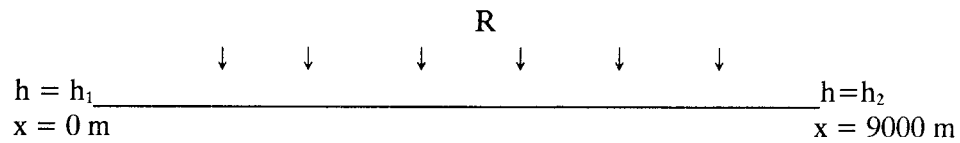
- a very low groundwater level (approx. 70 m below ground surface i.e. a hydraulic head of +105 m.a.s.l.) in percussion borehole HLJ 03.
- a relatively large vertical hydraulic gradient prevails throughout the length (500 m) of core borehole KLJ 01.

Several sets of geometrical configurations of fracture zones have been considered, and the resulting hydraulic head distributions have been compared to measurements from borehole KLJ 01.

The approach for the calculations has been to apply a two-dimensional model describing a vertical profile, coinciding with a section between KLJ 01 and HLJ 03. The underlying assumptions for the calculations is that flow takes place in a porous, isotropic and heterogeneous medium. The calculations have been carried out using the finite element code SUTRA, Voss (1984).

### 8.4.2 Verification of Hydraulic Boundaries

A possible origin for the low head in HLJ 03 are Lake Övre Lansjärv (SW of the site) and River Ängesån (NE of the site). To verify the possibility of these boundaries, a simple, onedimensional model have been used. The model consists of a line connecting Övre Lansjärv and Ängesån, and can be described as:



where  $h_1 = 86$  m.a.s.l. (Övre Lansjärv)  
 $h_2 = 90$  m.a.s.l. (Ängesån)

$R$  (m/s) is the recharge rate, and is assumed to be constant in the  $x$ -direction. If a confining layer exists,  $R$  corresponds to a leakage rate. The boreholes HLJ 03 and KLJ 01 are located at approximately  $x = 5000$  m.

The solution in terms of hydraulic head in the  $x$ -direction is:

$$h(x) = h_1 + \frac{h_2 - h_1}{9000} \cdot x + \frac{R}{2K(x)} \cdot (9000 \cdot x - x^2)$$

where  $K(x)$  = hydraulic conductivity in the  $x$ -direction(m/s).

The observed hydraulic head in HLJ 03 is +105 m.a.s.l. Assuming a hydraulic conductivity of  $1 \cdot 10^{-4}$  m/s, the recharge rate required to maintain that head is approximately 6 mm/year which is entirely reasonable. Thus, the assumption of Lake Övre Lansjärv and River Ängesån as far field hydraulic boundaries is realistic.

Assuming a confining layer with a vertical hydraulic conductivity  $K(z)$ , the  $R$  can be expressed as:

$$R = P' \cdot K(z)$$

where  $P'$  = vertical hydraulic gradient.

$P'$  is estimated from borehole measurements to 0.04, which results in a contrast in hydraulic conductivities,  $K(x)/K(z)$ , of the order of  $2 \cdot 10^4$ . This ratio was later used in the two-dimensional model, to define fracture zones and rock mass, respectively.

### 8.4.3 Modelled Cases and Results

The two-dimensional modelling in a vertical profile was generally performed with an internal boundary region defining the low pressure as measured in HLJ 03, at a depth of approximately 70 m. The flow discharge resulting from this region is considered as outflow perpendicular to the vertical plane, in the direction of either Övre Lansjärv or Ängesån. Definition of other boundaries is rather arbitrary. In general, the upper boundary and parts of the vertical boundaries is set at constant head = 0.0. The lower boundary is considered as a no-flow boundary.

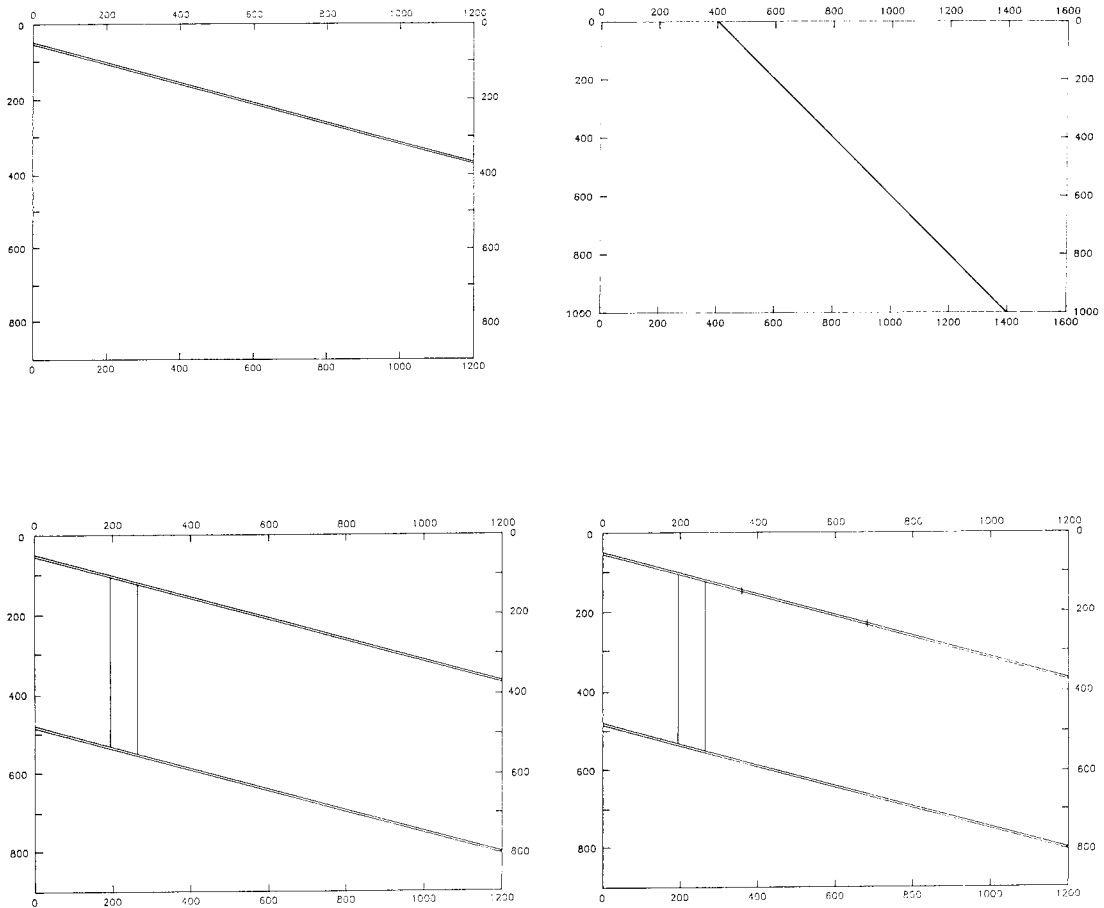


*Figure 8-6. Model geometries for case 1 (top left), case 2 (top right), case 3 (bottom left) and case 3B (bottom right).*

The results of the numerical modelling can be divided into three main cases:

1. One fracture zone with an inclination of  $15^\circ$  (representing a fracture zone intersecting the upper part of KLJ 01).
2. One fracture zone with an inclination of  $45^\circ$  (representing a fracture zone located below the bottom of KLJ 01).
- 3A. Two fracture zones with an inclination of  $15^\circ$ , and separated by approximately 400 m in the vertical direction (the upper zone intersecting KLJ 01).
- 3B. Identical to 3A, except for a discontinuity of low hydraulic conductivity introduced in the upper fracture zone.

The geometries of the modelled cases are illustrated in Figure 8-6.

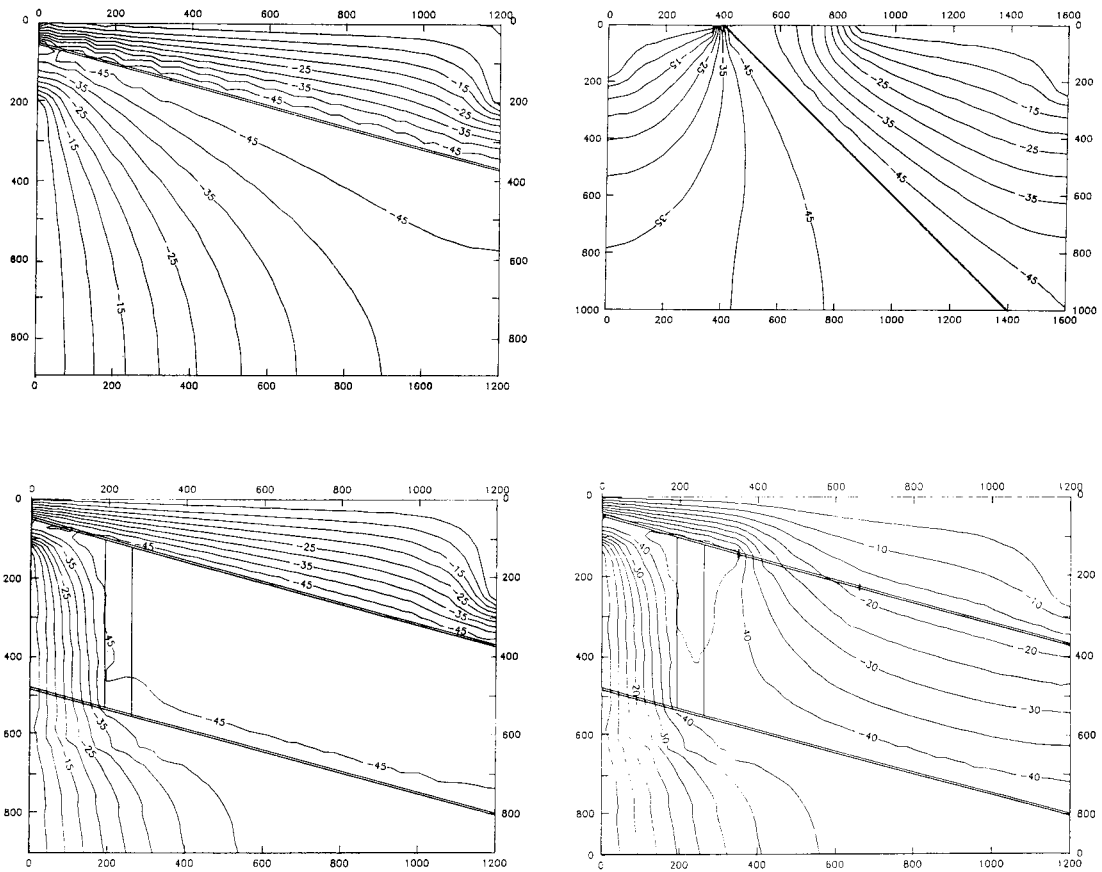


Figure 8-7. Simulated hydraulic head distribution for case 1 (top left), case 2 (top right), case 3A (bottom left) and case 3B (bottom right).

The results are illustrated in Figure 8-7, which plots hydraulic head for each case.

**Case 1:** As expected, the fracture zone acts as a line sink, causing hydraulic gradients directed towards it.

**Case 2:** The resulting flow pattern is analogous to the one for case 1.

**Case 3A:** Case 3A consists of, in addition to the two horizontal fracture zones, a vertical fracture zone connecting the horizontal ones. The striking result in this case is how readily the low hydraulic heads are conducted down to significantly deeper regions.

**Case 3B:** The results are somewhat similar to case 3A, but with a different hydraulic head distribution in the region between the horizontal fracture zones. It can be remarked that the result would be similar if the vertical connection between the upper and lower zones is replaced by a low head in the lower zone.

Comparison of the different simulated cases with the observed hydraulic head distribution (c.f. Figure 8-2) shows that cases 1 and 3A represent conditions that contradict measured results. Case 1 results in partly negative vertical gradients, while in case 3A the gradient is practically zero in the region between the horizontal fracture zones.

Cases 2 and 3B appear to represent realistic hydraulic conditions, resulting in vertical gradients that are approximately equal to the observed gradients in KLJ 01.

#### 8.4.4 Concluding Remarks

The modelling described here has clearly pointed out some missing pieces of information needed in order to explain the hydraulic conditions in the Lansjärv area. Although none of the cases attempts to in detail describe reality, some possible geometrical configurations can be identified.

The existence of an upper, **continuous** fracture zone with an inclination of 15° (case 1 and 3A) does not explain observed hydraulic data. Parallel fracture zones of 15° inclination may explain data, if the upper zone is **discontinuous** (case 3B). Another possibility would be a steeper inclination of the upper fracture zone (case 2).

#### 8.5 REFERENCES

**Andersson J-E, Ekman L and Winberg A 1988:**

Detailed investigations of fracture zones in the Brändan area, Finnsjön study site.

SKB AR 88-08.

**Carlsson L, Winberg A and Rosander B 1984:**

Investigations of hydraulic properties in crystalline rock.

Mat Res Soc Symp Proc Vol 26. Boston, Elsevier.

**Carlsson L, Grundfelt B and Winberg A 1987:**

Hydraulic modelling of the final repository for reactor waste (SFR). Evaluation of the groundwater flow situation at the SFR.

SKB Progress Report SFR 86-07

**Hansson K 1989:**

Hydrogeological investigations in the Lansjärv area.

SKB AR 89-11, Stockholm.

**Lindholm T, Sehlstedt S and Stenberg L 1983:**

Borehole geophysical investigations in the study site Kamlunge. (In Swedish).

SKBF/KBS AR 83-22

**Moye D G 1967:**

Diamond drilling for Foundation Exploration. Civ. Eng. Trans.

Inst. Eng. Australia, pp 95–100.

**Sehlstedt S 1988:**

Geophysical borehole logging in Lansjärv, KLJ 01.

SKB Borrhålsrapport KLJ 01, Stockholm

**Voss C 1984:**

A finite-element simulation model for saturated-unsaturated fluid density dependent groundwater flow with energy transport or chemically reactive single species solute transport.

U.S. Geological Survey, Water Resources Investigations Report 84-4369.





# 9 MINERALOGICAL AND GEOCHEMICAL STUDIES OF FRACTURE-INFILLINGS IN DRILLCORE KLJ 01

*Ove Landström<sup>1</sup>, John Smellie<sup>2</sup>, Eva-Lena Tullborg<sup>3</sup>*

<sup>1</sup>Studsvik Energiteknik AB, S-611 82 Nyköping, Sweden

<sup>2</sup>Swedish Geological Co, Box 1424, S-751 44 Uppsala, Sweden

<sup>3</sup>Swedish Geological Co, Pusterviksgatan 2, S-413 01 Göteborg, Sweden

## 9.1 INTRODUCTION

This study forms part of the overall investigation of the Lansjärv post-glacial fault zone. The main objectives are:

- to identify any mineralogical and/or microstructural evidence that might support recent reactivation movements along the tectonic zone (i.e. since the last ice-age ca. 10 000 yrs. ago),
- to determine whether low temperature rock/water reactions have contributed to changes in the fracture mineralogy and chemistry.

The studies have been carried out on drillcore material from borehole KLJ 01 drilled to a depth of 500 m to intercept an assumed neotectonic zone. The core has been systematically sampled, the sampled locations being based on available geological, geophysical and hydrological logging data.

## 9.2 RESULTS FROM THE CORE LOGGING

Drillcore KLJ 01 is characterised by a high fracture frequency mostly corresponding to high hydraulic conductivity in the upper 300 m. Below this depth the fracture frequency decreases drastically. From the borehole logging it can be clearly seen that chlorite and iron-oxyhydroxides are a common fracture constituent throughout the complete length of the borehole while calcite is depth dependent becoming most noticeable at approx. 200 m depth, although minor amounts have been observed at 54 m, 64 m, 110 m and from 165–180 m, Albino (1988). The relative absence of calcite at higher levels is most likely due to the high fracture frequency and high conductivity of the upper 300 m of the bedrock. This has provided an effective groundwater flow through the fracture systems thus dissolving and flushing out the carbonate minerals. Subordinate hydrothermal minerals like epidote, zeolites and prehnite occur in the fractures throughout the drillcore.

## 9.3 SAMPLING AND ANALYSES

The samples were collected from a series of open and sealed fracture zones with special emphasis on the zone at approx. 140 to 150 m, in addition to other fracture zones considered to be water-conducting.

Geochemical sampling consisted of scraping the mineral coatings from the fracture faces; care was taken to ensure that a minimum of host-rock material was included which otherwise would result in contamination and erroneous elemental concentrations. In addition, analyses were carried out on samples

from the wall rock, 7 to 15 mm from the fracture edge (i.e. B-samples) and in some cases also more than 20 mm from the fracture surface (i.e. C-samples). For comparison, some samples of unfractured, fresh granite are also included. Analysis on the fracture powders, as well as on the rock samples, was carried out using Instrumental Neutron Activation (INA) at Studsvik AB. The elements measured were Na, Fe, Cr, Co, Zn, Sb, Sr, Rb, Cs, Zr, Hf, Ta, Th, U, Sc and the lanthanides (excluding Pr, Pm, Gd, Dy, Ho, Er, Tm).

Sections for microscopic examination were selected, when possible, perpendicular to the fracture faces in order to trace the extent of alteration from the fracture into the host-rock.

X-ray diffractometry (XRD) was used in order to identify especially fine-grained mineral coatings within the fractures. These analyses were carried out at SGAB in Luleå.

## 9.4 MINERALOGY – RESULTS OF MICROSCOPY

The host-rock penetrated by borehole KLJ 01 is a medium to fine-grained granite comprising roughly equal amounts of quartz and feldspar. Interstitially are mafic aggregates comprising magnetite and biotite with subordinate amounts of sphene, apatite and accessory zircon; sporadic pyrite also occurs. All sections show varying degrees of alteration in which the feldspar breaks down to fine-grained mica (mainly sericite with subordinate muscovite), biotite to chlorite, and magnetite to hematite and hydrous oxides. In some cases, depending on the availability of Ca, minor epidote forms in association with the breakdown of both biotite and magnetite.

Within 1–2 cm from the fracture face, the granite itself has usually undergone some minor fracturing (e.g. samples from 114.80 m, 420.00 m), and in extreme cases completely crushed with only fragmented quartz representative of the primary mineral phases (e.g. samples from 76.21 m, 287.70 m, 319.80 m). Here the feldspar has been totally altered contributing to a very fine-grained matrix comprising alteration mica phases (sericite, chlorite), recrystallised quartz, and sometimes fine granular epidote and sphene. For those fracture zones considered water-conducting, the matrix adjacent to the fracture is usually highly charged with iron oxyhydroxides, present as fine dustings of amorphous hydrous oxides and/or hematite as aggregates and flakes. The former impregnates especially the altered feldspar, the degree of impregnation corresponding to the extent of alteration. Hematite forms mostly in the matrix and partly to completely pseudomorphs primary magnetite.

In addition to the micro-fracturing described above, which is very localised around the major fractures, the sample from 242.20 m represents a major mylonite zone and thus exhibits extreme deformation textures. This section is composed dominantly (50–90% of the section) of clay phases (montmorillonite, sericite, chlorite) with recrystallised quartz and minor amounts of remnant feldspar and magnetite grains. Primary zircon (commonly fractured) and later sphene and epidote are present in accessory amounts. The micas and quartz form a dense crenulated schistosity along which trails of recrystallised magnetite have formed. Although not as common as in some of the other sections, the fabric is impregnated by hydrous iron oxide dustings.

Subsidiary micro-fractures, formed coeval with hydrothermal events and located adjacent to the main fractures zones being studied, occur in some of the sections (e.g. 38.61 m, 242.20 m, 287.70 m). These are normally parallel to the major fracture plane and cross-cut existing textures; several distinctive types occur which include:

- simple variety (e.g. 38.61 m) up 0.6 mm wide and containing a very fine aggregate of sericite/chlorite and epidote; centrally, representing the final stage of crystallization, is quartz. The fracture margins are rich in iron oxyhydroxides.
- complex variety (e.g. 287.70 m) up to 1 mm wide and exhibiting a series of mineral generations within an open fracture. Marginal to the fracture, and even sometimes central, are euhedral quartz crystals. These give way to very fine granular aggregates of mostly epidote and iron-oxyhydroxides with sporadic grains of recrystallised quartz. The last infilling mineral phase is a mosaic of well-developed calcite crystals; marginal to these within the epidote-rich phase is commonly a dense concentration of iron oxyhydroxides. Another phase, zeolite, occurs as an aggregate of well-developed laths (coloured brown due to iron oxide impregnations) which have crystallised prior to the calcite but possibly subsequent to epidote. Epidote, zeolite and calcite, together with iron-oxyhydroxides, have crystallised irregularly throughout the rock matrix (other examples include 319.80 m).

The sequence of hydrothermal crystallization, in order of decreasing temperature can be summarized as follows: hematite/quartz, epidote and finally zeolite; calcite is the final phase and may or may not be hydrothermal in origin. Hydrous iron oxide dustings are commonly associated with epidote and especially zeolite, but these are believed to be mostly late-stage, probably preceding calcite, and have therefore totally impregnated the area of hydrothermal influence.

Tectonic reactivation along some of the fractures is evident both through microstructural and mineralogical observations. In one case the former is seen as an extreme mylonitisation texture (strong schistosity) accompanied by the formation of low-grade metamorphic minerals such as plagioclase feldspar, muscovite and magnetite. In other cases superimposed fracturing is observed, normally parallel to the existing tectonic pattern and with infillings such as quartz, epidote, zeolites and calcite; iron oxyhydroxides are widespread and intimately associated with especially epidote and zeolite. However, because of their hydrothermal mineral content, these fractures are considered to have formed coeval with late-stage granite emplacement and are not recent in origin. Nevertheless, as observed from borehole logging, later fracturing has undoubtedly occurred, although this is not readily discernable from the thin sections studied.

## 9.5 CHEMISTRY

The chemical analyses are presented in Tables 9-1 and 9-2. There is a wide range of concentration for all the measured elements, in some extreme cases varying from a few ppm to several hundreds. This study specially focuses on the variation of U, Th, and REE, (Rare Earth Elements), from the fracture surfaces into the wall rock as well as their variation with depth.

In order to evaluate the enrichment or depletion of elements that characterise the fracture coatings, the trace-element concentrations in the fracture samples have been normalized to concentrations representative of the host rock (reference values). We have chosen concentration averages of four rock samples (see Table 9-2) which are not close to the fracture surfaces and, moreover, apparently have not been influenced by alteration processes to any great extent. As seen in Table 9-2 the reference averages agree well with the average of all the wall rock samples analysed; a few exceptions should, however, be noted:

Table 9—1  
INNA results for fracture infills from borehole KLJ 01, Lansjärv

Element	1	2	3	4	5	6*	7**	8	9	10	11	12	13	14
Na %	0.93	0.66	0.16	0.63	3.1	0.51	< 0.7	1.1	0.76	1.3	3.6	0.62	1.4	2.0
Fe %	8.0	6.5	19.5	8.0	1.4	5.5	16.5	4.2	3.2	28.7	3.5	2.7	4.9	14.2
Cr ppm	18	206	14	79	8.4	230	4880	3112	4.9	8.6	10.7	14.3	37	111
Co	11	19	9.4	19	2.1	7.5	14.3	12	6.4	3.5	3.4	1.0	3.8	31
Zn	130	<150	33	90	-	-	-	70	110	47	30	30	75	420
Sb	1.1	-	0.2	-	-	-	-	-	< 0.5	0.65	0.3	-	< 0.5	-
Rb	< 100	87	< 75	140	150	260	< 150	390	880	< 150	250	< 50	< 50	150
Sr	< 350	< 350	-	-	-	-	-	-	< 100	< 100	-	< 400	< 150	-
Ba	< 500	250	240	< 250	330	2100	< 500	3024	< 500	< 200	780	< 200	370	< 500
Cs	2.6	2.0	0.6	2.3	2.3	5.0	< 1	8.7	18.8	1.8	1.1	< 0.75	< 1	2.7
Zr	~ 570	-	-	-	-	-	-	-	490	-	-	-	-	-
Hf	18.5	8.8	0.4	3.4	9.1	4.3	2.0	1.3	14.6	1.4	6.5	1.1	3.7	13.2
Ta	6.8	4.3	1.1	0.76	4.8	4.9	~ 1.8	< 0.9	4.8	0.65	1.8	0.53	1.4	5.9
Th	64.5	11.6	3.7	5.8	76.6	11.1	12.6	2.7	81.7	6.0	19.9	3.9	6.1	33.7
U	10.1	6.3	6.7	9.7	13.9	8.8	11.7	4.5	13.5	31.0	14.7	11.0	145	15.7
Sc	9.2	106	3.9	25.4	37.5	30.4	72.0	5.1	10.7	3.0	3.7	5.9	8.2	30.6
La	552	533	41.6	104	77.4	230	1703	27.3	161	188	298	81.1	118	54.6
Ce	997	757	58	517	112	238	2117	29.9	131	171	539	154	168	97.1
Nd	493	314	24	95	73	202	1367	22.3	95	90	211	59	80	39
Sm	78	37	5.0	20	13.4	29	211	4.6	15.3	11.4	26	9.1	15	9.1
Eu	8.9	3.7	0.80	2.9	1.5	3.6	23.9	0.46	1.7	1.8	2.8	1.0	1.7	0.93
Gd	-	-	-	-	-	-	-	-	-	-	-	-	-	-
Tb	9.6	3.9	1.2	3.7	3.0	3.1	16.6	0.66	2.4	1.7	2.0	0.89	3.1	2.1
Yb	16.9	10.8	4.6	10.0	8.2	4.3	13.2	1.6	6.3	5.8	2.6	3.2	7.9	8.4
Lu	2.5	1.6	0.62	1.5	1.2	0.59	1.6	0.22	0.98	0.88	0.42	0.55	1.2	1.4

\*) sealed fracture

\*\*) open

\*\*\*) calcite dominated fracture

Table 9—2  
INNA results for rock samples from borehole KLJ 01, Lansjärv

Element	38.63 m		57.65 m		76.20 m		114.80 m		131.40 m		242.20 m		287.40 m		420.0 m		425.13 - 452.03 m		452.03 - 452.17 m		Average of all selected samples *	
	B		B		B	C	B		B	C	B	C	B	C	B		B		B		all samples	selected samples *
Na %	2.1	1.8	3.6	3.3	3.5	2.7	2.4	0.85	2.7	3.1	4.2	2.4	2.4	2.5	2.7	2.8	2.7	2.8	2.7	2.8	2.7	2.8
Fe %	0.81	0.92	1.2	0.96	2.3	0.93	0.76	0.62	0.76	0.77	1.9	2.0	2.0	1.7	1.2	1.4	1.2	1.4	1.2	1.4	1.2	1.4
Cr ppm	1.5	9.8	2.8	3.2	10	4.5	5.2	3.0	3.0	3.2	17	2.8	3.0	5.0	5.4	3.6	5.4	3.6	5.4	3.6	5.4	3.6
Co	1.6	2.8	4.7	2.8	4.2	2.6	2.6	2.6	2.0	1.5	6.5	2.1	2.0	3.3	3.0	2.4	3.0	2.4	3.0	2.4	3.0	2.4
Zn	19	8	22	21	34		74		14	14	66	20	22	32	32	19	32	19	32	19	32	19
Sb					< 1						< 1											
Rb	256	233	190	188	145	137	166	717	216	206	77	259	226	232	220	220	232	220	232	220	232	220
Sr		< 450		< 250		< 300		105	< 120	103	135	147	262	623	670	670	623	670	623	670	623	670
Ba	716	931	300	590	396	640	680	915	736	465	110	590	1035									
CS	0.63	0.95	0.84	0.86	0.95	0.52	0.80	14.2	0.91	0.80	0.86	0.64	1.5	1.9	0.95	1.9	0.95	1.5	1.9	0.95	1.5	0.95
Zr						430	280	94	165	112	260	390	350	280	280	280	280	350	280	280	280	280
HF	8.5	11.1	4.4	4.0	12.0	11.4	8.0	3.3	4.6	3.3	7.9	13.7	9.1	7.8	7.5	7.5	7.8	9.1	7.8	7.5	7.8	7.5
Ta	2.2	3.8	15.1	3.2	2.6	3.6	2.8	0.33	0.36	0.38	1.6	2.9	2.1	3.2	2.1	2.1	3.2	2.1	3.2	2.1	3.2	2.1
Th	7.2	30.0	38.7	34.5	25.0	36.9	26.5	6.4	22.5	17.5	11.4	3.3	20.3	21.6	24.1	24.1	21.6	24.1	21.6	24.1	21.6	24.1
U	2.5	2.4	5.8	4.2	5.5	5.5	5.7	5.2	5.3	3.6	3.2	2.8	3.6	4.3	3.6	3.6	4.3	3.6	4.3	3.6	4.3	3.6
Sc	1.7	14.3	3.3	2.5	6.9	35.5	26.0	1.7	2.4	2.0	7.3	2.3	3.8	8.5	2.7	2.7	8.5	2.7	8.5	2.7	8.5	2.7
La	27	125	71	46	74	70	64	37	30	18	44	11	89	54	41	41	54	89	54	41	54	41
Ce	102	220	141	87	141	195	162	34	39	42	71	31	158	110	79	79	110	158	79	110	79	110
Nd	21	99	68	38	59	61	52	18	13.6	12.8	32	23	65	43	35	35	43	65	35	43	35	43
Sm	3.6	16	13.4	7.1	11.3	11.5	9.7	2.7	2.7	2.3	5.6	5.5	10.9	7.9	6.5	6.5	7.9	10.9	6.5	7.9	6.5	6.5
Eu	0.52	1.7	1.8	0.98	1.4	1.2	0.95	0.26	0.40	0.36	0.51	0.82	1.0	0.92	0.79	0.92	1.0	0.79	0.92	0.79	0.92	0.79
Gd																						
Tb	0.59	2.0	1.8	1.1	1.8	1.8	1.6	0.56	0.44	0.39	0.77	0.98	1.5	1.2	0.99	1.2	0.99	1.5	1.2	0.99	1.5	0.99
Yb	2.4	4.3	5.5	2.6	5.0	5.4	3.5	1.5	1.5	1.3	2.4	3.9	3.2	3.3	2.8	2.8	3.3	3.2	3.3	2.8	3.3	2.8
Lu	0.38	0.65	0.83	0.41	0.79	0.91	0.59	0.24	0.23	0.20	0.34	0.60	0.53	0.52	0.44	0.44	0.52	0.53	0.44	0.52	0.44	0.53

Sample B: 7 - 15 mm from the fracture surface

" C: 20 - 40 "

\*) Average of samples 76.20 C, 287.40 C, 425.13-26 and 452.03-17 (used for normalization)

- The REE averages are somewhat lower (about 25 %) in the reference samples. This could be due to an enrichment of the REE in the “near fracture” samples by secondary processes, or alternatively, that the concentrations of the granite reference samples are not representative of the host rock. However, the chondrite-normalised REE patterns are almost identical in shape for the two averages.
- Sc is lower (by a factor of 3) in the reference samples. Rather high Sc values, which are not normal for granitic rocks, are observed in some of the rock samples (as well as in the corresponding fracture coatings) and may be the result of hydrothermal events or, less probable, due to the inclusion of mafic material.

### 9.5.1 Reference Normalized Granite v.s Fracture Filling Phases

The rock-normalized concentration values of the fracture filling samples have been grouped according to their characteristic mineral phases and are illustrated in Figure 9-1. Five groups can thus be distinguished; samples respectively dominated by hematite/Fe-oxyhydroxide, chlorite, clay minerals (montmorillonite?), calcite and tectonized and hematized quartz-feldspar coatings. Two of the samples (319.8 m and 373.6 m) are anomalous to these groups; the Fe content is relatively low in these two samples although microscopy suggests hematite as the dominant phase.

Relative to the granite reference, average Na is depleted and Fe is enriched in all fracture samples, (exception 131.40 m). Besides Na, Ba and Rb seem to have been mobilized as they show lower ratios ( $<1$ ) in several samples, e.g. the chlorite and hematite/Fe-oxyhydroxide groups. It is interesting to note, however, that Rb/Cs show a positive correlation (not presented) in samples 146.9 m, 152.2 m and 242.2 m, all of which are rich in clay minerals and feldspar.

U, usually mobile, is enriched in most of the fracture samples and is especially high in 373.6 m (145 ppm, Table 9-1). In contrast, Zr, Hf, Ta and Th, which are considered to be more or less immobile elements, show a tendency to be: a) depleted in the hematite/Fe-oxyhydroxide and quartz/feldspar groups and in samples 319.80 m and 373.60 m, and b) enriched in the clay mineral and chlorite groups. The depletion can be a dilution effect due to a combination of volume increase by fracture opening and supply of material by precipitation.

Sc is enriched in the most fracture samples and especially in the chlorite and clay mineral groups. In contrast, however, the Fe/Sc ratio shows little variation, both in the rock as well as in the fracture samples; Sc seems to vary sympathetically with Fe. Important exceptions occur in samples 76.20 m and 287.7 m where Fe is considerably increased relative to Sc. As Sc is probably less mobile during low temperature conditions than Fe, the observed relationship at these levels could indicate a “late” precipitation of Fe-oxyhydroxide from recent groundwater. Rock normalized concentrations of the elements Fe, Sc, Th, U, La, Yb, Na and Cs for the fracture coatings (A) and the wall rock samples B and C are compared for the two levels (Figure 9-2). Most of the elements show a slight increase from the C to B samples which can be due to removal of material by leaching processes or be an effect (supply) of hydrothermal influences. Striking differences between the two borehole levels are, however, noticed for the U, Cs, Na, REE (especially the light REE) concentrations in the fracture coating samples relative to those in the wall rock samples. In sample 76.20 m a decrease of these elements in the fracture coating is noted whereas in sample 287.40 m a distinct enrichment of the same elements is recorded in the fracture sample. This can be indicative of a low temperature redistribution of these elements described as leaching in the near surface region and a sorption of especially LREE and U

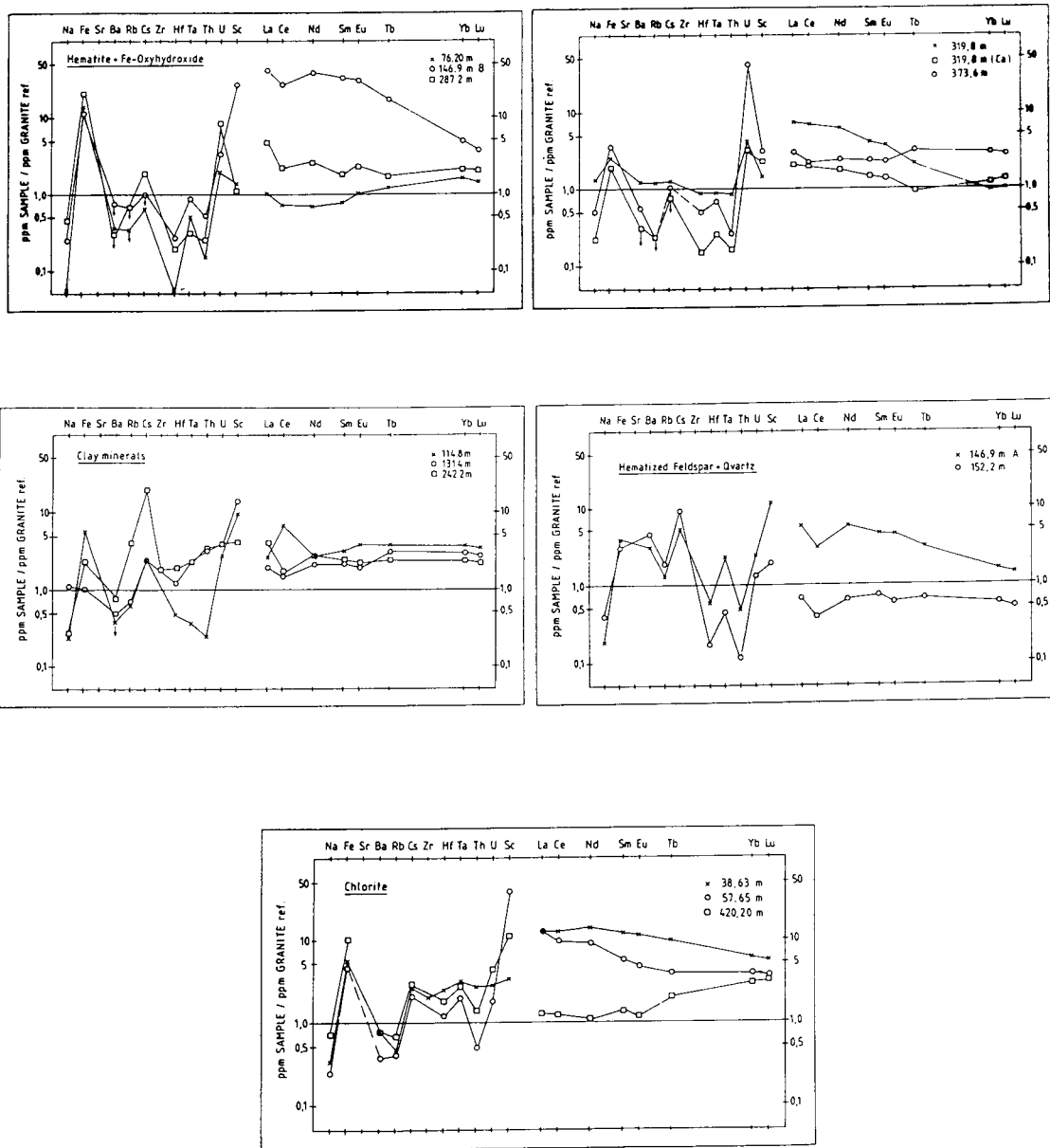


Figure 9-1. Concentration ratios of fracture coatings related to the granite reference at different depths from borehole KLJ 01, Lansjärv.



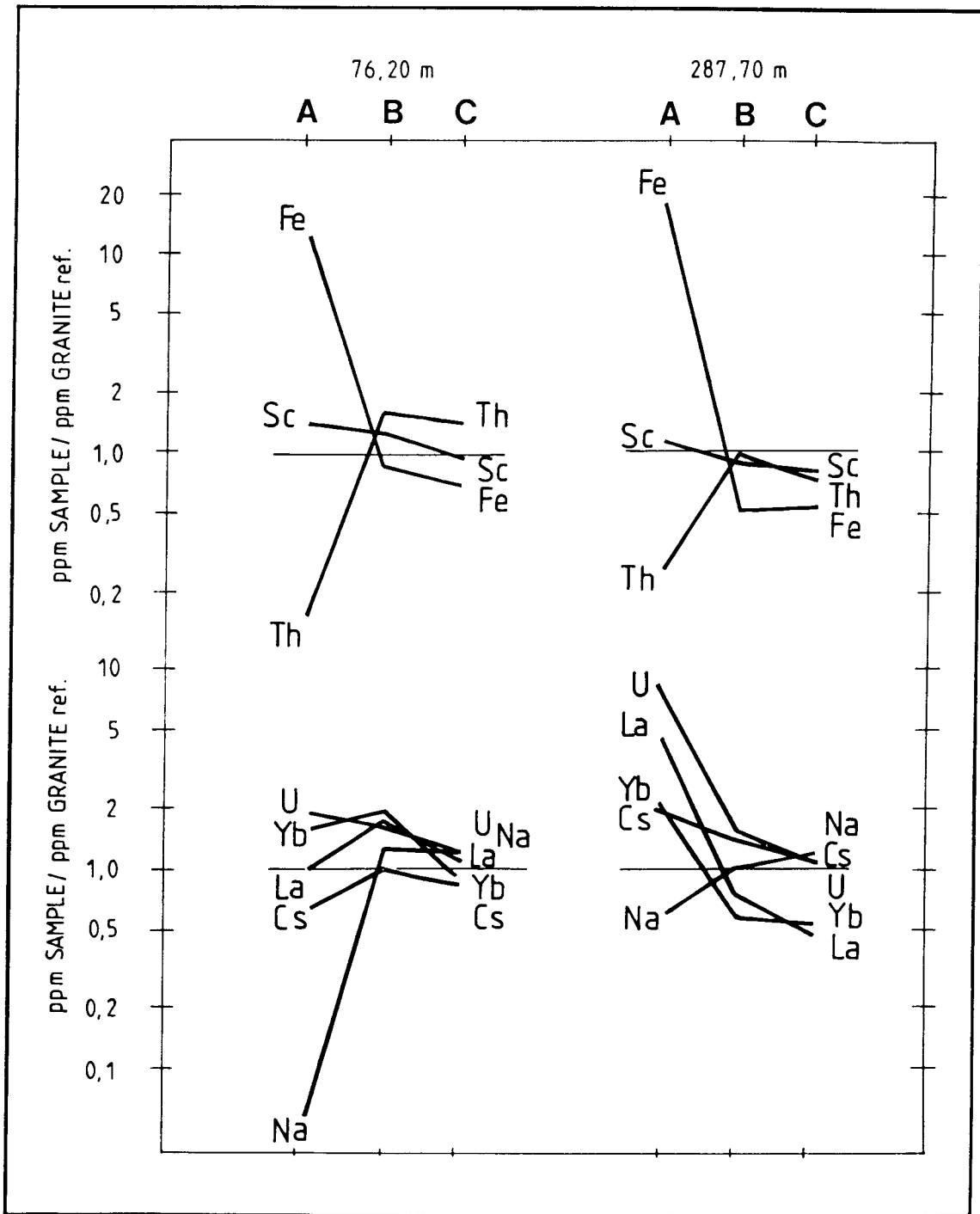


Figure 9-2. Variation of element distribution from the fracture surface (sample A) into the wall rock (samples B and C).

onto hematite/Fe-oxyhydroxide phases. The absence of a positive Ce-anomaly in the sample 76.20 m speaks in favour of non-oxidising conditions.

### 9.5.2 REE Fractionation Trends

One of the main objectives of the present work is to utilize the observed fractionation of the REE to interpret earlier and present geochemical environments in the bedrock. This is based on the following criteria:

- the sensitivity to redox conditions for the elements Ce and Eu. In nature  $Ce^{3+}$  can be oxidized to  $Ce^{4+}$  and  $Eu^{3+}$  reduced to  $Eu^{2+}$ . The different chemical properties of  $Ce^{4+}$  and  $Eu^{2+}$  thus result in a marked divergence from the normally trivalent REE valency states; these Ce and Eu “anomalies” are well exemplified in the illustrated chondrite-normalized REE patterns (Figures 9-3 and 9-4),
- REE are usually mobile as different ligand complexes; variations of these complex stabilities can cause a fractionation of, e.g. light REE/heavy REE, which is dependent on chemical environment parameters such as pH,  $pO_2$  etc.,
- the selective uptake of the REE by different minerals can give a distinctive character to the REE pattern of the composite fracture coatings.

The REE data are presented as chondrite normalised plots (Figures 9-3 and 9-4) which generally show typical curves characterised by an Eu anomaly. What is different, however, is the anomalous behaviour of Ce. Cerium shows a distinctive negative anomaly in several fracture coating samples and a significant positive anomaly in one sample (curve 4; sample 114.80 m, Figure 9-3). Positive as well as negative Ce-anomalies have also been recorded within the wallrock samples (c.f. 38.63 m and 131.40 m (positive anomaly) and 242.20 m (negative anomaly) Figure 9-4). The fresh granite samples, in common with most of the wall rock samples, do not show any Ce-anomaly (Figure 9-4) supporting the conclusion that a Ce anomaly is not a primary feature of the granite, but rather a result of later influences restricted to the fractures.

Besides the Ce anomalies, rock normalized REE curves show different fractionation patterns (relative to the host granite). The following main trends may be distinguished:

- The three clay minerals (samples 4, 5 and 9), as well as the feldspar sample 152.2 m (8) and sample 373.6 m (13) show no fractionation relative to the granite which possibly implies that the REE have not been mobilised. The difference in concentrations may be either; a) primary (original) or b) caused by the removal (e.g Na) of material during weathering processes or c) by the addition of trace elements during the formation of minerals.
- More or less pronounced light REE/heavy REE fractionations are found at 38.63 m (1), 57.65 m (2), 146.9 m (6 and 7) and 319.8 m (11), which probably implies light REE mobility (at low temperature conditions?)
- Heavy REE/ light REE fractionations are observed at 420.20 m and less distinct at 76.20 m. Whether this indicates a leaching of light REE or an enrichment of heavy REE is difficult to ascertain.

What is noteworthy and partly supports (possibly late) light REE mobilization is the small variation in the Yb-Lu concentration ratios compared to the light REE ratios (Figure 9-3) in the fracture minerals, especially distinct in the hematite/Fe-oxyhydroxide group. This observations can be interpreted as an

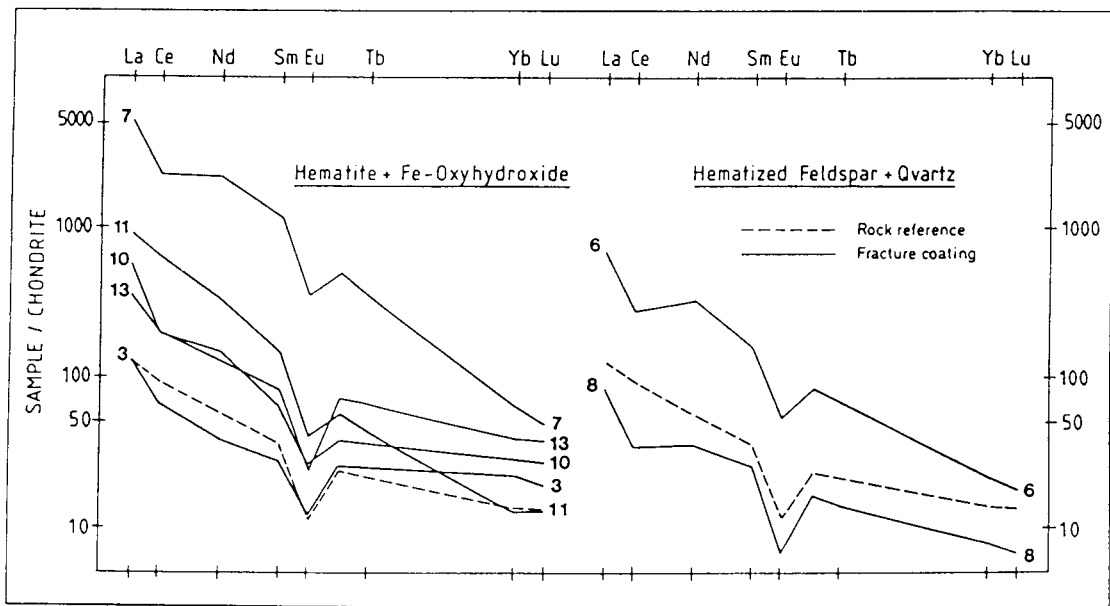
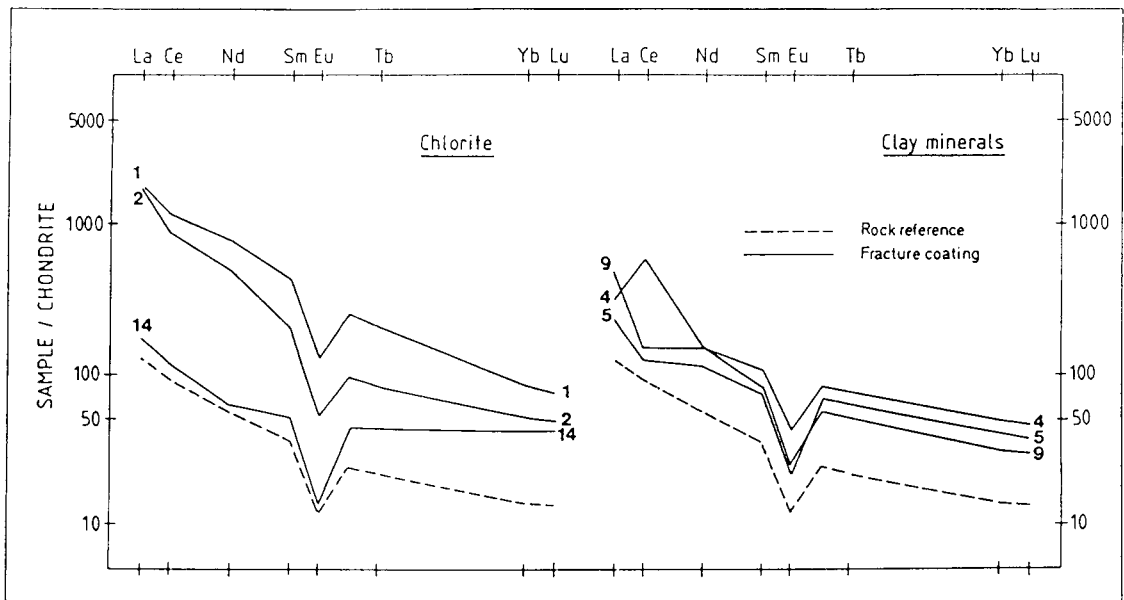


Figure 9-3. Chondrite normalised REE-curves for fracture fillings of samples listed in Table 9-1.

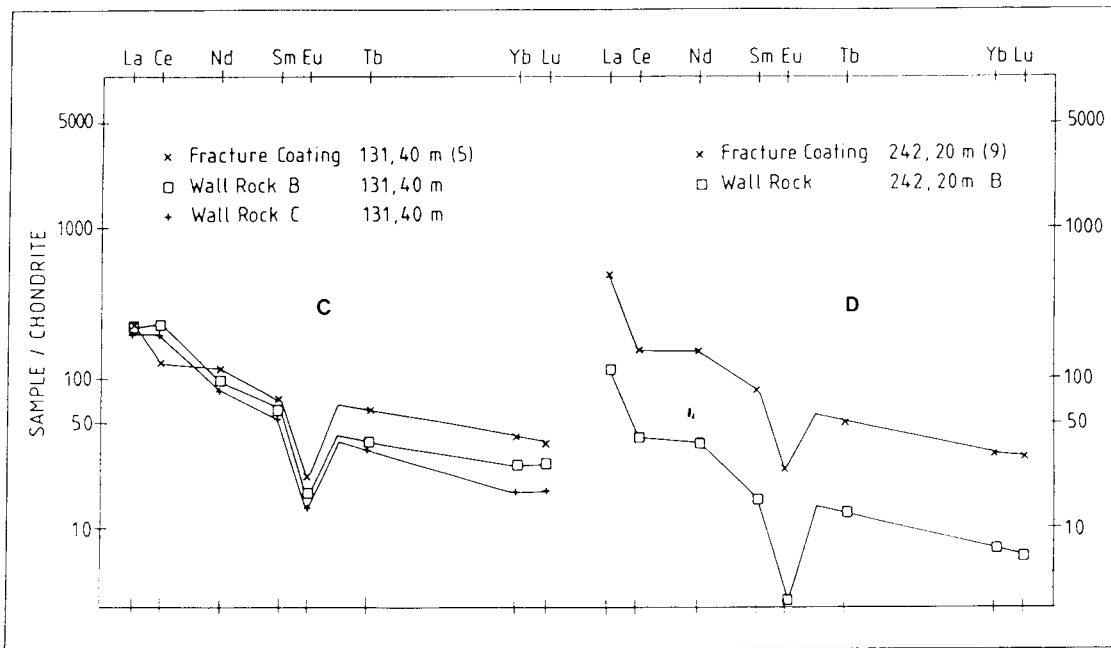
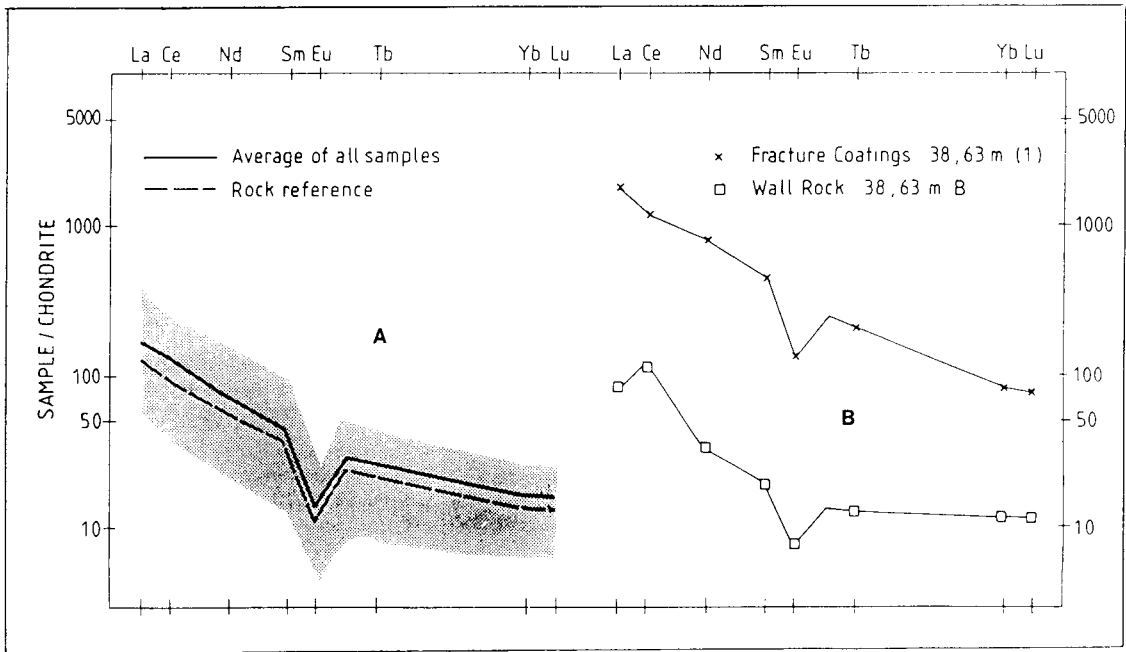


Figure 9-4. Chondrite normalized REE-curves for rock samples

- a) range of REE-curves and averages for granite samples,
- b), c) and d) wall rock samples with Ce-anomalies and their corresponding fracture coating.

initial hydrothermal enrichment of all REE in the fracture coatings, overprinted by a later (low temperature) mobilization (leaching-sorption) of the light REE.

### 9.5.3 Depth Related Trends

Figure 9-5 shows the variation of the Ce-anomalies versus depth. It is interesting that positive Ce-anomalies occur only in the upper part of the drillcore whereas the more pronounced negative Ce-anomalies are found deeper down. This observation, as well as the somewhat obscure enrichment of U in the fracture coatings in the deeper part of the drillcore support an influence of "near surface" groundwater and low temperature conditions down to several hundred metres depth.

The La/Th variation with depth (Figure 9-5) points to an extensive mobility i.e. enrichment of La in some of the fracture coatings in relation to the less mobile Th (at low temperature conditions). A corresponding enrichment of light REE is e.g. recorded in a water conducting hematite/Fe-oxyhydroxide bearing zone in Klipperås, Landström & Tullborg, (in manuscript). A fracture filling study in the Eye-Dashwa Lakes Pluton, Kamineni (1986) shows in particular an enrichment of the light REE in the low temperature mineral phases.

Zr, Hf and Ta are considered to be rather immobile during weathering processes; if this can be proved they could be used for normalization in estimates of the gain or loss of elements. The main host minerals of Hf is zircon and Hf is thus a rough measure of the content of this mineral (and of Zr). As seen in Figure 9-5 the Hf/Ta ratio varies between the different sampling levels. In the upper part of the borehole (i.e. in samples 38.93 m, 57.65 m, 76.20 m, 114.80 m and 131.40 m) the Hf/Ta ratio is, however, about the same for the fracture infillings and the wall rock samples which is an indication (but not an evidence) of immobility. The surprisingly low Ta values of the wall rock samples at 242.20 m and 287.40 m results in a large discrepancy between the Hf/Ta ratios of the fracture coatings and the wall rock. An (original?) non-uniform distribution of the host minerals of Ta and Hf may be the explanation.

### 9.5.4 Uranium Decay Series Measurements

Results of the uranium decay series measurements are presented in Table 9-3 and Figure 9-6. Comparing the uranium and thorium values with those reported using INAA (Tables 9-1 & 9-2) reveals a close correlation for uranium (except for sample 373.60 m) but not with thorium. For thorium these methods normally closely agree, McKenzie et al. (1986), and it is therefore suspected that sample heterogeneity has resulted in the observed analytical variations. However, this is not expected to affect the overall interpretations of the uranium decay series data, as the majority of samples exhibit excessive isotopic disequilibrium.

Of the samples measured, insufficient material was available to determine thorium in sample 242.20 m; samples 132.30 m and 146.9B m are in the process of being analysed even though only small quantities are available.

The uranium decay series data show the following features:

- a) Two samples (38.63 m and 43.50 m) show secular isotopic equilibrium and it can be concluded that they have not undergone any rock/water interaction within the last million years or so.
- b) Two samples (287.70 m and 319.80B m) show marginal disequilibrium. This may indicate a slight rock/water interaction over a long period of time (i.e. last 250 000 years), or, a very recent phenomenon.

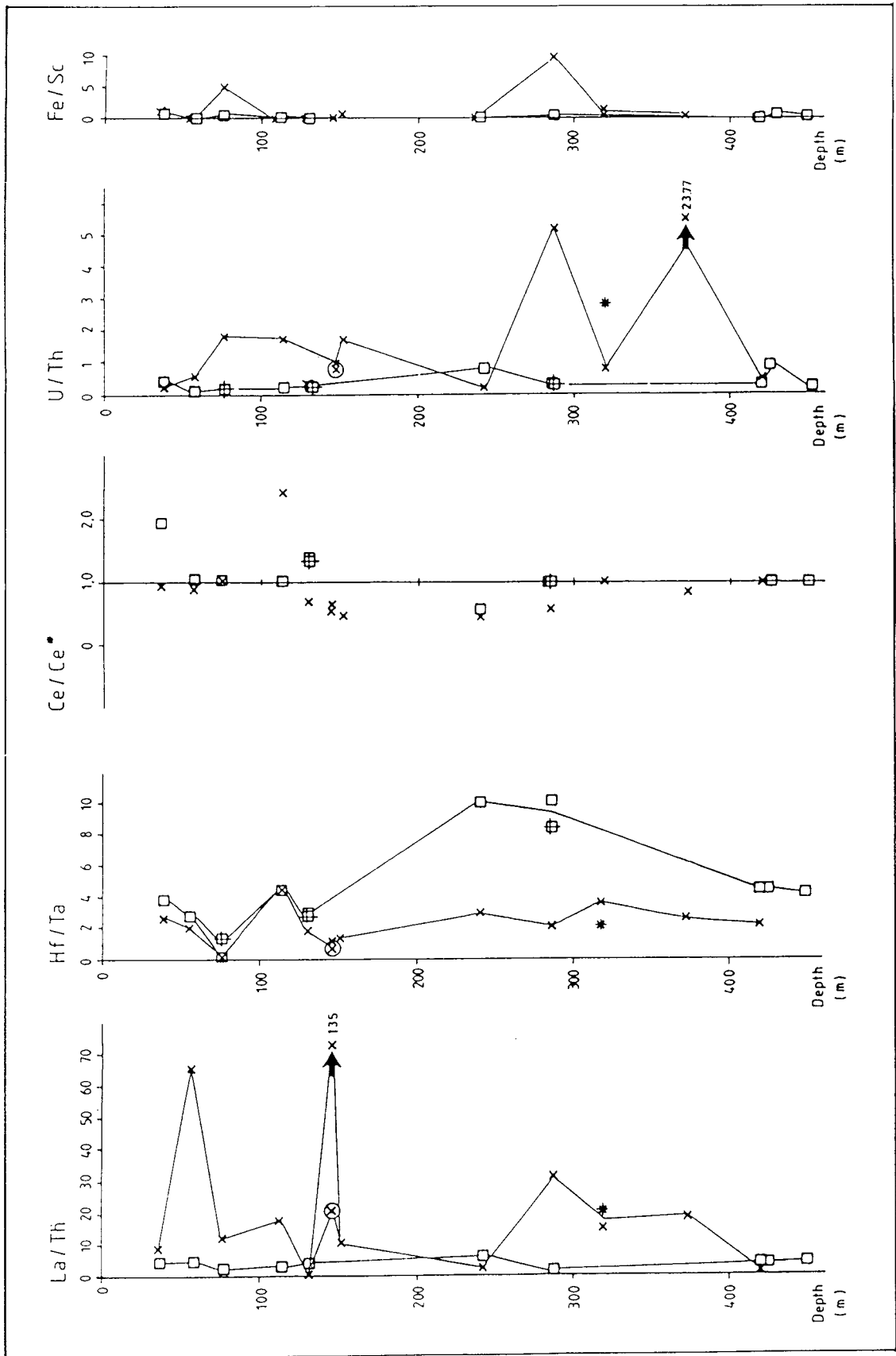


Figure 9-5. Variation of element ratios versus depth.   
 x = fracture coating = wall rock samples B, + = wall rock samples C,   
 \* = fracture coating dominated by calcite, x = sealed fracture 146.9 m.

Table 9-3. Uranium decay series data given in Bq/kg.

SAMPLE	$^{238}\text{U}$	$^{234}\text{U}$	$^{234}\text{U}/^{238}\text{U}$	$^{232}\text{Th}$	$^{230}\text{Th}$	$^{230}\text{Th}/^{234}\text{U}$
KLJ 01 38.63	155±7	155±7	1.00±0.04	73±5	148±8	0.95±0.06
KLJ 01 43.50	268±8	271±8	1.01±0.02	80±7	265±20	0.98±0.06
KLJ 01 57.65	61.8±3.3	71.7±5.0	1.16±0.07	87.0±4.0	97.8±4.3	1.36±0.07
KLJ 01 76.20	98.2±6.2	166.7±8.3	1.70±0.11	11.7±1.7	120.5±5.8	0.72±0.04
KLJ 01 86.0	212±7	214±6	1.01±0.04	267±12	333±13	1.56±0.07
KLJ 01 114.80	90.0±8.8	139.0±11.3	1.54±0.18	28.2±2.7	118.0±6.2	0.85±0.08
KLJ 01 131.40	160±5	194±6	1.21±0.05	75±3	130±5	0.67±0.04
KLJ 01 132.30	423±13	642±13	1.52±0.04	--	--	--
KLJ 01 146.9b	206.5±20.3	332.5±26.5	1.61±0.19	--	--	--
KLJ 01 242.20	168±7	157±5	0.93±0.03	--	--	--
KLJ 01 287.70	370±8	409±5	1.00±0.02	80±12	392±26	0.96±0.07
KLJ 01 319.80a	163±8	204±7	1.25±0.06	58±3	152±7	0.75±0.04
KLJ 01 319.80b (Ca)	96.7±5.0	101.2±5.0	1.05±0.05	21.7±2.8	88.0±5.0	0.87±0.05
KLJ 01 373.60	135.8±5.0	158.3±6.7	1.16±0.05	30.5±1.8	177.0±5.5	1.12±0.04

- c) Four samples (76.20 m, 114.80 m, 131.40 m, 319.80A m) clearly show uranium precipitation, which indicates a redox transition from oxidising to reducing groundwater conditions, possibly still in progress and points to extensive water/rock interaction at least within the last 250 000 to 1 million years.
- d) Of the remaining three samples (Figure 9-6), one is borderline (373.60 m), showing possible additions of uranium, or, a complex origin, one maybe complex in origin (57.65 m), and one may suggest some uranium removal (86.0 m) due to circulation of oxidising groundwater within this fracture.
- e) Of the three samples measured only for uranium isotopes (242.20 m, 132.30 m and 146.90B m), all show disequilibrium and have been affected by rock/water interaction processes within the last million years.

In summary, all but two samples exhibit isotopic disequilibrium and this can be attributed to varying degrees of rock/water interaction within recent geological time (the last million years). Unfortunately, periods of fracture reactivation during this time interval, which may have resulted in the sealing/opening of conductive fractures, cannot be ascertained from the present data.

## 9.6 DISCUSSION AND CONCLUSION

All the samples studied from borehole KLJ 01 show varying degrees of alteration, both within the relatively intact adjacent granite host-rock, and especially marginal to the major fracture zones sampled. Primary textures in some cases are readily distinguished, whilst in other cases deformation and crushing have all but destroyed the primary mineral phases. The mineralogy of these altered zones indicate that both hydrothermal and low-temperature weathering events have influenced the rock in the near vicinity of the fractures. Predominantly oxidising hydrothermal solutions, probably representing late-stage deuteric ef-

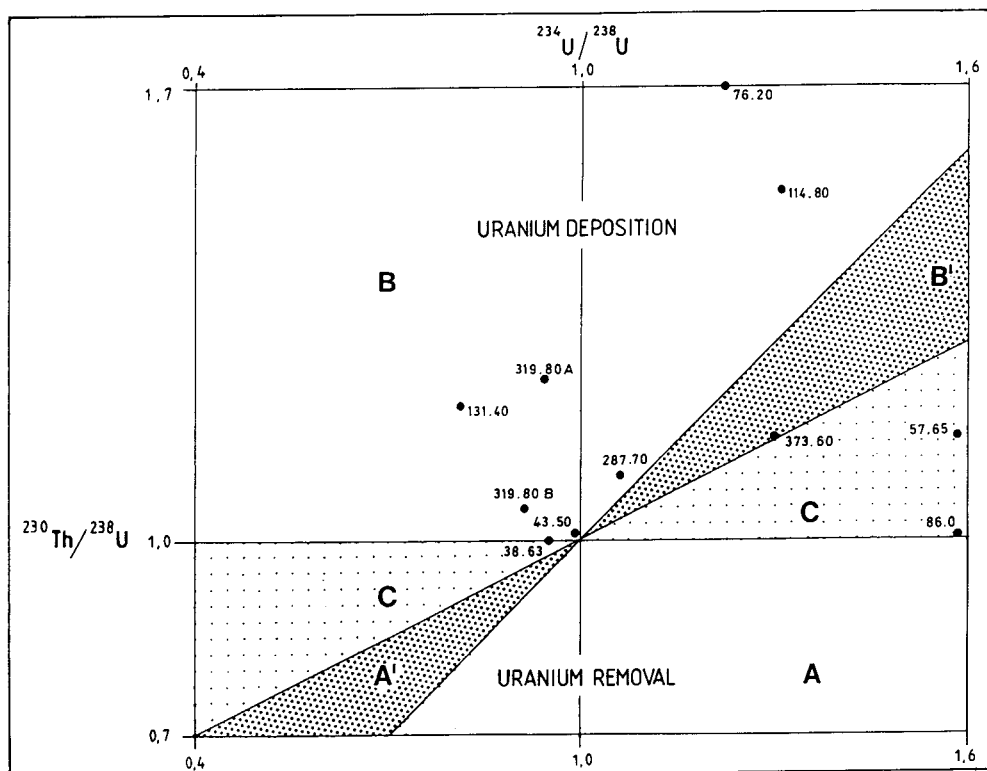


Figure 9-6. Thiel plot of uranium decay series data.

A' and B' = Forbidden for continuous single process.

C = Forbidden for any single process.

ects during emplacement of the granite massive, have resulted in the alteration of primary mineral phases such as feldspar, biotite and magnetite producing breakdown products such as sericite, chlorite, hematite and amorphous iron hydrous oxides. In some cases, Ca in these solutions has given rise to epidote formation.

Concerning the geochemical study, the trace elements in the Lansjärv samples vary within a wide range. The distribution of elements can be due to:

- 1) Original variation of the element distribution within the granite itself. (Affecting all elements).
- 2) One or more periods of hydrothermal activity causing redistribution of elements like U, Th, REE, Fe, Sc, Ba, Sr, Cs, Rb, and Na.
- 3) Circulation of low temperature groundwater resulting in redistribution of especially U, Fe and light REE.

Furthermore, it appears that the chemical behaviour, and thus the redistribution, of cerium differs from the other lanthanides in that under oxidising groundwater conditions it can exist in the less mobile four valency state. Thus, oxidation of cerium(III) present in the fracture mineral coating or in the adjacent wall rock, together with the mobilization and removal of the trivalent REE's, can cause a positive Ce-anomaly in the mineral phase (visible in several of the samples in the upper 150 m, Figure 9-5) whilst the transporting medium (i.e. groundwater or hydrothermal fluids) is depleted in Ce compared to the other REE. Mineral/water interactions, e.g. sorption and/or mineral precipitation in-



volving Ce-depleted water, may give rise to negative Ce-anomalies in the minerals along the water conducting fractures (c.f Figure 9-5 where negative Ce anomalies are found below 130 m depth). One hypothesis is that the oxidation, and thus the formation of the positive anomalies, is of hydrothermal origin. This is supported by the extent of the Ce-anomaly, which not only penetrates the fracture coatings, but also the fracture wall to at least 10 mm from the fracture edge. Furthermore, the extensive formation of hematite/Fe-oxyhydroxide during hydrothermal conditions point to a oxidising environment during this period.

Assuming that hydrothermal activity has resulted in an anomalous Ce distribution within and marginal to the fractures, this may, in addition, be further modified by more recent water/rock reactions. For example, low temperature groundwater in the upper part of the bedrock may result in the leaching of REE and U from the fracture coatings. Ce present in its four valence state is less mobile and the water will thus show a negative Ce-anomaly.

The results from the microscopic and geochemical studies supports the following interpretation of water/mineral interaction in the fractures in Lansjärv:

- 1) Extensive hydrothermal activity, probably combined with circulation of hydrothermal fluids, have influenced the area causing mineralizations of hematite, quartz, epidote, zeolites and as a last phase calcite followed by Fe-oxyhydroxides. An enrichment of U, Th, Sc, Fe and REE, detected in the fracture coatings and in some of the near fracture rock samples, can be correlated to these hydrothermal mineralizations. In addition, the positive Ce-anomalies is suggested to result from hydrothermal circulation of oxidising fluids. It can not be excluded that several hydrothermal periods have affected the area although one of them seems to be the dominating and overprinting one.
- 2) Subsequent to the hydrothermal period(s) low temperature groundwaters have circulated causing redistribution of elements as well as minerals e.g. the dissolution of calcite and the leaching of U and light REE taking place in the water conducting fractures in the upper part of the borehole, followed, deeper down, by precipitation and sorption of the same elements onto Fe-oxyhydroxide phases (c.f. section 6.5.1). In terms of the Ce-anomalies there is, no evidence of low temperature oxidation of Ce in the analysed fracture coatings. However, these leaching/sorption processes will underline existing, or create new, negative Ce-anomalies (c.f. Figure 9-2 and 3) in accordance with the above given description of the Ce mobility.

Recent (i.e. within the last million years) water/rock reactions are supported by the uranium decay series analyses which exhibit isotopic disequilibrium for 12 out of 14 samples. Furthermore, six samples clearly show uranium precipitation which infers a redox transition from oxidising to reducing groundwater conditions in fractures at depths ranging from 76 to 320 m. Uranium removal, on the other hand, which indicates oxidising groundwater conditions, is only suggested from one fracture at 86 m depth.

In conclusion there are signs of extensive hydrothermal alteration during oxidising conditions, in connection with an intensive fracturing especially pronounced in the upper 300 m of the drillcore. Subsequently a less extensive, but distinct, low temperature mobilization of U and light REE is suggested to have taken place.

It must be pointed out that the Lansjärv area has suffered an extremely intensive fracturing and hydrothermal alteration compared e.g. with the other study sites investigated by SKB. Is this one of the reasons for manifestation of neotectonic activity in the area?

## 9.7 REFERENCES

### **Albino B 1988**

Results from the core mapping in KLJ 01, Lansjärv.  
SKB Borrhålsrapport KLJ 01, Stockholm.

### **Kamineni D Ch 1986**

Distribution of uranium, thorium and rare-earth elements in the Eye-Dashwa Lakes Pluton – A study of some analogue elements. Chemical Geology vol 55, pp 361-373.

### **MacKenzie A B, Scott R D and Smellie J A T 1986**

II: A comparison of neutron activation and alpha spectroscopy analyses of thorium in crystalline rocks.  
SKB TR 86-01, Stockholm.



# 10 MODELLING OF ROCK MASSES

*Ove Stephansson*

Division of Rock Mechanics  
Technical University of Luleå  
S-951 87 Luleå, Sweden

## 10.1 INTRODUCTION

A repository for radioactive waste must be located and designed to be protected against (i) natural changes of first order (faulting, glaciation, meteorite impact) and (ii) human activity (war, sabotage, mining). To protect the repository from first order faulting, Stephansson et al., (1978) suggested its location in a large block of a jointed rock mass surrounded by faults or shear zones. Any large scale movements will then appear along pre-existing faults and the repository in the centre of the large block will be protected. Later Stephansson (1983) presented mathematical models of a repository and deposition holes to demonstrate the stability of the underground constructions. In modelling large scale rock masses and the farfield stability of vaults for radioactive waste disposal, we are faced with new problems. Here there are a limited number of studies in which the behaviour of cubic kilometres of rock masses are simulated. One example is the modelling of compaction and subsidence of the Ekofisk oil and gas field in the North Sea, Barton et al., (1986).

In this study of large rock masses the problems and features to be modelled are defined and conceptual models are presented showing the sequence of modelling, the boundary conditions and the sub-structuring of the models in global and regional scale to the far-field of the rock mass surrounding a repository. This is followed by a brief description of the modelling techniques applied in this study. Before the modelling tools are applied to any problem related to final storage of high-level waste, the computer codes must be verified and validated. The thoroughly instrumented and carefully investigated block test at Colorado School of Mines have been used in the validating process of two codes, namely, the non-linear finite element method HNFEMP and the code MUDEC for the distinct element method. The stress state and the displacement in faulted rock masses have been determined in simple two-dimensional generic models. One set of horizontal and vertical faults and two sets of intersecting faults have been modelled in a 4 x 4 km large rock mass. Glaciation, glacial flow and glacial retreat have been simulated with both modelling techniques. Stresses and displacements obtained from the modelling are analysed and the implications on the stability of the waste vault are discussed.

## 10.2 PROBLEM DEFINITION AND CONCEPTUAL MODELS

Since we intend to model the crustal rock mechanics and the stability of large rock masses we need to know the loads affecting the rock mass. From the theory of plate tectonics we know that the Earth's lithosphere is dynamic and that the plates are moving at a velocity of a couple of centimetres to tens of centimetres per year. The plates form megatectonic units, i.e. very large structural features of the Earth and the plate boundaries converge, diverge or transform from the first order zone of deformation where most strains develop. The zone of deformation along the boundary of the plate acts as a tectonic barrier and to some extent protects the interior of the plate, cf. Figure 10-1A.

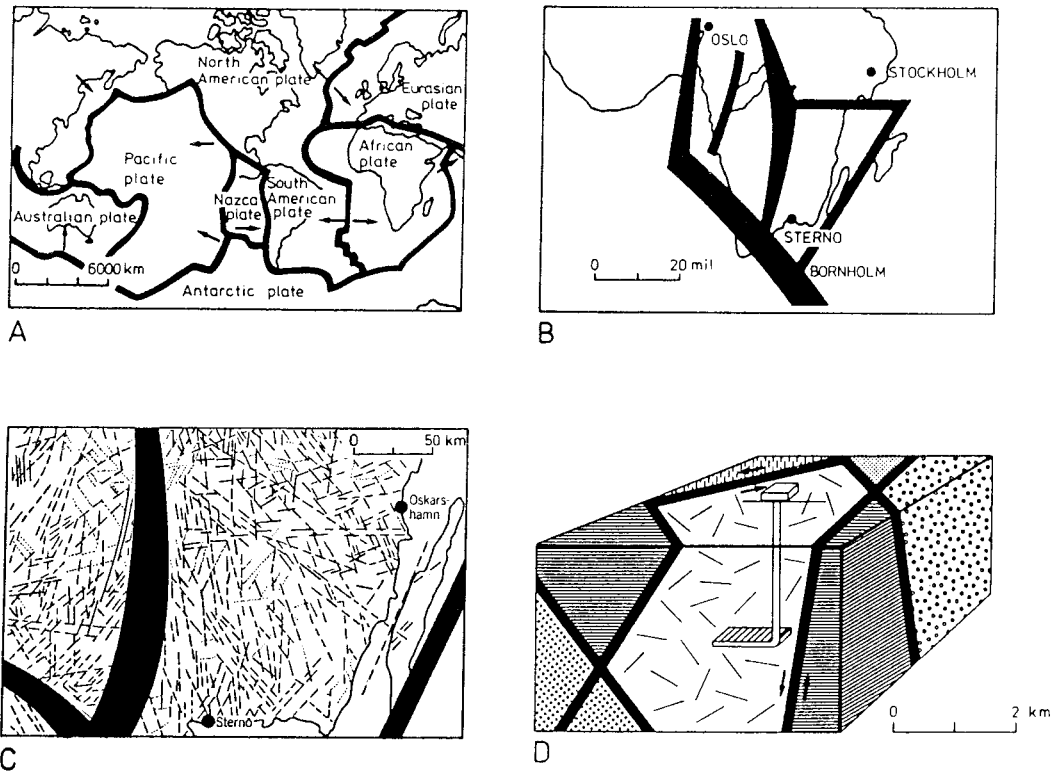


Figure 10-1. Deformation zones acting as barriers for repository of high level radioactive waste. A, Plate boundaries form the first order deformation zone. B, Second order deformation zones in southern Fennoscandia of the Eurasian plate. The zones define the megablock. C, Tectonic pattern of Southern Sweden according to Rös-hoff (1979). Fractures of 1st, 2nd, and 3rd order act as tectonic barriers for the interior of large blocks. D, Hypothetical model of a repository located in a rock block surrounded by faults and shear zones. Possible neotectonic movements will preferably take place along existing weak zones. After Stephansson (1983).

Intra-plate tectonics is still not established. One cannot therefore establish completely accurate models of deformation. Sometimes tectonic features are related to recent seismicity sometimes not. The Tornquist line, the Protogene zone, the Mylonite zone, the Oslo graben and its prolongation to the south form the second order zones of deformation in the Fennoscandian Shield; these second order deformation zones are characterized by repeated movements during several times of the geological evaluation and they act as tectonic barriers for the interior of the megablock, Figure 10-1B. The megablock of Southeastern Sweden is defined by the Tornquist zone in the south, the Protogene zone to the west, the fracture zone of Östergötland to the north and the sub-marine Öland-Gotland fracture zone to the east.

Inside a megablock of Precambrian rocks, the tectonic pattern is characterized by faults and fractures of various age and origin. The faults and fractures of 1st, 2nd and 3rd order act as a tectonic barrier for the interior of the blocks, Figure 10-1C. A generic model of a storage of highlevel waste located in the

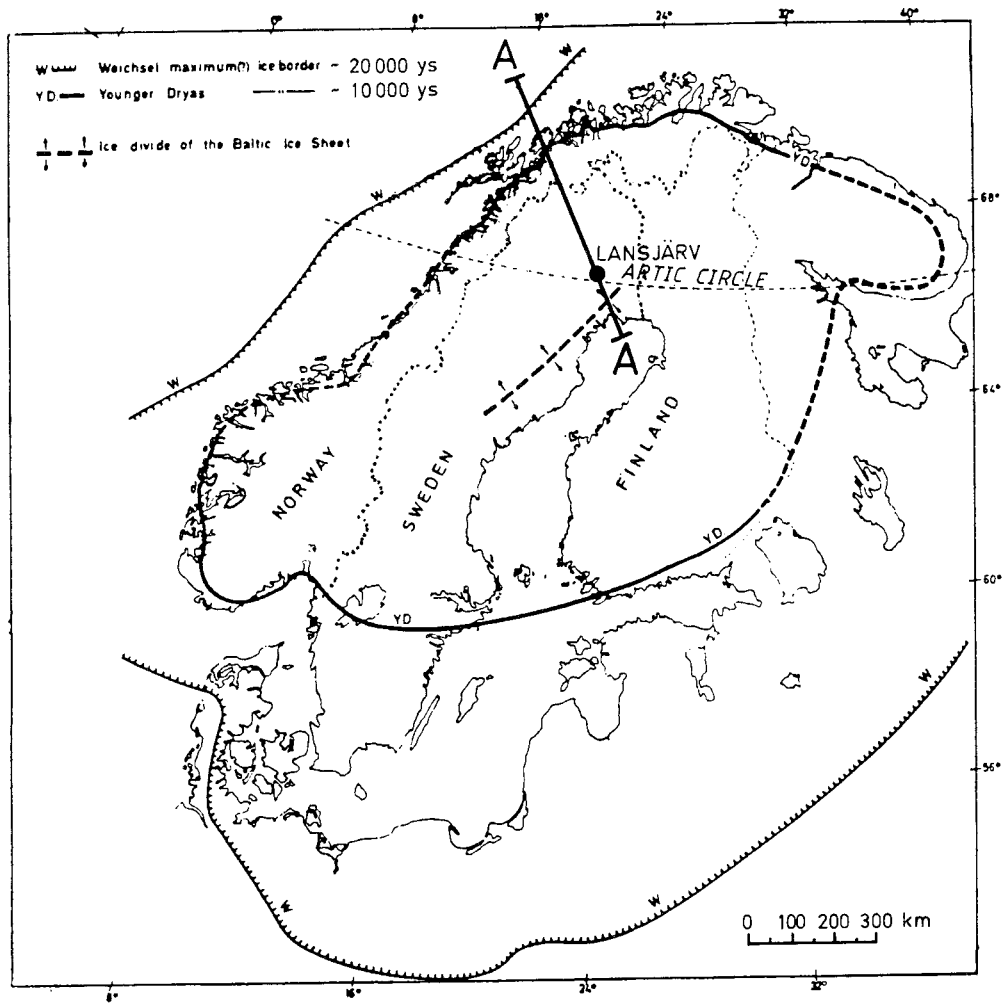


Figure 10-2. The most important Weichselian ice borders and the ice divide. After Bakkelid (1986). The figure also shows the suggested profile A—A for numerical modelling of crustal rock mechanics.

central portion of a jointed rock mass and surrounded by higher order faults and fractures is shown in Figure 10-1D. Possible neotectonic movements will preferably take place along existing weak zones in the rock mass.

The Lansjärv fault system and other neotectonic faults in Northern Fennoscandia are somehow related to the late stage of the Weichselian glaciation. This glacial ice began about 75.000 years BC and increased to a maximum ice extension of the Weichselian ice and the ice border at Younger Dryas (10.000–11.000 BC) and Pre-Boreal (9.000 BC) is reproduced after Bakkelid (1986) in Figure 10-2. In the figure is also shown the suggested profile A-A for numerical modelling of crustal rock mechanics. The main reasons for selecting this profile are listed below:

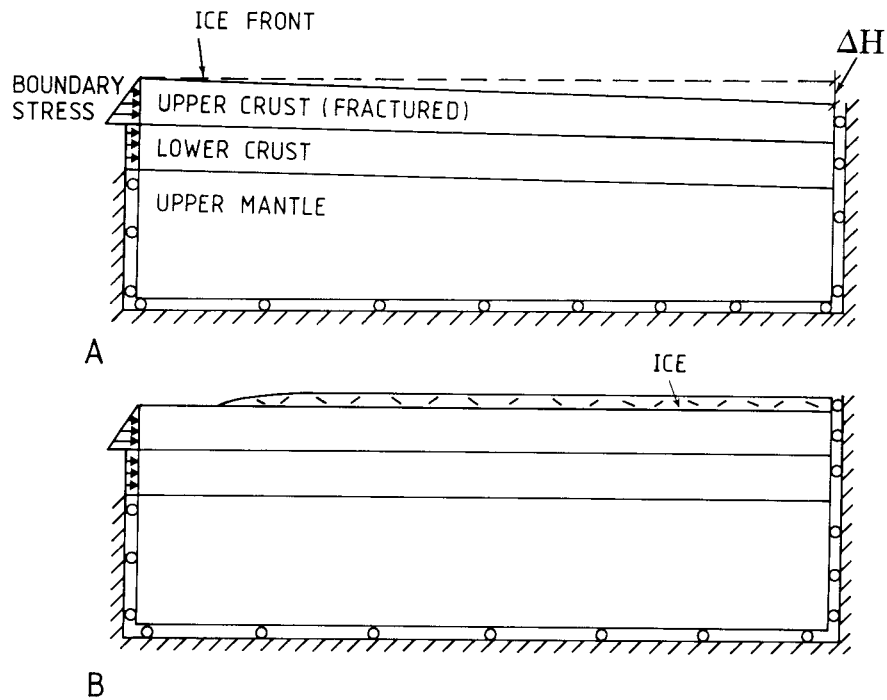


Figure 10-3. Suggested modelling of rock mass response from glaciation, deglaciation and glacial rebound for a NW-SE traverse in Northern Fennoscandia. A, Simulation of glacial rebound at the centre of uplift,  $\Delta H$ . B, Simulation of ice load from a glacial ice sheet. Boundary stress from ridge push and gravity loading will be applied to the crust.

- the profile strikes parallel to the direction of maximum horizontal stress, governed in principle by ridge push at the Mid-Atlantic Ridge,
- it strikes parallel to the major set of regional fracture zones in Northern Sweden,
- the point of zero vertical displacement at the NW end and the point of maximum vertical displacement and the ice divide at the SE end of the profile are points of symmetry,
- the profile A-A intersects the major neotectonic fault zone of Pärvie and Lansjärv.

In modelling the effect of glaciation, deglaciation and glacial rebound on crustal rock mechanics and stability, two modelling approaches are suggested. In the first approach the upper surface and bottom of the crust is given a shape in accordance with the glacio-isostatic deformation of an elastic crust overlaying a viscous mantle. The glacial uplift,  $\Delta H$ , can be varied in accordance with existing data of total, present and remaining uplift, Figure 10-3A.

The other two-dimensional approach uses ice as a surface load, Figure 10-3B. The profile of the top surface of the ice sheet is governed by known shape functions, Stephansson (1987) and the retreat of the ice sheet can be modelled so that the ice edge is located at a potential neotectonic fault system.

Global models presented in Figure 10-3 make it possible to increase our overall understanding of the change in stresses and deformations. They can also provide the boundary conditions for regional and far-field models as indicated in Figure 10-4. In this study regional models with dimension 4 x 4 km have been used to simulate the rock mass response to glaciation, glacial flow and deglaciation. The boundary stresses have been applied in accordance with the stress data

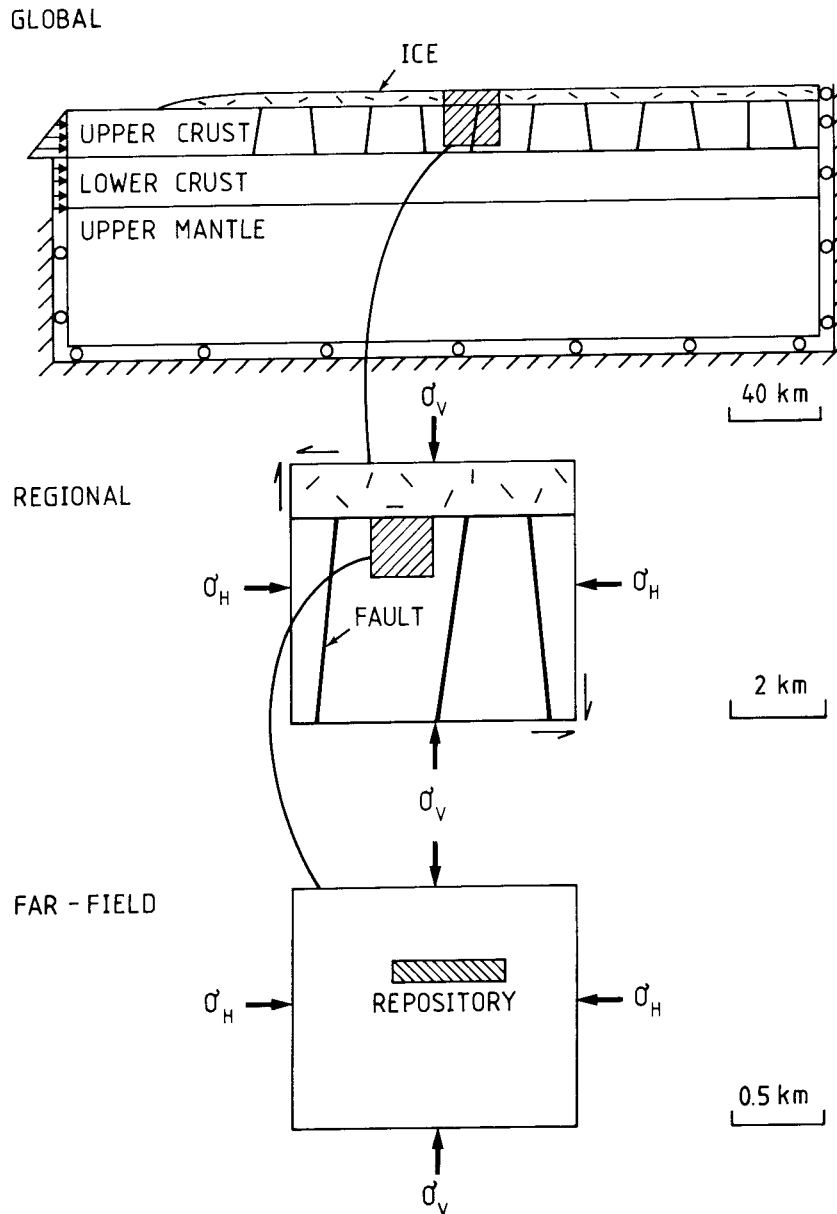


Figure 10-4. Illustration of the scale of modelling, where a global model gives the boundary conditions for the regional and the far-field models. Regional models with dimension 4 x 4 km have been used in this study.

presented in the Fennoscandian Rock Stress Data Base, Stephansson et al., (1986).

### 10.3 MODELLING TECHNIQUES

In principle, two approaches can be used in modelling jointed rock masses: continuum or discontinuum. The first approach uses a material constitutive model that accounts for the properties of the intact rock and the joints without including the joints as separate entities. The joints are assumed to be planar and the mechanical properties of the intact rock and joints are averaged, and distributed throughout the rock mass in proportion to the spacing of the defined joint sets.



Since the joint system consisting of one or several sets of joints are smeared out in a unit volume of rock, the method is sometimes called the “smeared out” approach or the “equivalent material approach”, Pande (1985), Olofsson (1985), and Zimmerman and Blanford (1985).

The discontinuum approach implies that jointed rock masses are modelled by describing the response of every joint separately. Goodman (1976) developed a special joint element for rocks and implemented it in a finite element program. The distinct element method, Cundall (1980), is another technique for analysing problems in which fracturing or jointing controls the rock mass response. This method models the rock mass as a series of blocks separated by joint planes. The MUDEC code is based on the distinct element method and has been applied to loading tests on a large basalt block at Hanford test station in the US, Hart et al., (1985).

### 10.3.1 Jointed Rock Continuum Model, HNFEMP

A jointed non-linear rock continuum model has been formulated by Olofsson (1985) for modelling jointed rock mechanical response in continuum-based numerical codes. The recoverable normal and shear joint deformations are assumed to depend linearly on the applied stresses so that the joint elastic compliance is regarded as a constant property. The intact rock is considered to be a linearly elastic material and for an elastically isotropic material the compliance matrix may be determined from the Young’s modulus and the Poisson’s ratio.

In Olofsson’s model (op. cit.) a joint has two failure models, (i) shear failure, and (ii) normal failure. Shear failure is initiated when the shear stress exceeds the frictional forces in the joint plane. Normal failure can either be tensile or compressive. The viscoplastic yield function,  $F$ , for a single joint in the rock mass is illustrated in Figure 10-5. This function depends on the following parameters:

- cohesion,  $c_0$
- angle of dilation,  $\Phi_i$
- basic friction angle,  $\Phi_s$
- asperity angle,  $\Phi_a$
- normal compressive strength of asperity,  $N$

The fundamental Mohr-Coulomb failure criterion in the  $\sigma_n - \sigma_s$  co-ordinate system is transformed to a joint plane co-ordinate system to obtain the equations for the final yield function. Equations to relate the dilation angle and other unknowns to the well-known empirical formulations of joint shear and normal behaviour by Barton and Bandis (1982) and Barton’s parameters JRC, JCS and joint length,  $L$  are included in the model.

The equivalent rock mass model for the mechanical behaviour of continuous rock joints has been implemented in a finite element code called FEMP, Nilsson and Oldenburg (1983), and the special version containing the non-linear model of the rock joints is called HNFEMP.

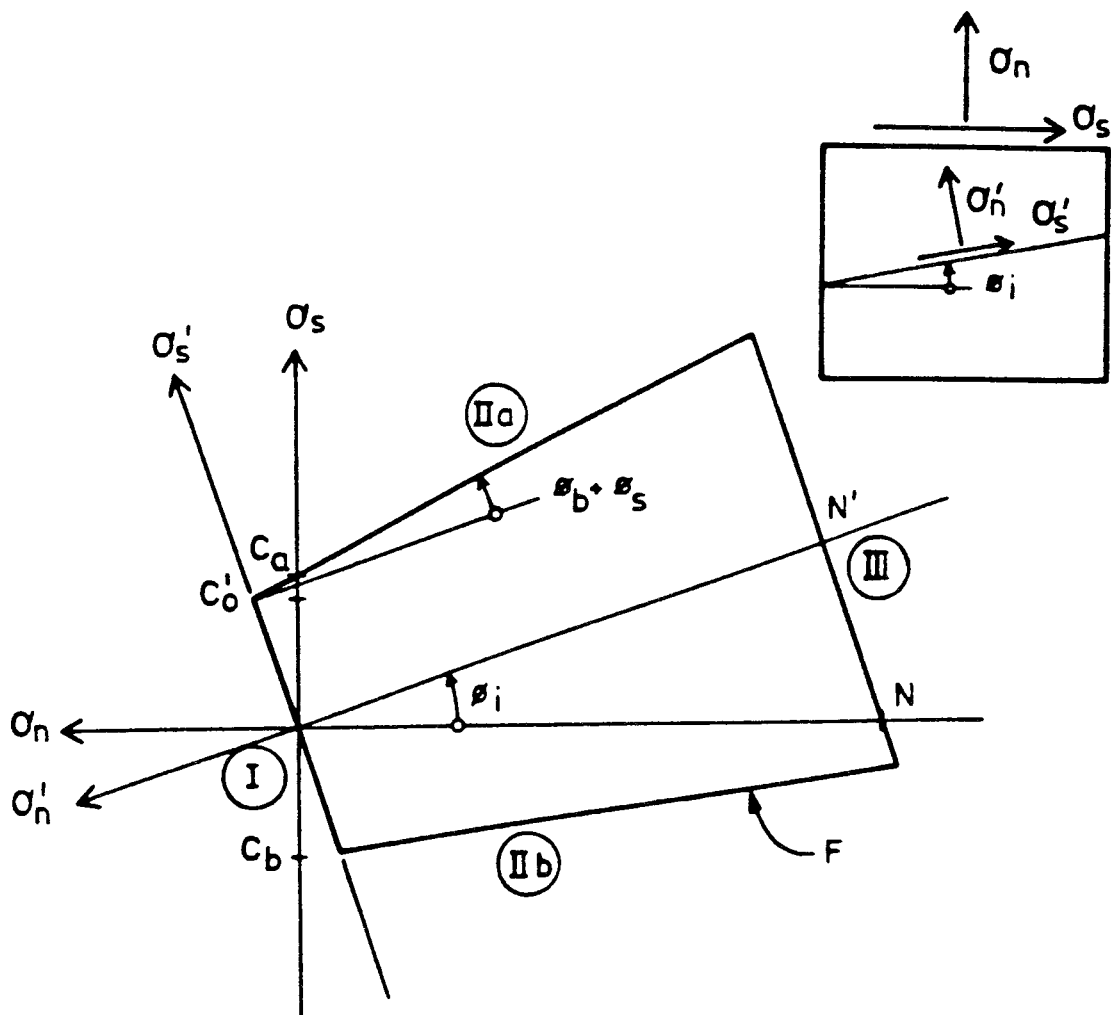


Figure 10-5. Viscoplastic yield function,  $F$ , for a single joint. After Olofsson (1985).

### 10.3.2 Distinct Element Program for Modelling Jointed Rock Masses, MUDEC

The distinct element method is a recognized discontinuum modelling approach for simulating the behaviour of jointed rock masses. The Micro Universal Distinct Element Code, MUDEC, provides in one code modelling variable rock deformability, plastic behaviour and fracturing of intact rock, fluid flow and fluid pressure generation in joints and voids and linear and non-linear inelastic behaviour of joints. In this study we apply both linear and nonlinear behaviour of the joint parameters. The shear-dilation-conductivity coupling of each joint set is modelled in accordance with the method suggested by Barton et al., (1985) and called the Barton-Bandis joint model. The model allows for changes in stiffness as a function of the number of loading cycles and the applied stresses. Typically, data are selected after the fourth loading cycle.

MUDEC contains logics to account for generation of fluid pressure in inner domains of the model. This facility has been applied in generating boundary loadings from flat jacks. The boundary element program coupled to MUDEC is a direct formulation which gives an integral equation in terms of the boundary values of tractions and displacements.

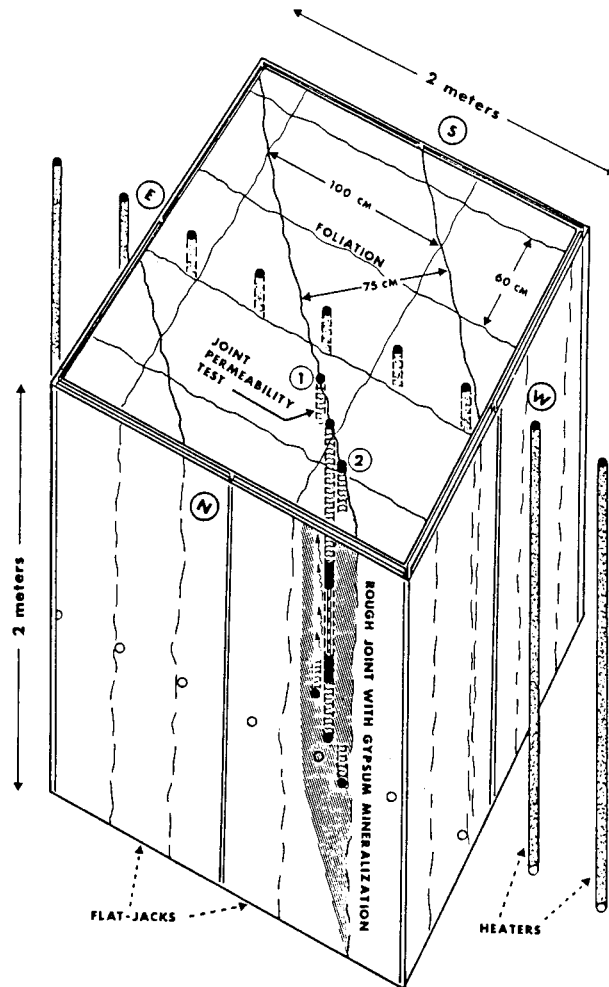


Figure 10-6. Schematic block diagram showing the relationship of the average joint structure to the flatjacks, the line of borehole heaters and the joint permeability test. After Hardin et al. (1981).

#### 10.4 AN ATTEMPT TO VALIDATION OF ROCK MECHANICS CODES AGAINST COLORADO SCHOOL OF MINES BLOCK TEST DATA

A series of mechanical and hydrological experiments is being conducted with an in-situ block of fractured gneissic rocks at the Colorado School of Mines (CSM) Experimental Mine at Idaho Springs, Colorado. In recent years the project has included studies of applied stresses versus deformation, stress and fracture conductivity, together with studies of fracture deformation versus fracture conductivity.

The block and the specially-excavated drift (the block location) have been the sites for several rock mechanics and hydrological studies. Results from these studies are reported by Barton et al., (1988) and Stephansson and Savilahti (1988).

The test block is a two-meter cube of Precambrian gneiss excavated by Terra Tek, Inc. in 1979, Figure 10-6. They subjected the block to bi-axial and uniaxial loading at ambient and elevated temperatures, using flatjacks and a line of borehole heaters for measuring hydro-thermal-mechanical properties of the rock mass. Joint permeability, static modulus, dynamic modulus, joint normal and

shear stiffness, coefficient of thermal expansion, thermal conductivity and diffusivity were investigated under various conditions of stress (0–6.9 MPa, uniaxial and biaxial) and temperature (12–74° C mean block temperature). After Terra Tek completed their program, CSM began a second series of experiments with new hydraulic flatjacks, decoupled recording displacements with a fixed external reference frame and an updated recording system.

#### 10.4.1 Mechanical Properties

Extensive laboratory tests on intact rocks from the experimental mine have resulted in the following elastic constants for the intact rock matrix:

$$E_R = 58.6 \text{ GPa for all rock types, all directions}$$

$$\nu = 0.25$$

Based on joint parameters recorded in the mine and the known hydro-mechanical coupled joint behaviour the parameters for the Barton system of joint characterization for the foliation set and the diagonal joint set were as follows:

$$JRC = 8.2$$

$$JCS = 62.2 \text{ MPa}$$

$$\Phi_r = 26.5^\circ$$

For a representative normal stress level of 3.5 MPa the cohesion, friction angle and peak dilation angle is found to be

$$c = 0.4 \text{ MPa}$$

$$\Phi = 32^\circ$$

$$d = 6.7^\circ$$

The parameters associated with the joint-shear and normal stiffness properties of the CSM block have been determined by three different methods. Average stiffnesses according to Barton's system of the foliation and diagonal joint set for representative normal stresses in the range 0–7 MPa are shown in Table 10-1.

**Table 10-1. Stiffness data obtained for the CSM block.**

Stiffness	Barton System Linear [MPa/mm]	Terra Tek Field Measurements* [MPa/mm]	CSM Field Measurements† [MPa/mm]
Normal	67.2	117.3	35.4
Shear	2.7	16.7	24.0

\* Whittmores pins, Hardin et al., (1981)

† Triangulation array, Richardson (1986)

During the first phase tests conducted by Terra Tek the surface of the block was instrumented with some thirty pairs of Whittmore pins. By subtraction of the deformation of the intervening intact rock from the overall gauge response, the

net joint deformation was obtained. The average normal stiffnesses of the diagonal and foliation joints are shown in Table 10-1.

Joint normal and shear displacement curves were also constructed for the tests run by CSM using a field measuring system and an evaluation technique described by Richardson (1986). In principle, tests were selected for which there were two displacement measuring stations on each side of a joint. This yielded four possible triangular rosettes. These were averaged to give a single joint normal curve and a single joint shear curve. Based on measurements of joint stiffness data for the four major joints in the block conducted at three levels in the block, Richardson (op. cit.) obtained the average stiffnesses shown in Table 10-1.

It is believed that the difference between the CSM results and the Terra Tek results presented in Table 10-1 indicate the following: (i) possible surface decoupling in the Terra Tek results, (ii) the lower peak stress level (5 MPa versus 7 MPa) used in the CSM test, and (iii) broader array spacing for the deformation measurements in the CSM test. The difference between the stiffness results may also be due to increased stiffness resulting from the attached bottom. All the stiffness values presented were therefore included in the validation with HNFEMP.

#### 10.4.2 Modelling with HNFEMP and Comparison of Numerical and Field Test Results

A continuum model of the CSM block was constructed using the HNFEMP code. The dimensions of the block, its orientation and the three sets of continuous joints and their average spacing are shown in Figure 10-6.

Six different material models were tested. Two of these had identical normal and extreme shear stiffnesses, see Table 10-2.

East-West uni-axial loading (1), N-S uni-axial loading (2) and bi-axial loading (3) directions were modelled and the peak stresses were as shown in Figure 10-7. Each model tested is assigned a two-digit number, where the first digit denotes the material number (1-6), and the second for the loading conditions (1-3).

**Table 10-2. Material models tested with HNFEMP.**

Joint Stiffness [MPa/mm]	Material Model					
	1 Isotropic, Linearly Elastic	2 Field Data Barton System	3 Block Test Terra Tek	4 Block Test CSM	5 Sensitivity Analysis	6 Sensitivity Analysis
Normal	∞	67.2	117.3	35.4	117.3	17.3
Shear	∞	2.7	16.7	24.0	2.7	00.0

A total of 18 models (6 materials and 3 loadings) of the CSM block were analysed and the results are presented in Stephansson and Savilahti (1988). As an example of the results obtained principal stress vectors and y-displacement are shown for Model 2.3 (stiffnesses according to Barton's system and biaxial loading), Figure 10-8.

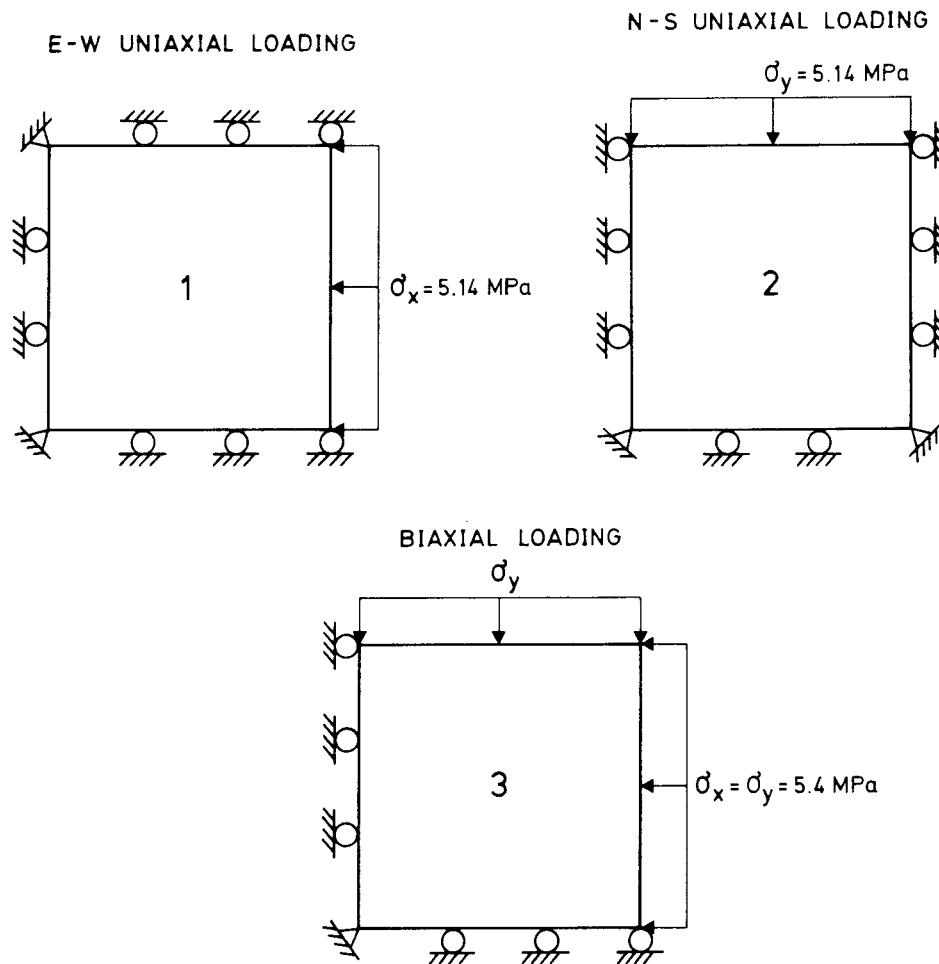


Figure 10-7. Loading configurations (1—3), applied peak loads and boundary conditions for finite element modelling with HNFEMP.

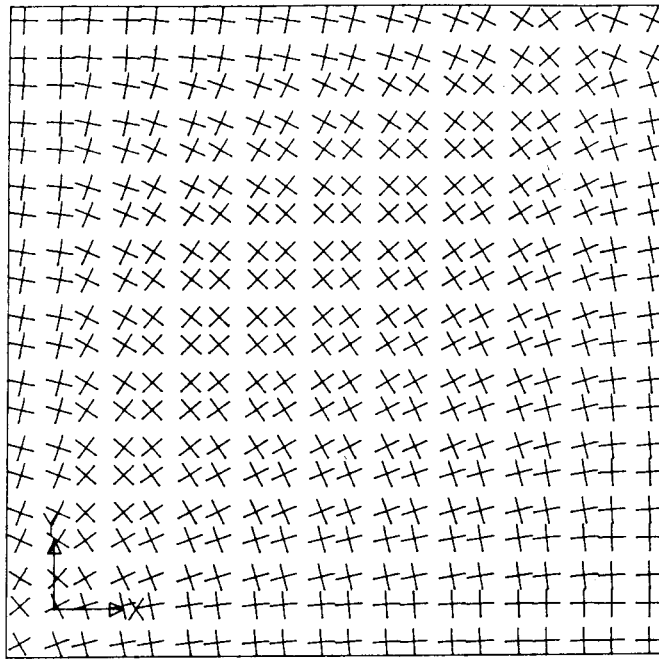
To demonstrate the applicability of the smeared out approach to rock mass modelling, comparison between model predictions of the block behaviour and the recorded and analysed field data is essential. The following tests are used for the validation of HNFEMP:

- Peak-load displacement vectors, CSM test
- Equivalent modulus of deformation, CSM test
- Block deformation modulus, Terra Tek test
- Rock deformation modulus, CSM tests
- Rock stresses, CSM tests

With the fixed frame anchored into the mine back in the CSM test, absolute displacements of station points at various depths within the block during loading could be measured. In principle there is fair agreement in the magnitude and orientation of the displacement vector obtained from the field tests and the HNFEMP-modelling, see Figure 10-9. Modelling results always give smaller magnitudes for displacements than those obtained from the field data.

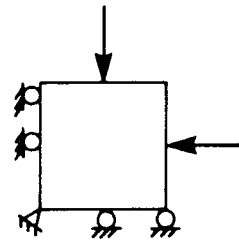
The effective Young's modulus of the CSM block was determined from the calculated overall strains between four block corners and discontinuous deformation analysis (DDA). The average Young's modulus of 12.4 GPa calculated from DDA is found to be in good agreement with the result (12.0 GPa) of

CSM-BLOCK MODEL 2.3 : PRINCIPAL STRESS VECTOR



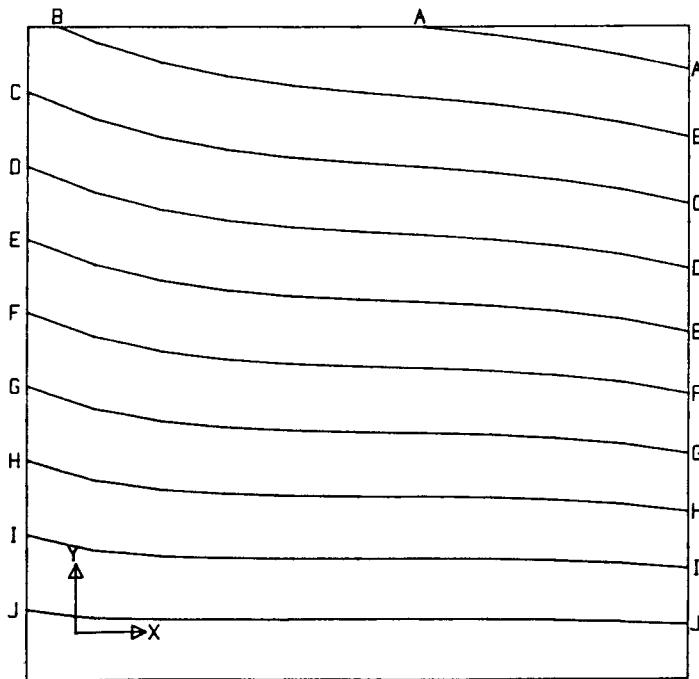
FACTOR  
1.0E-7

0 10 [MPa]

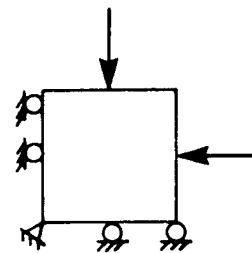


A

CSM-BLOCK MODEL 2.3 : Y-DISPLACEMENT



A=-5.0E-04 [m]  
B=-4.5E-04  
C=-4.0E-04  
D=-3.5E-04  
E=-3.0E-04  
F=-2.5E-04  
G=-2.0E-04  
H=-1.5E-04  
I=-1.0E-04  
J=-5.0E-05  
K=-1.2E-10



B

Figure 10-8. HNFEMP model of CSM block, Model 2.3, Barton's joint system and bi-axial loading 5.14 MPa. A, Principal stress vectors. B, y-displacement.

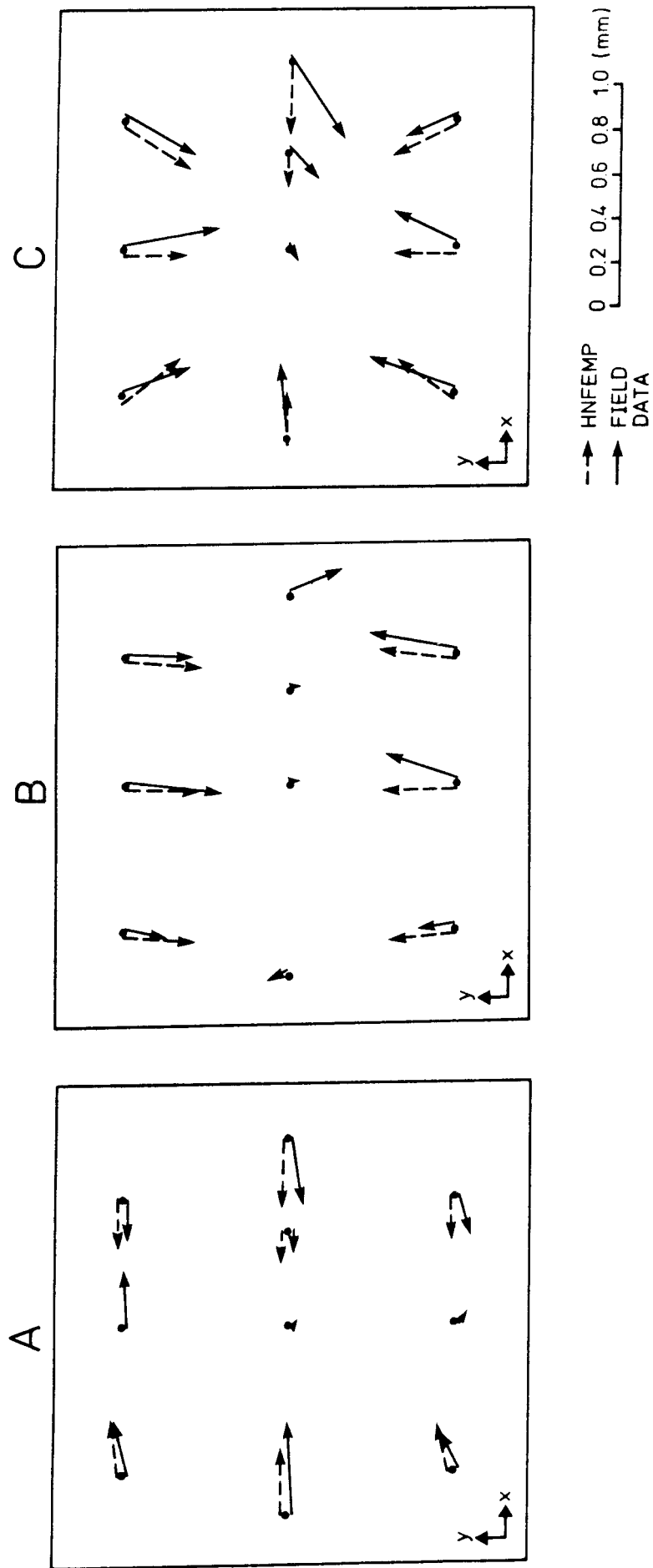


Figure 10-9. Displacement vectors at peak loads from field tests and modelling with material model 4, CSM test. A, Uni-axial E—W loading. B, Uni-axial N—S loading. C, Bi-axial loading.



the finite element modelling with the stiffness parameters suggested by Richardson (1986), material model 4.

The Terra Tek research group measured the aperture of the boundary crack in the grout above the flatjacks. They calculated the effective elastic modulus of the block. Using the stiffness values suggested by Terra Tek (material model 3), the modulus was calculated to be 24.0 GPa. This is in close agreement with the calculated value of 24.2 GPa.

Stress monitoring during flatjack loading of the CSM block was conducted with two instrumentation systems — the USBM Borehole Deformation Gauge (BDG) and the Luleå University of Technology gauge (LUT). Excluding a few measuring stations at the centre of the block, the monitored directions of the principal horizontal stress were in fair agreement with the modelled results. Furthermore, the magnitude of the average maximum horizontal stress from the BDG monitoring agreed best with the results of the modelling and the applied loading from the flatjacks.

In conclusion, the five different comparisons between model predictions of the block behaviour and the recorded and analysed field data show fair to close agreement and this demonstrates the applicability of the smeared out approach to rock mass modelling.

#### **10.4.3 Modelling with MUDEC and Comparison of Numerical and Field Test Results**

Two versions of the MUDEC code have been tested against the measured results from the CSM block test, namely MUDEC-linear, where the joint properties are assumed to vary linearly with applied stress, and MUDEC-BB where joint stiffnesses are assumed to vary non-linearly with stress in accordance with the Barton-Bandis joint model. For simplicity, the CSM block was modelled by three joints and four principal blocks, see Figure 10-10.

Boundary conditions were varied in an attempt to simulate flatjack loading more realistically. Block models with linear joint behaviour (Model A) and Barton-Bandis joint behaviour (Model B) were analysed with simple uniform stress boundaries, Barton and Chryssanthakis (1989). More realistic boundary conditions were achieved by applying fluid pressure loading in rectangular slots simulating the flatjacks and with rigid boundaries resisting displacements behind them. These boundary conditions were applied only to the MUDEC-BB models (Model C). Results have been presented for principal stresses, shear stresses, deformation vectors, shear displacements along the joints, block rotation and for the case of MUDEC-BB also joint mechanical and conducting apertures. Typical results for the principal stresses and block rotations inside the model are shown in Figure 10-11 for the case of bi-axial loading of Model C (flatjack simulation and Barton-Bandis joint behaviour). Notice that stresses tend to be transmitted perpendicularly across the joints, Figure 10-11A. In general, the stress magnitudes are of the order of 4 to 7 MPa compared with the maximum applied boundary stresses of 5.4 MPa. Stress concentrations associated with block rotation and corner loadings increase the stresses in the range of 9.1–14.3 MPa for linear joint behaviour and 7.9–23.2 MPa for non-linear joint models. A summary of the numerical results for the three models A, B and C is presented in Table 10-3.

Comparison of the numerical results with measurements of displacement vectors and shear displacements, Richardson (1986), measurements of shear displacement, shear stiffness and conducting aperture, Hardin et al., (1982) and stress measurements performed, Brown et al., (1986) show good agreement in

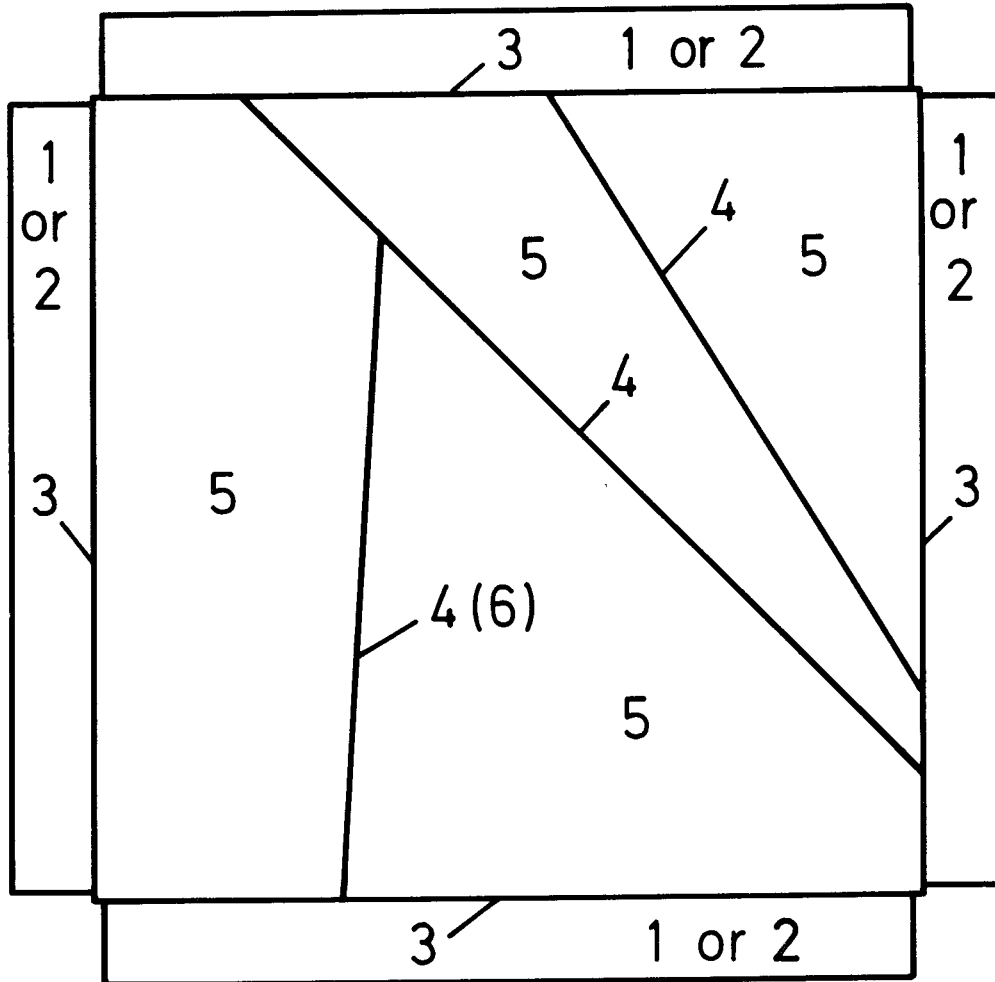
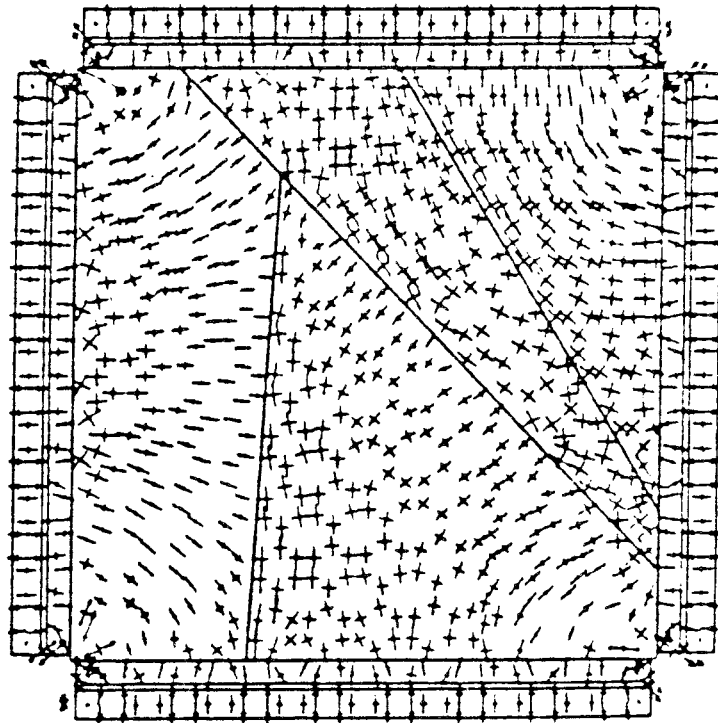


Figure 10-10. Modelling of the CSM block with MUDEC. Three joints and four rock blocks are simulated and the material properties are given.

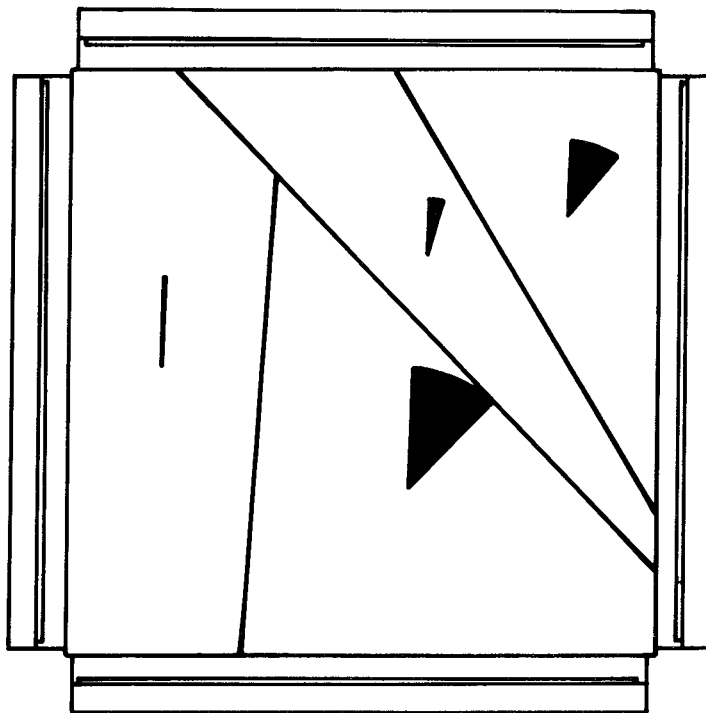
general, cf. Table 10-4. Excellent agreement was obtained for joint shear displacements and joint conductive apertures.

### 10.5 MODELLING THE EFFECT OF GLACIATION, ICE FLOW AND DEGLACIATION ON LARGE ROCK MASSES

The effect of glaciation and deglaciation has been studied in two-dimensional generic models of faulted rock masses. Six loading cases were modelled two-dimensionally for a 4 x 4 km rock mass, Figure 10-12. After consolidation and application of boundary stresses, where the models were loaded by horizontal stresses from one side and both sides respectively (case 1), an ice sheet, three kilometres thick, was applied at the surface of the model (case 2). A special interface was introduced at the ice-rock boundary. Ice flow was then simulated either by a velocity applied at the vertical boundary or by shear stresses applied



A



B

Figure 10-11. MUDEC-BB modelling of the CSM block in bi-axial loading and flat-jack simulation. A, Principal stresses where the maximum principal stress is 17 MPa. B, Rotation of individual blocks in the model. After Barton and Chryssanthakis (1988).

**Table 10-3. Summary of the numerical results obtained from MUDEC showing the maximum displacement vectors, the maximum shear displacements on joints, maximum principal stresses and mechanical and conducting apertures inside the CSM block. After Barton and Chryssanthakis (1988).**

Type of Model	Direction of loading	Maximum displacement vectors	Maximum shear displacement	Maximum principal stresses	Mechanical or real aperture	Conducting or theoretical aperture
		[mm]	[mm]	[MPa]	[ $\mu\text{m}$ ]	[ $\mu\text{m}$ ]
<b>MODEL A</b>						
Stress boundaries and linear joint model	Biax	0.10	0.06	11.3	-	-
	N-S	0.28	0.15	14.1	-	-
	E-W	0.29	0.15	9.1	-	-
<b>MODEL B</b>						
Stress boundaries and Barton-Bandis joint model	Biax	0.12	0.11	8.6	137	36.9
	N-S	0.53	0.75	23.2	162	49.9
	E-W	0.40	0.33	8.5	160	49.2
<b>MODEL C</b>						
Fluid pressure boundaries model and Barton-Bandis joint model	Biax	0.19	0.13	15.9	136	34.7
	N-S	0.32	0.30	21.9	152	49.6
	E-W	0.37	0.29	7.9	158	48.6

**Table 10-4. Summary of the numerical and experimental results obtained from Terra Tek and CSM tests concerning the maximum displacement vectors, total block displacement, shear displacement and maximum principal stress. After Barton and Chryssanthakis (1988).**

	Maximum displacement vector	Total block displacement	Shear displacement	Maximum principal stress [MPa]	
	[mm]	[mm]	[mm]	DBG method	LUT method
CSM test Richardson (1986)	0.5 Biax 0.6 N-S 0.6 E-W	0.725 Biax	- Biax 0.225 (N-S) 0.20 (E-W)		
Terra Tek test Hardin et al. (1982)	* * *	~0.23 Biax ~0.23 N-S ~0.23 E-W	- Biax 0.22 (N-S) 0.13 (E-W)		
CSM test Brown et al. (1986)				20.0 Biax 24.7 N-S 16.3 E-W	11.6 Biax 8.4 N-S 11.8 E-W
Numerical results from Models A, B, C	0.10-0.19 Biax 0.28-0.53 N-S 0.29-0.40 E-W	0.20-0.38 Biax - N-S - E-W	0.06-0.13 Biax 0.15-0.75 N-S 0.15-0.33 E-W	8.6-15.9 Biax 14.1-23.2 N-S 7.9-9.1 E-W	

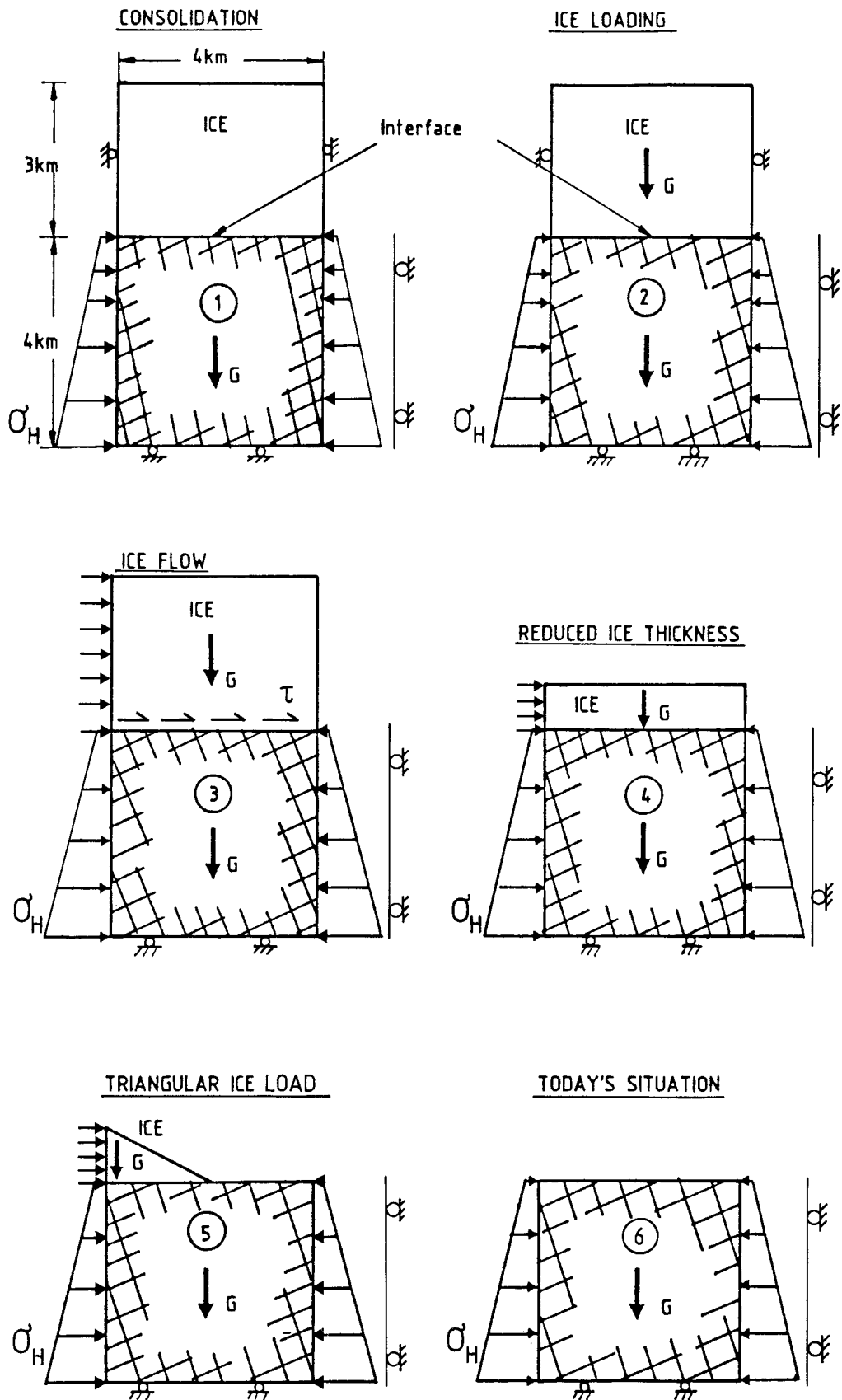


Figure 10-12. Generic models for glaciation, glacial flow and deglaciation. Loading cases, boundary conditions and geometry. Two different boundary conditions were used. During consolidation, loading case 1, no ice load was applied.

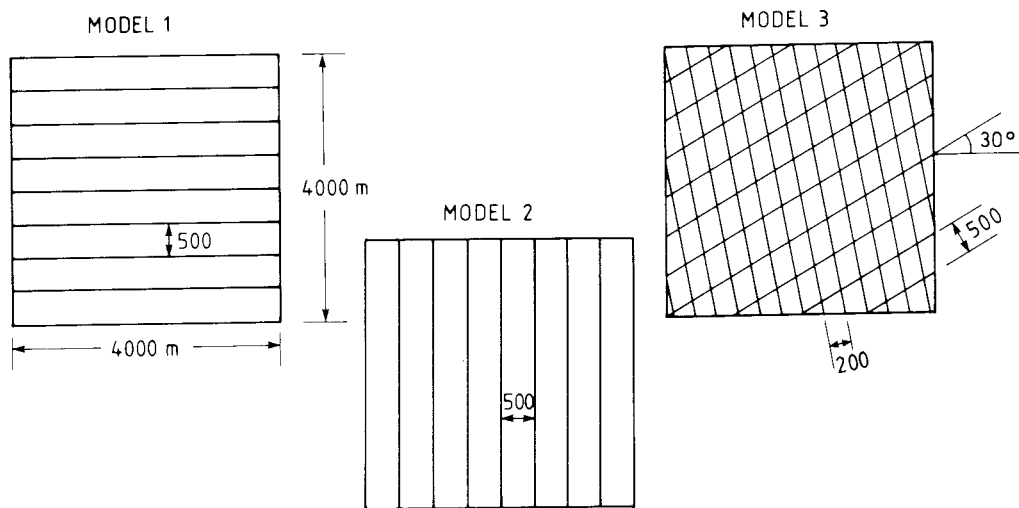


Figure 10-13. Sections of fault set geometries in generic modelling.

at the top surface of the rock mass (case 3). For simulation of deglaciation the ice thickness was reduced in two steps. First 2/3 of the ice sheet was removed and the response in stress and displacement was studied (case 4). Later all ice was removed from one half of the model and a triangular ice load was left (case 5). Finally, all ice was removed to represent today's situation (case 6). In modelling the effect of glaciation and deglaciation the displacements at bottom of the model are restricted to vertical. In nature the ice load will cause subsidence and rebound due to the viscoelastic behaviour of the earth's mantle. These effects are not considered in this study.

Three different fault set geometries were analysed, Figure 10-13. Models 1 and 2 consist of a rock mass with one set of faults having a spacing of 500 m and oriented horizontally and vertically, respectively. Model 3 has two sets of faults with a spacing of 200 m and 500 m, respectively. The fault geometry of Model 3 approaches closest to the situation at Lansjärv.

### 10.5.1 Modelling with HNFEMP

Each of the Models 1–3 is subjected to an initial horizontal stress  $\sigma_H = 5 + 32 \cdot z$  acting at one of the vertical boundaries and a vertical stress  $\sigma_v = 27 \cdot z$ , where  $z$  is the depth in kilometres and the stresses are in MPa. The finite element mesh contains 289 nodes and 256 elements and plane strain conditions are assumed. Two types of material properties were considered, namely, a soft fault stiffness and a fault system 60 times stiffer, cf. Table 10-5.

Displacement vectors and principal stress vectors from ice loading and ice flow for Model 3.3, i.e. loading case 3 according to Figures 10-12 and Model 3.3 with two intersecting sets of faults with large normal and shear stiffnesses (stiff faults according to Table 10-5) are shown in Figures 10-14. Due to the large ice load, which is less than the horizontal stress, displacements will be directed towards the right boundary, where the tectonic stress is applied.

The modelling approach with HNFEMP uses a material constitutive model that accounts for the properties of the intact rock and the joints without including the joints as separate entities, see section 10.3.1. This modelling technique results in continuous displacements and stresses throughout the model.

**Table 10-5. Material properties for HNFEMP-modelling of glaciation and deglaciation.**

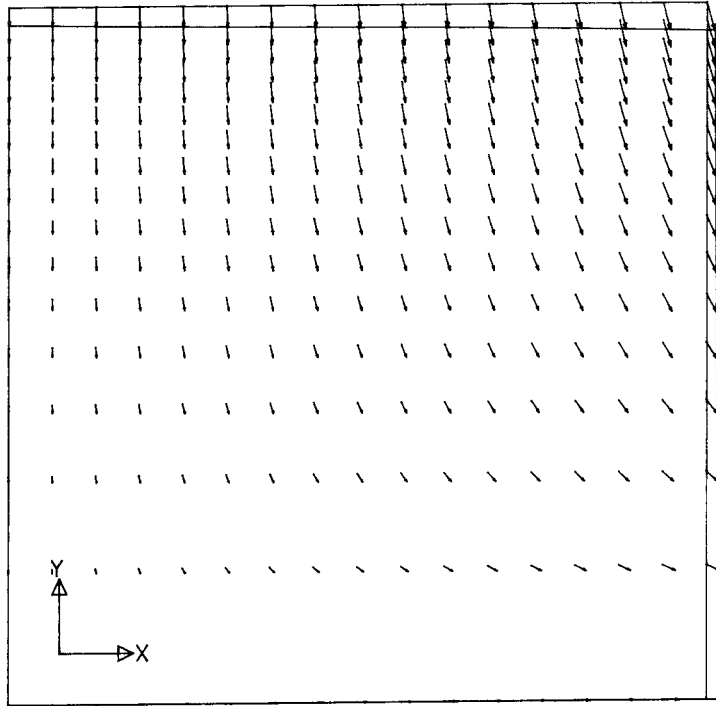
Material	Parameter	Soft Faults	Stiff Faults
Intact rock	Density, kg/m <sup>3</sup>	2700	2700
	Young's modulus, GPa	40	40
	Poisson's ratio	0.2	0.2
Fault	Normal stiffness, MPa/m	10.0	600.0
	Shear stiffness, MPa/m	1.0	60.0
	Cohesion, MPa	0.1	0.1
	Dilation angle, degree	5.0	5.0
	Tensile strength, MPa	0.0	0.0
	Friction angle, degree	35.0	35.0
	JRC	6	6
	JCS, MPa	50.0	50.0
	$\Phi_r$ , degree	25.0	25.0
Ice	Density, kg/m <sup>3</sup>	900	900
	Shear stress, MPa	0.1	0.1

Vertical displacement at the midpoint of the ground surface for Model 1–3 with soft and stiff faults are shown in Figures 10-15. Models with a soft fault stiffness have large displacements. The total vertical displacement is governed by the thickness of the model. The results obtained demonstrate the relative importance of fault stiffness and fault geometry. Ice loading and removal cause changes in the stresses as shown in Figures 10-16 for a point located 500 m below the ground surface. The stress changes are  $\Delta\sigma_x \sim 3$  MPa and  $\Delta\sigma_y \sim 27$  MPa for Model 3 with two sets of intersecting faults, where x is the horizontal direction.

### 10.5.2 Modelling with MUDEC, Linear Fault Stiffness

The three generic models, Models 1–3 with different fault set geometry, were analysed with the MUDEC code, Jing and Stephansson (1988). The 4 x 4 kilometre rock mass is treated as an assembly of elastic rock blocks separated by discontinuities with linear stiffnesses and Mohr-Coulomb failure properties. Two different joint stiffnesses were used, the ice was simulated as an elastic medium and a distributed load at the ground surface, respectively. The interface between the ice and the rock mass was simulated by means of a soft, low-strength and low-friction discontinuity. Two different tectonic, horizontal stresses were simulated and a total of seven models were analysed and presented by Jing and Stephansson (op. cit.). Results for Model 3 with identical geometry, material properties and boundary stresses to those presented in section 10.5.1 (stiff faults) are shown in Figures 10-17 and 10-18. Horizontal and vertical stresses versus loading cases for points along the central line and various depths below the ground surface are shown in Figures 10-17. Since modelling is conducted in time steps the fictitious time is also shown. The flattening of the stress curves for each loading case and depth indicates stable conditions. At a depth of 400 m changes of horizontal stress during ice loading and unloading are of the order of  $\Delta\sigma_x \approx 10$  MPa. The stress magnitudes are less than those obtained from the HNFEMP-modelling, cf. Figure 10-16. Slip along inclined faults causes the stress release. The change in vertical stress reflects the loading and removal of the ice

GENERIC MODEL 3.3 : DISPLACEMENT VECTOR

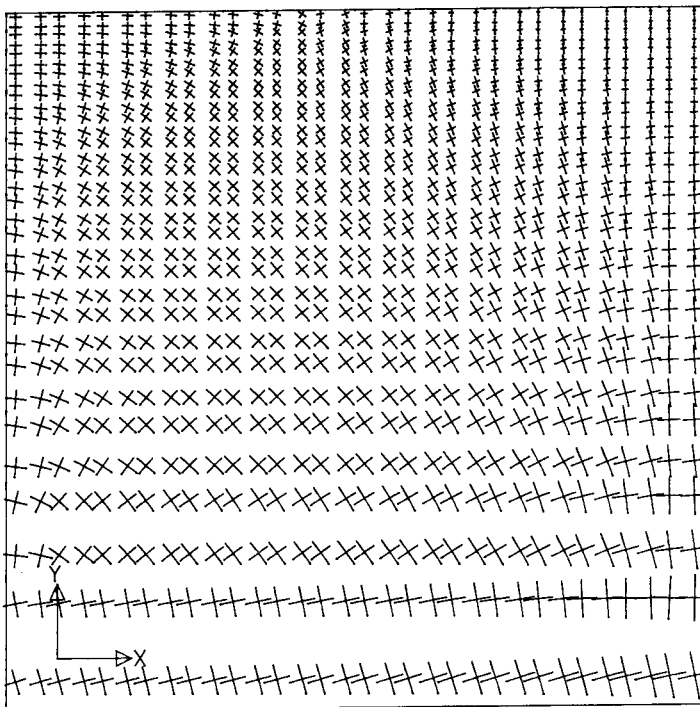


FACTOR  
0.1

0 20 40 m

A

GENERIC MODEL 3.3 : PRINCIPAL STRESS VECTOR



FACTOR  
5.0E-9

0 100 200 MPa

B

Figure 10-14. Results for HNFEMP-modelling of ice loading and ice flow according to case 3 in Figure 10-12. A, Displacement vector. B, Principal stress vector.



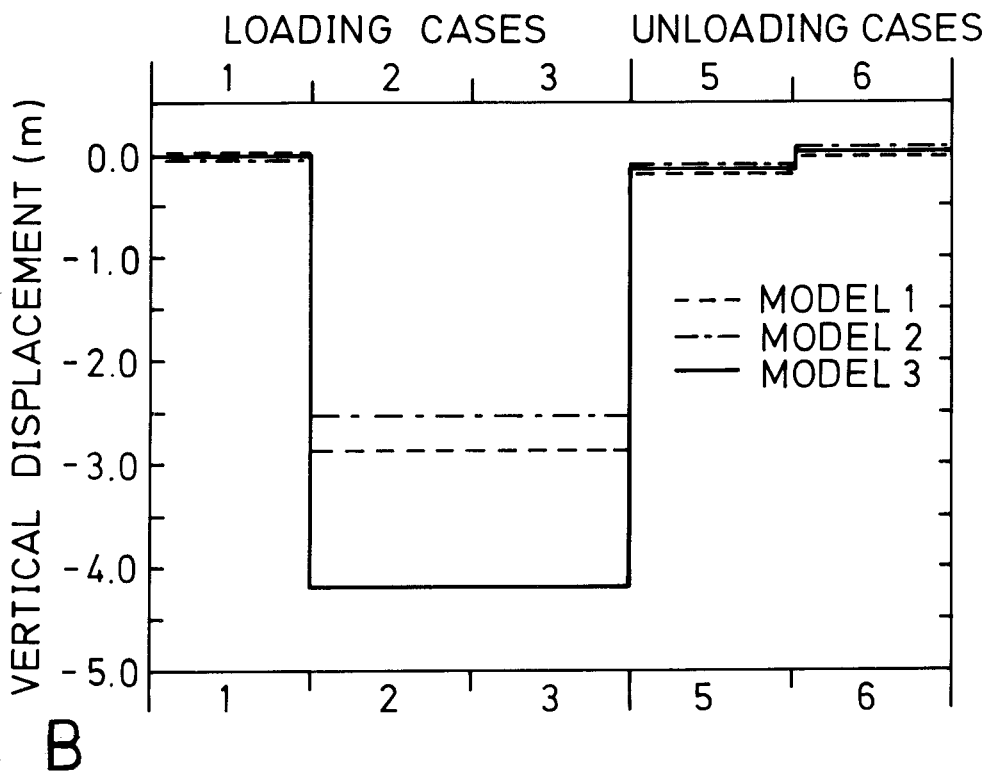
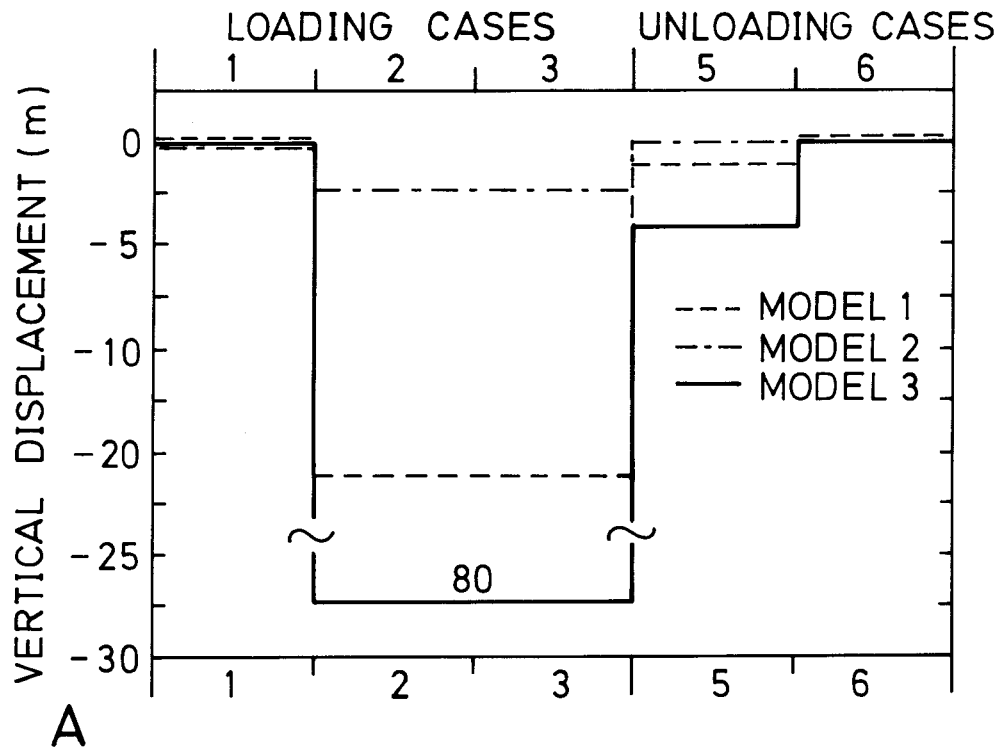


Figure 10-15. Results from HNFEMP-modelling of vertical displacement at the ground surface for Models 1—3. A, Soft faults. B, Stiff faults.

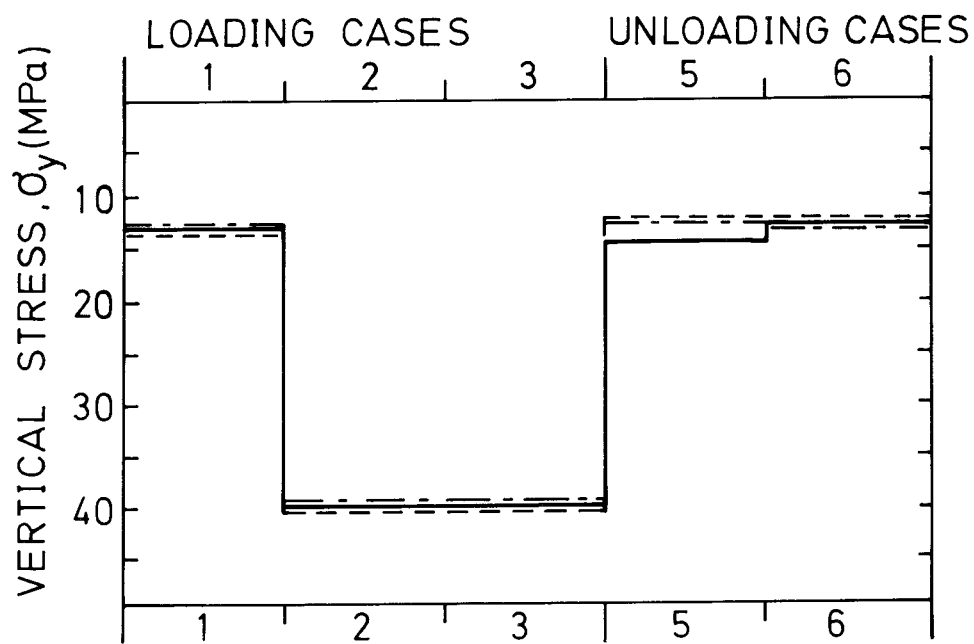
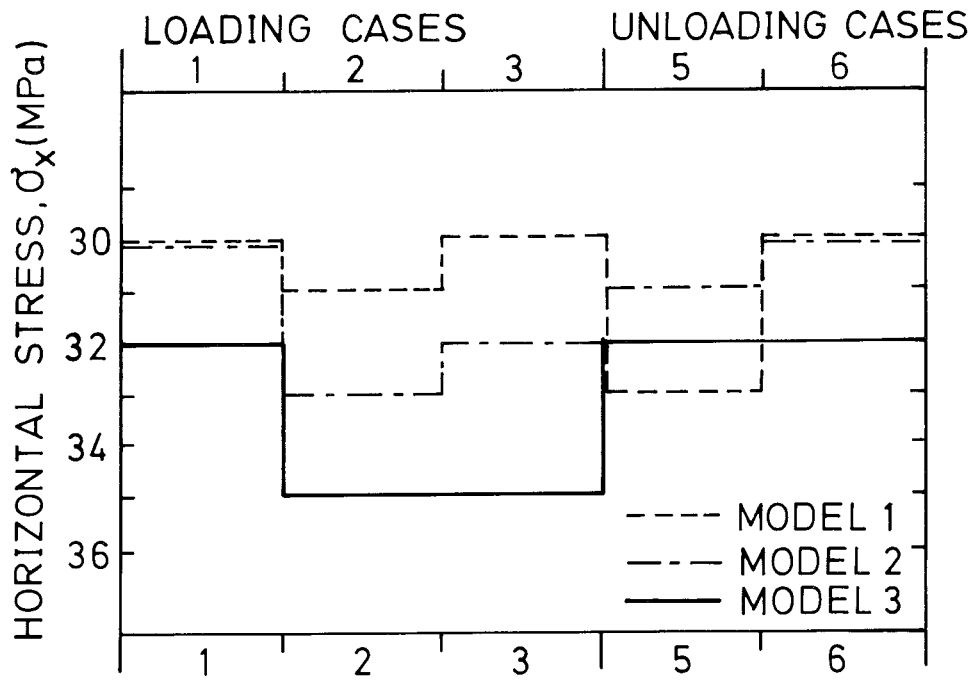


Figure 10-16. Results from HNFEMP-modelling of horizontal and vertical stress at 500 m depth in the centre of Models 1—3. Stresses are similar for soft and stiff faults. Loading and unloading cases according to Figure 10-14.

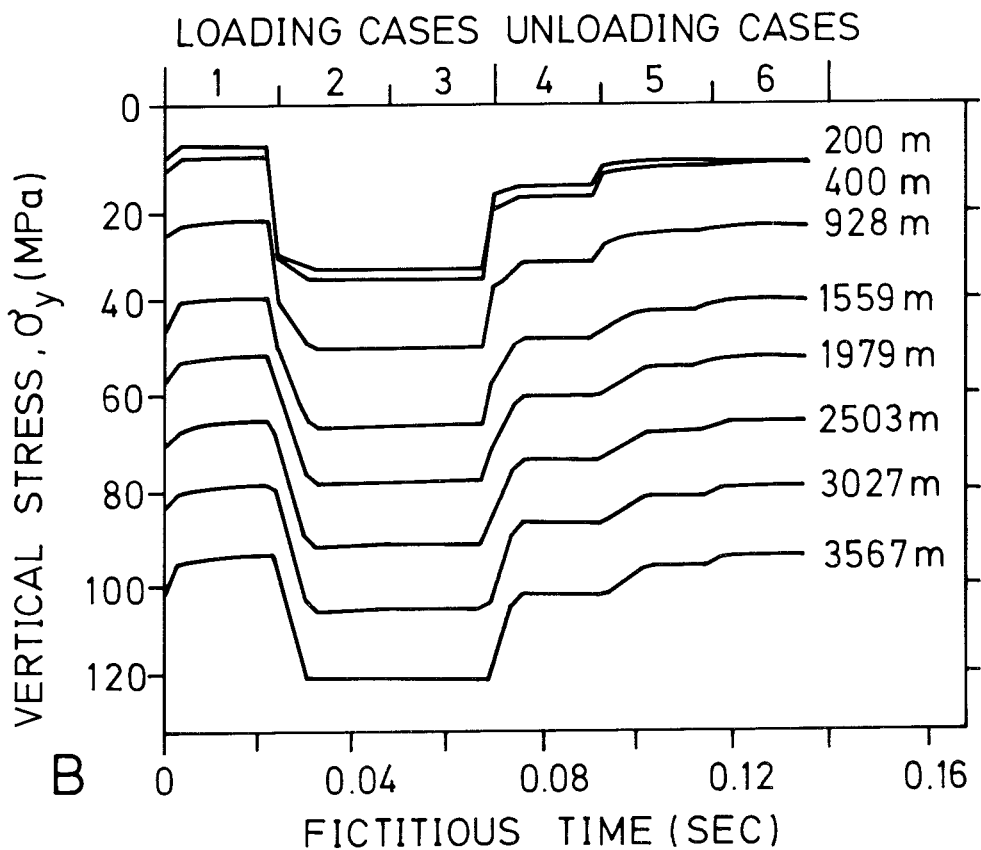
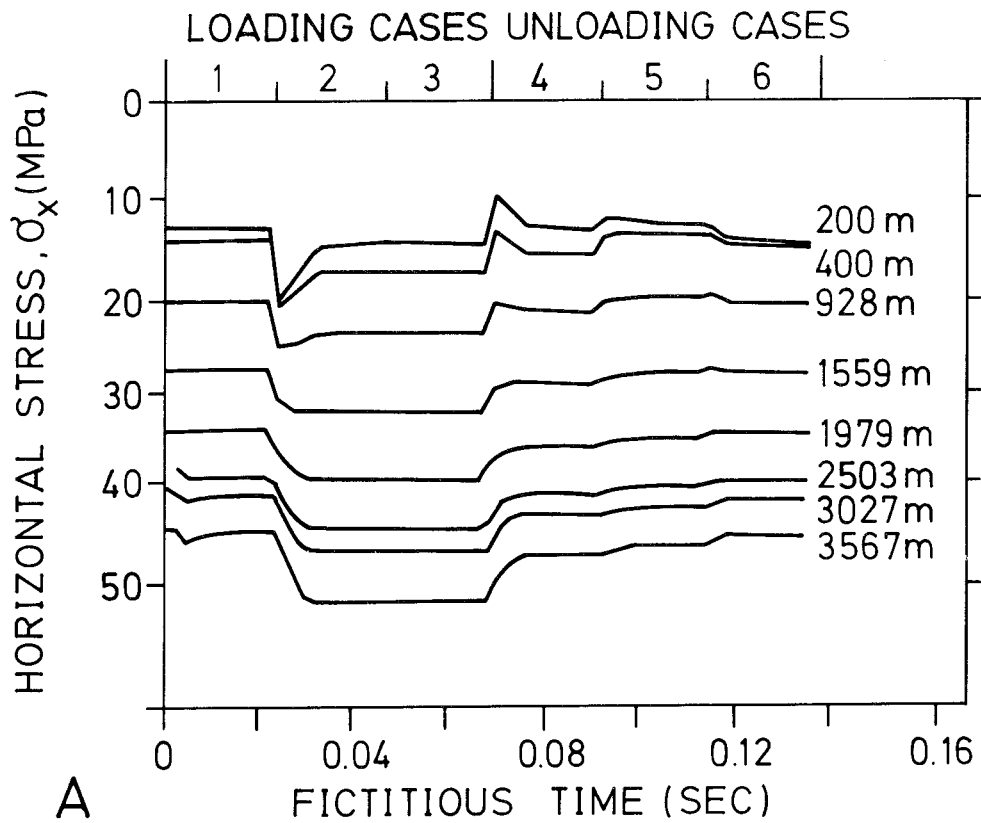


Figure 10-17. Results from MUDEC-modelling of Model 3 with linear fault stiffness. Normal stresses versus loading cases and fictitious computational time is shown for points at various depth. A, Horizontal stress. B, Vertical stress.

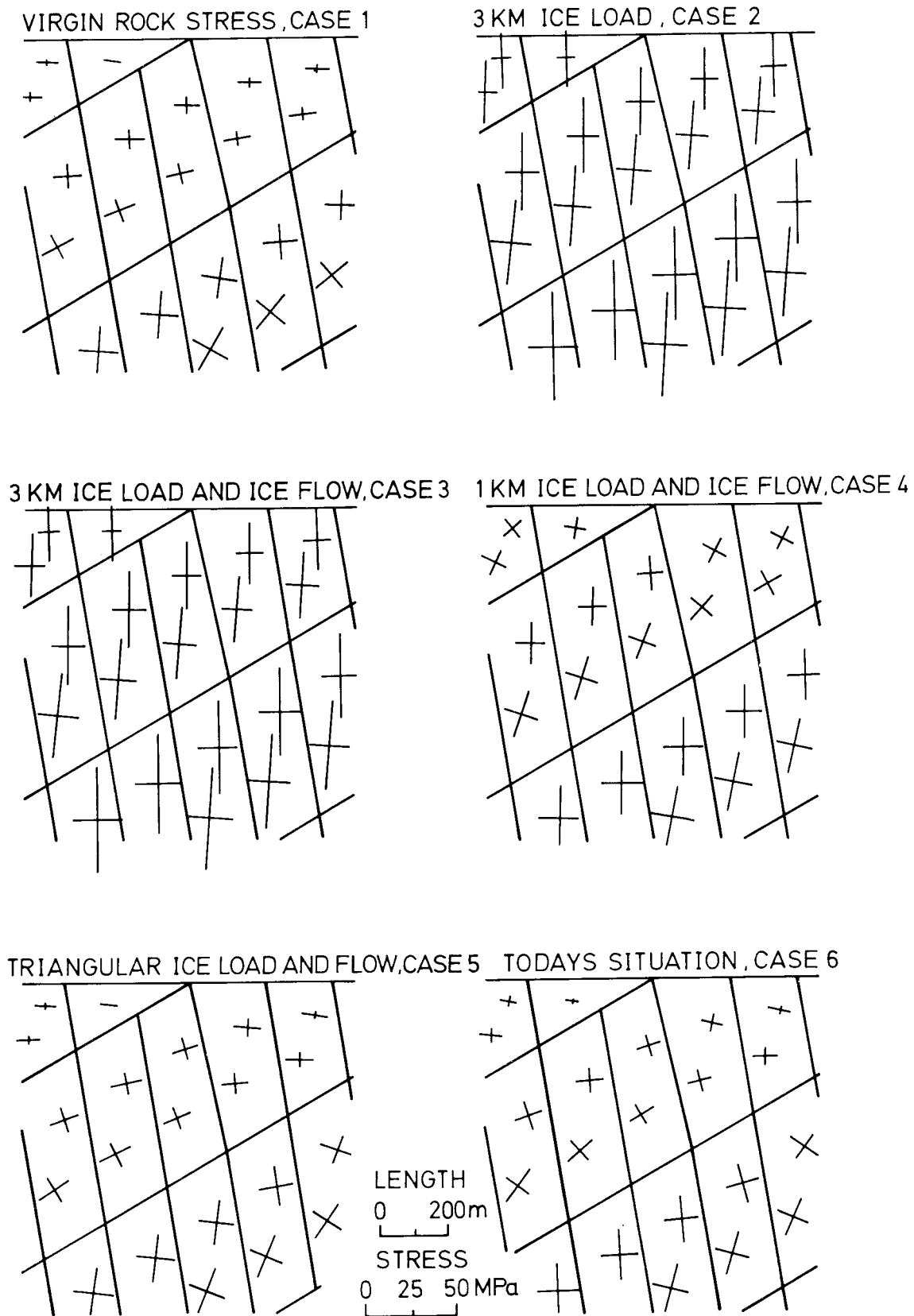


Figure 10-18. MUDEC-modelling of generic Model 3 with stiff faults. Changes in magnitude and orientation of principal stresses for the uppermost 1000 m of the rock mass.

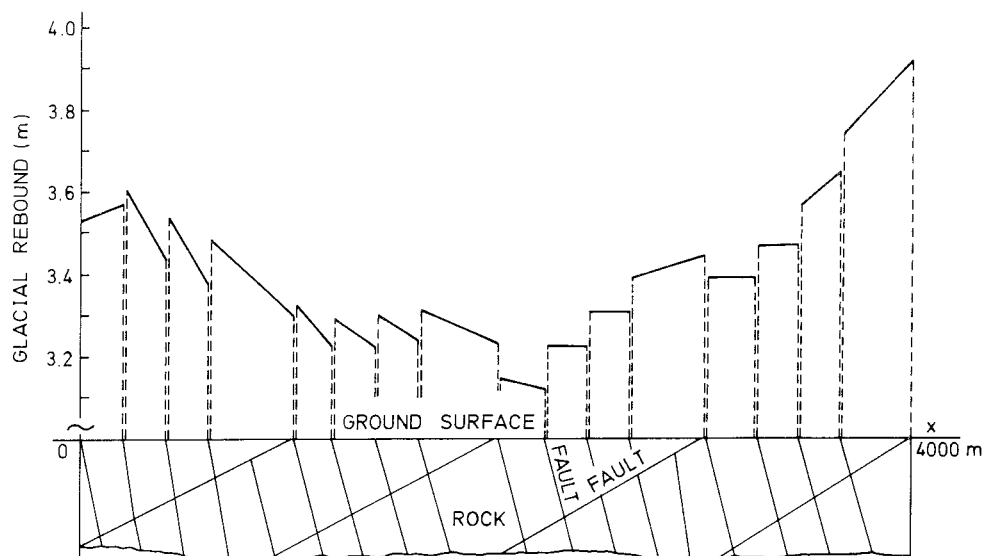


Figure 10-19. MUDEC-modelling of Model 3 with stiff faults showing rebound of the ground surface after deglaciation. The relative displacement between adjacent rock blocks are 5 to 10 cm.

sheet and the results obtained from HNFEMP and MUDEC modelling are in close agreement.

The variation in magnitude and orientation of the principal stresses for the uppermost 1 km of the rock mass and the three loading and unloading cases are shown in Figure 10-18. The re-orientation of the stresses is caused by translation and rotation of the rock blocks surrounded by the two sets of faults.

The individual displacement of the uppermost blocks of the model at the ground surface is shown in Figure 10-19, where the relative displacement between individual blocks are of the order of 5 to 10 cm. A complete deglaciation of the model gives a rebound of 3 to 4 m as indicated by the uppermost line for the blocks. This excludes the global scale upheaval from the glaciation. The total rebound of the ground surface is represented by the uppermost solid line. Relative displacement between individual blocks and rebound are slightly less but of the same magnitude at 500 m depth.

The results obtained from the HNFEMP and MUDEC modelling are in close agreement, cf. Figure 10-16. The effect of a glacial sheet on the remaining stress state will be almost negligible when the process of ice retreat is completed. However, the stresses do tend to rotate and become aligned with the boundary of the rock blocks after deglaciation, as indicated for case 6 in today's situation, Figure 10-18. At greater depth, the reorientation is less pronounced.

### 10.5.3 Modelling with MUDEC and Barton-Bandis Joint Model

Three different generic models of large rock masses with a fault geometry as for Model 3 (see Figure 10-13) were analysed with the non-linear MUDEC code and Barton-Bandis joint model, Barton, Chrystanthakis (1989). Results from two of the generic models — called Model 3A and Model 3B — are presented. The geometry, boundary conditions and loading cases are the same as for model-

ling with linear MUDEC, except that effective tectonic stresses were applied to two of the models. Model 3A has fault stiffnesses that are two to four orders of magnitude stiffer than the faults for Model 3B. The material properties are presented in Table 10-6.

The large problem size and the difference between the joint stiffnesses and the surrounding rock mass in Model 3B, resulted in a very long consolidation procedure (loading case 1) which proceeded slowly during successive loading and unloading stages. The vertical displacements of the ground surface after ice loading were found to be 3.78 m and 3.90 m for Models 3A and 3B, respectively. This is in close agreement with the results obtained from the HNFEMP and linear MUDEC modelling, cf. Figures 10-15 and 10-19. The application of effective tectonic stresses to the model make no major changes in magnitudes of stresses and displacements.

The computational mesh used in the central and uppermost 1000 m of Model 3B was made finer to study in detail the change in displacements and stresses in the vicinity of a repository. Figure 10-20 shows the slight re-orientation of the principal stresses due to ice loading and ice flow from left to right for Model 3B. The principal stress plots for all three models analysed indicate no dramatic changes in terms of stress rotation under the various loading and unloading cases. Changes in horizontal and vertical stresses at 500 m depth below ground surface are in close agreement with other modelling results except for the low stresses due to deglaciation in Model 3B, cf. Figure 10-21.

Modelling with the MUDEC and Barton-Bandis joint models permits determination of mechanical and hydraulic joint/fault aperture. Model 3A exhibits a small variation in aperture and closure down to a depth of 200–300 m. They then reach the maximum closure value of about 100  $\mu\text{m}$  for the sub-horizontal faults and 40  $\mu\text{m}$  for the sub-vertical fault set. Model 3B exhibits an aperture change of 90  $\mu\text{m}$  at the top of the model to 40  $\mu\text{m}$  at the bottom.

The shear displacements obtained vary between 1.2 mm and 80 mm for Model 3A down to a depth of 1000 m. A maximum shear displacement of 0.89 m was obtained for the “soft faults” in Model 3B. For more details about mechanical and hydraulic apertures the reader is referred to the work by Barton, Chrissanthakis (1989).

**Table 10-6. Rock material and joint properties used for Model 3A and Model 3B. After Barton, Chrissanthakis (1989).**

Properties	Intact Rock	Model 3A †		Model 3B		Ice	Interface between ice and rock
		Subvertical	Subhorizontal	Subvertical Fault Set	Subhorizontal Fault set		
Young's Mod. (GPa)	39.9*						
Poisson's ratio	0.19*						
Density (kg/m <sup>3</sup> )	2700					900	
Bulk Mod. (MPa)	2.1E4*					8.8E3	
Shear Mod. (MPa)	8.2e3*					3.4E3	
JRC (Joint roughness coefficient)		5	10	5	10		4
JCS (MPa) (Joint compress. strength)		150	150	150	150		5
PHIR (degrees) Residual friction		30	30	30	30		8
LO (m) Lab-scale joint length		0.10	0.10	0.10	0.10		0.10
Sigma C (MPa) Uni-axial compress. strength of intact rock		220	220	220	220		5
JKN (MPa/m) Joint normal stiffness limit		2.4E8	1E9	2.4E4	1E5	5.8E6	5.8E8
JKS (MPa/m) Joint shear stiffness limit		2.9E4	7.8E4	2.0E2	6.0E2	3E3	3E3
KN (MPa/m) Point contact normal stiffness		2.4E7	1E8	2.4E3	1E4	5.6E6	5.8E6
KS (MPa/m) Point contact shear stiffness		2.9E3	7.8E3	2.0E1	6.0E2	1.2E3	1.2E3
APER (mm) Zero load aperture		0.150	0.200	0.150	0.200		0.015
JCOH (MPa) Joint cohesion						0.01	
JFRIC (tangent) Joint friction coefficient						0.10	
JTENS (MPa) Joint tensile strength						1.0	

\* equivalent properties

† effective tectonic stresses applied

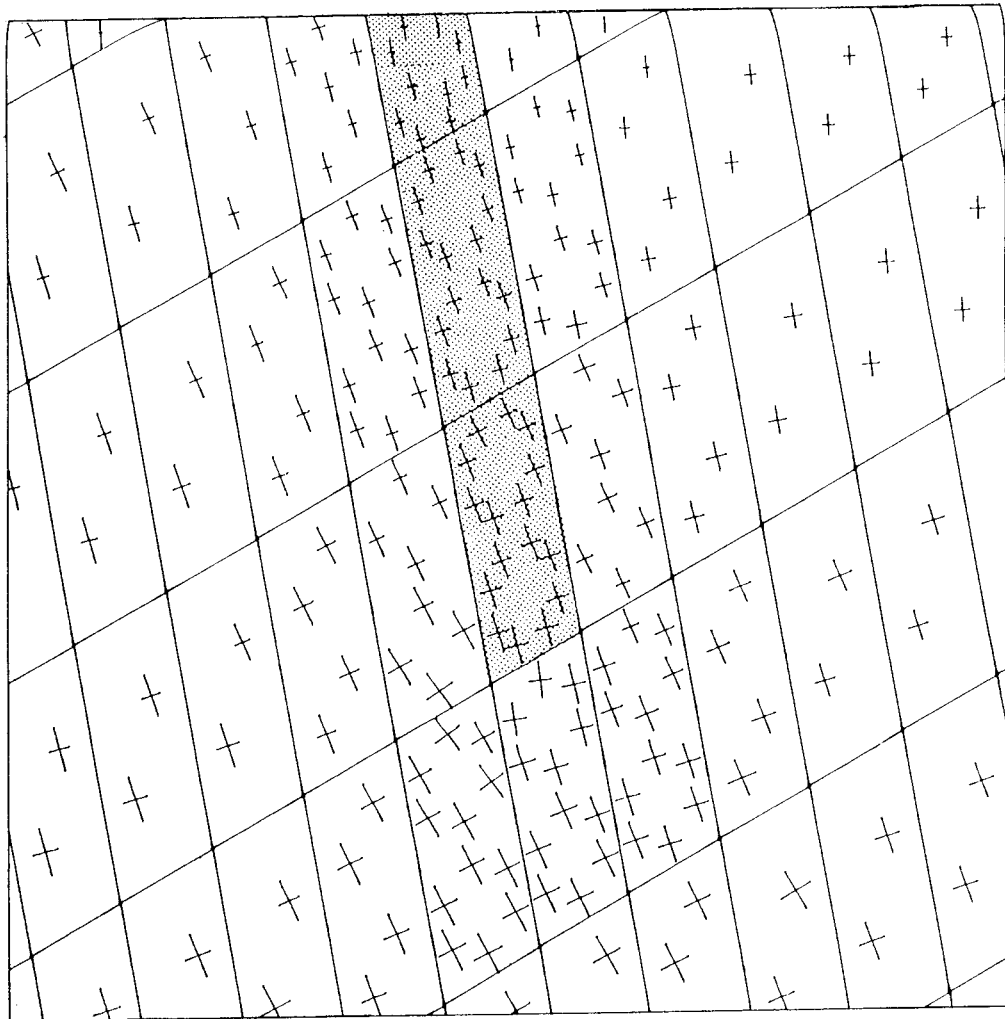


*Figure 10-20. Principal stress vectors in the central portion of Model 3B. Loading case 3 with 3 km of ice and ice flow analysed with MUDEC and Barton-Bandis joint model. After Barton, Chryssanthakis (1989).*



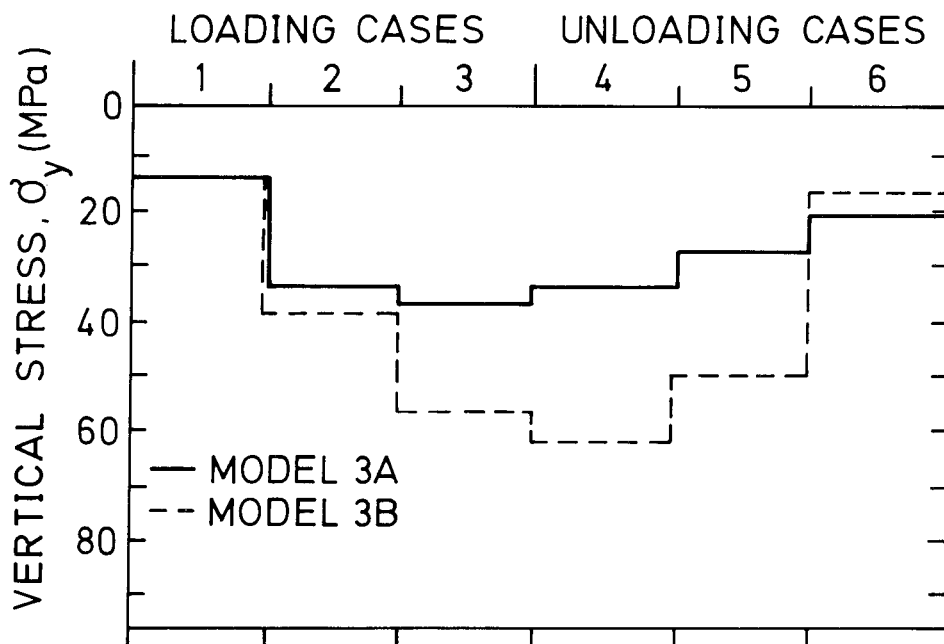
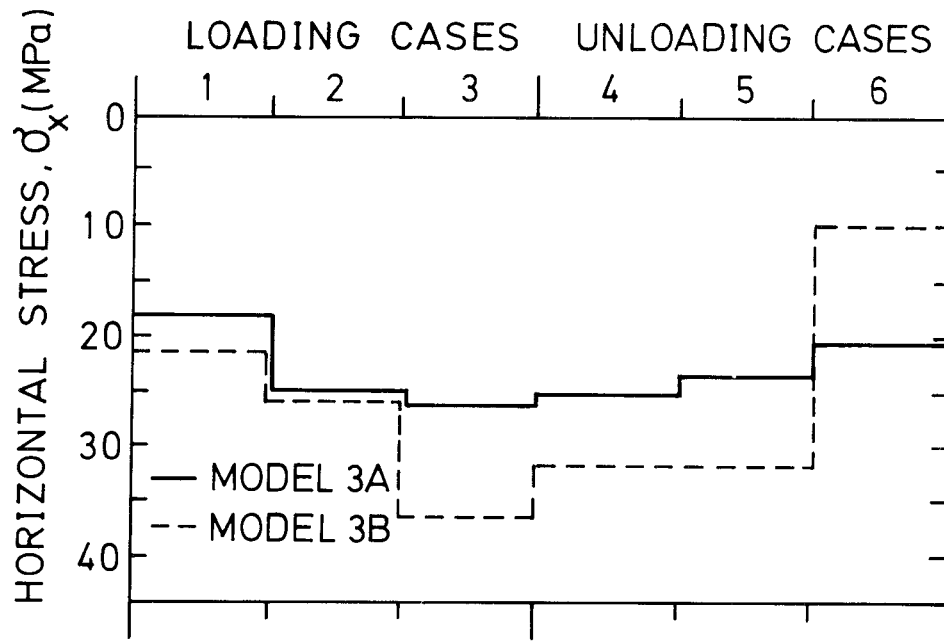


Figure 10-21. Horizontal and vertical stresses at 500 m depth versus loading and unloading cases for Models 3A and 3B, MUDEC with Barton-Bandis joint model. Based on data taken from Barton, Chryssanthakis (1989).

## 10.6 SUMMARY

- Inside a megablock of Precambrian rocks, the tectonic pattern is characterized by faults and fractures of various ages, origin and character. Faults and fractures of 1st, 2nd and 3rd order are assumed to act as deformation barriers for the interior of the block of jointed rock mass. It is suggested that a potential repository for highlevel waste be located in the interior of such a large rock block.
- In modelling the effect of glaciation, deglaciation and glacial rebound on crustal rock mechanics and stability, two modelling approaches are suggested. (i) The upper surface and the bottom of the crust is assigned a shape consistent with glacio-isostatic deformation of an elastic crust overlying a viscous mantle and the glacial uplift is varied in accordance with total, present and remaining uplift. (ii) An ice sheet with known shape and thickness is applied on top of a crustal model and the ice flow and ice retreat are modelled.
- Modelling of rock mass response to glaciation and deglaciation is suitable for a sub-structuring approach. Models on the global scale provide the boundary conditions for regional models which in turn provide the boundary conditions for the farfield models, cf. Figure 10-4.
- Two modelling techniques have been applied in this study of the rock mass response to glaciation. The first approach uses a material constitutive model that accounts for the properties of the intact rock and the faults without including the faults as separate entities. This model is implemented in the finite element code called HNFEMP. The other approach implies that faulted rock masses are modelled by describing the response of every fault and deformable block separately. The Micro Universal Distinct Element Code, MUDEC, has been applied with linear fault stiffness properties and nonlinear stiffnesses according to Barton-Bandis.
- The HNFEMP code and the MUDEC code with Barton-Bandis fault properties were tested against the Colorado School of Mines (DSM) block test data at Edgar Mine. Good agreement is obtained for the orientations and magnitudes of the displacement vector and modulus of deformation between the field test and the HNFEMP-modelling. In the monitoring of the principal horizontal stress by the USBM borehole deformation gauge, good agreement with the applied loading in the field and the numerical results by HNFEMP and MUDEC was obtained. Excellent agreement was obtained for joint shear displacements and joint conductive aperture with the MUDEC-modelling. Hence, the two modelling approaches have been shown to adequately represent rock mass deformation from known boundary loadings.
- The effect of glaciation, glacial flow and deglaciation has been studied in two-dimensional, generic models of faulted rock masses. Six loading cases have been simulated in a two-dimensional 4 x 4 km region for three different fault geometries (Figure 10-13).
- HNFEMP-modelling with stiff faults gave a vertical displacement at the ground surface between 2.5 and 4.2 m where the model with two intersecting faults gave the largest displacements. Horizontal stresses at a depth of 500 m varied between 30 and 35 MPa for the loading and unloading cases. The load of a 3 km thick ice sheet superimposed on the virgin vertical rock stress give a vertical stress of 40 MPa (Figure 10-16).
- MUDEC-modelling with linear fault stiffnesses gives smaller horizontal stresses but similar vertical stress compared with the HNFEMP-modelling results. The loading and unloading of the models cause variation in magnitude and orientation of the principal stresses for the uppermost ~ 1000 m of the rock mass.

A major part of the re-orientation of the stresses is caused by rigid body translation and rotation of the rock blocks.

- For MUDEC-modelling with linear fault stiffness the glacial rebound of the ground surface after deglaciation is found to be 3.2 to 4.0 m and about the same as that obtained from the HNFEMP-modelling. The relative vertical displacement between individual rock blocks are 5 to 10 cm.
- For MUDEC-modelling with the Barton-Bandis joint model, the vertical displacement of the ground surface after deglaciation was found to be 3.8 and 3.9 m for Models 3A (stiff faults) and 3B (soft faults) respectively. This is in fair agreement with results obtained from the HNFEMP and linear MUDEC modelling. Modelling with stiff faults was satisfactory while modelling two sets of intersecting fault sets and soft fault stiffnesses gave very high vertical stresses when ice flow is introduced. Application of effective tectonic stresses, i.e. total stress minus pore pressure, make no major change in magnitude of stresses and displacements.
- Modelling with the MUDEC and Barton-Bandis joint model permits determination of mechanical and hydraulic fault aperture. Aperture changes of 40–100  $\mu\text{m}$  have been obtained.

## 10.7 CONCLUSIONS

- Two approaches for modelling rock masses have been applied in this study, namely the finite element method of continuous faults (HNFEMP) and the distinct element method of discontinuous faults (MUDEC). Despite the different modelling approach their application to the CSM block test gave similar results and fair to good agreement with data recorded in the field test. The moderate loading of the block and minor excess over shear strength of existing joints favour elastic deformations and enhance the agreements between the modelling techniques and between the models and the block test.
- The effect of glaciation, glacial flow and deglaciation has been studied in two-dimensional, generic models of faulted rock masses with the two modelling approaches. Altogether ten loading cases have been simulated in a two-dimensional 4 x 4 km region for three different fault geometries. Models with two intersecting sets of faults always give the largest displacements of the studied fault geometries. Local glacial rebound of the ground surface after deglaciation is found to be about 4 m for all models with realistic fault stiffnesses; this faulting is independent of modelling approach. Models with larger dimension (but all other parameters unchanged) will increase the rebound.
- For MUDEC modelling with linear fault stiffness the relative displacement between individual blocks of dimension 200 x 500 m are found to be 5 to 10 cm. The relative displacement of the blocks will most likely cause changes in the mechanical and hydraulic aperture of the faults and thereby change the groundwater flow during a cycle of glaciation and deglaciation.
- The load of a 3 km thick ice sheet superimposed on the virgin vertical rock stress gives a vertical stress of 40 MPa. This stress will be superimposed on the virgin state of rock stress. Construction of a repository, thermal loadings and loading from swelling bentonite will further influence the stress around the deposit.

## 10.8 REFERENCES

### **Bakkeliid S 1986**

The determination of rates of land uplift in Norway. *Tectonophysics*, Vol. 130, pp. 307–326.

### **Barton N R and Bandis S C 1982**

Effect of block size on the shear behaviour of jointed rock. *Proc. 23rd U.S. Symposium on Rock Mechanics*, pp. 739–760.

### **Barton N R, Bandis S C and Bakhtar K 1985**

Strength, deformation and conductivity coupling of rock joints. *Int. J. Rock Mech. Min. Sci. & Geomech. Abstr.*, Vol. 22, No. 3, pp. 121–140.

### **Barton N R et al. 1986**

Numerical analyses and laboratory tests to investigate the Ekofisk subsidence. *Proc. 27th U.S. Symposium on Rock Mechanics*, Univ. of Alabama, June 23–25, 1986.

### **Barton N and Chryssanthakis P 1988**

Validation of MUDEC against Colorado School of Mines block test data. SKB TR 88-14, 94 p, Stockholm.

### **Brown S M, Leijon, B A and Hustrulid W A 1986**

Stress distribution within an artificially loaded jointed block. *Proc. Int. Symposium on Rock Stress and Rock Stress Measurements*, pp. 429–439, Centek Publishers, Luleå.

### **Barton N, Chryssanthakis P 1989**

Distinct element modelling of the influence of glaciation and deglaciation on the behaviour of a faulted rock mass. SKB AR 89-19.

### **Cundall P A 1980**

UDEC — A generalized distinct element program for modelling jointed rock. Report PCAR-1-80, Peter Cundall Associate, Contract DAJA 37-79-C-0548, European Research Office, U.S. Army.

### **El Raba A W M A 1981**

Measurements and modelling of rock mass response to underground excavation. M.S Thesis T-2470, Colorado School of Mines, Golden, Colorado.

### **Goodman R E 1976**

Methods of geological engineering in discontinuous rocks. West Publ. Co., St Paul.

### **Hardin E L, Barton N R, Lingle R, Board M P and Voegele M D 1982**

A heated flatjack test to measure the thermomechanical transport properties of rock masses. Office of Nuclear Waste Isolation, Columbus, OH, ONWI, 260 p.

### **Hart R D, Cundall P A and Cramer M L 1985**

Analysis of a loading test on a large basalt block. *Proc. 26th U.S. Symposium on Rock Mechanics*, pp. 759–768.

**Jing L and Stephansson O 1988**

Distinct element modelling of the influence of glaciation and deglaciation on the state of stress in faulted rock masses. SKB AR 88-23, 16 p, Stockholm.

**Nilsson L and Oldenburg M 1983**

FEMP — An interactive, graphic finite element program for small and large computer system. Technical Report 1983:07 T, Luleå University of Technology, Luleå.

**Olofsson T 1985**

Mathematical modelling of jointed rock masses. Doctoral Thesis 1985:42 D, Luleå University of Technology, Luleå.

**Pande G N 1985**

A constitutive model of rock joints. Proc. Int. Symposium on Fundamentals of Rock Joints, pp. 429–439, Centek Publishers, Luleå.

**Richardson A M 1986**

In-situ mechanical characterization of jointed crystalline rock. Ph.D. Thesis T-3256, Colorado School of Mines, Golden, Colorado, 543 p.

**Singh U, Savilahti T and Stephansson O 1988**

Generic model analysis of large faulted rock masses with soft faults using HNFEMP computer code. SKB AR 88-21, 13 p. and 13 App., Stockholm.

**Singh U, Savilahti T and Stephansson O 1988**

Generic model analysis of large faulted rock masses with hard fault stiffness. SKB AR 88-22, 13 p. and 15 App., Stockholm.

**Stephansson O 1983**

The need of discontinuities and horizontal stresses in geological storage of radioactive waste. Proc. 4th Int. Conf. on Basement Tectonics, pp. 35–47.

**Stephansson O 1987**

Modelling of crustal rock mechanics for radioactive waste storage in Fennoscandia. SKB TR 87-11, 79 p., Stockholm.

**Stephansson O, Bäckblom G, Groth T and Jonasson P 1978**

Deformation of a jointed rock mass. Geol. Fören. Stockholm Förh., Vol. 100, pp. 387–394.

**Stephansson O, Särkkä, P and Myrvang A 1986**

State of stress in Fennoscandia. Proc. Int. Symposium on Rock Stress and Rock Stress Measurements, pp. 21–32, Centek Publishers, Luleå.

**Zimmerman R M and Blanford M L 1985**

Evaluation of the accuracy of continuum-based computational models in relation to field measurements in welded tuff. Proc. Int Symposium on Fundamentals of Rock Joints, pp. 233–245, Centek Publishers, Luleå.

# 11 GENERAL CONCLUSIONS

*The interdisciplinary researchers and co-ordinators.*

Three objectives were set for the Lansjärv study. They were:

- assess the mechanisms that caused present-day scarps,
- clarify the extent of any recent fracturing,
- clarify the extent of any ongoing movements.

At the end of the research project the following eight questions were listed and answered by the interdisciplinary research group.

## **1. ARE THE POST-GLACIAL FAULTS (PGF) NEW OR REACTIVATED FAULTS?**

The Lansjärv post-glacial fault reactivated pre-existing old structures. Natural outcrops close to the scarp show parallel foliations developed at high temperatures in Proterozoic times (c. 1.7 Ga), vein systems developed in Greenschist facies, and old fracture zones. Any new fractures at the surface (i.e. younger than 10,000 years) appear to be confined to within a few metres of the scarp. Even in excavations across the PGF, most of the fractures exhibit extensive oxidation produced at elevated temperatures well before the Quaternary. The upper 300 m of drill core KLJ 01 displays a high fracture frequency and zones of intense hydrothermal alterations developed in oxidising conditions. Negative magnetic anomalies indicate the regional extent of zones of oxidation along old fracture zones like that reactivated by the Lansjärv post-glacial fault.

The inferred three dimensional pattern of the post-glacial fault is consistent with the reactivation of pre-existing structures to release NW compressive stresses on a regional scale.

## **2. WHAT ARE THE CAUSES OF POST-GLACIAL MOVEMENTS?**

The pattern and kinematics of the PGFs do not indicate the radial or tangential extension expected of post-glacial uplift. Instead, they fit the pattern of plate tectonics better. Loading by ice sheets allows the build up of rock stresses. Deglaciation leads to release of stored energy, and, in the Lansjärv region, at least, one large earthquake.

## **3. WHY DO THE PGF SCARPS TREND NNE?**

Fault plane solutions and in-situ stresses indicate a maximum horizontal compression trending N 60° W. The crust is expected to shorten horizontally along pre-existing NNE trending faults in such a stress regime and the resultant dip-slip displacements are visible in the low-relief ground surface.

#### **4. WHY ARE PERSISTENT PGF FEATURES DISTINCT IN A TECTONICALLY COMPLICATED AREA?**

The PGFs distinct strike distribution is attributed to the concentration of post-glacial movements to there being only a few pre-existing structures with appropriate orientations with respect to the reported stress field.

#### **5. ARE THE PGFs SURFICIAL PHENOMENA?**

The existence of local shallow thrust flakes is still an open question but the general length of the PGF indicates significant depth extent (e.g. crustal scale).

#### **6. PRESENT MOVEMENTS?**

The Lansjärv region is near the centre of fastest (~1 cm/y) post-glacial uplift in Fennoscandia and is straining actively, mostly by strike-slip and reverse faults. Although the size of PGFs indicate major earthquake(s) ( $M_L \geq 7$ ) at end-glacial times, the frequent earthquakes of the last 400 years all have  $M_L < 4$ . A large proportion of the current regional strain may be aseismic.

Only geodetic measurements can constrain the rates of regional strain and constrain the ratio of seismic to aseismic strain. Measurements of local networks proposed for particular sites, however, were considered too expensive and of questionable reliability.

#### **7. IS THE LANSJÄRV AREA, WITH ITS PGFs ANOMALOUS COMPARED TO THE REST OF FENNOSCANDIA?**

##### **Regional Scale**

- PGFs in Northern Fennoscandia are remarkable tectonic features of late origin in the Earth's crust and appear in several well defined zones e.g. Pärvie, Lansjärv, Lainio. Some of them are associated with NE-SW trending deformation zones.
- The bedrock in Northern Fennoscandia is characterized by a relatively large number of major shear zones with NW-SE and N-S strike.
- The PGFs at Lansjärv were reactivated by tectonic movements which appear to have been triggered by deglaciation.
- The stress field in Northern Fennoscandia is less consistent in direction of maximum horizontal stress compared to the rest of Fennoscandia. The stress field in the region is most likely caused by plate tectonics related to the Mid-Atlantic and Arctic Ocean Ridges.
- The orientation of pre-existing weak zones in the stress field of Northern Fennoscandia favours thrusting and reverse faulting PGFs.
- Earthquakes in the Lansjärv region occur in the upper crust (0–12 km).
- PGFs in Northern Fennoscandia are located in areas with low relief and moderate to large present uplift.

## Local Scale

The core drilling KLJ 01 has not confirmed the existence of a subhorizontal PGF at Lansjärv.

This may be because the uppermost 300 m of the core demonstrates such a very high fracture frequency that we cannot be certain of distinguishing single PGF in the core.

- The core shows signs of extensive hydrothermal activity, probably combined with circulation of hydrothermal fluids. The positive Ce-anomalies suggest hydrothermal circulation of oxidizing fluids.
- The rock stress measurements at the Lansjärv borehole reveal a state of stress with extremely low minimum stress magnitudes compared to existing data of rock stresses in deep boreholes in Fennoscandia. The maximum horizontal stress rotates about 90°, over a depth interval of about 200 m in the borehole.
- The vertical hydraulic gradient and the low hydraulic heads at depth are anomalous in view of the current geological model on which the borehole was sited.
- The hydraulic conductivity in KLJ 01 does not differ significantly from conditions found in other study sites of the SKB site investigation programme.

## 8. WHAT IS THE POTENTIAL IMPACT OF PGFs ON REPOSITORY DESIGN AND PERFORMANCE ASSESSMENT?

A principle for design of a repository is to avoid potential zones of movement that may damage the canisters. It is evident from this study that post-glacial fault movements reactivated pre-existing, old, heavily fractured and altered zones at least several metres across.

Such zones would be localized in the site characterization for a repository. Even if such a zone is not identified from surface or borehole investigations, it could still be avoided when canister positions are selected. This study concludes that the post-glacial fault movement was associated with at least one major earthquake(s). The impact on the wall rock of the Lansjärv post-glacial fault is still unclear. New fracturing within a few metres is indicated on one excavated bedrock surface.

In the KBS-3 study, SKBF/KBS (1983), a so-called “respect distance” of at least 100 m along fracture zone was specified as a design condition. With respect to the performance assessment of a repository it is of utmost importance to recognize whether these fault movements will dramatically affect the ground water flux around the repository and/or affect the groundwater chemistry. The borehole at Lansjärv is located in a very tectonized and complex geological area in the Baltic Shield.

In spite of the very dramatic structures and events that are described in this report, the results from the hole are comparable to results from other potential sites for a repository in Sweden. This is specifically true for the results of hydraulic conductivity and groundwater chemistry for deep bedrock conditions.

However, below a depth of approx. 300 m, it has not been possible to recognize changes in rock conditions due to the latest deglaciation. The present conditions represent the accumulated effects of the tectonic activity since the Atlantic rifting began at about 58 Ma. and several glaciations and deglaciations.

This study indicates that post-glacial fault movements are associated with low-dipping fracture zones, though the PGF itself may have a dip exceeding 40°. This fact must be recognized in the site characterization for a repository so that investigations are performed sufficiently deep under a potential repository level.





# List of SKB reports

## Annual Reports

1977-78

TR 121

### **KBS Technical Reports 1 – 120.**

Summaries. Stockholm, May 1979.

1979

TR 79-28

### **The KBS Annual Report 1979.**

KBS Technical Reports 79-01 – 79-27.

Summaries. Stockholm, March 1980.

1980

TR 80-26

### **The KBS Annual Report 1980.**

KBS Technical Reports 80-01 – 80-25.

Summaries. Stockholm, March 1981.

1981

TR 81-17

### **The KBS Annual Report 1981.**

KBS Technical Reports 81-01 – 81-16.

Summaries. Stockholm, April 1982.

1982

TR 82-28

### **The KBS Annual Report 1982.**

KBS Technical Reports 82-01 – 82-27.

Summaries. Stockholm, July 1983.

1983

TR 83-77

### **The KBS Annual Report 1983.**

KBS Technical Reports 83-01 – 83-76

Summaries. Stockholm, June 1984.

1984

TR 85-01

### **Annual Research and Development Report 1984**

Including Summaries of Technical Reports Issued during 1984. (Technical Reports 84-01–84-19)

Stockholm June 1985.

1985

TR 85-20

### **Annual Research and Development Report 1985**

Including Summaries of Technical Reports Issued during 1985. (Technical Reports 85-01-85-19)

Stockholm May 1986.

1986

TR 86-31

### **SKB Annual Report 1986**

Including Summaries of Technical Reports Issued during 1986

Stockholm, May 1987

1987

TR 87-33

### **SKB Annual Report 1987**

Including Summaries of Technical Reports Issued during 1987

Stockholm, May 1988

1988

TR 88-32

### **SKB Annual Report 1988**

Including Summaries of Technical Reports Issued during 1988

Stockholm, May 1989

## Technical Reports

1989

TR 89-01

### **Near-distance seismological monitoring of the Lansjärv neotectonic fault region Part II: 1988**

Rutger Wahlström, Sven-Olof Linder,  
Conny Holmqvist, Hans-Edy Mårtensson  
Seismological Department, Uppsala University,  
Uppsala  
January 1989

TR 89-02

### **Description of background data in SKB database GEOTAB**

Ebbe Eriksson, Stefan Sehlstedt  
SGAB, Luleå  
February 1989

TR 89-03

### **Characterization of the morphology, basement rock and tectonics in Sweden**

Kennert Röshoff  
August 1988

TR 89-04

### **SKB WP-Cave Project Radionuclide release from the near-field in a WP-Cave repository**

Maria Lindgren, Kristina Skagius  
Kemakta Consultants Co, Stockholm  
April 1989

TR 89-05

### **SKB WP-Cave Project Transport of escaping radionuclides from the WP-Cave repository to the biosphere**

Luis Moreno, Sue Arve, Ivars Neretnieks  
Royal Institute of Technology, Stockholm  
April 1989

TR 89-06

**SKB WP-Cave Project**  
**Individual radiation doses from nuclides contained in a WP-Cave repository for spent fuel**

Sture Nordlinder, Ulla Bergström  
Studsvik Nuclear, Studsvik  
April 1989

TR 89-07

**SKB WP-Cave Project**  
**Some Notes on Technical Issues**

- Part 1: Temperature distribution in WP-Cave: when shafts are filled with sand/water mixtures  
Stefan Björklund, Lennart Josefson  
Division of Solid Mechanics, Chalmers University of Technology, Gothenburg, Sweden
- Part 2: Gas and water transport from WP-Cave repository  
Luis Moreno, Ivars Neretnieks  
Department of Chemical Engineering, Royal Institute of Technology, Stockholm, Sweden
- Part 3: Transport of escaping nuclides from the WP-Cave repository to the biosphere.  
Influence of the hydraulic cage  
Luis Moreno, Ivars Neretnieks  
Department of Chemical Engineering, Royal Institute of Technology, Stockholm, Sweden

August 1989

TR 89-08

**SKB WP-Cave Project**  
**Thermally induced convective motion in groundwater in the near field of the WP-Cave after filling and closure**

Polydynamics Limited, Zürich  
April 1989

TR 89-09

**An evaluation of tracer tests performed at Studsvik**

Luis Moreno<sup>1</sup>, Ivars Neretnieks<sup>1</sup>, Ove Landström<sup>2</sup>  
<sup>1</sup> The Royal Institute of Technology, Department of Chemical Engineering, Stockholm  
<sup>2</sup> Studsvik Nuclear, Nyköping  
March 1989

TR 89-10

**Copper produced from powder by HIP to encapsulate nuclear fuel elements**

Lars B Ekbom, Sven Bogegård  
Swedish National Defence Research Establishment  
Materials department, Stockholm  
February 1989

TR 89-11

**Prediction of hydraulic conductivity and conductive fracture frequency by multivariate analysis of data from the Klipperås study site**

Jan-Erik Andersson<sup>1</sup>, Lennart Lindqvist<sup>2</sup>  
<sup>1</sup> Swedish Geological Co, Uppsala  
<sup>2</sup> EMX-system AB, Luleå  
February 1988

TR 89-12

**Hydraulic interference tests and tracer tests within the Brändan area, Finnsjön study site**  
**The Fracture Zone Project – Phase 3**

Jan-Erik Andersson, Lennart Ekman, Erik Gustafsson, Rune Nordqvist, Sven Tirén  
Swedish Geological Co, Division of Engineering Geology  
June 1988

TR 89-13

**Spent fuel**  
**Dissolution and oxidation**  
**An evaluation of literature data**

Bernd Grambow  
Hanh-Meitner-Institut, Berlin  
March 1989

TR 89-14

**The SKB spent fuel corrosion program**  
**Status report 1988**

Lars O Werme<sup>1</sup>, Roy S Forsyth<sup>2</sup>  
<sup>1</sup> SKB, Stockholm  
<sup>2</sup> Studsvik AB, Nyköping  
May 1989

TR 89-15

**Comparison between radar data and geophysical, geological and hydrological borehole parameters by multivariate analysis of data**

Serje Carlsten, Lennart Lindqvist, Olle Olsson  
Swedish Geological Company, Uppsala  
March 1989

TR 89-16

**Swedish Hard Rock Laboratory –**  
**Evaluation of 1988 year pre-investigations and description of the target area, the island of Åspö**

Gunnar Gustafsson, Roy Stanfors, Peter Wikberg  
June 1989

TR 89-17

**Field instrumentation for hydrofracturing stress measurements  
Documentation of the 1000 m hydrofracturing unit at Luleå University of Technology**

Bjarni Bjarnason, Arne Torikka  
August 1989

TR 89-18

**Radar investigations at the Saltsjötunnel – predictions and validation**

Olle Olsson<sup>1</sup> and Kai Palmqvist<sup>2</sup>  
<sup>1</sup> Abem AB, Uppsala, Sweden  
<sup>2</sup> Bergab, Göteborg  
June 1989

TR 89-19

**Characterization of fracture zone 2, Finnsjön study-site**

**Editors: K. Ahlbom, J.A.T. Smellie, Swedish Geological Co, Uppsala**

- Part 1: Overview of the fracture zone project at Finnsjön, Sweden  
K. Ahlbom and J.A.T. Smellie. Swedish Geological Company, Uppsala, Sweden.
- Part 2: Geological setting and deformation history of a low angle fracture zone at Finnsjön, Sweden  
Sven A. Tirén. Swedish Geological Company, Uppsala, Sweden.
- Part 3: Hydraulic testing and modelling of a low-angle fracture zone at Finnsjön, Sweden  
J-E. Andersson<sup>1</sup>, L. Ekman<sup>1</sup>, R. Nordqvist<sup>1</sup> and A. Winberg<sup>2</sup>  
<sup>1</sup> Swedish Geological Company, Uppsala, Sweden  
<sup>2</sup> Swedish Geological Company, Göteborg, Sweden
- Part 4: Groundwater flow conditions in a low angle fracture zone at Finnsjön, Sweden  
E. Gustafsson and P. Andersson. Swedish Geological Company, Uppsala, Sweden
- Part 5: Hydrochemical investigations at Finnsjön, Sweden  
J.A.T. Smellie<sup>1</sup> and P. Wikberg<sup>2</sup>  
<sup>1</sup> Swedish Geological Company, Uppsala, Sweden  
<sup>2</sup> Swedish Nuclear Fuel and Waste Management Company, Stockholm, Sweden
- Part 6: Effects of gas-lift pumping on hydraulic borehole conditions at Finnsjön, Sweden  
J-E. Andersson, P. Andersson and E. Gustafsson. Swedish Geological Company, Uppsala, Sweden  
August 1989

TR 89-20

**WP-Cave - Assessment of feasibility, safety and development potential**

Swedish Nuclear Fuel and Waste Management Company, Stockholm, Sweden  
September 1989

TR 89-21

**Rock quality designation of the hydraulic properties in the near field of a final repository for spent nuclear fuel**

Hans Carlsson<sup>1</sup>, Leif Carlsson<sup>1</sup>, Roland Pusch<sup>2</sup>  
<sup>1</sup> Swedish Geological Co, SGAB, Gothenburg, Sweden  
<sup>2</sup> Clay Technology AB, Lund, Sweden  
June 1989

TR 89-22

**Diffusion of Am, Pu, U, Np, Cs, I and Tc in compacted sand-bentonite mixture**

Department of Nuclear Chemistry, Chalmers University of Technology, Gothenburg, Sweden  
August 1989

TR 89-23

**Deep ground water microbiology in Swedish granitic rock and its relevance for radionuclide migration from a Swedish high level nuclear waste repository**

Karsten Pedersen  
University of Göteborg, Department of Marine microbiology, Gothenburg, Sweden  
March 1989

TR 89-24

**Some notes on diffusion of radionuclides through compacted clays**

Trygve E Eriksen  
Royal Institute of Technology, Department of Nuclear Chemistry, Stockholm, Sweden  
May 1989

TR 89-25

**Radionuclide sorption on crushed and intact granitic rock  
Volume and surface effects**

Trygve E Eriksen, Birgitta Locklund  
Royal Institute of Technology, Department of Nuclear Chemistry, Stockholm, Sweden  
May 1989

TR 89-26

**Performance and safety analysis of  
WP-Cave concept**

Kristina Skagius<sup>1</sup>, Christer Svemar<sup>2</sup>

<sup>1</sup> Kemakta Konsult AB

<sup>2</sup> Swedish Nuclear Fuel and Waste Management Co  
August 1989

TR-89-27

**Post-excavation analysis of a revised  
hydraulic model of the Room 209 fracture,  
URL, Manitoba, Canada**

**A part of the joint AECL/SKB character-  
ization of the 240 m level at the URL,  
Manitoba, Canada**

Anders Winberg<sup>1</sup>, Tin Chan<sup>2</sup>, Peter Griffiths<sup>2</sup>,  
Blair Nakka<sup>2</sup>

<sup>1</sup> Swedish Geological Co, Gothenburg, Sweden

<sup>2</sup> Computations & Analysis Section, Applied  
Geoscience

Branch, Atomic Energy of Canada Limited,  
Pinawa, Manitoba, Canada

October 1989

TR 89-28

**Earthquake mechanisms in Northern  
Sweden Oct 1987 — Apr 1988**

Ragnar Slunga

October 1989

TR 89-29

**Interim report on the settlement  
test in Stripa**

Lennart Börgesson, Roland Pusch

Clay Technology AB, Lund

November 1989

TR 89-30

**Seismic effects on bedrock and under-  
ground constructions. A literature sur-  
vey of damage on constructions,  
changes in groundwater levels and flow,  
changes in chemistry in groundwater  
and gases**

Kennert Röshoff

June 1989